

Doctoral thesis

Doctoral theses at NTNU, 2021:240

Ane Dalsnes Storsæter

Designing and Maintaining Roads to Facilitate Automated Driving

NTNU
Norwegian University of Science and Technology
Thesis for the Degree of
Philosophiae Doctor
Faculty of Engineering
Department of Civil and Environmental
Engineering



Norwegian University of
Science and Technology

Ane Dalsnes Storsæter

Designing and Maintaining Roads to Facilitate Automated Driving

Thesis for the Degree of Philosophiae Doctor

Trondheim, August 2021

Norwegian University of Science and Technology
Faculty of Engineering
Department of Civil and Environmental Engineering



Norwegian University of
Science and Technology

NTNU

Norwegian University of Science and Technology

Thesis for the Degree of Philosophiae Doctor

Faculty of Engineering

Department of Civil and Environmental Engineering

© Ane Dalsnes Storsæter

ISBN 978-82-326-6579-2 (printed ver.)

ISBN 978-82-326-5241-9 (electronic ver.)

ISSN 1503-8181 (printed ver.)

ISSN 2703-8084 (online ver.)

Doctoral theses at NTNU, 2021:240

Printed by NTNU Grafisk senter

“We are stuck with technology when what we really want is just stuff that works.”

Douglas Adams, *The Salmon of Doubt*

Abstract

Designing and Maintaining Roads to Facilitate Automated Driving

by Ane Dalsnes STORSÆTER

Advanced Driver Assistance Systems (ADAS) are common in modern cars. ADAS features such as lane keeping and Adaptive Cruise Control (ACC) represent forms of lateral and longitudinal vehicle control, i.e., the basis for automated driving. The sensors and software on which such functionalities depend also determine some of their driving characteristics and abilities. Current road infrastructure has been designed for human drivers. With driving automation becoming commonplace and expected to take on a greater role in transportation, it is time that automated drivers are included as road users and considered in road design and maintenance standards. Automated drivers have, however, not been defined to the extent needed to make this possible. This thesis establishes a unified framework for including automated drivers as new road users and suggests starting points for adapting road design and maintenance to facilitate automated driving. Practical research from laboratory, test site, and real-life settings were performed using available data from ADAS applications for the latter. Based on these examples, suggestions for adaptations to design and maintenance to support automated drivers are presented. Furthermore, how ADAS functionality can be used to monitor the state of road assets is demonstrated.

1. The main findings of this thesis related to including the automated driver as a new road user are:
 - Development of a new unified framework for automated and human driving that for the first time includes all driving processes and identifies characteristics of automated drivers based on existing technology.
 - Characteristics of automated drivers found to be of special importance to transport engineering are:
 - Increased electromagnetic sensitivity range.
 - Greater field of view.
 - Fundamental differences in cognitive processes.
2. The findings related to geometric road design for automated drivers are:
 - Three parameters need to be redefined in the short-term for automated drivers: *Eye height*, *Object height* and *Reaction time*. New definitions of parameters could include replacing *Eye height* and *Object height* with new design parameters describing line of sight and object detection by automated drivers.

- A new manual for road design for transportation without human occupants is advised. The following geometric road design parameters can be revised with regards to automated freight transport: *Vertical acceleration*, *Relative vertical speed*, *Minimum vertical curve radius (sag)*, *Clothoid parameter*, and *Minimum horizontal curve radius (tunnels)*.
 - The shapes and dynamic properties of vehicles should continue to be monitored for changes including *Vehicle height*, *Vehicle width*, *Wheel distance*, *Overhang*, *Acceleration*, *Deceleration*, and *Reaction time*.
3. The following findings relate to adaptations to road design for automated users:
- Colors, patterns, and textures can be used to make existing road infrastructure elements such as guardrails, dividers, and road markings gain higher visibility to facilitate automated detection.
 - Visibility of traffic control devices in parts of the electromagnetic spectrum beyond the visible light can be used to add information for automated users, e.g., barcode layer in the near-UV for positioning.
 - Contrast between road marking and road pavement is more important for camera-based lane detection than measures of retroreflectivity.
 - Camera based Lane Departure Warning (LDW) systems appear to be independent of exterior lighting (other than headlights).
 - Yellow road markings have higher visibility and contrast to the road surface and snow in color spaces HSL (Hue, Saturation, and Lightness), HSV (Hue, Saturation, and Value), and YUV (luminance, color component U and color component V).
 - Yellow road markings can facilitate automated driving in snow better than white markings.
 - The type and thickness of road marking may affect successful detection by camera based lane departure warning.
4. The following results of the thesis are related to road maintenance for human and automated users:
- Lane Departure Warning functionality demonstrates that Advanced Driver Assistance Systems can be used to monitor the state of road markings.
 - Lane Departure Warning functionality can be used to identify when conditions such as snow prevent detection of road marking.
 - Data from Advanced Driver Assistance Systems can be used to define Operational Design Domains (ODDs) and Infrastructure Support Levels for Automated Driving (ISAD).

This research has established automated drivers as new road users and suggested starting points in processes to adapt road design and maintenance to facilitate automated driving.

Acknowledgements

Thank you to my knowledgeable and supportive supervisors:
Dr. Kelly Pitera and Dr. Edward McCormack.

Thanks to my family, boyfriend, friends and coworkers for all their help and motivation, especially to my kids for their patience.

Thanks also to all the staff at NTNU for support in all matters ranging from procurement to prototyping and testing.

Thanks to the Norwegian Public Roads Administration
for the possibility to pursue a PhD.

Contents

Abstract	v
Acknowledgements	vii
1 Introduction	1
1.1 Motivation	1
1.2 Research Objectives	3
1.3 Thesis Structure	3
1.4 Scope of the Thesis	3
1.5 List of Papers	5
1.5.1 Author Contributions for All Papers	5
2 Designing and Maintaining Roads to Facilitate Automated Driving	7
2.1 The Automated Driver	10
2.2 Road Design	12
2.2.1 Geometric Road Design	12
2.2.2 Road Markings	13
2.3 Road Maintenance	14
3 Research Design	17
3.1 Theoretical Foundation	18
3.1.1 Paper I	18
3.1.2 Paper II	20
3.2 Practical Research - Road Markings	22
3.2.1 Paper III	22
3.2.2 Paper IV	26
4 Discussion of Results	33
4.1 Research Objective 1	33
4.2 Research Objective 2	36
4.2.1 Design Parameters in Need of Revision in the Short Term	36
4.2.2 Geometric Road Design Parameters in Need of Revision in the Long-Term	39
4.3 Research Objective 3	44
4.3.1 Paper I	44
4.3.2 Paper II	45
4.3.3 Paper III	45
4.3.4 Paper IV	48
4.4 Research Objective 4	54

4.4.1	Sensor Data from Automated Driving Systems and Suggested Applications.	54
4.4.2	Findings From Practical Experiments and Suggestions for Applications	55
4.5	Summary of Main Results	59
4.6	Further Work	61
5	Conclusion and Further Perspectives	65
	Bibliography	69
A	Paper I	77
B	Paper II (in progress)	103
C	Paper III	131
D	Paper IV (preprint)	151
E	Code for Data Analyses in Paper III	191
F	Code for Image Analyses in Paper IV	197

List of Figures

2.1	Regulations related to automated driving adapted from (Ertrac, 2019).	8
3.1	Norwegian design parameters from manual v120 (Statens vegvesen, 2019b). Basic parameters are shown in blue and design parameters in white.	21
3.2	Retroreflector mounted on the side of the test vehicle.	23
3.3	Illustration of ROC curve plots.	26
3.4	Difference in width of thermoplastic marking before (left-hand side) and after (right-hand side) melting.	28
3.5	Snow application with sifter and 0.5 cm wooden frame.	28
3.6	Snow removal equipment. Ribbed plow on the left-hand side and brush on the right-hand side.	29
3.7	Example of histogram of pixel intensities.	31
4.1	Unified framework for human and automated driving (Storsæter, Pit- era, and McCormack, 2020).	34
4.2	Parameters of geometric road design affected by the automated driver derived from Manual V120 (Statens vegvesen, 2019b).	36
4.3	The effect of lower reaction times on Stopping sight distances.	39
4.4	Example of accelerations experienced in a horizontal curve.	42
4.5	Sign with traditional layer and an added layer visible in the near in- frared. Source: Snyder et al. (2018).	44
4.6	Data resolution for the car (blue) and retroreflector (red).	46
4.7	Plots of position data for 1) Daytime and night-time on freeway, 2) Daytime on county roads, and 3) Night-time on county roads. Visual- ization: http://geojsonviewer.nsspot.net	47
4.8	Overlapping section of county roads with lane detection results for daytime (left-hand side) and night-time (right-hand side) driving. . . .	47
4.9	Example of visibility of lane markings in different color spaces, visu- ally (left-hand side) and by pixel values (right-hand side).	49
4.10	Laboratory road model with 0.5 cm snow (birds-eye view) and corre- sponding histograms for RGB and grayscale representations.	50
4.11	Histogram plots for HSL, HSV and YUV color space representations of Figure 4.10	51
4.12	Public road in evening with partial snow cover (RGB and grayscale representations) and corresponding histogram plots.	52
4.13	Histogram plots for HSL, HSV and YUV color space representations of the public road driving image (Figure 4.12).	53
4.14	Receiver operating characteristics curves.	57

4.15 Example of similarity of different road infrastructure elements considering automated detection. Photo: NPRA. 62

List of Tables

1.1	The research objectives of the thesis.	3
1.2	Overview of Automated Driving.	4
2.1	Infrastructure Support levels for Automated Driving (ISAD) based on (Ertrac, 2019).	9
2.2	The levels of automation defined by SAE International, adapted from (SAE International, 2018).	10
3.1	Relationship between research objectives and papers in the thesis.	17
3.2	Overview of methodology used in the thesis.	18
3.3	Lane detection values and their conversion from four discrete values to a binary outcome.	24
3.4	Composition of stone sizes in asphalt (Ab2).	27
4.1	Significances of predictor variables for lane detection by LDW.	45
4.2	Visibility of yellow and white road markings for cases with snow coverage based on histogram plots.	54
4.3	Classification of all cases: freeway and county roads in daytime and night-time.	56

List of Abbreviations

ADAS	Advanced Driver Assistance System
AADT	Average Annual Daily Traffic
AASHTO	American Association of State Highway and Transportation Officials
ABS	Anti-lock Braking Systems
ACC	Adaptive Cruise Control
ADAS	Advanced Driver Support System
ADS	Automated Driving System
AI	Artificial Intelligence
ATSSA	The American Traffic Safety Services Association
AUC	Area Under Curve
AV	Automated Vehicle
CAV	Connected and Automated Vehicle
CCAM	Cooperative, Connected and Automated Mobility
CEDR	Conference of European Directors of Roads
DAS	Driver Assistance System
DDT	Dynamic Driving Task
EM	Electromagnetic
HAV	Highly Automated Vehicle
IMU	Inertial Measurement Unit
IR	Infrared
ISAD	Infrastructure Support levels for Automated Driving
ISO	International Organization for Standardization
ITS	Intelligent Transportation Systems
LAV	Lower-level Automated Vehicle
LDW	Lane Departure Warning
Lidar	A portmanteau of “light” and “radar”, also referred to as an acronym for Light Detection And Ranging (LiDAR) and Laser imaging, Detection, And Ranging (LADAR).
MAXCC	MAXimum Correct Classification
MAXSS	MAXimize Sensitivity and Specificity
ML	Machine Learning
MUTCD	Manual on Uniform Traffic Control Devices for Streets and Highways
NHTSA	National Highway Traffic Safety Administration
NPRA	Norwegian Public Roads Administration
NTNU	Norges Teknisk-Naturvitenskapelige Universitet AKA Norwegian University of Science and Technology
OEDR	Object and Event Detection and Response
ODD	Operational Design Domain
πnonevent	Nonevent rate

ROO	R oad O wners and O perators
SAE	S ociety of A utomotive E ngineers
SPSS	S tatistical P ackage for the S ocial S ciences
UV	U ltraviolet

For my kids

Chapter 1

Introduction

1.1 Motivation

Advanced driver support systems (ADAS) are common in modern vehicles, providing support functions such as lane keeping for lateral control and adaptive cruise control (ACC) for longitudinal control. These are core functionalities used also in higher levels of automation and, eventually, fully automated driving. On these foundations, a new automated road user is emerging: the automated driver.

The automated driver represents a significant shift in transportation. For over a century the design of vehicles and roadways has been based on characteristics of human physiology and psychology. Now, the vehicle industry is in a race to create fully automated driving systems. The introduction of the automated driver raises questions on to what extent the road infrastructure needs to be modified to support automated driving. The automated driver is under development, with different choices in sensors and software for different developers, and the knowledge the automakers possess is not willingly shared. This makes it challenging for road authorities and transportation researchers to suggest what changes to the roadway should be addressed and how.

The time frame envisioned to achieve fully automated driving on public roads is not known. Lutin, Kornhauser, and Lerner-Lam (2013) referenced the expectation of Audi, BMW, GM, and Nissan to introduce self-driving cars by 2020. This prophecy was proven wrong and new estimates suggest that the 2040s, or even 2050s, may be the decades in which most vehicles have become fully automated (Litman, 2018). Still, lower levels of automation such as ADAS in today's vehicles have already been found to provide safety benefits (Kusano et al., 2014; Kusano and Gabler, 2015; Östling et al., 2019). For instance, lane departure warning (LDW) was shown to be able to prevent 28.9 % of road departure crashes caused by drivers drifting out of the lane in a simulation study (Kusano et al., 2014). Making sure that the road infrastructure is easily and correctly interpreted is therefore beneficial even in the current vehicle fleet.

Beyond contributing to traffic safety, automated driving is suggested to have cost-reducing effects for road infrastructure. The reasoning behind this claim is that automated drivers can provide opportunity for designing roads that have horizontal and vertical curvature with smaller radii which can reduce the amount of earthwork needed during road construction (Khoury, Amine, and Saad, 2019; Statens vegvesen, 2019c). Today's road design furthermore requires consecutive curves to be similar in radii to make the roadway more predictable for human drivers. This might not be

needed for automated drivers allowing for more flexibility in road design (Paulsen, 2018) and, subsequently, reducing the area needed for road construction. Another consequence of automated driving is the potential to remove safety features such as speed safety buffers. Automated drivers can be programmed to adhere to the speed limit, or even dynamically set speed limits dependent on, e.g., the weather. This would remove the need for a buffer in the speed limit which is part of today's road design to mitigate human drivers' tendency to speed.

The first step in adapting the road infrastructure to support automated drivers, is to acknowledge the automated driver as a new road user. Road design is based on human traits such as eye height and reaction time. To be able to assess whether road design parameters should be revised to include the automated driver, there is a need to identify the characteristics of automated drivers and determine how they differ to those of human drivers. Existing taxonomies, such as the SAE International's levels of automation (SAE International, 2018), or standards such as the automotive functional safety standard ISO 26262 (International Organization for Standardization, 2011), do not provide details of hardware (i.e., sensors) and software needed to establish these characteristics for automated driving systems. Once a framework for automated drivers as new road users is developed, the characteristics of automated and human driver can be compared to evaluate current road design and maintenance.

Road markings are the most widely used traffic control devices today, and high visibility lane markings are beneficial for the safe operation of human drivers (Fares et al., 2010; Thamizharasan et al., 2003). Lane detection functionality is likewise considered to be important for any driving automation system (Aly, 2008; Chen et al., 2015; Farah et al., 2018; Yi, Chen, and Chang, 2015). Road marking therefore represents a natural starting point for exploring how road design and maintenance can be adapted to facilitate automated driving.

Road authorities have several incentives to develop knowledge on the automated driver. First and foremost, is the aim to reduce death and injury in transportation. Exploring how automated drivers differ from human drivers give insights into how roads can be adapted to enhance the safety effects of driving automation, it also makes it possible to assess the need for new standards for automated driving that can allow greater flexibility in road design. Last but not least, automated driving functionality is dependent on sensors that observe the road environment, these sensors can be used for crowd-sourced monitoring of road assets. Automated driving functionality has thus far been developed without input or interference by road owners and operators (ROOs). Adapting road infrastructure to support driving automation has furthermore been given little attention in research (Farah et al., 2018; Nitsche, Mocanu, and Reinthaler, 2014). At the same time emerging frameworks such as the Infrastructure Support levels for Automated Driving (ISAD) proposed by The European Road Transport Research Advisory Council (ERTRAC) (Ertrac, 2019) are creating expectations of road infrastructure that facilitates driving automation. Given that roads are planned to serve the traffic needs in the subsequent 20 years (Statens vegvesen, 2018) the time to start adapting our road design and maintenance standards and strategies is now.

1.2 Research Objectives

The aim of this thesis is to initiate the process of including the automated driver as a new road user. This thesis furthermore identifies starting points for adapting road design and maintenance to facilitate automated driving including practical examples of how the road design and infrastructure can be adapted to support both human and automated user.

TABLE 1.1: The research objectives of the thesis.

Research Objectives	
RO1	Establish automated drivers as new road users including identifying their characteristics and how they compare to human drivers’.
RO2	Evaluate geometric road design parameters with regards to automated drivers, in both the short and long term.
RO3	Examine how road infrastructure design and maintenance can facilitate automated driving.
RO4	Examine how driving automation systems can act as sensors to monitor the state of road infrastructure.

1.3 Thesis Structure

Part 1 forms the main part of the thesis and consists of five chapters and a bibliography. Chapter 1 motivates and defines the research; Chapter 2 gives a theoretical background for how to design and maintain roads for automated driving. Chapter 3 covers the methodology used in the four papers. The results from the individual papers are discussed in Chapter 4 and linked to the research objectives. Chapter 5 offers conclusions from the thesis work and suggestions for further research efforts in designing and maintaining roads for automated drivers. The second part of the thesis contains the four full papers written within the PhD studies, and examples of code used in these.

1.4 Scope of the Thesis

Automated driving is a complex set of functionalities encompassing a diverse set of knowledge domains, e.g., hardware and sensors, software development, robotics and cybernetics, physics, geometric road design, transport technology, law, regulation, ethics, etc. To approach this vast domain from a research perspective, a scope must be defined. Automated driving can be described in general terms as consisting of hardware and sensors, software and processing, and, lastly, control or steering. These are listed in the left-hand side column of **Table 1.2** and discussed in Paper I. These driving processes determine key characteristics of the automated driver such as how it observes the environment, how it interprets the input, and how it acts based on these inputs. The research in this thesis considers how these automated driver

characteristics can be used to adapt the other main component required for driving: the physical road infrastructure.

TABLE 1.2: Overview of Automated Driving.

Automated Driving System /Vehicle	Regulatory	Intersection of Automated Driving and Regulation
Hardware/sensors	Road Design	Operational Design Domain (ODD)
Software/processing	Road Maintenance	Infrastructure Support levels for Automated Driving (ISAD)
Control/steering	Driver's License Vehicle Inspection	

The strategies for design and maintenance of road infrastructure lie within the regulatory domain of road authorities in the middle column of **Table 1.2**. How to adapt design and maintenance of roads to facilitate automated driving is the main objective of this research. Road authorities are also responsible for driving licenses and periodic check vehicle inspections. These will need to be evaluated for driving automation systems but will not be covered in this thesis.

Road design and maintenance are the main focuses of Paper II, III and IV. From the framework describing automated driving developed in Paper I, current road design parameters for road design were evaluated considering automated drivers in Paper II. Papers III and IV used both laboratory and field tests to assess how road design and maintenance can be adapted to support automated driving features and how the sensors used in driving can be used to monitor the state of road infrastructure including challenging Nordic weather conditions. For these experiments, road markings were the use case as they are the most widely used traffic control device. This thesis uses lower levels of automation, i.e. Advanced Driver Assistance Systems (ADAS), to show how the knowledge needed to start adapting road infrastructure design and maintenance is available today and how this can be used to enable a proactive approach to including the automated driver in design and maintenance of roads.

Finally, the right column in **Table 1.2** represents the intersection of driving automation and regulation of road infrastructure. First, are the Operational Design Domains (ODDs) and, secondly, the newly defined Infrastructure Support Levels for Automated Driving (ISAD). ODDs are a sets of driving conditions that allow different levels of driving automation. ODDs are related to road infrastructure in terms of both the class of road, e.g., freeway versus county road, and the physical infrastructure present, e.g., guardrails, barriers, and intersections. Another part of ODDs is weather, which is also related to levels of winter maintenance. The ISAD framework is under development and represents interaction between automated road users and the road infrastructure. The support levels of the ISAD framework range from conventional road infrastructure such as signage and road markings to roads that monitor all activity and communicates relevant events to automated vehicle systems in real-time. ODDs and ISAD will be discussed in this thesis as they represent suggested efforts towards adapting the road design and maintenance to support automated driving.

1.5 List of Papers

I

Storsæter, Ane Dalsnes, Kelly Pitera, and Edward D. McCormack.
"The Automated Driver as a New Road User." *Transport Reviews*. 2020,
doi: 10.1080/01441647.2020.1861124.

II

Storsæter, Ane Dalsnes, Kelly Pitera, and Edward D. McCormack.
"Preparing for Automated Drivers - An Evaluation of Current Road Design Parameters." In progress.

III

Storsæter, Ane Dalsnes, Kelly Pitera, and Edward D. McCormack.
"Using ADAS to Future-Proof Roads - Comparison of Fog Line Detection from an In-vehicle Camera and Mobile Retroreflector." *Sensors*. 2021; 21(5),
doi: 10.3390/s21051737.

IV

Storsæter, Ane Dalsnes, Kelly Pitera, and Edward D. McCormack.
"Camera Based Lane Detection - Can Yellow Road Marking Facilitate Automated Driving in Snow?" Submitted to *Journal of Field Robotics*.

1.5.1 Author Contributions for All Papers

Conceptualization, Data curation, Formal analysis, Funding acquisition, Investigation, Project administration, Visualization, Writing - original draft: Ane Dalsnes Storsæter.

Methodology: Ane Dalsnes Storsæter, Kelly Pitera, Edward McCormack.

Supervision, Writing - review & editing: Kelly Pitera, Edward McCormack.

Chapter 2

Designing and Maintaining Roads to Facilitate Automated Driving

This chapter provides background to set the context for exploring how road infrastructure can support automated driving. Automated driving represents a complex and interdisciplinary field (Koopman and Wagner, 2017). While the technology driving the automation of transportation has seen rapid development in recent years, the same cannot be said for the design and maintenance of the physical road. It may be argued that automated drivers will need to adhere to current, human-oriented road design and maintenance, however, the idea of infrastructure adapting to automated road users is becoming more prevalent. For instance, the European Commission states that it is a research priority to determine how road infrastructure can and should support automated driving (European Commission, 2018). ERTRAC has furthermore proposed a taxonomy for Infrastructure Support levels for Automated Driving (ISAD). ISAD will be an addition to other regulations related to automated driving, such as the homologation (i.e., the granting of approval by an official authority) framework that governs motor vehicle type approval, the operational design domain which governs where and under which conditions the automated system can operate, and the traffic regulations framework which governs the manuals for road design and traffic control devices (Ertrac, 2019; Erhart et al., 2020) shown in **Figure 2.1**.

The ISAD framework describes five levels of infrastructure support for automated driving shown in **Table 2.1**. In **Table 2.1** VMS refers to Variable Message Signs. Today's road networks are at level E and D, i.e., *Conventional infrastructure*. Level E, the lowest level, represents road infrastructure designed for human drivers such as road markings and signs. Level D represents the addition of static map information in digital form. Levels C-A are labelled as *Digital infrastructure*. At level C, the infrastructure is described as being able to share "All dynamic and static infrastructure information." to automated vehicles (AVs). The ISAD taxonomy is vaguely described and the question of what "all" data means remains unanswered. The data road owners possess will vary in type, quality, and sensitivity. How this data is stored, e.g., the data format, will also be of importance for sharing. Regarding dynamic data, even more questions arise. What types of dynamic events are expected to be known and

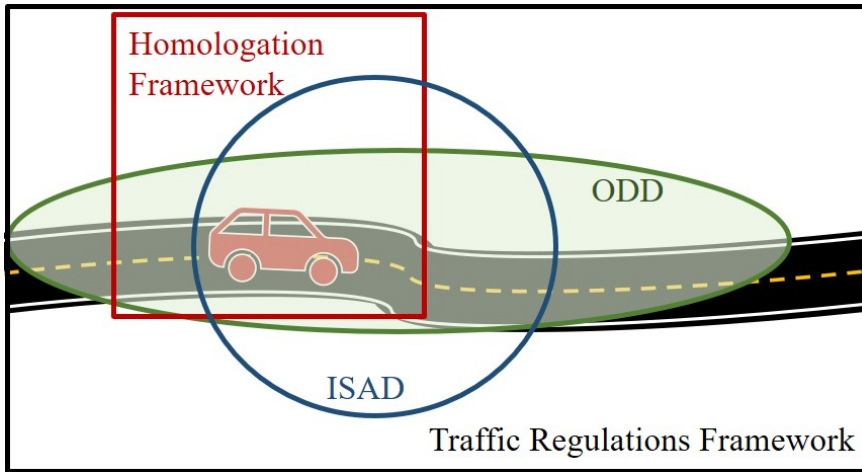


FIGURE 2.1: Regulations related to automated driving adapted from (Ertrac, 2019).

what is the required level of service in terms of accuracy and latency of this information?

At levels A and B, the road infrastructure is required to understand the movement of road users and objects in real time and to convey this information to AVs. This would require major investments in sensors, surveillance, and communication services on public roads. Furthermore, it would shift the responsibility of perceiving objects and events from the driver to the road infrastructure. The ISAD framework is presented as a part of a *Connected Automated Driving Roadmap* developed by ERTRAC's Working Group on *Connectivity and Automated Driving* (Ertrac, 2019). This group, according to ERTRAC, gathers experts from the industry, research providers, and public authorities. The road map states that it is necessary to establish what the prerequisites towards the infrastructure are from the vehicle side and suggests that the most basic step towards this is a classification of the road infrastructure (ISAD).

The ISAD framework is a signal for ROOs to be proactive in their approach to how driving automation will impact on strategies for road design and maintenance. Level D, which represents making conventional road infrastructure such as signs, signals, and static maps available digitally, is on its own a task worth approaching with the concept of accuracy and accountability. For example, what are the requirements on ROOs on the quality of such services? What is the liability if the level of service is not met? Establishing these levels of services for level D is an on-going process for road owners and other relevant actors such as map and communication infrastructure providers (Kartverket, 2020).

The higher levels of the ISAD framework suggest a drastic change from the reigning concept that the driving system must be able to handle the dynamic driving environment to shifting some of the responsibility for safe driving over on new and upgraded road infrastructure. While it would be possible to create roads that monitor and report all movement, weather, and incidents to road users, this would require a substantial investment in both road and communication infrastructure as well as added resources on technology and communication within the ROOs. Leaving the

TABLE 2.1: Infrastructure Support levels for Automated Driving (ISAD) based on (Ertrac, 2019).

Level	Name	Description	Digital map, static road signs	VMS, warnings, incidents, weather	Microscopic traffic situation	Guidance: speed, gap, lane advice
A	Cooperative driving	Based on real-time information on vehicle movements, infrastructure can guide AVs to optimize overall traffic flow.	X	X	X	X
B	Cooperative perception	Infrastructure can perceive microscopic traffic situations and share data to AVs in real-time.	X	X	X	
C	Dynamic digital information	All dynamic and static infrastructure information is available digitally and can be provided to AVs.	X	X		
D	Map support	Static digital inc. signage available, possibly also physical reference points. Signals, short-term roadworks and VMS to be recognized by AVs.	X			
E	No AV support	Conventional infrastructure, no digital information. AVs need to recognize road geometry and signage.				

responsibility of perceiving and understanding the road environment to the moving road users, i.e., vehicles, is likely to have a higher cost-efficiency than making all roads capable of the same. Conventional road infrastructure is known to face substantial shortcomings in level of maintenance. If the future road infrastructure in addition features scores of sensors requiring low-latency and reliable communication, it would open for liability issues for ROOs in the event of sensor or communication failure. The ISAD framework is immature but highlights the need for road authorities to be a part of decision-making processes on the requirements on physical road infrastructure and digital representations of these, i.e., digital twins.

This thesis initiates the process of including the automated driver in road design and maintenance, suggests ways to adapt road infrastructure to support driving automation, and shows examples of how the sensors used for ADAS can be used to monitor the road infrastructure. The road infrastructure considered in this work includes the road geometry, the road surface and traffic control devices (e.g., signage, signals, markings, dividers, and guardrails).

2.1 The Automated Driver

This section addresses the ambiguity of terminology and definition of automated driving, e.g., *automated driving*, *autonomous driving*, and *self-driving*.

The first driver assistance system (DAS) introduced in the market is considered to be the Anti-lock Braking System (ABS) more than 50 years ago (Galvani, 2019). While DAS relies solely on input from the vehicle's internal sensors, e.g., inertial measurement unit (IMU) and odometers, ADAS has the advantage of sensing the surroundings to provide more information about the driving situation and offer more advanced driver support features (Galvani, 2019). ADAS are commonplace in newer vehicles, e.g., lane keeping assistance and adaptive cruise control.

ADAS introduces the idea of shared responsibility of driving tasks between human driver and driving automation system, e.g., ACC can brake and accelerate and lane keeping functionality can control the lateral position. A taxonomy for how these roles are shared for different levels of automation has been developed by The Society of Automotive Engineers (SAE) International (Table 2.2). In Table 2.2, *Fallback* refers to taking over the dynamic driving task (DDT) if the driving automation system fails.

TABLE 2.2: The levels of automation defined by SAE International, adapted from (SAE International, 2018).

		Dynamic Driving Task (DDT)			
Level	Name	Sustained lateral and longitudinal control	Object/Event Detection and Response	Fallback	Operational Design Domain (ODD)
0	No driving automation	Driver	Driver	Driver	N/A
1	Driver Assistance	Driver/System	Driver	Driver	Limited
2	Partial Driving Automation	System	Driver	Driver	Limited
3	Conditional Driving Automation	System	System	Fallback-ready user	Limited
4	High Driving Automation	System	System	System	Limited
5	Full Driving Automation	System	System	System	Unlimited

In the SAE taxonomy, Level 0 represents only the use of DAS systems and no driving automation. Levels 1 is driving where the human is in control and is assisted by ADAS functionality. At level 2 the driving automation system is able to

have sustained lateral and longitudinal control of the vehicle, examples of such systems include General Motor's *Super Cruise* and Tesla's *Autopilot*. At level 2, the driving automation systems are not capable of handling object and event detection and response (OEDR), e.g., driving in the vicinity of road works, requiring the human driver to monitor the driving system at all times. Level 3 is the first level where the driving automation system can drive on its own with OEDR capability and the human acting as a fallback-ready user. At the two highest levels, 4 and 5, the automated driving system is responsible for all the driving tasks without the need for a fallback user. The difference between level 4 and 5 lie in the operational design domain, where level 4 may have restrictions on where and when it can operate which are not present at level 5.

The SAE International (SAE International, 2018) defines the automated driving system (ADS) as:

"The hardware and software that are collectively capable of performing the entire [Dynamic Driving Task] DDT on a sustained basis, regardless of whether it is limited to a specific operational design domain (ODD)"

This definition only applies to levels 3-5, while they assign the generic term *driving automation system* to any 1-5 level system.

As a note on terminology, this thesis does not use the term *autonomous* following the recommendation from SAE:

"Additionally, in jurisprudence, autonomy refers to the capacity for self-governance. In this sense, also, 'autonomous' is a misnomer as applied to automated driving technology, because even the most advanced ADSs are not 'self-governing.' Rather, ADSs operate based on algorithms and otherwise obey the commands of users."

Terminology on driving automation sometimes refers to automated *driving systems* and other times to automated *vehicles*. In this thesis, the automation will be attributed to the hardware and software that allows for driving, in line with the SAE definition of an ADS. While the vehicle and its attributes will have impact on the characteristics of an ADS and the uses of such automation, this work will focus on the sensors and software that are currently used to provide automated driving features. The term *automated vehicle* (AV), or the associated *highly automated vehicles* (HAV) referring to levels 3-5 of the SAE taxonomy, or the term *lower-level automated vehicle* (LAV) referring to levels 0-2 (Li et al., 2019) will therefore not be used. Instead, this thesis will refer to the terms *automated driver* and *driving automation system*. These describe driving support functionality performed by the use of sensors and software to aid the human driver in control of the vehicle (e.g., LDW), as well as driving by the use of sensors, software and actuators to actively control the vehicle such as controlling the lateral and longitudinal position.

The automated driver is under development and much remains unknown with regards to what array of sensors they will have, where the sensors will be positioned, and how the software that interprets and acts on the sensor data will evolve. The focus of this research is, therefore, on the present level of automation, i.e., ADAS, and how it can be used to assess the impact of automation in driving on road design and maintenance. Using existing technology, it is possible to gain insights into driving

automation at an early stage to create strategies for including automated drivers in the design and maintenance of roads.

Terminology regarding automated driving is often seen in conjunction with the ability for the driving system to communicate. Although a driving system does not strictly need to be connected to be automated, connectivity allows the automated driver to obtain information beyond its own sensors and a priori data, such as updates on the weather, friction, or incidents ahead. This linking of connectivity and automation is seen in several widely used terms, e.g., *Connected and Automated Vehicle (CAV)* and *Cooperative, Connected, and Automated Mobility (CCAM)*. In the latter term, the distinction between connected and cooperative can be defined as the difference in being able to communicate externally, e.g., connectivity, and using this information for steering and navigation, e.g., cooperativity (Shladover, 2018).

2.2 Road Design

The aim of this thesis is to investigate how automated driving can be facilitated through the design and maintenance of roads. The manuals governing the design of roads in Norway and the United States are presented in this section and the impact of automated driving on adapting these manuals are discussed. This is followed by an introduction to road maintenance strategies in section 2.3.

This thesis examines the standards of road design used in Norway and also in comparison to those of the United States, as a commonly known standard worldwide. The design of roadways in Norway is governed by the *Handbook of Road and Street Design N100* (Statens vegvesen, 2019a) and the *Handbook of Geometric Road Design V120* (Statens vegvesen, 2019b). U.S. road design is primarily governed by the American Association of State Highway and Transportation Officials' (AASHTO) guidelines in *A Policy on Geometric Design of Highways and Streets* (American Association of State Highway and Transportation Officials, 2011). While these guidelines are specific to these countries, they are based on theoretical concepts in physics and geometry that are universally related to road design, and thus have international relevance.

2.2.1 Geometric Road Design

Geometric road design governs the alignment, profile, and cross section of road design. The design guidelines for geometric road design are based on a century of accumulated knowledge on human driving, vehicles, and tire-road surface physics. Parameters used in geometric road design are related to, among other things, human anatomy such as eye height and human physiology in terms of comfort. These parameters need to be evaluated considering automated drivers to ensure the optimal design of roads for both human and automated drivers.

Geometric design parameters are not regularly updated in either Norway or the U.S. (Elvik, 2017; Khoury, Amine, and Saad, 2019; Wood and Donnell, 2017). Due to this, some road design parameters have remained unchanged for decades. For instance, the stopping sight distance (Ds) parameter used in the U.S. was developed in the 1940s with minor revisions in the mid-eighties (Khoury, Amine, and Saad, 2019) and mid-nineties (Transport Research Board, 1997; Wood and Donnell, 2017), while perception-reaction time for drivers dates back to 1954 (Khoury, Amine, and

Saad, 2019). Some even question the theoretical foundation of the design parameters claiming they are based partly on old experiments and partly on theories scarcely supported by research (Elvik, 2017; Khoury, Amine, and Saad, 2019; Wood and Donnell, 2017).

With the advent of automated drivers, these new road users must be included in geometric road design to obtain the safest and most cost-efficient roads for the future. The automated driver, including lower levels of automation such as ADAS, relies on sensors and software to drive. These sensors and software provide an objective way to monitor how well current infrastructure works for automated drivers and identify areas that need to be improved. This means that data produced by automated driving functionality can be used to identify where changes to the physical road infrastructure need to happen. In this way, geometric road design, and road design and maintenance in general, can be adapted based on empirical data collected from vehicles.

2.2.2 Road Markings

Road markings are the most widely used traffic control devices today (Thamizharasan et al., 2003) and have been identified as being of particular importance to driving automation (Hadi and Sinha, 2011; Hallmark, Veneziano, and Litteral, 2019; Hoang et al., 2017; Kusano and Gabler, 2015). While road markings are most commonly used in lane keeping features, they are generally useful for positioning and navigation for automated drivers at all levels of automation.

Road surface markings were introduced as early as 1911, when white markings were used to divide traffic in Michigan U.S.A. (OECD Road Research Group, 1975). Pavement markings provide visual information that is intended to provide better traffic flow, higher driving comfort and safer traffic for human drivers (Gibbons, Hankey, and Pashaj, 2004; Hallmark, Veneziano, and Litteral, 2019; OECD Road Research Group, 1975). To serve these goals, the road marking has the following main functions (Carlson, Park, and Andersen, 2009; Statens vegvesen, 2015):

1. Leading traffic; through enhancing the road geometry, road delineation and lanes.
2. Notifying drivers; through information on specific stretches of road that require more attention, or adaption of driving.
3. Regulating traffic; through road markings that assign rules to the use of the road.

LDW, which relies on road markings, has been proven to have safety benefits. Kusano et al. (2014) used a simulation to reconstruct 481 single-vehicle collisions extracted from the database of fatal and non-fatal injuries maintained by the National Highway Traffic Safety Administration (NHTSA) for the year 2012. Each crash was simulated under two conditions: 1) as it occurred, and 2) with a lane departure warning (LDW) system. They concluded that a LDW system could potentially prevent 28.9% of all road departure crashes caused by the driver drifting out of his or her lane, resulting in a 24.3% reduction in the number of seriously injured drivers. Sternlund (2017) investigated lane departure crashes (head-on, single-vehicle, and overtaking/lane changing crashes) in Sweden, and found that approximately half (51%)

of all head-on and single-vehicle crashes were identified as being a consequence of drifting, where LDW systems had the potential to prevent the majority (33–38%) of these crashes. He states that the typical lane departure crash happens without prior loss of control, and that they occurred on undivided roads in rural areas with posted speed limits ≥ 70 km/h, where the center and side road markings were visible. To achieve these traffic safety effects from driving automation, there is a need to understand to what extent road markings are suitably designed for detection by automated systems. This requires investigating how automated drivers sense the road marking (e.g., LDW systems) and whether existing quality parameters designed for human drivers also assure lane detection by automated systems.

The functionality, i.e., whether it is visible to human and automated driver, of pavement markings is influenced both by its color and the marking material. Road marking materials are commonly divided into four categories: thermoplastics, multi-component/epoxy, preformed plastic, and paints. Retroreflectivity and contrast in service are higher for white than for yellow markings, and are higher for more durable pavement markings (Migletz et al., 1999). Epoxies and thermoplastics are more durable than solvent or water based paints (Bagot, 1995; Cruz, Klein, and Steiner, 2016). The durability and cost-benefit of a specific material is dependent on several factors such as Average Annual Daily Traffic (AADT), climatic conditions, road geometry, share of heavy vehicles, use of studded tires, and levels of maintenance.

The visibility of pavement markings depends on the visual size of the markings, its contrast with the background against which it is seen, the amount, pattern and angle of incoming light sources, retroreflectivity characteristics of the markings, the visual function of the observer, and sources of glare (Hills, 1980; Migletz et al., 1999; Satterfield, 2014).

The quality of road markings is usually measured by the retroreflection, R_L , and the coefficient of luminosity, Q_D . Q_D is a measure of visibility under daylight conditions, during which natural light hits the marking and is dispersed in all directions. R_L is used under nighttime or otherwise dark conditions, during which an active light source is directed toward the marking and reflection is measured. The coefficient of retroreflected luminance, R_L , measured in millicandelas per lux per square meter ($mcd/m^2/lux$), is defined by the American Society for Testing and Materials as the ratio of the luminance of a projected surface to the normal illuminance at the surface on a plane normal to the incident light (American Society for Testing and Materials, 2005). Migletz, Fish, and Graham (1994) suggest that conspicuity of markings is more related to contrast than to luminance, since contrast defines how easily an object can be seen against its background. Contrast has been identified as important for humans to be able to detect road markings (Hills, 1980; Zwahlen and Schnell, 2000) as well as for automated drivers (Hadi and Sinha, 2011; Pike, Carlson, and Barrette, 2018; Pike, Barrette, and Carlson, 2019).

2.3 Road Maintenance

Road maintenance strategies are in place to ensure that the road infrastructure elements (e.g., pavement, markings, signage, and signals) maintain their intended function. For instance, optimal driving conditions for human drivers is dependent on

adequate road surface quality, visible markings, signage, working signals, that the road has enough available friction and is cleared of snow and obstacles.

The process of monitoring the road infrastructure and updating the asset inventory is a manual and time-consuming process using specialized equipment and personnel (Gargoum et al., 2017; Kruse and Simmer, 2003; Osichenko and Spielhofer, 2018). The Conference of European Directors of Roads (CEDR) financed a project called PREMiuM (Practical Road Equipment Measurement, Understanding and Management) with the aim of improving road equipment management. In interviews with stakeholders they found that although keeping a robust and accurate inventory of road assets was seen as essential to evaluate the performance of the assets, many asset inventories were out of date and incomplete, and that the characteristics of the assets were not routinely measured (Erdelean and Osichenko, 2014). Efforts have been made to include new ways of monitoring the state of the road infrastructure, for instance by using cameras and image analyses, however, there is still a need to establish ways to more consistently monitor the roadway and traffic control elements (Gargoum et al., 2017; Osichenko and Spielhofer, 2018).

There is a considerable body of research available on sign detection and quality assessment based on images, radar and lidar (Ai and Tsai, 2016; Bahlmann et al., 2005; Chauhan, Luthra, and Ahmad Ansari, 2020; Gargoum et al., 2017; Wang, Hou, and Gong, 2010). Despite this, signage was found to be inadequately inventoried and monitored by road owners and operators (ROOs) (Osichenko and Spielhofer, 2018). The same problem was identified for road marking maintenance management, which is also a quite mature field within both camera-, radar- and lidar-based automated detection (Xing et al., 2018).

Modern cars are equipped with cameras and radars that can provide a way to crowd-source the considerable effort needed to monitor road assets. Cars also have sensors (e.g., Inertial Measurement Units (IMUs) and damping systems) that sense irregularities in the road that can be used to identify damages to the road surface or slippery conditions. With higher levels of automation, commercial vehicles may also have lidars that are able to create 3D point clouds of the road infrastructure. 3D road models based on laser scanning are also widely used by ROOs, for instance to check for wear to the road such as rutting (Vegdirektoratet, 2017), or to analyze whether large freight vehicles can safely navigate through winding roads and tunnels (Oregon Department of Transportation, 2017). These point clouds should be shared with the public in efforts to provide openly available map data for automated driving.

Crowd-sourced monitoring provides an efficient way to determine what parts of the road infrastructure the automated driving features senses and which are missed. This information is useful for evaluating current road design and maintenance strategies. Furthermore, the detection of road infrastructure elements can be used for asset management by comparing the automated detections to the digital inventories of road infrastructure. Changes in how the road infrastructure elements are perceived over time, i.e., effects of wear or weather, can be used as input for predictive maintenance strategies.

Chapter 3

Research Design

The overall aim of this thesis was to examine how road design and maintenance can be adapted to facilitate automated driving. This was done through a series of four papers. The research focused on existing levels of driving automation represented by ADAS functionality. By utilizing existing technology, characteristics of automated drivers could be established, and practical research experiments could be executed to demonstrate how to include automated drivers in road design and maintenance. **Table 3.1** lists the four research objectives (ROs) and their relation to the papers.

TABLE 3.1: Relationship between research objectives and papers in the thesis.

	Research Objectives	Research Response
RO1	Establish automated drivers as new road users including identifying their characteristics and how they compare to human drivers’.	Paper I, II
RO2	Evaluate geometric road design parameters with regards to automated drivers, in both the short and long term.	Paper II
RO3	Examine how road infrastructure design and maintenance can facilitate automated driving.	Paper I, II, III, IV
RO4	Examine how driving automation systems can act as sensors to monitor the state of road infrastructure.	Paper I, III, IV

There were no existing frameworks that described all driving processes, nor identified the characteristics that define an automated driver. Therefore, the first part of the thesis was used to establish a framework for describing the automated driver. In Paper I a unified framework was developed, making it possible to determine characteristics of automated drivers and compare these to those of human drivers. This enabled the next step; to use this newly established framework to evaluate current geometric design parameters considering automated drivers (RO2) in Paper II. Paper I and II thus form a theoretical foundation for the thesis where the automated driver is established as a new road user (RO1), which then informs applied research in the latter of the thesis.

Paper III and IV utilized laboratory and field experiments as case studies to examine how road infrastructure design and maintenance can facilitate automated driving (RO3) and how driving automation systems can act as sensors to monitor the state of road infrastructure (RO4). The methods used in the thesis are summarized in **Table 3.2**.

TABLE 3.2: Overview of methodology used in the thesis.

Paper	Method	Analytical approach	Objective	Data
I	Literature review and synthesis	Qualitative, exploratory review	Framework for automated drivers	Journal and conference papers, reports
II	Literature review and synthesis	Qualitative, exploratory review	Automated drivers' impact on design parameters	Manuals, journal and conference papers, reports
III	Field experiments	Quantitative by Logistic binary regression, area under the curve	Compare LDW detection by car and retroreflectometer	LDW output, Lane detection by retro-reflectometer
IV	Laboratory and field experiments	Visual quantitative assessment, pixel intensity histograms for qualitative assessment	Examine the effect of road marking color on visibility in snowy conditions	Images of road model, images from field experiments

3.1 Theoretical Foundation

3.1.1 Paper I

Paper I is the response to the first research objective; to establish the automated driver as a new road user including identifying its characteristics and how they compare to human drivers'. Establishing the automated driver as a new road user started by investigating the current literature on human driver models, automated driving, and mobile robotics, including standards and taxonomies related to the automation of driving. The motivation was to see if an inductive approach could be used to define the automated driver, i.e., was there existing literature that covered the automated driver and that identified its characteristics? The databases searched were Google Scholar and Oria (a database of literature available via Norwegian universities and research institutions). No restrictions were used on publication date as theories on human driving and mobile robotics were established 40-50 years ago. As discussed in section 2.1 there are many terms used for driving automation systems where some refer to the automation of vehicles and some to the systems that governs the driving. In addition, the interdisciplinarity of the topic, as well as the rapidly increasing

number of publications on automated driving, mean that literature searches generate a large number of returns. The immaturity of the taxonomy and definitions on automated driving are an obstacle in the research on how to include automated driving in road design and maintenance, and underlines the need for accuracy and consistency in the terms used in associated research (Chan, 2017). The literature search also found a gap in the research on automated drivers and how they can be included in road design and maintenance. The search terms used in the literature search for Paper I were:

- *(driver OR Driving OR drivers) AND (model OR models)*
- *Driving AND (automation OR autonomous)*
- *Vehicle AND (automated OR autonomous)*
- *Mobile AND robotics*

From the literature returned by these searches, relevant research was selected. The overall impression was that there were few hits concerning lower levels of automation. While there was substantial research on level 3 automation where the driving tasks are shared between human and driver, as well as research on levels 4 and 5 of driving automation (full automation). Two known frameworks that are relevant for automated driving, the SAE J3016 and the ISO 26262, were investigated and found to not cover all driving processes nor discuss the automated driver with a combination of hardware and software that could identify key characteristics.

Based on the initial literature search, it was concluded that it was not possible to use induction to establish a framework for automated drivers, thus, an abductive approach was chosen. In an abductive approach, a provisional hypothesis is selected or invented to explain an empirical case and pursued through further investigation (Kennedy and Thornberg, 2018). The framework developed in Paper I combined the theories of human driving and mobile robotics into a unified framework for both human and automated driving. This would constitute the provisional hypothesis which can be refined through further investigations.

The unified framework identified that sensing was integral to all parts of the driving processes for both human and automated driver. From the first rounds of searches, the most common sensors used in automated driving had been identified. The human senses were then researched and compared to the sensors used by automated drivers. The review of the sensory processes of automated and human driver followed an inductive approach where existing data, i.e., the state of the art on hardware and software used in driving automation, was used to reveal characteristics of the automated driver. The literature on sensors used by driving automation systems largely focused on identifying optimal sensors and software without considering how road design and maintenance factor into the success of the sensor system. One exception, however, was regarding road markings where issues such as wear, pavement cracks, and rutting are widely reported as having negative impact on automated lane detection.

Another distinction between human and automated driver uncovered in developing the framework, was the difference in cognition, i.e., how the different road users process the sensory input. This led to a new inductive process. Literature searches

within machine learning (ML), artificial intelligence (AI), and object detection by machines were performed to identify cognitive traits of the automated driver.

The inductive process of establishing traits of automated drivers has weaknesses as new sensors or software can change the characteristics of the automated driver. The traits attributed to the automated driver will therefore need to be reconsidered over time as the technology matures. However, the characteristics found, e.g., how passive sensors such as cameras see the road infrastructure versus how an active sensor, e.g., a lidar or radar observes the same, is valuable in the short-term for including driving automation in the design and maintenance of roads. Furthermore, although the sensors and software itself will develop, their basic functionality may well stay the same, i.e., there will be better cameras, but they all depend on available radiation in their range of electromagnetic sensitivity.

3.1.2 Paper II

Paper II used the framework and characteristics from Paper I to evaluate geometric road design parameters with regards to automated drivers, in both the short and long term, (RO2). The review in Paper II provided a qualitative evaluation of current geometric road design parameters, i.e., parameters that govern the alignment, profile, and cross section of road design. This also relates to RO1; establishing automated drivers as new road users.

Geometric road design is based on a century of accumulated knowledge on human driving, vehicles, and tire-road surface physics. As the laws of physics and physiology of humans are the same internationally, road geometry considerations based on Norwegian road design have international significance. For further relevance, the design parameters used in Norway were compared to U.S. equivalents from the *A Policy on Geometric Design of Highways and Streets* (AASHTO, 2011).

The paper reviewed the geometric design parameters from the manual on geometric road design in Norway, *Håndbok V120 Premisser for geometrisk utforming av veg* (Statens vegvesen, 2019b). The review was separated into basic parameters and design parameters following the structure of manual V120 as shown in **Figure 3.1**.

Literature searches were performed using Google Scholar and Oria to identify existing literature relating automated driving to adaptations in geometric road design. No restriction on publishing year was applied due to the limited number of relevant hits. The searches showed that there is little research considering how automated drivers impact road design and maintenance. The literature that does focus on physical road infrastructure tends to cover level 5 automation. The search terms: *geometric road design* AND (*automated* OR *autonomous*) AND (*driving* OR *driver* OR *vehicle*) gave two relevant results in Google Scholar and one relevant result in Oria. Of these, one reviewed the road design parameters: stopping sight distance, decision sight distance, and length of sag and crest vertical curves (Khoury, Amine, and Saad, 2019). Another study used a vehicle dynamics model to investigate the performance margin of a vehicle given certain conditions of effective friction and road geometry (slope and cross-slope) (Kang and Ferris, 2018), and the final paper pointed out the lack of research on the impact of driving automation on physical road infrastructure (Farah et al., 2018). From the paper by Khoury, Amine, and Saad (2019) more references were found relating automated driving to design parameters *Stopping sight distances*, *Vertical curve radii*, and *Horizontal curve radii*.

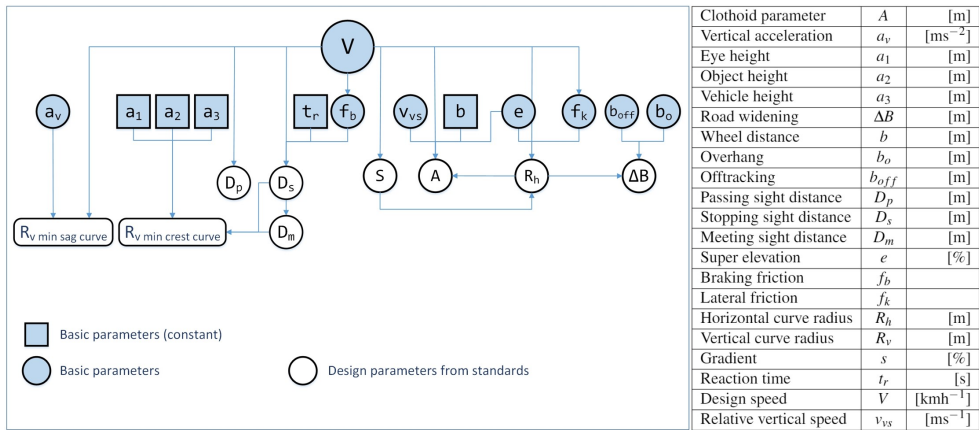


FIGURE 3.1: Norwegian design parameters from manual v120 (Statens vegvesen, 2019b). Basic parameters are shown in blue and design parameters in white.

Due to limited available research on geometric road design the review followed an abductive approach. The hypothesis of the abductive approach was that the characteristics of automated driving identified in Paper I show fundamental differences between human and automated drivers that are relevant when considering road design for automated drivers.

The design parameters of the Norwegian manual V120 were evaluated using the unified framework developed in Paper I and compared to the equivalent U.S. parameters. Based on the differences between human and automated driver established in Paper I, the impact on the different parameters was assessed. The findings were supported by additional searches on specific road design parameters.

The review used a qualitative evaluation of the differences between human and automated driver to assess which parameters would be affected by the new road user. Geometric design parameters that need to be completely redefined for automated drivers, and which need to be re-evaluated as the development of automated drivers continues, were suggested. The abductive approach created a provisional hypothesis which can be further developed over time as the research on the impact of driving automation on road infrastructure design and maintenance develops. A weakness for the abductive approach, used in creating the unified framework of driving and the review of geometric road parameters considering automated drivers, is that there might exist more than one legitimate way of describing automated drivers (Kennedy and Thornberg, 2018). As driving automation is under development, it is expected that the unified framework can be further developed and changed, and that subsequent reviews of geometric design for automated users will be needed.

3.2 Practical Research - Road Markings

3.2.1 Paper III

In Paper III field testing on public roads was performed to compare lane detection by the ADAS function LDW to lane marking assessment by a mobile retroreflectometer. The comparison was used to shed light on both 1) how road infrastructure design and maintenance can facilitate automated driving (RO3), and 2) how driving automation systems can act as sensors to monitor the state of road infrastructure (RO4). Both road design and road maintenance are large domains and road markings were chosen as a case both since it is a ubiquitous traffic control device and due to the availability of data. The methods used for data capture and analyses are described in detail in Paper III and supplemented in this section with further explanations and reasoning.

The investigation into RO3 followed an inductive approach where information on how ADAS functionality works was used as the data on which to induce consequences for road design and maintenance. For RO4, a deductive approach was taken. The theory for the deduction was that a LDW system could be used to monitor the state of road markings, the theory was then examined through an experiment.

In the experiment, the mobile retroreflectometer was attached to a car with an LDW system to allow for simultaneous data capture. Through collaborations with a car manufacturer, data from the LDW system was available directly from the car allowing for more accurate and dense data capture than solutions that use video capture of the dashboard, such as García, Camacho-Torregrosa, and Padovani Baez (2020). Furthermore, by using a mobile retroreflectometer attached to the vehicle with the LDW system, simultaneous data capture syncing the ADAS data with the reference retroreflectometer data was possible (**Figure 3.2**). This provided a higher accuracy than using different vehicles for LDW data and reference data, as seen in research by Matowicki, Pribyl, and Pribyl (2016) and Nayak et al. (2020), where differences in position in the lane, traffic and time of day provide a less consistent data set.

From the retroreflectometer, retroreflectivity of markings was measured. As this is based on actively transmitted lasers and their reflections, this value is not sensitive to ambient light. The LDW system in the vehicle is based on a video camera which, on the other hand, is dependent on available light. The vehicle with the LDW functionality also reported the available ambient light, which was used to investigate whether ambient light, i.e., daylight versus headlights, affected the detection of road markings by the LDW feature.

Retroreflectivity is the most common measure of lane marking quality. However, the contrast between marking and surrounding pavement has also been identified as an important factor for road marking visibility for both humans (Hills, 1980; Zwahlen and Schnell, 2000) and machines (Hadi and Sinha, 2011; Pike, Carlson, and Barrette, 2018; Satterfield, 2014). Contrast was therefore used as an additional quality parameter.

The lane detections, given as discrete values, were logged by the vehicle manufacturer, and shared after the experiment. The position of the vehicle, i.e., latitude and longitude, was logged by both the vehicle and the retroreflectometer. This was meant to provide verification of synchronization of the two data sources.



FIGURE 3.2: Retroreflectometer mounted on the side of the test vehicle.

There are some important limitations to address with regards to the data capture. The first is that the laser beams from the retroreflectometer need to hit the road markings to provide correct data. The car was manually driven by the author of this thesis. The laser beams had an impact width of about three times the width of the freeway markings and about five times the width of the county road markings (because of the difference in road marking widths). Although the laser beams are thought to have hit the road markings for most of the time driven, there are likely to be some discrepancies. The data was averaged over 30 meters (recommended setting); therefore, is not thought to have given false negatives, but could potentially lower the average retroreflection value.

The retroreflectometer failed to log data on one of the nighttime data captures. This was, according to the manufacturer, due to the temperatures being too low for the retroreflectometer causing it to malfunction. This meant that there was no set of daytime and nighttime recordings for one of the routes used in the analysis (county roads). For this reason, the analyses for county road in daytime and nighttime, respectively, were performed on different stretches of road. The roads used in the two cases were checked and found to be similar in terms of conditions of road surface and road marking.

Another issue is that the vehicle recorded data at regular time intervals while the retroreflectometer logged averages over a given distance. Having one data source in time intervals and the other in distance intervals meant that the sample rate for the two data sources was different at different speeds. At lower speeds, the time-based data recorded data more often than the distance-based measurement. The higher the speed, the more data was recorded by the distance-based retroreflectometer per unit

time, while the time-based vehicle logging will have fewer recordings per distance unit at higher speeds than at lower speeds. This caused the data from the retroreflectometer and the car to be unevenly distributed. This issue was remedied by using interpolation techniques (Li and Heap, 2008).

The chosen procedure for combining the data set from the vehicle and from the retroreflectometer, was to resample the data with interpolation to match the resolution of the discrete Lane detection by the vehicle. The Lane detection data had four values as shown in **Table 3.3**: no detection, left-hand side marking detected, right-hand side marking detected and marking on both sides of the vehicle detected.

TABLE 3.3: Lane detection values and their conversion from four discrete values to a binary outcome.

Original value	Binary value
0 = No detection	0
1 = Left hand marking detected	0
2 = Right hand marking detected	1
3 = Both sides detected	1

These values were converted to binary values where no detection and left-hand detection were set to 0 and right-hand detection and detection on both sides were set to 1. This was to match the readings of the retroreflectometer which only measured the right-hand side lane marking.

The reason for choosing *Lane detection* as the reference sample rate, was that performing interpolation on the binary lane detection values would change them from discrete values to an artificial continuous set of values which would alter the meaning of the data. The data preparation was performed using the programming language Python and the data analysis library Pandas. The data were time-series data which are classified as an ordered data type. They could therefore be merged on the time variables using the Pandas function `pd.merge_ordered` with forward fill. Forward fill propagates the last valid observation forward in the case of missing values. The code used is shown in Appendix A, and is available at the following GitHub repository: <https://github.com/ResearchAne/DataAnalysesLDW>.

3.2.1.1 Binary Logistic Regression

The outcome under investigation in Paper III was the success or failure of the LDW related to the quality of the road marking. The quality of the road marking was a continuous (averaged) measurement used traditionally for quality assessments. The lane detection by the car were binary values and dependent on the car's camera-based perception of the visibility of the road markings. The analyses were aimed at assessing the causality between the road marking quality (in terms of retroreflectivity and contrast to the surrounding road) to the discrete outcome of the LDW. This is commonly done by using binary logistical regression (Nathanson and Higgins, 2008). The regression analyses returned the likelihood of predicting the correct outcome of the car's lane detection (lane detected or not detected) based on the input variables

to assess whether the LDW feature of a production car could be used as a quality measure for road markings (RO4).

The lane detection from the car and the retroreflectometer were examined through binary logistic regression in SPSS (Statistical Package for the Social Sciences). To investigate whether the data from the retroreflectometer could predict the outcome of the car's lane detection, the predictors used were *Retroreflection*, *Contrast*, *Vehicle speed*, and *Ambient light*, and the dependent variable was *Lane detection*. In binary logistic regression analyses, a cut point needs to be set. A cut value of 0.5 is the default setting and most commonly used in regression analyses to predict classifications (Weiss and Dardick, 2020). In this case, a probability of the lane marking being detected greater than 50% is forecast as a positive detection (=1).

There are alternatives to using the standard value (0.5) as the cut point. (Weiss and Dardick, 2020) reviewed the standard cut value along with three other strategies in simulated logistic regression:

- Highest classification rate (MAXCC): the cut point that results in the highest correct classification rate (i.e., the minimum percent of incorrect predictions).
- Nonevent rate ($\pi_{nonevent}$): the cut-point is selected using a priori information to select a cut-point. One type of a priori information is the proportion of persons in the nonevent group in the population.
- Maximize sensitivity and specificity (MAXSS): the cut-point is determined by a priori information on the cost of incorrect predictions.

Their results showed that the 0.5 and MAXCC methods performed similarly across all conditions investigated. Weiss and Dardick (2020) advise against using the $\pi_{nonevent}$ method as it does not result in fewer misclassifications in large groups and has the highest misclassification of all methods for small groups. While the MAXSS approach may be suitable for classifying small groups. The $\pi_{nonevent}$ and MAXSS are based on a priori information and such information was not available in this case. The MAXCC approach was, furthermore, not considered as the advantages of using this approach compared to using the standard value are negligible (Weiss and Dardick, 2020). The cutoff point was therefore kept at the standard value of 0.5.

3.2.1.2 Receiver Operating Characteristic Curves

Receiver Operating Characteristic (ROC) Curves summarize the trade-off between the true positive rate and the false positive rate for a predictive model (Fawcett, 2006). ROC curves can also be used to identify threshold values for successful detection (Metz, 1978). This was used in Paper III to try to identify a threshold of retroreflection or contrast that gave positive lane detection by the LDW system.

ROC curves are plotted as 1-specificity (x-axis) versus sensitivity (y-axis), where specificity and sensitivity are defined by **Equations 3.1** and **Equation 3.2**:

$$\text{Specificity} = \frac{\text{True negatives}}{\text{True negatives} + \text{True positives}} \quad (3.1)$$

$$\text{Sensitivity} = \frac{\text{True positives}}{\text{True positives} + \text{True negatives}} \quad (3.2)$$

Figure 3.3 illustrates how ROC curves may appear, with the false positive rate (1-specificity) on the x-axis and the true positive rate (sensitivity) on the y-axis.

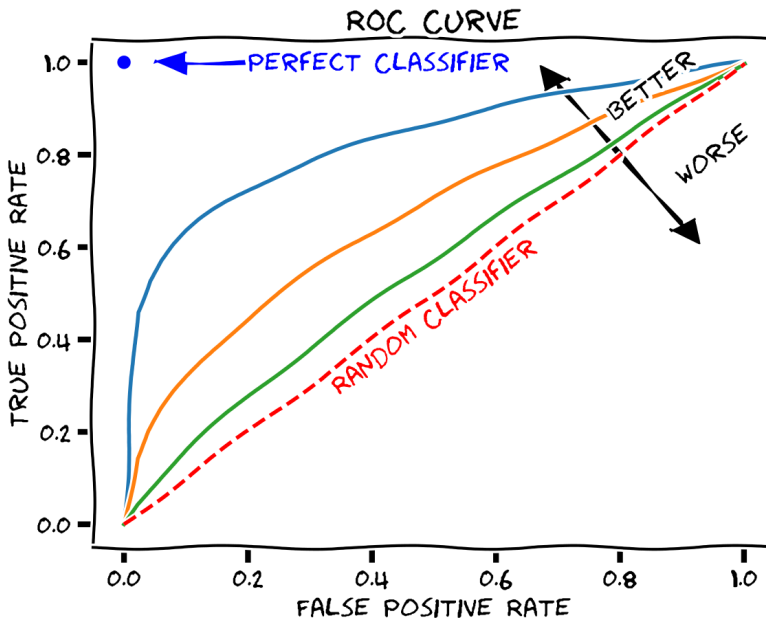


FIGURE 3.3: Illustration of ROC curve plots.

A threshold can be chosen as a tradeoff between these two measures of accuracy, i.e., how many false positives and negatives are acceptable for what rate of true positives and true negatives. The aim of these analyses was to try to locate indications of threshold values for the predictor variables (*Ambient light*, *Retroreflection*, *Contrast* and *Vehicle speed*) that would result in successful lane detection. This is a step towards establishing how road infrastructure design and maintenance can facilitate automated driving (RO3).

3.2.2 Paper IV

Paper IV used road markings as a case for investigating how the design and maintenance of roads could be adapted to support automated driving. Paper IV used both laboratory and field research to examine how well camera-based road marking detection works in snowy conditions and whether yellow markings were more easily identified than white markings in such conditions. Laboratory research was chosen due to the possibility of controlling variables, e.g., temperature, snow depth, snow quality and ambient light, in the on-site winter laboratory at NTNU. Two different field experiments, one at a closed airfield and one on public roads, were used in addition to the laboratory work to provide a wider range of cases. Images from the laboratory and field were then subsequently utilized for image analysis. Details of

the methods used to capture and analyze data are found in Paper IV while this section offers additional information on the methods used and reasoning for the research design choices.

Similar to the previous paper, Paper IV addressed 1) how road infrastructure design and maintenance can facilitate automated driving (RO3), and 2) how driving automation systems can act as sensors to monitor the state of road infrastructure (RO4). For RO3 an inductive approach was taken where data on how snow affected lane detection were collected. In addition, deduction was used with the hypothesis that yellow markings could be more visible in snowy conditions when exploring images in different color spaces. In relation to RO4, the empirical results were planned to provide input on how ADAS can be used to monitor the state of the road related to visibility of road markings in the event of snow. This follows an inductive strategy where the empirical results were the basis for evaluating how in-vehicle cameras can be used to monitor the road conditions.

3.2.2.1 Laboratory Experiment

A road model of a lane in 1:10 scale was created to be used in the winter laboratory (for details on the road model refer to Paper IV). The material used to make the road model was a custom asphalt concrete with gravel sizes of 2 mm and less, called *Ab2* from the Norwegian term *Asfaltbetong* and the maximum gravel size. The gravel and rock sizes conventionally used in asphalt concrete are 4, 8, 11, 16 and 22 mm (Statens vegvesen, 2005). At 1:10 scale, this range is between 0.4 and 2.2 mm and the *Ab2* gravel, thus, was to scale. The asphalt was made at NTNU according to the composition in **Table 3.4** using bitumen as binder.

TABLE 3.4: Composition of stone sizes in asphalt (*Ab2*).

Stone size [mm]	Percentage
0 - 0.25	5%
0.25 - 0.5	15%
0.5 - 1	30%
1 - 2	50%

The road marking used was white and yellow melt-in-place preformed thermoplastic tape (Geveko Premark) that was applied using a heat gun. This marking type is used for smaller, manual application such as marking out parking spaces and symbols, but the product is considered equivalent to thermoplastics used for road applications in terms of material type and function according to the contractor. The preformed tape was cut into strips and melted to find the width of the markings after melting (**Figure 3.4**). The aim was to have one-centimeter-wide markings after application, i.e., 1:10 the normal road marking width.

A custom sifter was crafted to help apply an even layer of snow (**Figure 3.5**). Through trials of snow application, it was determined that the lowest depth where a consistent snow depth could be achieved was 0.5 cm. A wood frame with a height of 0.5 cm was made to achieve the correct snow depth and provide more consistent snow application (**Figure 3.5**).



FIGURE 3.4: Difference in width of thermoplastic marking before (left-hand side) and after (right-hand side) melting.

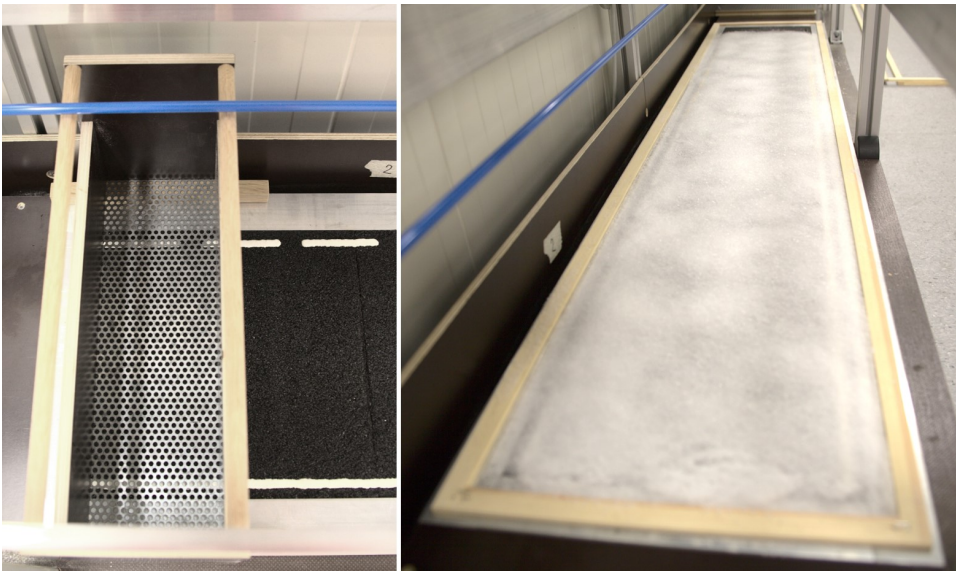


FIGURE 3.5: Snow application with sifter and 0.5 cm wooden frame.

Tests with more snow, 1 cm, were also performed (using a wooden frame 1 cm in height) but were found to leave the road markings undetectable by the camera.

In the laboratory experiment there were some parts of the set-up that could not be scaled down, i.e., the height of the road markings and the snow crystals themselves. However, the physical interaction of light, snow and road marking is the same as in real-life testing and the set-up, therefore, assumed to be valid. The camera was attached to a moving rig to simulate the movement of a car. The speed of the camera was not to scale as speeds higher than 8.33 m/s caused the camera to move in the rig.

8.33 m/s is equivalent to approximately 30 km/h while the road model was based on a road with a 60 km/h speed limit.

It could also be noted that there are high-end cameras that have higher resolutions and video capture frame rates than those used in the experiment. Unfortunately, there was no time to procure such cameras before the available laboratory slot and the laboratory was subsequently restricted for use due to the Covid-19 pandemic.

3.2.1.2 Airfield Experiment

The first field experiment was executed at a closed airfield with a 43.5 cm wide marking of type ViaTerm C35E applied in liquid form by a road marking application truck. According to the contractor the product is equivalent to the melt-in place Geveko Premark used in the lab experiment. The experiment coincided with a test of snow removal equipment used primarily for sidewalks and bicycle lanes. Three different cases were tested, determined by the weather and the available equipment on site. These cases featured only yellow marking as this was the only marking on the airfield. The first case was from natural snowfall which provided a starting case of 2.5 cm of snow. The next two cases were created by the snow removal equipment that was available on site shown in **Figure 3.6**. The left-hand side image shows snow removal using a plow with a perforated steel edge with two-centimeter-high ribs and the right-hand side image shows snow removal by brush. The perforated steel edge is an efficient way of scraping the road and works optimally in temperatures close to 0° Celsius (Vegdirektoratet, 2012). Removal of snow by brush is most commonly used for sidewalks and bicycle lanes in Norway but is being tested on national roads in efforts to reduce the need for salting (Barbøl, 2017).



FIGURE 3.6: Snow removal equipment. Ribbed plow on the left-hand side and brush on the right-hand side.

3.2.2.3 Public Road Data Capture

The last case used for image analyses in Paper IV was from afternoon driving on a snowy public road. This provided a case from a public road with naturally occurring snow and driving tracks in low ambient light. Where the bare road model from the laboratory experiments provided a best-case scenario, new asphalt concrete, new road marking, no dirt, no weather and good ambient light, the public road case provided a close to worst case comparison. This meant that results from the experiments

could be analyzed across a selection of cases to increase the relevance of the findings. The public road case featured both yellow and white road marking in a challenging, but not uncommon, driving situation in Norway which was of importance in answering the question of whether yellow center road markings should be the design standard.

3.2.2.4 Image Analyses

The aim of the image analyses was to test the hypothesis that yellow road markings had higher visibility than white markings in snowy conditions. The literature review had found that in the most commonly used color spaces, *Red, Green and Blue* (RGB) and *grayscale*, white markings had the highest visibility and contrast to the road surface. However, in cases with snow, or other environmental factors such as dirt or ash, white markings appear similar to the environmental pollutants making it challenging to detect road markings. Research indicated that other color spaces could increase the visibility of road markings. Three color spaces seemed particularly promising based on results from field experiments of camera based lane detection (Lee and Moon, 2018; Podpora, Korbaś, and Kawala-Janik, 2014; Rezwanul Haque et al., 2019): *Hue, Saturation and Lightness* (HSL), *Hue, Saturation and Value* (HSV) and *luminance, color component U and color component (YUV)*.

The analyses of the data (images) were done by visual inspection and by histogram plots. The visual inspection was chosen as it represented the way human drivers perceive road markings. Although the visual inspection presented in Paper IV is a subjective measurement performed by the author of this thesis, it provides an example of a human assessment. The images analyzed were provided in the paper to give readers the possibility to do their own visual assessment.

Histograms showing the pixel intensities of the road markings versus the surroundings (road surface or snow) were chosen as an objective measure for the visibility of road markings. Histograms were chosen as a deliberately direct way of showing the pixel intensities without using algorithms to enhance contrasts or otherwise alter the results. This was done to show the effect of road marking color on machine vision visibility in snowy conditions in a raw format rather than suggest or assess different algorithms to detect edges or lanes. An example of a histogram representation is shown in **Figure 3.7**.

The image of the bare road model is an ideal case for road marking visibility with dark and new asphaltconcrete and newly laid white markings. As the histogram sums the pixel values for each column of the picture, the road markings create very distinct peaks in the histogram plot. These are easily identifiable mathematically either by searching for changes, i.e., gradients in the pixel values, or simply by setting thresholds for the sums of columns to identify road markings. These procedures additionally positions the road markings in the image.

The effect of snow depth on road marking visibility was also investigated. The original idea was to research several depths of snow in the snow lab, however, this proved unfeasible as mentioned previously. The limited snow depths researched still provided input on needed winter maintenance efforts for camera-based lane detection.

An example of code to perform the color conversions and create the histograms is found in Appendix B. The code used is also available from the following GitHub

repository: <https://github.com/ResearchAne/Can-Yellow-Road-Markings-Facilitate-Automated-Driving>.

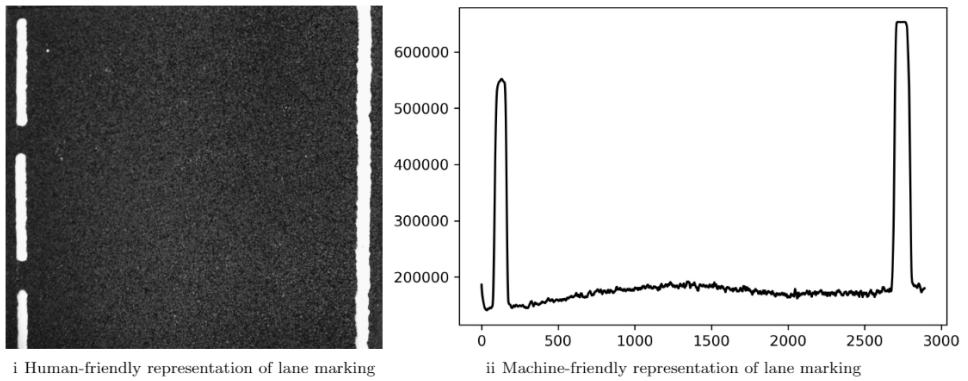


FIGURE 3.7: Example of histogram of pixel intensities.

Chapter 4

Discussion of Results

The overall aim of the thesis was to initiate the process of including automated drivers in the design and maintenance of roads. The research conducted has used existing and available driving automation functionality, i.e., ADAS, to identify traits of automated drivers and to prepare for automated road users.

The main results of the research are presented in part within this chapter to set a context for the discussion of results, with a more complete description of the results found within the individual papers. The findings are discussed in relation to the four research objectives from section 1.2.

4.1 Research Objective 1

Currently, road infrastructure is made for human drivers. To leverage the safety potential of automated drivers and start adapting road infrastructure to support automated driving features, there is a need to understand how automated drivers differ from humans. The first research objective, RO1, was to define automated drivers including identifying their characteristics and how they compare to human drivers'.

Current taxonomies and definitions, such as the SAE's levels of automation and the ISO 26262, do not cover the entire set of driving processes for automated drivers. For instance, the SAE defines a framework for describing driving automation based on models of human driving, such as Michon (1985), but it does not cover the planning stage, e.g., route determination, which is considered the initiation of the driving processes. Nor does it cover the hardware and software that comprises the automated driving abilities and gives the automated driver some of its driving characteristics. The ISO 26262 framework considers the functional safety features of components and software needed for automated driving but does not examine these in a way that can define automated drivers as new road users. These two frameworks therefore represent two separate areas with little overlap. A unified framework was therefore developed in Paper I (**Figure 4.1**).

This framework is the first to describe all driving processes for human and automated drivers and was founded on existing theories on human driver models and mobile robotics. It was called a unified framework as it covers both the traditional human driver and the new automated driver. Furthermore, it is aimed at unifying the different domains involved in creating automated drivers and the infrastructure these new road users need.

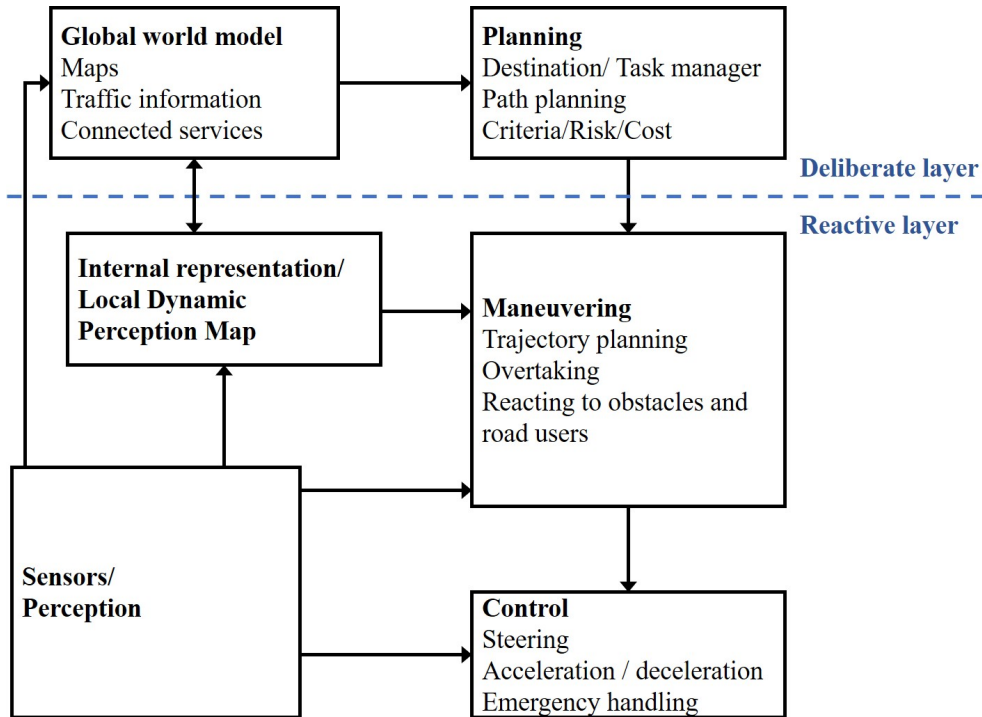


FIGURE 4.1: Unified framework for human and automated driving (Storsæter, Pitera, and McCormack, 2020).

The same lack of cooperation and unity is seen in the separation of traditional traffic engineers from disciplines related to robotics such as electronics, IT, and cybernetics. While it is obvious that driving is related to a transportation device such as a vehicle and the road on which it drives, this simple fact is not transferring to collaboration between experts representing development of vehicles and roads, respectively. Communication is also an important domain to consider in the future of transport as expectations on both vehicles and roads being able to communicate are increasing, e.g., the ISAD taxonomy.

The unified framework for driving represents the first step towards establishing the automated driver as a road user. The framework showed that on a macroscopic level, driving for both human and automated drivers can be described by the same processes. The unified framework allowed for these overall processes to be analyzed in more detail, revealing important differences between human and automated drivers.

Due to their importance for both human and automated driving, sensing and cognition were reviewed in Paper I. Based on the state of the art of sensor technology and automation software available today, the sensing and cognitive processes of automated drivers were analyzed and compared to equivalent human processes to identify similarities and differences. Although sensors and software will develop and mature over time, it was possible to identify traits that define automated drivers. A major difference between human and automated driver was found to be field of view

(FOV). A human driver's binocular vision (for subjects with no visual impairment) is approximately 200° in the horizontal median, and 150° in the vertical in the direction of view. An automated driver on the other hand, can have sensing abilities in all directions simultaneously.

Another main difference between human and automated road users is in the electromagnetic (EM) sensitivities of the two drivers. Humans are sensitive to EM radiation in the range of 380 to 750 nanometers. The automated driver, in comparison, can have an EM range, depending on equipment, from ultraviolet (UV) or near-ultraviolet (cameras), through the visible spectrum (cameras), infrared (IR) (cameras), microwaves (radar) and other radio waves (ground penetrating radar).

Beyond sensing, cognition is also identified as an important characteristic that is distinctively different for human and automated driver. Cognition converts sensory input to information. While it is possible to assess the performance of components of automated driving, such as latency in signal response from a sensor, e.g., a radar, or the processing time for the software to interpret and act on such a system, e.g., response time of an ACC, it is challenging to do this when considering the automated driver as a system with several such components. The latency of sensor and software is related to reaction time, which is anticipated to be lower for automated drivers. However, the more sensor input or other data the system needs to process the longer the reaction time will be as long as the available resources of the automated driver, e.g., memory and processing power, are limited. Further, the way in which an automated driver recognizes elements of the driving environment is different to how humans interpret their surroundings. Take for instance object recognition. In road design for humans, the detection of an object is related to how much of the object is visible to the human eye at a given distance. This is not directly transferable to an automated driver that uses an array of sensors and, thus, represents a fundamental change between the two road users that need to be addressed in road design.

Machines are inherently different to humans, e.g., it is assumed that humans will drive safely and there is, at least to some extent, a generic understanding of what safe driving is. The same cannot be said for automated driving. The idea of safe behavior that make certifying human drivers possible is not applicable to machines. This is important with regards to testing and certification of automated drivers. The technical concerns that deal with sensor functionality and redundancy are under development (Koopman and Wagner, 2017), but the successful operation of an automated driver will depend also on the software. Software efforts have in recent research focused on machine learning (ML) and artificial intelligence (AI) (Koopman and Wagner, 2017; Wang, Hou, and Gong, 2010; Xing et al., 2018) as these can provide more efficient procedures for interpreting sensor input and have the capability of learning. However, this complicates the process of certifying the driving automation system, as if you certify a system at one point in time it might react differently in the future. Furthermore, it will not suffice to observe the behavior of the automated driver, e.g., it stopped for a pedestrian, and assume that its actions were intended to protect a vulnerable road user. It is necessary to know that it was the pedestrian it detected and not other infrastructure elements and that the automated system would also do so if the pedestrian was in a wheel chair or there was bad weather such as snow drift (Koopman and Wagner, 2017). This can be assured by requiring information and accountability to be part of the software, i.e., making the automated driver able to state what it detects and what decisions it makes, often referred to as explainable AI.

The main differences described, FOVs, EM sensitivities, and cognition are important findings in relation to RO1; examine how the automated driver's characteristics differ to that of human drivers. Along with the unified framework, these differences are essential towards defining the automated driver (RO1) but also affect the geometric road design (RO2) described in the next section. Furthermore, the characteristics of the automated driver serve as useful information in the process of including automated drivers in the design and maintenance of roads (RO3) as well as investigating how automated drivers senses and cognition can be used to monitor the road infrastructure (RO4) which are covered in sections 4.3 and 4.4., respectively.

4.2 Research Objective 2

The second research objective was to evaluate geometric road design parameters with regards to automated drivers, in both the short and long term. This was made possible by the definition of automated drivers and their characteristics established in Paper I.

Paper II reviewed Norwegian geometric road design parameters as well as their U.S. equivalents, considering the transition from human to automated driver. The geometric road design parameters that were found to be affected when considering automated drivers are shown in **Figure 4.2**. The short-term effects are indicated by a red edge color in the figure and discussed in subsection 4.2.1.

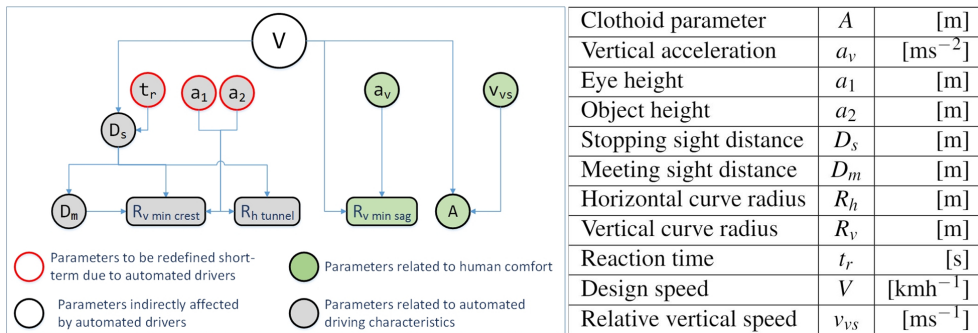


FIGURE 4.2: Parameters of geometric road design affected by the automated driver derived from Manual V120 (Statens vegvesen, 2019b).

The long-term effects of automated driving on geometric design parameters are presented in section 4.2.2. The parameters are in the following referred to by italic lettering to make them easier to locate in the text.

4.2.1 Design Parameters in Need of Revision in the Short Term

The review and synthesis identified that three parameters need to be addressed in the short term: *Eye height*, *Object height* and *Reaction time*, shown as red circles in **Figure 4.2**. They are constant values used in road design for humans.

Eye height is an average value describing the vertical distance between the road surface and human eyes. *Eye height* influences the sight lines of human drivers and

is used for determining minimum crest curve radii as shown in **Figure 4.2**. For an automated driver, the *Eye height* would be represented by the position of the sensor relative to the ground which can be lower than human eye height, e.g., parking sensors, at approximately the same height as human eye height, such as cameras in the rear-view mirror sensor cluster, and higher than human sight, e.g., roof-mounted lidars. Increased “eye” height above ground allows for smaller vertical crest curves in current geometric road design, while lower sensor heights could provide vision underneath vehicles not available to human drivers. The position of the vehicle’s sensors, i.e., the eyes and ears of the car, is different not only with regards to height above the ground, but also the lateral position on the vehicle. For instance, sensors mounted to the extremes of the vehicle’s width would provide improved sight lines through horizontal curves. The *Eye height* parameter is used in current human-oriented design to determine available sight distances for curvatures and stopping distances. As the eye height cannot be applied to automated drivers in the same way as for human drivers, the concept of eye height for automated drivers needs particular attention.

Object height, as defined for a human drivers, is the height of an object that a driver can detect and stop for. More specifically, in the Norwegian standard, it is quantified as a human being able to see a sector of the object covered by an angle of one arcminute (Statens vegvesen, 2019b). *Object height* is used conjointly with *Eye height* to determine the minimum *Vertical curve radii* for crest curves. Automated drivers sense the road using a set of sensors that operate differently to human vision. Sensors can have positions that are different both with respect to the height above ground and laterally across the car’s width. Different sensors have different methods of detection, e.g., cameras are dependent on external light while radars and lidars actively emit radiation. In addition, sensors of the same type also have different ranges and inaccuracies making it hard to generalize their performance. Software will also be an important part of object detection as this is where the sensor input is interpreted, such interpretation can rely on one sensor or a fusion of a set of sensors.

A new definition for object recognition is needed for automated drivers addressing both *Eye height* and *Object height*. How automated drivers detect objects depend on their sensors and software. For instance, objects can be found by identifying the right pixels in images, by interpreting reflections by radars or shapes by lidars, or combinations of these sensor data. Furthermore, characteristics of the objects are of importance. An object in the road can be harmless, e.g., a plastic bag or a shadow, or dangerous, e.g., a boulder. Where humans can distinguish between objects that are safe to hit and which are not, this must be taught to machines which are known to struggle with generalization (Branson et al., 2014; Fleuret et al., 2011; Linsley et al., 2017). One option when redefining eye height and object height is to combine them into new parameters for sight lines and object detection for automated drivers. In this way, the definition could be based on the functionality of the combination of sensors and software that gives the automated driver its sight and object detection characteristics.

Human and automated drivers sense and interpret sensory input differently. This is also of importance to the geometric design parameter *Reaction time*. *Reaction time* is the time taken to receive, process, and act on sensory input and is a basic design parameter that features conjointly with speed in design parameters *Stopping sight distance* (D_s) and *Meeting sight distance* (D_m). Indirectly, *Reaction time* also influences *Horizontal curve radius* (R_h) and *Vertical crest curve radius* ($R_{v,crest}$) as these consider

stopping and, in some instances, meeting sight distances. For horizontal curves, this is not in the initial design, but instead in consideration of the clear distance adjacent to the inside of the curve. The reaction time of automated drivers is by some researchers expected to be lower than for human drivers (Collin et al., 2019; Farah et al., 2018; Teoh and Kidd, 2017). If lower reaction times are obtained, this would reduce sight distances and curve radii for a given speed. For a given curve radii, a lower reaction time would allow for an increased design speed. This holds significant potential for creating a more flexible road design and, with that, lowering construction costs.

The reaction time of an automated driver depends on the sensors it uses, how many sensors there are, how much data is processed from each sensor, the efficiency, accuracy and safety of the software, and the hardware used (e.g., processors and memory). The reaction time can therefore also be adjusted, for instance filtering out data at an early stage leaves less data to process and thus lower reaction times. Similarly, having multiple sensors can provide better accuracy, as well as redundancy in case of sensor failure, but is also likely to add to the reaction time of the driving automation system. For human drivers, the reaction time used in road design is based on an 85th percentile value reaction time of human beings. The reaction time of an automated driver needs a new definition that considers the functionality and safety of the system. If not, there might be an incentive for driving automation systems to sacrifice accuracy in detection or redundancy of sensor input (by using fewer sensors or less data) to obtain lower reaction times.

The impact of lower reaction times on *Stopping sight distance* is defined by **Equation 4.1**, where D_r is the reaction distance in meters, D_b is the braking distance in meters, t_r is the *Reaction time* in seconds, V is the *Design speed* in km/h, g is gravitational acceleration (9.81 m/s^2), f_b is the *Braking friction* and s is the *Slope*:

$$D_s = D_r + D_b = t_r \times \frac{V}{3.6} + \frac{\left(\frac{v}{3.6}\right)^2}{g \times (f_b + s)} \quad (4.1)$$

If automated drivers have lower reaction times than human drivers, the required *Stopping sight distances* for given Design speeds would decrease. Alternatively, lower reaction times can allow for higher *Design speeds* for a given stopping sight distance requirement. **Figure 4.3** shows how *Stopping sight distance* would be affected by lower *Reaction times* at different design speeds. As an example, at 80 km/h a reaction time of 2 seconds gives a *Stopping sight distance* of 99.5 meters, while a reaction time of 1 second reduces the distance to 77.3 meters. It can be noted that as the reaction time decreases, the difference in stopping sight distances decreases between two given speeds.

Meeting sight distance is linearly related to *Stopping sight distance* as defined by **Equation 4.2** and would therefore be affected accordingly if reaction times decrease.

$$D_m = 2 \times D_s + 10 \quad (4.2)$$

Reaction time affects the *Stopping* and *Meeting sight distances*, as shown. Furthermore, *Eye height*, *Object height* and *Stopping/Meeting sight distance* are used when calculating minimum *Vertical curve radius* for crest curves, and for determining the minimum *Horizontal curve radius* for tunnels. These relationships are examined in section 4.2.2.2 which covers automated driving characteristics.

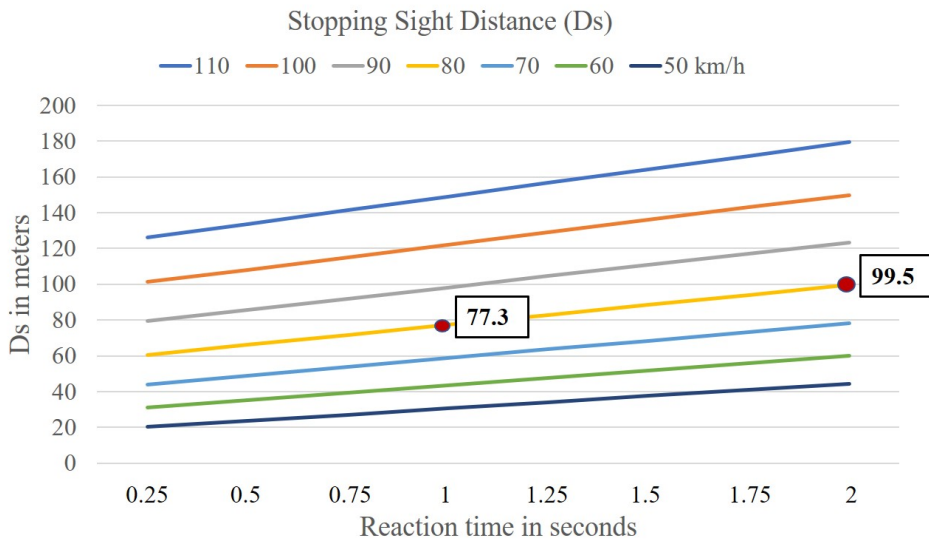


FIGURE 4.3: The effect of lower reaction times on Stopping sight distances.

4.2.2 Geometric Road Design Parameters in Need of Revision in the Long-Term

The long-term effects are divided into two categories: 1) parameters primarily related to vehicle characteristics, including dynamics, and 2) parameters primarily related to human comfort, as shown in **Figure 4.2**. These categories are not mutually exclusive. Parameters that depend on characteristics of automated driver and the shape of the vehicle are discussed in the following section (4.2.2.1). Design parameters related to human comfort are explored in the subsequent section (4.2.2.2) to see if more flexible road design could be possible for automated freight applications.

4.2.2.1 Geometric Road Design Parameters Related to Vehicle Characteristics

Driving automation is under development and characteristics of the automated driver will evolve. This subsection discusses the geometric design parameters that are related to the characteristics of the driving automation system and the physical shape of vehicles. These parameters include the vehicle dynamics of vehicles controlled by automated drivers.

The impact of automated driving on the *Reaction time* and *Object height* were discussed in detail in section 4.2.1. These parameters describe characteristics of automated drivers and the vehicles they control in terms of the performance and placement of sensors, internal networks and communication and software. The sensing capabilities and functionality of automated drivers need to be monitored as automated driving matures, including effects of connectivity which adds complexity to the driving automation systems.

Acceleration and *Deceleration* are dependent on vehicle characteristics including the physical shape of the vehicle, its weight, and its powertrain. The shape of the vehicle also factors in in terms of rolling resistance, area of the front of the vehicle, air resistance characteristics, and the power to weight ratio. *Acceleration/Deceleration* could increase due to higher road adhesion and improvements in powertrain and braking technologies (Washburn and Washburn, 2018). This would decrease the *Stopping sight distance*, *Meeting sight distance* and *Passing sight distance*. Furthermore, it can affect the length required for ramps and passing/climbing lanes. However, road design must consider the lower end of vehicle performance, therefore, such changes would only be realistic if changes are seen in the general vehicle population. Changes to both the vehicle performance and shape should therefore be monitored for changes but are not assumed to be applicable for changes in road design at present time.

Vertical curve radius for crests will also be impacted by the characteristics of vehicles operated by automated drivers. Crest curves are defined by the available *Stopping sight distance*, *Eye height* and *Object/Vehicle height* as shown in **Equation 4.3**. Lower reaction times will decrease the *Stopping sight distance* if the *Design speed* is unchanged and thus decrease the minimum radii of crest curves. Furthermore, a higher *Eye height* or *Object/Vehicle height* will also lower the minimum radii. As argued, for automated users the basic parameters *Eye height* and *Object height* need to be redefined. It follows that the vertical crest curve would need revision in the longer term when *Eye height* and *Object height* have been defined for automated drivers.

$$R_{v,min} = \frac{1}{2} \times \left(\frac{D_s(m)}{\sqrt{a_1} + \sqrt{a_2(3)}} \right)^2 \quad (4.3)$$

For *Horizontal curve radii*, tunnels are of particular interest when considering vehicle and automated driver characteristics, as their minimum radii are greatly influenced by the available sight distance on the inside of the curve. As shown in **Equation 4.4**, the *Horizontal curve radius* in tunnels is related to the *Stopping sight distance*, D_s (m), and the distance from the center of the lane to the tunnel wall, B (m). A lower *Reaction time* would decrease the *Stopping sight distance*, thus, allowing for decreased *Horizontal curve radii*. Furthermore, sensor placement could further the lateral extents of the automated driver's sight lines represented by the variable B .

$$R_{h,min} = \frac{(D_s)^2}{8B} \quad (4.4)$$

The physical shape of vehicles also affects geometric design parameters. The width and length of vehicles are related to the wheel distance, overhang, and offtracking abilities, which is relevant when considering both widening around sharp horizontal curves and lane widths. At present time, driving automation has not indicated any clear trend in changes to vehicle sizes. Automated driving is envisioned in everything from small pods (Duarte and Ratti, 2018) to platoons of trucks (Lutin, Kornhauser, and Lerner-Lam, 2013). Larger cargo volumes for goods are desirable, thus, driving a desire towards bigger freight vehicles. On the other hand, bigger vehicles will, generally, have poorer vehicle dynamics due to issues including air resistance, power to weight ratios, and smaller margins of error on existing roads.

The shape and dynamic properties of vehicles should be monitored for significant and consistent changes. Currently there are no clear indications of changes in

the shape of vehicles as a result of automation. Changes in the dynamic performance of vehicles driven as a result of driving automation systems could improve performance such as increased acceleration and deceleration. However, road design must take into consideration the lower end of vehicle performance. It is possible to design roads, based on changes in vehicle performance, for specific uses if vehicles using the stretch of road can be required to have certain characteristics such as a minimum *Acceleration/Deceleration* or maximum *Vehicle width, Overhang*, etc. The next section explore how road design can change if human comfort is not a requirement, i.e., the case for a separate road design standard for automated freight.

4.2.2.2 Geometric Road Design Parameters Related to Human Comfort

A lower reaction time in theory allows for smaller radii of horizontal and vertical curvatures and/or higher design speeds. However, there are limitations on these design parameters relating to the forces, due to accelerations, acting on human drivers or passengers to ensure comfortable and safe driving. It could therefore be useful to develop two sets of road design standards, one for transportation involving humans as drivers or passengers, and one for transportation without humans (automated freight). The latter would allow for exploring the flexibility and cost-efficiency of roads without concern for human comfort.

Transportation where humans are drivers and passengers involve accelerations that induce forces on the human body. If these forces are too great, humans experience discomfort and, in the extremes, injury (Kumar and Norfleet, 1992). Accelerations are caused by changes in velocities, i.e., changes in speed, direction, or both.

Linear accelerations are caused when the speed changes, but the direction remains the same, e.g., accelerating or deceleration without changing the heading. Accelerations upwards and downwards are vertical accelerations experienced with vertical displacement. The *Vertical acceleration* parameter is used to limit the vertical acceleration experienced by humans in vertical curves and is therefore used in the design parameter *Vertical curve radius*. The effect of vertical acceleration is found in both crest and sag curves, but it is more severe in sag curves as it in this case adds to the gravitational acceleration acting downwards. The minimum vertical sag curve is related to *Design speed* (km/h) and *Vertical acceleration* (m/s^2) as shown in **Equation 4.5**. Increases in the allowed vertical acceleration for a given speed will decrease the minimum sag radii allowing for more flexibility in road design.

$$R_{v,min} = \frac{\left(\frac{V}{3.6}\right)^2}{a_v} \quad (4.5)$$

While crest vertical curves are currently designed for sight distance, if connectivity could reduce the need for lines of sight significantly, vertical acceleration and the associated comfort could then have more of an impact on the determination of minimum vertical crest curve radii.

Higher deceleration rates, as proposed by Washburn and Washburn (2018), could result in reductions in braking lengths which, like *Reaction time*, would have the effect of reducing *Stopping sight* and *Meeting sight distances*. A higher rate of acceleration could also decrease the required *Passing sight distances*. Yet, for transport with human passengers, accelerations are limited by human physical comfort (Washburn

and Washburn, 2018). Research has showed that humans have a higher tolerance towards longitudinal linear acceleration (Kumar and Norfleet, 1992) which might indicate that higher limits for acceleration and deceleration are possible also with human passengers on straight stretches of road. However, there is also the aspect of human mental comfort and trusting the safe operation by an automated driving system. Human mental comfort is likely to become more important when the automated driver is in control of the vehicle (Hartwich, Beggiato, and Krems, 2018; Manchon, Bueno, and Navarro, 2020) and should receive more attention in designs for automated transport of human passengers in the future.

For freight transport, making use of higher acceleration/deceleration rates could result in shorter ramps and climbing/passing lanes. However, as previously stated, these geometric elements are limited by the vehicles with the poorest power to weight ratios when designing roads. It is therefore doubtful that significant changes could be possible until an eventual increase in performance of all vehicles using the road.

Accelerations are also experienced laterally, for instance in horizontal curves. **Figure 4.4** shows a car driving through a curve, seen from a plan perspective. The car and

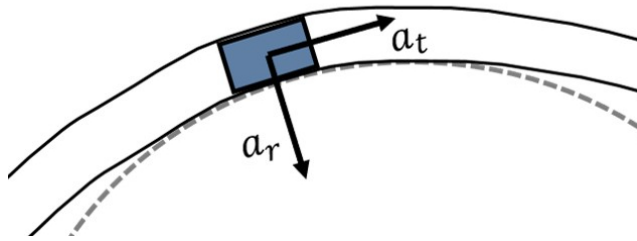


FIGURE 4.4: Example of accelerations experienced in a horizontal curve.

its occupants experience a radial acceleration, a_r , (also referred to as a centripetal acceleration) when the car turns around the curve, while changes in the forward speed are expressed as a linear tangential acceleration, a_t .

The radial/centripetal acceleration, a_r , is expressed by **Equation 4.6** where v is the speed and r is the radius of the curve the car is traversing:

$$a_r = \frac{v^2}{r} \quad (4.6)$$

This means that the design parameters *Design speed* and *Horizontal curve radius* affect the accelerations felt by the car's occupants. However, the design requirements for minimum *Horizontal curve radius* are not based on human comfort, but instead based on keeping the vehicle inside the curve, as shown in **Equation 4.7**, where V is the *Design speed* in km/h, g is gravitation (9.81 m/s^2), e_{max} is the maximum *Superelevation*, and f_k is the side friction.

$$R_{h,min} = \frac{\left(\frac{V}{3.6}\right)^2}{g \times (e_{max} + f_k)} \quad (4.7)$$

Although the *Superelevation* does affect the comfort of human occupants, the main limiting factors are avoiding skidding and rollover of vehicles. While it could be possible to increase *Superelevation* to reduce the associated horizontal curve radius, due

to issues related to available side friction in inclement weather and rollover issues, this is unlikely (Easa and Dabbour, 2003).

Comfort is considered when determining the length and parameter value associated with *Clothoids*, the spiral transition curves used in horizontal alignments to transition between different radii curves. At a constant speed, a clothoid allows for a gentle change in lateral forces between two different radii where the length of the clothoid affects how fast this change occurs. Within the Norwegian standards, the minimum Clothoid parameter is defined by **Equation 4.8**.

$$A_{min} = \sqrt{R_{h,min} \times L_{e,min}} \quad (4.8)$$

Where

$$L_{e,min} = \frac{b \times V \times e_{max}}{3.6 \times v_{vs}} \quad (4.9)$$

$L_{e,min}$ represents the minimum distance required to generate the *Superelevation*, e , and is also related to *Wheel distance*, b (m), the *Design speed*, V (km/h), and the *Relative vertical speed*, v_{vs} (m/s). The parameters related to comfort are e_{max} and v_{vs} . Increasing the e_{max} has already been ruled out leaving the possibility for higher *Relative vertical speeds*. *Relative vertical speed* describes the difference in vertical speed of wheels on the same axle which occurs in cornering. The Norwegian definition of the *Clothoid* parameter differs from the U.S. standards where a value for the rate of increase of lateral acceleration is used, as shown in **Equation 4.10** where V is the *Design speed* (km/h), R is the *Horizontal curve radius* (m), and C is the rate of increase of lateral acceleration (m/s^3):

$$A_{min} = \frac{\left(\frac{V}{3.6}\right)^3}{R \times C} \quad (4.10)$$

Values for C are in the range of 0.3–0.9 m/s^3 and higher values could be considered for automated freight. Based on both the Norwegian and U.S. standards, the minimum Clothoid parameter could be reassessed for automated freight.

4.2.2.3 Road Design for Automated Freight

In summary, the review of road design parameters in Paper II found that the following parameters related to 1) vehicle characteristics, including dynamics (section 4.2.2.1), and 2) human comfort (section 4.2.2.2) show the most immediate potential in terms of creating more flexible road design for automated freight:

- *Vertical acceleration*
- *Relative vertical speed*
- *Clothoid parameter*
- *Minimum vertical curve radius (crest)*
- *Minimum vertical curve radius (sag)*
- *Minimum horizontal curve (tunnel)*

These indicate increased flexibility in road design primarily for vertical alignments. Horizontal curves are limited by requirements to avoid slipping and rollover, with the exception of tunnels where the lateral placement of sensors can provide the possibility of smaller radii curves. Additionally, if higher *Acceleration/Deceleration* rates could be ensured, *Stopping, Meeting, and Passing sight distances* can be decreased.

4.3 Research Objective 3

The third research objective was to examine how road infrastructure design and maintenance can facilitate automated driving. In the following, suggestions on areas of research for adapting road infrastructure elements to automated drivers are suggested as well as concrete results and findings that are relevant for current road design and maintenance.

4.3.1 Paper I

Using currently available technology, Paper I shed light on how sensors used in driving automation perceive the driving environment as described in section 4.1. In understanding these sensing capabilities lie a potential for adaptations to road design and maintenance. For example, the increased electromagnetic (EM) sensitivity allows for higher dimensionality of information as information can be embedded with visibility at different wavelengths. One such application has been demonstrated by the company 3M who produced traffic signs with both a layer visible to the human eye (the visible spectrum) and a layer visible in the near-infrared range. This is shown in **Figure 4.5** where the image on the left-hand side is visible to the human eye and cameras, and a second layer underneath is visible to cameras with near-IR sensitivity when filtering at the correct wavelength.



FIGURE 4.5: Sign with traditional layer and an added layer visible in the near infrared. Source: Snyder et al. (2018).

The barcode is visible in the near-IR, has high contrast, and is well suited for machine readability. This second layer of information can be used to convey information

such as the position of the sign in geographic coordinates, thus acting as a landmark to help with positioning. This could be especially useful in areas where there are known problems in communicating with position services, e.g., tunnels.

4.3.2 Paper II

Paper II used the unified framework of driving to investigate how geometric road design would be affected by automated drivers. The results, discussed in the previous section (4.2), provided suggestions on geometric road design parameters in need of redefinition in the short term and in the long term. A separate regulation for automated freight transport was also suggested, both due to the limitations imposed by human comfort (subsection 4.2.2.2) and due to the possibility of changes to vehicle dynamics as a result of driving automation (subsection 4.2.2.1).

4.3.3 Paper III

In Paper III, the visibilities of road markings were measured by a mobile retroreflector attached to a passenger car with an LDW system. Data capture on county roads and freeways during night and day were performed to compare lane detection by LDW system to a conventional retroreflector. The retroreflector measured the retroreflectivity of the road marking and the contrast to the road surface. These readings, in addition to ambient light measured by the car, and the vehicle speed, were used as predictor variables in a binary logistic regression to predict whether the LDW system detected road markings. **Table 4.1** shows the significance of the predictor variables in correctly predicting the outcome of the LDW system in the difference cases (combinations of freeway/county road and daytime/night-time).

TABLE 4.1: Significances of predictor variables for lane detection by LDW.

	County road daytime				County road night-time			
	B	S.E.	Sig.	Exp(B)	B	S.E.	Sig.	Exp(B)
Retroreflection	0.003	0.000	0.000	1.003	-0.010	0.012	0.000	0.990
Contrast	0.538	0.000	0.000	1.712	0.514	0.067	0.000	1.672
Vehicle Speed	1.127	0.002	0.000	3.087	3.097	0.012	0.000	22.127
Ambient Light	0.000	0.000	0.000	1.000	0.003	0.001	0.000	1.003
Constant	-19.30	0.043	0.000	0.000	-50.89	0.207	0.000	0.000
	Freeway daytime				Freeway night-time			
	B	S.E.	Sig.	Exp(B)	B	S.E.	Sig.	Exp(B)
Retroreflection	0.003	0.000	0.000	1.003	0.004	0.000	0.000	1.004
Contrast	0.538	0.008	0.000	1.713	0.495	0.017	0.000	1.640
Vehicle Speed	1.076	0.002	0.000	2.932	0.429	0.001	0.000	1.536
Ambient Light	0.000	0.000	0.000	1.000	-0.011	0.000	0.000	0.989
Constant	-18.39	0.043	0.000	0.000	-8.100	0.023	0.000	0.000

The results showed that retroreflectivity did not affect the outcome of the car's lane detection with log odds (Exp(B)) of approximately 1 in all cases. Contrast was found to be positively related to successful predictions, contributing in the range of 1.64 to 1.71 for the different scenarios, with slightly higher values for daytime

conditions. This means a unit change in contrast would result in 1.64–1.71 times the odds of getting a correct prediction. This result indicates that contrast is a better indicator of whether the LDW system detected markings than the more widely used retroreflection quality parameters Q_D or R_L . The retroreflector emits laser beams and detects their reflection and is therefore not affected by ambient light. The LDW system of the car was camera-based and, thus, dependent on the availability of light. Ambient light was therefore thought to have an effect on the LDW detections. The analyses presented in **Table 4.1** show that this was not the case as ambient light has log odds of approximately 1 in all cases. The freeways are lit by streetlights while the county roads were largely without lighting. This indicates that the headlights of the car are sufficient for LDW-based lane detection and that these systems are not dependent on streetlights.

Vehicle speed was the most significant predictor in all cases except freeway at nighttime where contrast was more influential. This is because the retroreflectorometer logged data as an average over distance (30 m) while the car logged in regular time intervals. As a result, the data sample rate differed between the two data sources depending on the vehicle speed. This difference is illustrated in **Figure 4.6**.

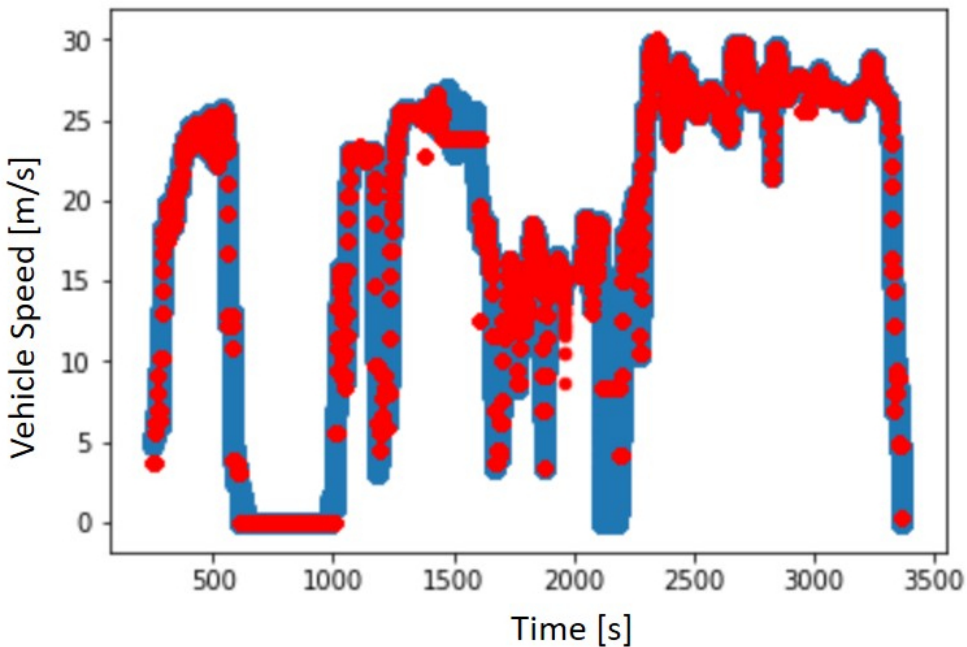


FIGURE 4.6: Data resolution for the car (blue) and retroreflectorometer (red).

To investigate this finding, an overlapping portion of the daytime and night-time data sets for the county roads was extracted. The overlapping segment is represented by orange squares in **Figure 4.7**.

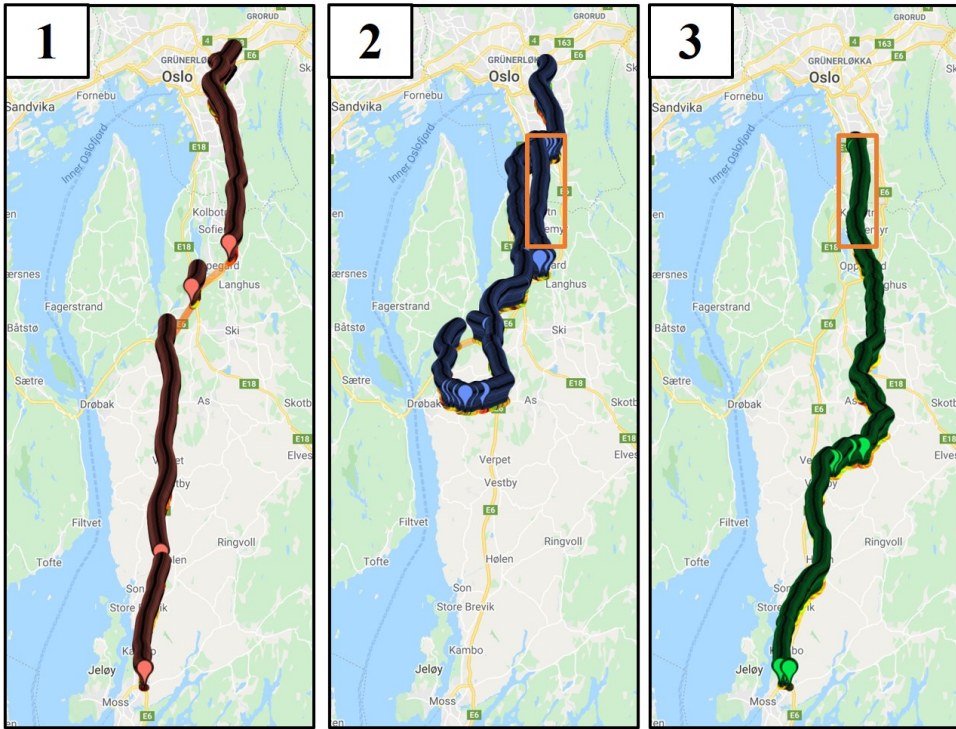


FIGURE 4.7: Plots of position data for 1) Daytime and night-time on freeway, 2) Daytime on county roads, and 3) Night-time on county roads. Visualization: <http://geojsonviewer.nsspot.net>.

When the lane detections made by the LDW system were investigated on the stretch of road indicated by the orange box in **Figure 4.7** it was evident that the night-time driving had a much lower rate of positive detections than the daytime data collection. This is illustrated in **Figure 4.8**.

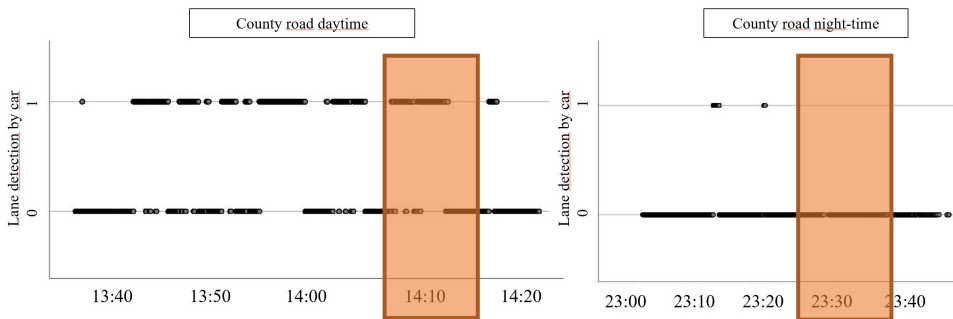


FIGURE 4.8: Overlapping section of county roads with lane detection results for daytime (left-hand side) and night-time (right-hand side) driving.

The same difference in positive lane detections between daytime and night-time was not seen in the freeway cases. Manual searches in the NPRA's Vegkart web service (Statens vegvesen, 2021) were performed to shed additional light on the difference in lane marking detection. These searches found that the night route, in general, had more spray thermoplastics (1-1.5 mm thickness) than the day route, which had almost entirely preformed thermoplastics (3 mm). This could explain the overall trend of much fewer successful lane detection for night versus day. For the overlapping segment, however, the marking was thermoplastic which still showed a much poorer performance for camera-based detection at night. According to the Vegkart service the marking used on county road 152 was 2 mm thick thermoplastic compared to the 3 mm thick thermoplastic used on the freeway (E6).

In addition to thickness, application and wear can factor into the marking's visibility. As ambient light has been shown not to be a predictor for the LDW's, the material and thickness used for road marking could be investigated as a predictor for automated lane detection in future studies.

4.3.4 Paper IV

Colors and patterns have a long history in alerting drivers and commanding attention when it comes to signage. The same use of colors for other road infrastructure elements is less common. Roads are generally gray and black, most commonly road markings are white, and dividers are often found in their natural concrete gray coloration. Norway will be the only country in the Nordics using yellow road markings when Finland finish phasing out yellow markings, a change which is due by the end of March 2023 (Finnish Transport and Communications Agency, 2020). Road markings are a major expense for road agencies (Pike and Bommanayakanahalli, 2018) and using one color is more cost-efficient than two. LDW systems have been proven to provide safety benefits. They represent core functionality also used in higher levels of automation and have a high dependency on road markings. It is therefore of importance to make sure that road markings are designed and maintained to ensure sufficient visibility for both human and automated drivers also in adverse weather. Adverse weather, and particularly snow, is known to cause problems for automated lane detection. However, there is a lack of research indicating weather yellow road markings (used in Norway and in the U.S.) can provide added visibility for automated drivers in adverse weather such as snow.

To this effect, the use of yellow road markings to enhance visibility in snowy driving conditions was the subject of Paper IV. Literature suggested that the use of different color space representations could affect the visibility of road markings in images. First, the most commonly used color spaces, RGB and grayscale were assessed. The results showed that although the yellow road markings are visible to the human eye in snowy conditions, they are hard to detect by automated and mathematical processes. An example is shown in the image from the plowed airstrip in **Figure 4.9**. This case only has yellow markings. These are visible to the human eye in **Figure 4.9i** (RGB representation). However, in the histogram plot of the three channels that make up the RGB image (**Figure 4.9ii**), it is not easy to pick out any distinct peaks that corresponds to the road marking. For the grayscale image, **Figure 4.9iii**, and the corresponding histogram plot, **Figure 4.9iv**, the road marking is hard to discern in both representations and thus not suitable for detection by human or machine. The two

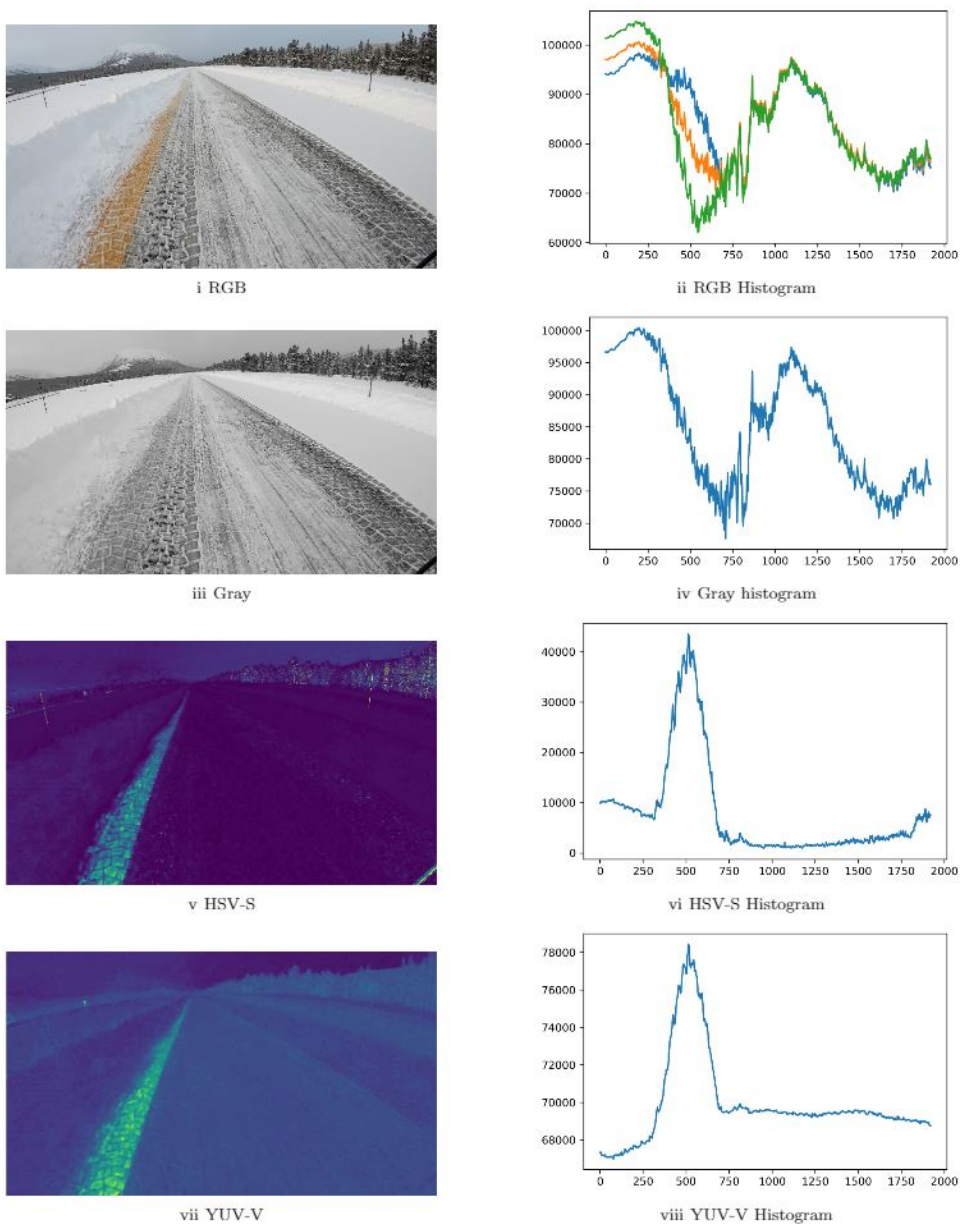


FIGURE 4.9: Example of visibility of lane markings in different color spaces, visually (left-hand side) and by pixel values (right-hand side).

lower representations of the same image (**Figure 4.9v, vii**) demonstrate how color space representations can be used to enhance road features. In both the S-channel of the HSV image and the V-channel of the YUV image, the yellow road markings have significantly different pixel intensities compared to both the road surface and the snow. The histograms confirm the finding from the visual inspection displaying

distinctive peaks in the position of the road markings (**Figure 4.9vi, viii**).

In **Figure 4.10** an example with both yellow and white markings is shown. This image is taken in the laboratory and shows the road model covered in 0.5 cm of snow. There are yellow road markings above the red dotted line and white markings below it.

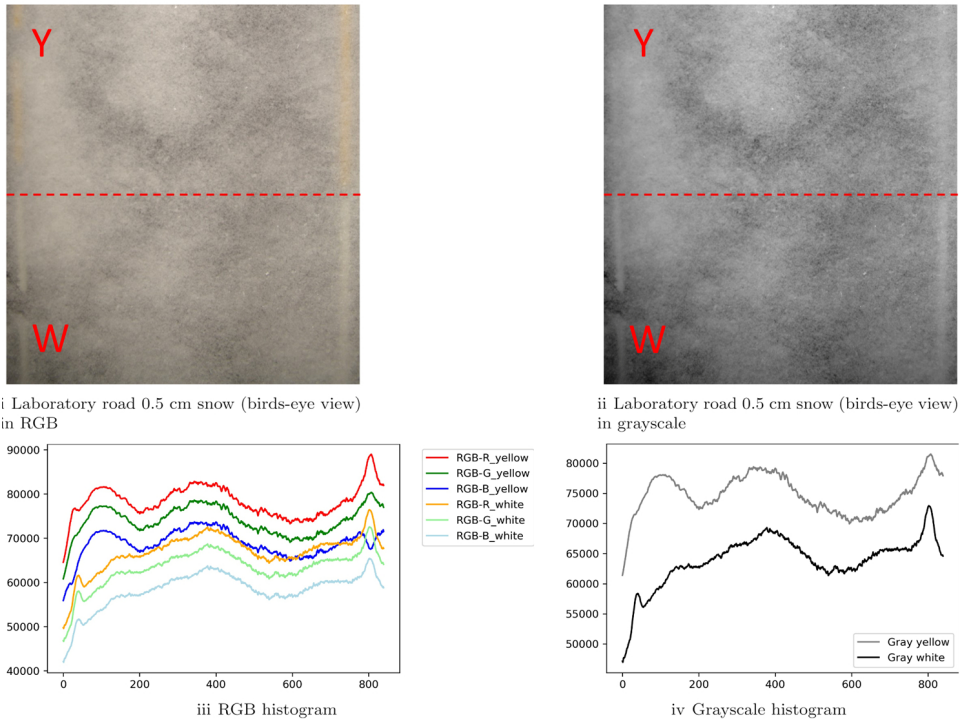


FIGURE 4.10: Laboratory road model with 0.5 cm snow (birds-eye view) and corresponding histograms for RGB and grayscale representations.

In the RGB and grayscale representations the continuous line (right-hand side marking) creates peaks in the histograms for both white and yellow markings. The dashed marking (left-hand side marking) on the other hand, is not possible to discern from the other peaks and troughs of either histogram plot.

White markings create slightly higher peaks due to their higher pixel values, but the overall plot is not optimal for identifying road markings based on gradients or thresholds. The following figure (**Figure 4.11**) shows the histogram plots corresponding to alternative color spaces for the same image. On the left-hand side all channels are shown in the same plot, while the right-hand side highlights the channels that are most successful in enhancing the road markings and the difference in visibility between white and yellow road markings.

The HSL-S, HSV-S, YUV-U and YUV-V channels enhance the pixel intensities for both yellow and white road marking, setting them apart from the road surface and the cover of snow. These four channels are therefore shown separately in the right-hand side in **Figure 4.11** which also allows for a comparison of the visibility of white versus yellow markings. The visibility of the yellow road markings (red and dark

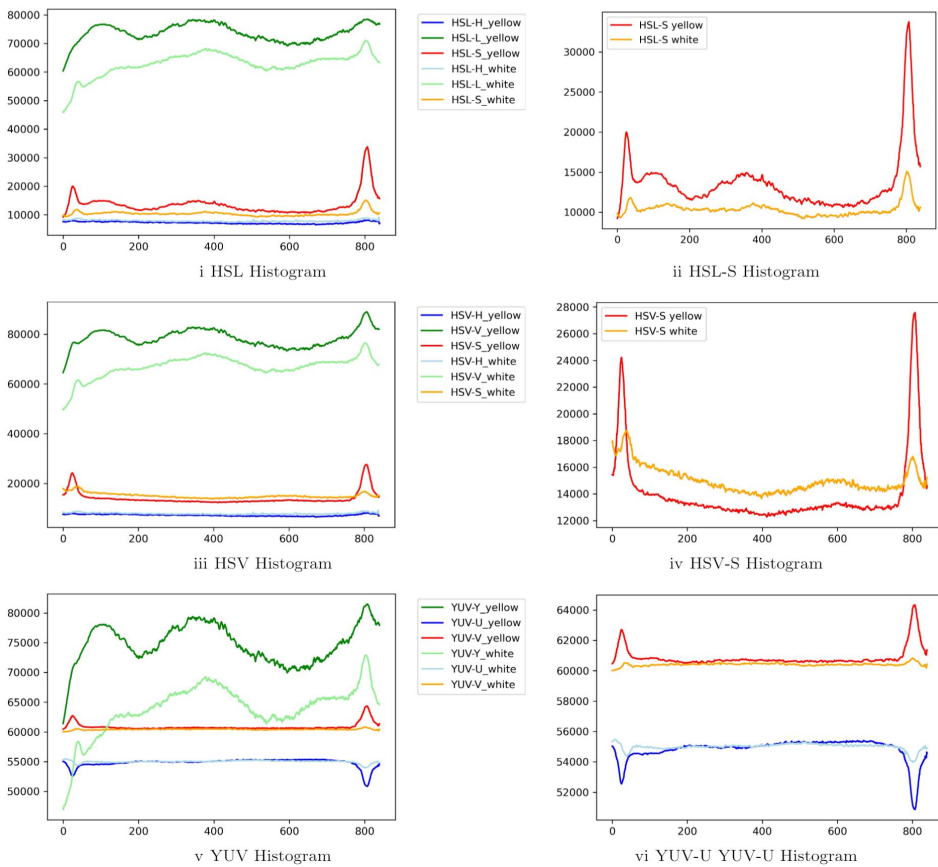


FIGURE 4.11: Histogram plots for HSL, HSV and YUV color space representations of **Figure 4.10**.

blue lines) is much greater than the white markings (yellow and light blue lines) as shown by the difference in peak heights. The continuous road markings create higher peaks than dashed lines as expected, as they have more marking pixels thus creating a higher pixel intensity sum (i.e., peak) in the histogram.

In the case of evening driving on public roads with partial snow cover, a small segment in the lower half of the image was used to compare the visibility of yellow and white road markings in different color spaces. Perspective view images as shown in **Figure 4.12**. give wider and lower peaks than the birds-eye perspective as the marking pixels are spread across more columns of the image. This can to some extent be corrected by perspective transformation. However, the perspective view was considered sufficient for examining how different color spaces affected visibility. This followed the overall methodology of using unaltered images in different color space representations to assess the impact of color space on the visibility of yellow versus white markings without introducing unintended effects from image manipulation.

The image in **Figure 4.12** has yellow markings on the left-hand side and white markings on the right-hand side in line with design standards in Norway and the

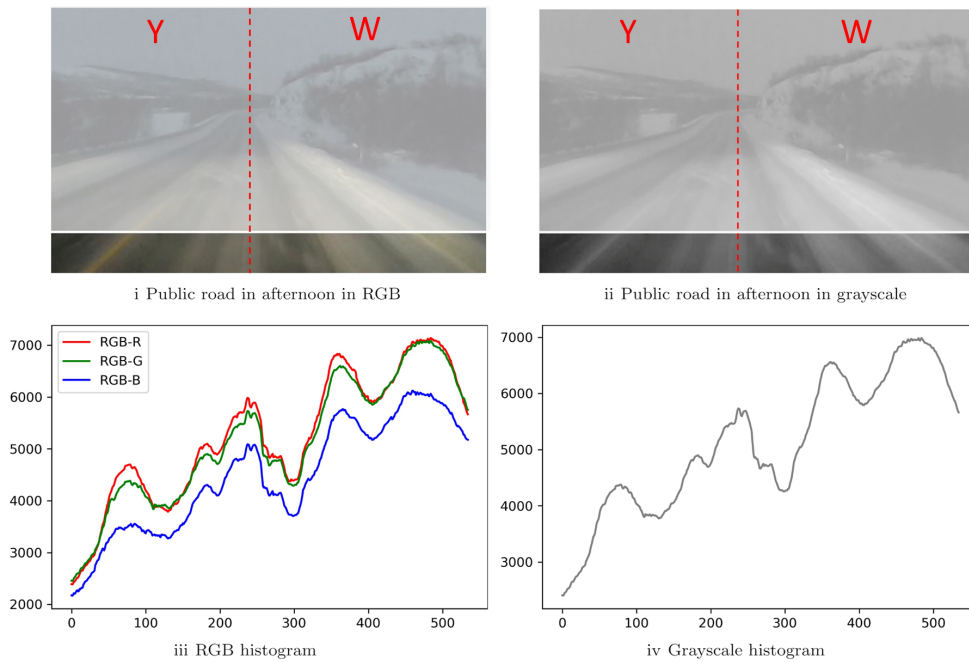


FIGURE 4.12: Public road in evening with partial snow cover (RGB and grayscale representations) and corresponding histogram plots.

U.S. Both the yellow and white lane markings are visible to the human eye, however, the histogram plots show that for automated detection RGB and grayscale representations are not well suited to locate either color road marking.

The histogram plots for the alternative color spaces for the public road case are shown in **Figure 4.13**. In these challenging conditions, the HSL-S and HSV-S channels provide distinct peaks corresponding to the yellow road marking (peak on the left-hand side of the histograms) while the white marking is hard to separate from the road surface or snow (peak on the right-hand side of the histogram). The YUV-U/V channels are not able to enhance the yellow or the white road marking.

The results for all cases with snow are summarized in **Table 4.2**. Overall, the HSV-S and HSL-S channels were the best at enhancing the road marking, but only for yellow road markings. The hypothesis stated that yellow road markings could be more easily visible to both human and automated drivers than white markings, which was confirmed by these findings. For complete results, refer to Paper IV.

Successful and safe automated driving will need redundancy and robustness in sensors and software. The added visibility and contrast of yellow road markings indicate that they can provide robustness for lane keeping in adverse weather situations where there are fewer reference points for the automated driver to depend on.

The value of yellow road markings for lane marking visibility is of importance to road authorities in relation to road design policies. Norway will soon be the only country in the Nordics that uses yellow road markings. In the EU, white road markings are currently the norm. Paper IV suggests that yellow road marking can facilitate automated driving in snowy conditions. Thus, the use of yellow road markings on

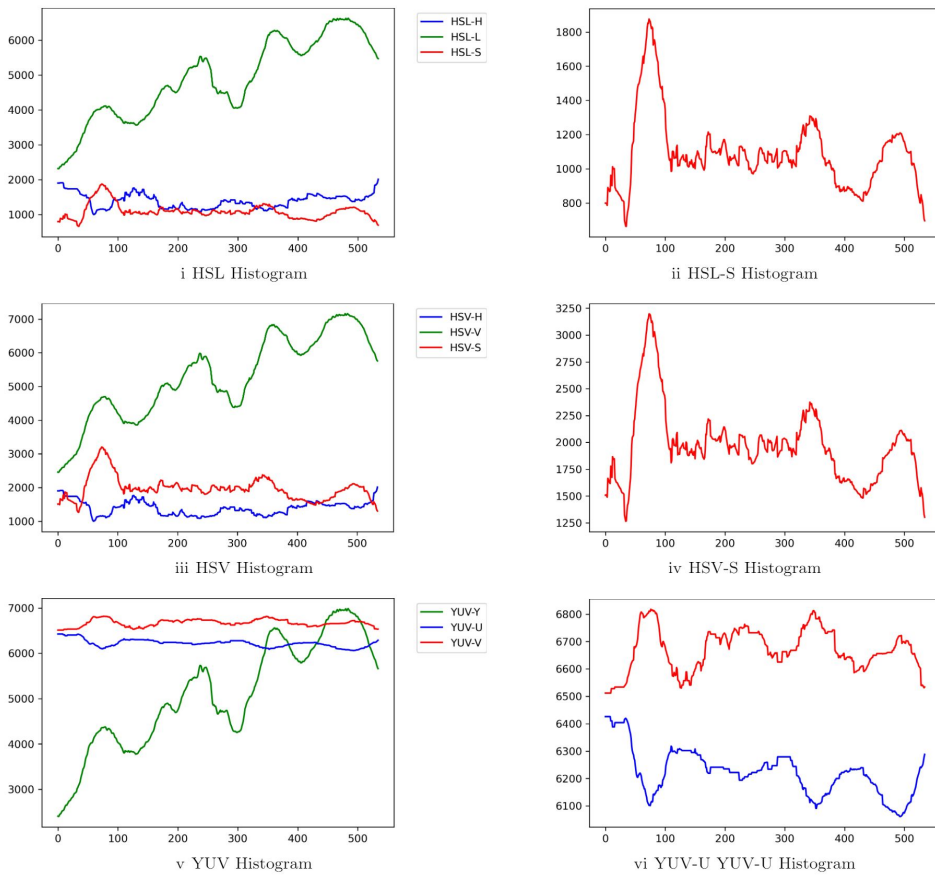


FIGURE 4.13: Histogram plots for HSL, HSV and YUV color space representations of the public road driving image (Figure 4.12).

at least one side of the lane is encouraged to enhance visibility of road markings for both human and automated driver based on the results of this research. The use of two colors adds information to the driver by indicating whether the adjacent lane is for the direction the driver is traveling in or for the opposite direction. This is vital information for all drivers and suggests that keeping two colors could continue to be beneficial for traffic safety. Continuous lines are easier to discern in adverse weather conditions and provide higher signal values for sensors such as cameras. The use of dashed versus continuous lines also relay information to drivers and the visibility of these compared to continuous lines can be further investigated in efforts to determine whether the higher visibility of continuous lines outweighs the importance of knowing the directionality of lanes as the latter can be communicated in other ways (e.g., through maps).

In summary, the third research objective was to examine how road infrastructure design and maintenance can facilitate automated driving. Paper I identified differences between human and automated driver in terms of sensing and cognition. These

TABLE 4.2: Visibility of yellow and white road markings for cases with snow coverage based on histogram plots.

	Image	Gray	RGB			HSL			HSV			YUV			
	Channel		R	G	B	H	S	L	H	S	V	Y	U	V	
Laboratory 0.5 cm snow	White	+	+	+	+		+	+			+	+	+	+	+
	Yellow		+								++	+	+	++	++
Airfield	Plowed										++			++	++
	Brushed						++	++		++	++			++	++
Public road	White														
	Yellow										++				

changes suggest that color and texture should be researched more actively in applications for road infrastructure elements to make them easier to detect and classify. Paper II used the characteristics of automated drivers identified in Paper I to review current geometric road design and suggested changes to these in the short and long term. Paper III investigated how road marking quality measures in traditional measurements compared to automated lane detection functionality. The results indicate that contrast is of higher importance than retroreflectivity for camera based lane detection. Furthermore, LDW functionality does not seem to rely on ambient lighting other than the car's headlights. The thickness, type, and wear of lane markings should receive more attention in future research efforts to design and maintain roads for automated drivers. Paper IV investigated whether yellow road markings could be beneficial to automated driving in adverse weather. The results suggest that yellow markings provide significantly higher visibility in snow when the color spaces HSV-S, HSL-S and YUV-U/V are considered. Yellow road markings are therefore encouraged on at least one side of lanes to enhance visibility for both human and automated driver.

4.4 Research Objective 4

4.4.1 Sensor Data from Automated Driving Systems and Suggested Applications.

Characteristics related to sensory and cognitive capabilities of automated drivers were identified in Paper I which shed light on how driving automation systems can be used as mobile sensor arrays to monitor the condition of road assets. Current levels of ADAS include cameras for LDW and sign recognition, radars for adaptive cruise control (ACC) and blind spot warning, and ultrasound for parking assistance. In higher levels of automation, the use of lidar is common. However, lidars are not yet used in publicly available vehicles due to their high cost. While most modern cars

have cameras available it is often difficult to obtain video data due to several factors. Videos require considerable storage space and most commercial vehicles have limited storage space available. Video may be stored in smaller sections which are later deleted to perform ADAS functions such as LDW. Getting access to this video would likely require both cooperation with the car manufacturer, the user acceptance of the vehicle owner and driver, and high bandwidth communication services. Fortunately, there are alternatives to gaining access to the video from vehicles. For example, the output from the ADAS functions themselves can provide useful interpretations of the road infrastructure such as the discrete lane detection values used in Paper III. This data is more easily available, requires much less storage and communication bandwidth, and is not associated with privacy issues. Detection of signs by automated drivers likewise represents a conversion of image information to less verbose information. It is therefore also suitable for sharing and can be correlated to road infrastructure asset management systems to see whether signs are present and in good condition. Other types of data derived from driving automation systems such as hard braking actions or tire slip also provide information that can be used to investigate what parts of the road infrastructure are more problematic than others. Patterns in such findings could reveal both issues related to road design, e.g., poorly designed curvature, and maintenance, e.g., trees causing shading issues or snow.

ADAS data is a combination of the sensing and cognition performed by automated drivers. While it does not provide access to raw data from sensors, it outputs the interpretations and actions of the automated driver which ultimately decide how it performs in the driving environment. Driving automation systems differ in terms of sensor use and placement, as well as software, which together form the product the manufacturers of automated drivers are selling. It is, therefore, proprietary information. The output of its functionality is less sensitive and, thus, easier to share and will give road engineers useful information from which to optimize road maintenance and design.

4.4.2 Findings From Practical Experiments and Suggestions for Applications

Papers III and IV demonstrated through practical research how ADAS can be used to monitor the state of road infrastructure and driving conditions using road markings as a case. Paper III examined how one of the most common ADAS features, LDW, can be used to monitor the condition of road markings. To evaluate the use of LDW for this purpose, a retroreflectometer was used as a reference. The test used known quality measures for lane marking obtained from the retroreflectometer, i.e., *Retroreflectivity* and *Contrast*, as predictor variables to see if a traditional way of assessing road marking quality coincided with the result from the LDW system. In addition, *Ambient light* and *Vehicle speed* were used as predictor variables predicting the outcome of the car's lane detection by LDW. Overall, the predictor variables could successfully forecast the result of the LDW system in 92–98% of cases depending on conditions (county road versus freeway, and night versus day). The results are shown in **Table 4.3**, where 0 indicates that no lane marking was detected, while 1 indicates that the road marking was found.

Table 4.3 shows that the outcome of the lane detection's functionality was correctly predicted by the model in 92.1% of cases for the freeway and 92.8% of cases for

TABLE 4.3: Classification of all cases: freeway and county roads in daytime and night-time.

Freeway daytime (mean lux = 9663)				Freeway night-time (mean lux = 10)			
Observed	Predicted Lane detection			Observed	Predicted Lane detection		
	0	1	Correct (%)		0	1	Correct (%)
LDW car 0	959887	55543	94.5	LDW car 0	369022	28771	92.8
LDW car 1	60635	401120	86.9	LDW car 1	35314	461956	92.9
Overall (%)			92.1	Overall (%)			92.8
County road daytime (mean lux = 9726)				County road night-time (mean lux = 6)			
Observed	Predicted Lane detection			Observed	Predicted Lane detection		
	0	1	Correct (%)		0	1	Correct (%)
LDW car 0	1256579	55058	95.8	LDW car 0	1064740	17027	98.4
LDW car 1	67802	401812	85.6	LDW car 1	7020	202021	98.1
Overall (%)			93.1	Overall (%)			98.1

county roads in daytime. Regarding nighttime, the results were 93.1% for the freeway and 98.1% for county roads. There was a higher accuracy level for no detection of lane marking on the freeway in both daytime and nighttime. The same was true for the county roads at nighttime, although the difference was not as distinct. With respect to the county road daytime case, the accuracy was similar between no marking detected and a marking found. The analyses suggest that LDW systems can be useful for monitoring road markings. Further testing with several makes of vehicles and ADAS systems should be performed to confirm this finding.

ROC curves were analyzed to see if threshold values for successful lane detection for the four predictor values could be identified (**Figure 4.14**). *Vehicle speed* has the largest area under the curve, and thus the highest accuracy in terms of ratio of true positives and negatives to false positives and negatives. The threshold values for vehicle speed lie between 56.14 and 57.02 km/h, which suggests that speeds lower than this provides insufficient data points from the distance based retroreflectometer. For further testing using LDW (or lane keeping functionality) and retroreflectometers, it is advised to keep this in mind by performing tests at speeds higher than 57 km/h, adjusting the sample rate of the retroreflectometer to less than 30 meters, or, if possible, using time-based sampling for all data collection.

Ambient light was found to have no predicting quality. This result could be confirmed by executing more tests using a greater range of ambient light conditions and several LDW or lane keeping systems.

Retroreflection and *Contrast* are the most influential predictors for night-time conditions. As *Ambient light* was found to have no effect on whether or not the LDW system detected road markings, this is of interest. It could be that low ambient light and the use of headlights create higher contrasts between the road marking and the road surface than in daylight conditions. Possible threshold values for *Retroreflection* and *Contrast* for county road and freeway are shown in **Figure 4.14**. As discussed in more detail in the methodology, the thresholds values obtained from ROC analyses are trade offs between the rate of true positives and negatives to false positives and

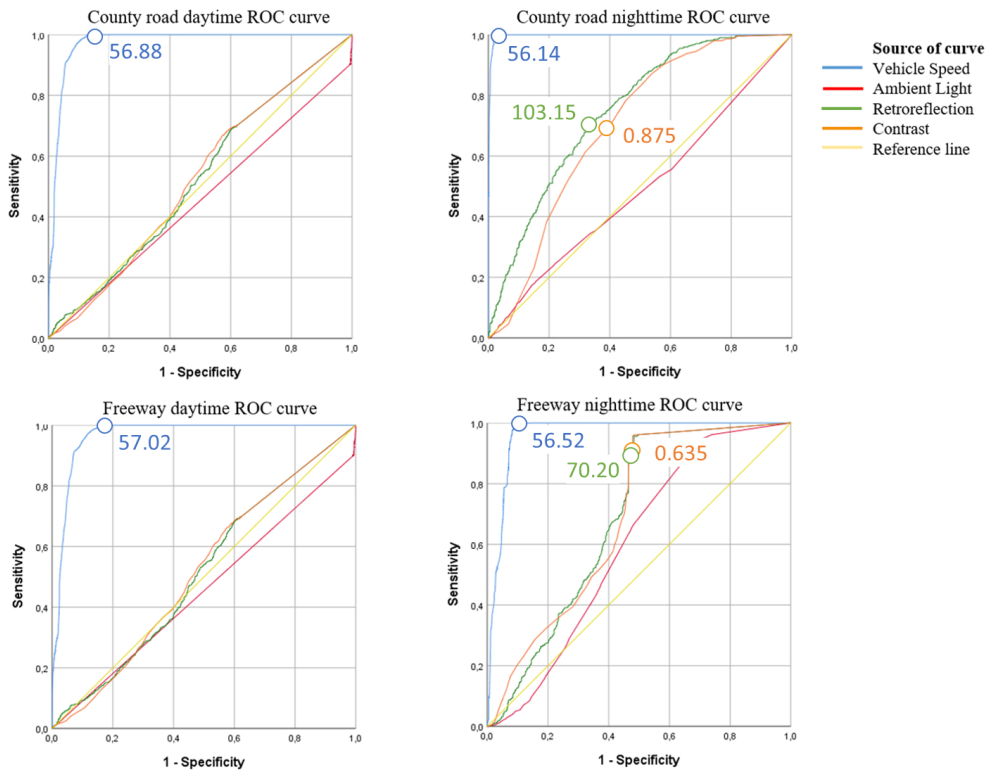


FIGURE 4.14: Receiver operating characteristics curves.

negatives. Therefore, a strategy for what level of accuracy is most beneficial for the intended use would affect the thresholds chosen.

Contrast ratios for road markings can provide useful input for ensuring road marking with high visibility for both human and automated driver. Unfortunately, this measure is not uniformly used or defined in research. In the literature review, only one research report was found that investigated the contrast ratio in association with successful lane detection by car (Lundkvist and Fors, 2010). The contrast ratio used in Paper III was defined by the supplier of the retroreflectometer and was not directly comparable to the one used by Lundkvist and Fors. Due to differences in how contrast ratio was defined, it was not possible to directly compare the results of the two studies.

The mobile retroreflectometer used in Paper III reported contrast values based on **Equation 4.11**:

$$C = 1 - \frac{\text{return signal (pavement)}}{\text{return signal (marking)}} \quad (4.11)$$

This value can be converted to a contrast ratio by **Equation 4.12** according to the supplier of the retroreflectometer:

$$CR = \frac{-1}{C - 1} \quad (4.12)$$

Substituting **Equation 4.11** for C in **Equation 4.12** would give **Equation 4.13** for determining contrast ratio (CR) for the study in Paper III, while Lundkvist and Fors (2010) used **Equation 4.14**. The equipment used in Paper III did not report $R_{roadsurface}$, therefore, it was not possible to calculate the contrast in the same way as in **Equation 4.14**.

$$CR = \frac{\text{return signal (marking)}}{\text{return signal (pavement)}} \quad (4.13)$$

$$C_{RL} = \left| \frac{R_{marking} - R_{roadsurface}}{R_{roadsurface}} \right| \quad (4.14)$$

If the $R_{roadsurface}$ value had been available, the measurements obtained in the test for Paper III could have been converted to the C_{RL} values used by Lundkvist and Fors, allowing for a way to compare the two findings.

In the data set from the vehicle, there were additional data that could be useful for road monitoring. The radar used for ACC logs the distance to vehicles in front of the test car which can be used in traffic engineering applications. The full feeds from sensors, such as images/video from in-vehicle cameras or radar reflections from the ACC system, require substantial resources in storage and communication bandwidth. The logged distance to the vehicle in front, however, is information that is easily stored and shared. Like the discrete lane detection data used in Paper III, this represents information that could be used at present time without the need of additional equipment, is easily shared, and do not represent personal data. ADAS data, e.g., discrete lane marking detections and radar ranges, are examples of ways to start using automated driving features to monitor road assets and road usage.

In Paper IV the effect of snow depth on the visibility of road markings for camera based lane detection was investigated. The smallest increment of snow depth achievable in the laboratory was 0.5 cm increments. The 0.5 cm depth of snow was successful in showing the difference in visibility of road markings in snowy conditions depending on the color space representation. At 1 cm snow coverage in the laboratory, the images produced showed road markings with too low visibility for machine vision applications. The road model used in the laboratory was at 1:10 scale while the snow was not possible to scale down. The physical interaction of light, snow, and road markings were similar in the lab and the real world and the model was therefore assumed to produce results applicable to real world settings. However, real world testing on the airfield showed that it was possible to detect road markings when a 2.5 cm layer of natural snow had been subject to a ribbed plow with 2 cm high ribs. The snow left by the ribbed plow was further altered by the wheel passage of the tractor to which the plow was attached. These results suggest that further investigations should be made into how the depth of snow and snow removal procedures affect the visibility of road markings in snow.

To summarize, the fourth research objective was examining how driving automation systems can act as sensors to monitor the state of road infrastructure. Paper I reviewed how automated drivers sense their surroundings and process the sensory input. The findings suggest that the automated driver has a number of sensors that can be used for road asset monitoring, the most common and applicable being cameras and radars. The raw feeds from such systems are resource intensive in terms

of storage and communication bandwidth and are seldom willingly shared. However, the derived information represented by ADAS functionality represent data that is more accessible and less sensitive providing data sources to monitor both the state of road assets, e.g., road marking quality, and challenging weather conditions. In Paper III this was demonstrated by using the discrete data set from an LDW system. Logistic regression analyses showed that the success of the LDW system could be predicted by traditional measuring equipment. This suggests that the output of the LDW system is useful both to monitor the state of road markings for (predictive) maintenance applications and to identify situations where the LDW systems fail. The latter is needed input to be able to include the automated driver in considerations of road design and maintenance needs (e.g., marking type, marking color and the need for reapplication). Paper IV investigated the visibility of road markings in snow providing an example of how automated driving features can alert of conditions that are challenging for automated driving systems. When ADAS functionality fails on roads where they usually work fine, it can indicate that there are weather conditions or other events that require maintenance actions. This input can be correlated to data from road weather stations for confirmation. Such data can shed light on how weather conditions such as rain or snow affect the functionality of ADAS features and higher levels of automation. Based on these data, road maintenance actions can be taken, predictive maintenance systems can be trained, and information on the needs of automated drivers can be collected for instance to be used in relation to ODDs and ISAD frameworks.

4.5 Summary of Main Results

The following section provides a concise summary of the results of each research objective.

RO1: Establish Automated Drivers as New Road Users Including Identifying Their Characteristics and How They Compare to Human Drivers’.

- A unified framework for automated and human driving was developed in Paper I (see **Figure 4.1**).
- The following characteristics of automated drivers were found to have high relevance to transport engineering:
 - Increased electromagnetic (EM) range.
 - Greater field of view (FOV).
 - Fundamental differences in cognitive processes.
- Evaluation of geometric design parameters in RO2 also contributed towards establishing automated drivers as new road users.

RO2: Evaluate geometric road design parameters with regards to automated drivers, in both the short and long term.

- Geometric road design parameters that need to be redefined in the short term were identified, these were:

- *Eye height, Object height, and Reaction time.* New definitions of parameters could include combining eye height and object height to new design parameters describing line of sight and object detection for automated drivers.
- A new manual for road design for transportation without human occupants is advised. The following geometric road design parameters can be revised with regards to automated freight transport: *Vertical acceleration, Relative vertical speed, Minimum vertical curve radius (sag), Clothoid parameter, and Minimum horizontal curve radius (tunnels).*
- Changes related to the shape and dynamic properties of vehicles should be monitored for changes including *Vehicle height, Vehicle width, Wheel distance, Overhang, Acceleration, Deceleration, and Reaction time.*

RO3: Examine how road infrastructure design and maintenance can facilitate automated driving.

- Color, pattern, and texture can be researched to create higher visibility and recognizable signatures for road infrastructure elements such as guardrails, dividers, and road markings.
- The higher range of electromagnetic sensitivity of automated users suggest that additional information can be embedded in road infrastructure elements visible only to automated drivers, e.g., a machine-readable layer in the near-UV for positioning.
- Contrast between road marking and road pavement is more important for visibility than retroreflectivity considering camera based Lane Departure Warning (LDW).
- LDW systems appear to not be dependent on exterior lighting (other than headlights).
- Yellow road markings have higher visibility and contrast to the road surface and snow in color spaces HSL, HSV, and YUV.
- Yellow road markings can facilitate automated driving in snow.
- Snow removal by a plow with a perforated steel edge appear to remove enough snow to make yellow road markings visible to cameras.
- The type and thickness of road marking may affect successful detection by camera based LDW.

RO4: Examine how driving automation systems can act as sensors to monitor the state of road infrastructure.

- LDW functionality demonstrates that ADAS can be used to monitor the state of road markings.

- LDW functionality can identify when conditions such as snow prevent detection of road marking.
- Output data from automated driving features (ADAS and higher levels of automation) represent data that is accessible, easy to share, and with few privacy concerns.
- ADAS data represent starting points for using data from driving automation systems to monitor and predict the maintenance needs of road assets.
- Data from ADAS systems can be used to define ODDs and ISAD levels.

4.6 Further Work

The unified model of driving was derived through an abductive approach and should thus be developed as the software and hardware that make up the automated driver evolves.

The characteristics identified for automated drivers, increased EM sensitivity, FOV and differences in cognition could be further investigated by:

- Researching the use of visibility in different parts of the EM spectrum for road applications.
- Researching the use of added information in existing road infrastructure for automated users (e.g., positions in signs).
- Researching how colors, patterns, and textures can be used actively to facilitate recognition of road infrastructure elements (e.g., guardrails, dividers, road markings).

Lidars do not see colors per se, and, unlike cameras, they actively transmit radiation making them independent of ambient light. Color still affects how visible an object is for lidars as lighter colors absorb less light than darker colors making lighter colored objects easier to detect. It could therefore be of interest to research the use of color and contrast in road infrastructure elements as it can be beneficial to human vision, camera-based vision, and lidars.

As an example, guardrails were found to be confused for lane markings in literature on automated lane detection. In **Figure 4.15** an image from a reference camera for a retroreflectometer is shown.

The image illustrates how guardrails and lane markings are similar in color and shape, thus causing confusion for automated detection. On the left-hand side of the vehicle the road markings are also white. These different traffic control devices and barriers can be hard to correctly identify, especially in the event of snow.

In addition to color, roughness and reflectivity of the objects also affect how they are perceived by active sensors such as lidars and radars. The surface qualities determine how much light is reflected back and how this signal appears, e.g., smooth surfaces reflect the light as a specular reflection, while rough surfaces create diffuse reflection. It is possible to take advantage of this phenomena and further investigate how the surface texture can help in classification of road environment objects such as curbs, dividers, road markings, and guardrails.



FIGURE 4.15: Example of similarity of different road infrastructure elements considering automated detection. Photo: NPRA.

The evaluations of geometric road design parameters suggested, in the short term, a redefinition of the *Eye height*, *Object height* and *Reaction time*. How these parameters are used in relation to automated drivers needs research and involvement from road authorities. In the longer term, developing a separate standard of geometric road design considering transportation without human passengers, i.e., automated freight, is encouraged.

The thesis demonstrated uses of camera based ADAS for 1) identifying how road design and maintenance can facilitate driving automation, 2) monitoring the state of road infrastructure assets, and 3) providing input towards defining ODDs and ISADS based on driving automation. However, the research findings of this thesis should be validated by additional tests.

The use of camera based LDW to monitor the quality of road markings shown in Paper III could be validated by performing additional testing with multiple vehicles with different makes of LDW/lane keeping systems. Testing during a greater range of ambient light conditions could verify the indication that LDWs are independent of external light sources (other than the car's headlights). The type of road marking used, the marking thickness, the time since application, and traffic volumes (including heavy vehicles) could shed additional light on the optimal design and maintenance of road markings for camera based lane detection. Additional testing to verify that contrast is a more relevant quality parameter for camera based lane detection than retroreflectivity is suggested. The importance of contrast for automated lane detection also implies that the asphalt used, and its condition, affects the success of automated lane detection. Darker colors are optimal to increase the contrast between road markings and road surface. Harmonization of the definition of contrast ratios used for road marking assessment is advised to enable comparison of research results. Alternatively, it is helpful to have access to the return signal of both road markings and road surface when using active measurements such as retroreflectometers.

To support the findings in Paper IV, further evaluation of the visibility of white and yellow road markings in snowy conditions for human and automated drivers could be performed. For visual analyses, a group of people could be used to achieve more representative evaluations of visibility of road markings for human vision. The classification of the visibility of road markings could be improved by using more categories than the three (not visible, somewhat visible, and clearly visible) used in

this research. For automated drivers, image or video capture by other types of cameras, including high-end cameras and in-vehicle cameras from different producers, are needed to verify the results of Paper IV that yellow road markings can provide better visibility than white markings in snowy conditions. For the maintenance aspects of Paper IV, investigating how different snow removal procedures affect the visibility of markings would be beneficial for establishing winter maintenance procedures to support automation and as input to ODD considerations. Further investigations on possible thresholds of snow depths related to automated lane detection and other ADAS functions are also advised as a means to establish maintenance procedures and ODDs for automated drivers.

This thesis investigated automated detection of road markings, the most widely used traffic control device, as an example of driving automation functionality. This is one of many automated driving features and other ADAS functionality including sign detection and ACC should be explored. More advanced automated driving features, such as tracking and classification of dynamic objects, and the general use of ML and AI, provide further options for research. As the field of driving automation is so vast and complex, the use of familiar ADAS features that are widely used on public roads could continue to provide a useful approach for research on how to design and maintain roads for both human and automated drivers.

Chapter 5

Conclusion and Further Perspectives

This research sought to initiate the process of including automated drivers as new road users by identify starting points for adapting road design and maintenance to facilitate automated driving.

The first paper established automated drivers as new road users. It introduced a unified framework for human and automated driver that for the first time covers all driving processes. Based on this framework, characteristics pertaining to automated drivers were identified and compared to human drivers. The main differences were found to be their field of view (FOV), electromagnetic (EM) sensitivities and cognition. The sensors and software used for automated driving features give automated drivers some of their driving characteristics. These are used in advanced driver assistance system (ADAS) functionality as well as in higher levels of automation. ADAS functionality such as lane departure warning (LDW) represent readily available data sources that road owners and operators (ROOs) can use to understand what parts of the road infrastructure are well suited for automated drivers and which are not. This information can be used to research adaptations to the physical infrastructure, such as the use of colors, textures, and patterns in road design to increase recognizability of different road infrastructure elements. This can make classification of objects faster and more accurate which could positively impact reaction times and traffic safety.

The characteristics of automated drivers established in Paper I were used to examine how automated driving will affect geometric design parameters in Paper II. Paper II provided suggestions for adapting geometric road design to facilitate automated driving in both the short term and the long term. In the short term, the geometric design parameters *Eye height*, *Object height*, and *Reaction time* need to be re-defined for automated users. *Eye height* and *Object height* can for instance be replaced with parameters describing sight distances and object detection. In the longer term, parameters that were found to have potential for creating more flexible road design for automated freight transport were identified: *Vertical acceleration*, *Relative vertical speed*, *Minimum vertical curve radius (sag)*, *Clothoid parameter*, and *Minimum horizontal curve radius (tunnels)*. Also, in a long-term perspective, parameters related to vehicle dynamics, e.g., *Reaction time*, *Acceleration* and *Deceleration*, should be monitored with changes in vehicles and increasing automation as these can affect design parameters including *Stopping*, *Meeting* and *Passing sight distances*.

Papers III and IV demonstrated that existing driving automation functionality such as LDW can be used to find avenues of applied research for adapting road design and maintenance to facilitate automated driving. Paper III compared lane detection by LDW to lane quality assessment by retroreflectometer. The results indicate that LDW systems can provide efficient ways of monitoring the state of road assets such as road markings. Paper IV demonstrated that yellow road markings have significantly higher visibility than white markings in snowy conditions in color channels HSV-S, HSL-S and YUV-U/V. Results indicate that the yellow road markings stayed visible in these color channels in snow depths of 0.5 cm. Snow removal procedures by plow with a perforated edge and brush were highly effective in making the yellow road marking visible. Two of the most commonly used color spaces, RGB and grayscale, were found to be less suited for lane detection in snow considering automated road marking detection.

ADAS constitutes mobile sensor systems that were shown to provide data useful for monitoring the state of road markings. Crowd-sourced data from other sources including mobile phones, road weather stations, camera surveillance and vehicles are also of interest in providing efficient ways of monitoring road assets. ADAS systems are at present time particularly valuable as the information produced by such systems are anonymous and compact. ADAS outputs are therefore easy to share both with respect to privacy issues and required communication infrastructure. Furthermore, ADAS are functionalities that are designed to help with driving tasks and represent lower levels of automation in driving. Where they fail are, therefore, as interesting as where they work as this provides insight into how to adapt road infrastructure to support automated driving.

ADAS, and other crowd-sourced data, can be used to optimize maintenance such as reapplication of painting or snow removal, as well as to determine the needed level of service to support driving automation. In essence, these data are descriptions of operational design domains (ODDs). The insight into the sensory performance of automated drivers should thus be a source of knowledge for deciding the conditions for which driving automation can be allowed. This should also affect how the ODDs themselves are defined. As the sensor systems of automated drivers might require other quality measures than human drivers (e.g., contrast versus retroreflectivity for road markings), there will be a need to consider new ways of classifying road infrastructure and driving conditions as seen from the perspective of the automated driver. For instance, ROOs might refer to road classes as part of an ODD, but it might be of greater importance what type of marking and pavement type (in relation to contrast between the two) was used, and their condition, to determine which roads are suited for automated driving. As such, automated drivers represent many unknowns but are also the proverbial well of Mimir for adapting the road design and maintenance to support automation.

This research has established automated drivers as new road users and suggested paths forward to adapt road design and maintenance to facilitate automated driving. These are starting points in processes to include automated drivers as new road users. Automated driving can make roads safer, but this requires cooperation between manufacturers of sensors, software, and vehicles, as well as road owners and regulators, in continued research efforts to improve driving automation and develop the road infrastructure to support it.

Bibliography

- Ai, Chengbo and Yichang James Tsai (2016). "An automated sign retroreflectivity condition evaluation methodology using mobile LIDAR and computer vision". In: *Transportation Research Part C: Emerging Technologies* 63, pp. 96–113. ISSN: 0968090X. DOI: 10.1016/j.trc.2015.12.002. URL: <http://dx.doi.org/10.1016/j.trc.2015.12.002>.
- Aly, Mohamed (2008). "Real time detection of lane markers in urban streets". In: *IEEE Intelligent Vehicles Symposium, Proceedings*. California Institute of Technology, Eindhoven, Netherlands, pp. 7–12. ISBN: 9781424425693. DOI: 10.1109/IVS.2008.4621152. arXiv: 1411.7113. URL: <https://arxiv.org/pdf/1411.7113.pdf>.
- American Association of State Highway and Transportation Officials (2011). *A Policy on Geometric Design of Highways and Streets*. 6th ed. Washington DC, USA: American Association of State Highway and Transportation Officials.
- American Society for Testing and Materials (2005). *ASTM E1710-05, Standard Test Method for Measurement of Retroreflective Pavement Marking Materials with CEN-Prescribed Geometry Using a Portable Retroreflectometer*. Tech. rep. West Conshohocken, Pennsylvania, USA: ASTM International. DOI: 10.1520/E1710-05. URL: www.astm.org.
- Bagot, Keith W. (1995). *Evaluation of Alternative Pavement Marking Materials*. Tech. rep. Springfield, VA, USA: Federal Aviation Administration.
- Bahlmann, Claus et al. (2005). "A system for traffic sign detection, tracking, and recognition using color, shape, and motion information". In: *IEEE Intelligent Vehicles Symposium, Proceedings 2005*, pp. 255–260. DOI: 10.1109/IVS.2005.1505111.
- Barbøl, Hans Kristian (2017). *Børsteoppsett for vintervedlikehold på vei*. URL: <https://www.at.no/anlegg/371475> (visited on 03/03/2021).
- Branson, Steve et al. (2014). "The ignorant led by the blind: A hybrid human-machine vision system for fine-grained categorization". In: *International Journal of Computer Vision* 108.1-2, pp. 3–29. ISSN: 15731405. DOI: 10.1007/s11263-014-0698-4.
- Carlson, Paul J., Eun Sug Park, and Carl K. Andersen (2009). "Benefits of pavement markings: A renewed perspective based on recent and ongoing research". In: *Transportation Research Record* 2017.1, pp. 59–69. ISSN: 03611981. DOI: 10.3141/2107-06.
- Chan, Ching Yao (2017). "Advancements, prospects, and impacts of automated driving systems". In: *International Journal of Transportation Science and Technology* 6.3, pp. 208–216. ISSN: 20460449. DOI: 10.1016/j.ijtst.2017.07.008. URL: <https://doi.org/10.1016/j.ijtst.2017.07.008>.
- Chauhan, Praveen, Prateek Luthra, and Irshad Ahmad Ansari (2020). "Road Sign Detection Using Camera for Automated Driving Assistance System". In: *SSRN Electronic Journal*, pp. 1–8. ISSN: 1556-5068. DOI: 10.2139/ssrn.3573876.

- Chen, Chenyi et al. (2015). "DeepDriving: Learning Affordance for Direct Perception in Autonomous Driving". In: *2015 IEEE International Conference on Computer Vision (ICCV)*. Princeton Vision and Robotics. Santiago. ISBN: 9780123739063. DOI: 10.1016/S1573-4285(07)00003-8. URL: <http://deepdriving.cs.princeton.edu>.
- Collin, Anne et al. (2019). "Autonomous driving systems hardware and software architecture exploration: optimizing latency and cost under safety constraints". In: *Systems Engineering* October 2018, pp. 327–337. ISSN: 15206858. DOI: 10.1002/sys.21528.
- Cruz, Marisa, Alexander Klein, and Viviana Steiner (2016). "Sustainability Assessment of Road Marking Systems". In: *Transportation Research Procedia* 14, pp. 869–875. ISSN: 23521465. DOI: 10.1016/j.trpro.2016.05.035. URL: <http://dx.doi.org/10.1016/j.trpro.2016.05.035>.
- Duarte, Fábio and Carlo Ratti (2018). "The Impact of Autonomous Vehicles on Cities: A Review". In: *Journal of Urban Technology* 25.4, pp. 3–18. ISSN: 14661853. DOI: 10.1080/10630732.2018.1493883.
- Easa, Said M. and Essam Dabbour (2003). "Design radius requirements for simple horizontal curves on three-dimensional alignments". In: *Canadian Journal of Civil Engineering* 30.6, pp. 1022–1033. ISSN: 03151468. DOI: 10.1139/103-022.
- Elvik, Rune (2017). "Can evolutionary theory explain the slow development of knowledge about the level of safety built into roads?" In: *Accident Analysis and Prevention* 106, June, pp. 166–172. ISSN: 00014575. DOI: 10.1016/j.aap.2017.06.008. URL: <https://doi.org/10.1016/j.aap.2017.06.008>.
- Erdelean, Isabela and Denitsa Osichenko (2014). *CEDR Contractor Report Asset Management and Maintenance*. Tech. rep. Vienna, Austria: AIT.
- Erhart, Jacqueline et al. (2020). "Infrastructure support for automated driving: Further enhancements on the ISAD classes in Austria". In: *Proceedings of 8th Transport Research Arena TRA 2020*. Vol. 43. 0. Helsinki, Finland. URL: <https://www.researchgate.net/publication/339339109>.
- Ertrac (2019). *Connected Automated Driving Roadmap*. Tech. rep. Brussels, Belgium: European Road Transport Research Advisory Council. URL: https://connectedautomateddriving.eu/wp-content/uploads/2019/04/ERTRAC-CAD-Roadmap-03.04.2019-1.pdf?fbclid=IwAR3ynV70pUc07z03Y1PqQKe4S5xgY_sW8kMbnocwTZ7S78Cfz8upjPKRKpo.
- European Commission (2018). *On the road to automated mobility: An EU strategy for mobility of the future*. Tech. rep. Brussels, Belgium: European Commission. DOI: 10.1142/S1793830917500227. URL: https://ec.europa.eu/growth/content/guidelines-exemption-procedure-eu-approval-automated-vehicles_en.
- Farah, Haneen et al. (2018). "Infrastructure for Automated and Connected Driving: State of the Art and Future Research Directions". In: *Road Vehicle Automation* 4, pp. 187–197. ISBN: 978-3-319-60933-1. DOI: 10.1007/978-3-319-60934-8. arXiv: 9605103 [cs]. URL: <http://link.springer.com/10.1007/978-3-319-60934-8>.
- Fares, Hussam et al. (2010). "Modelling the performance of pavement marking in cold weather conditions Modelling the performance of pavement marking in cold weather conditions". In: *Structure and Infrastructure Engineering*. DOI: 10.1080/15732479.2010.504212. URL: <https://www.tandfonline.com/action/journalInformation?journalCode=nsie20>.

- Finnish Transport and Communications Agency (2020). *New road markings and traffic signs* | Traficom. URL: <https://www.traficom.fi/en/transport/road/new-road-markings-and-traffic-signs> (visited on 09/16/2020).
- Fleuret, François et al. (2011). "Comparing machines and humans on a visual categorization test". In: *Proceedings of the National Academy of Sciences of the United States of America* 108.43, pp. 17621–17625. ISSN: 00278424. DOI: 10.1073/pnas.1109168108.
- Galvani, Marco (2019). "Classifications of Safety Systems". In: *IEEE Instrumentation & Measurement Magazine* 22.1, pp. 11–16. DOI: 10.1109/MIM.2019.8633345.
- García, Alfredo, Francisco Javier Camacho-Torregrosa, and Pedro Vinicio Padovani Baez (2020). "Examining the effect of road horizontal alignment on the speed of semi-automated vehicles". In: *Accident Analysis and Prevention* 146.March, p. 105732. ISSN: 00014575. DOI: 10.1016/j.aap.2020.105732. URL: <https://doi.org/10.1016/j.aap.2020.105732>.
- Gargoum, Suliman et al. (2017). "Automated highway sign extraction using lidar data". In: *Transportation Research Record* 2643, pp. 1–8. ISSN: 03611981. DOI: 10.3141/2643-01.
- Gibbons, Ronald B, Jonathan Hankey, and Irena Pashaj (2004). *Wet night visibility of pavement markings: Executive summary*. Tech. rep. Charlottesville, VI, USA: Virginia Transportation Research Council.
- Hadi, Mohammed and Prasoon Sinha (2011). "Effect of pavement marking retroreflectivity on the performance of vision-based lane departure warning systems". In: *Journal of Intelligent Transportation Systems: Technology, Planning, and Operations* 15.1, pp. 42–51. ISSN: 15472450. DOI: 10.1080/15472450.2011.544587.
- Hallmark, Shauna, David Veneziano, and Theresa Litteral (2019). *Preparing Local Agencies for the Future of Connected and Autonomous Vehicles*. Tech. rep. May. St. Paul, MN, USA: Minnesota Department of Transportation. URL: <http://mndot.gov/research/reports/2019/201918.pdf>.
- Hartwich, Franziska, Matthias Beggiano, and Josef F. Krems (2018). "Driving comfort, enjoyment and acceptance of automated driving—effects of drivers' age and driving style familiarity". In: *Ergonomics* 61.8, pp. 1017–1032. ISSN: 13665847. DOI: 10.1080/00140139.2018.1441448. URL: <https://doi.org/10.1080/00140139.2018.1441448>.
- Hills, B. L. (1980). "Vision, visibility, and perception in driving". In: *Perception* 9.2, pp. 183–216. ISSN: 03010066. DOI: 10.1068/p090183. URL: <https://journals.sagepub.com/doi/pdf/10.1068/p090183>.
- Hoang, Toan Minh et al. (2017). "Road lane detection robust to shadows based on a fuzzy system using a visible light camera sensor". In: *Sensors (Switzerland)* 17.11. ISSN: 14248220. DOI: 10.3390/s17112475. URL: <https://www.scopus.com/inward/record.uri?eid=2-s2.0-85032682621&doi=10.3390>.
- International Organization for Standardization (2011). *Road vehicles – Functional safety – Part 9: Automotive Safety Integrity Level (ASIL)-oriented and safety-oriented analyses*. URL: <https://www.iso.org/standard/51365.html> (visited on 04/03/2019).
- Kang, Yong Suk and John B. Ferris (2018). "Performance Margin for Geometric Road Design". In: *SAE International Journal of Passenger Cars - Mechanical Systems* 11.4, pp. 6–11. ISSN: 19464002. DOI: 10.4271/06-11-04-0022.
- Kartverket (2020). *Kartverkets innspill til stortingsmeldingen om datadrevet økonomi og innovasjon*. Tech. rep. Hønefoss, Norway: Kommunal- og moderniseringsdepartementet, pp. 1–5.

- Kennedy, Brianna L. and Robert Thornberg (2018). "Deduction, Induction, and Abduction". In: *The SAGE Handbook of Qualitative Data Collection*. Ed. by Uwe Flick. London, UK: SAGE Publications Ltd, pp. 49–64. ISBN: 9781473952133. DOI: 10.4135/9781526416070.
- Khoury, John, Kamar Amine, and Rima Abi Saad (2019). "An Initial Investigation of the Effects of a Fully Automated Vehicle Fleet on Geometric Design". In: *Journal of Advanced Transportation* 2019.May, pp. 1–10. ISSN: 20423195. DOI: 10.1155/2019/6126408.
- Koopman, Philip and Michael Wagner (2017). "Autonomous Vehicle Safety: An Interdisciplinary Challenge". In: *IEEE Intelligent Transportation Systems Magazine* 9.1, pp. 90–96. ISSN: 19391390. DOI: 10.1109/IMITS.2016.2583491.
- Kruse, Kellee Boulais and Tom Simmer (2003). *Asset Management of Roadway Signs through Advanced Technology*. Tech. rep. Fargo, ND, USA: Upper Great Plains Transportation Institute North Dakota State University.
- Kumar, K Vasantha and William T Norfleet (1992). *Issues on Human Acceleration Tolerance After Long-Duration Space Flights*. Tech. rep. National Aeronautics and Space Administration. URL: <https://ntrs.nasa.gov/search.jsp?R=19930020462>.
- Kusano, Kristofer et al. (2014). "Potential Occupant Injury Reduction in the U.S. Vehicle Fleet for Lane Departure Warning-Equipped Vehicles in Single-Vehicle Crashes". In: *Traffic Injury Prevention* 15, S157–S164. ISSN: 1538957X. DOI: 10.1080/15389588.2014.922684. URL: <https://www.tandfonline.com/action/journalInformation?journalCode=gcpi20>.
- Kusano, Kristofer D. and Hampton C. Gabler (2015). "Comparison of Expected Crash and Injury Reduction from Production Forward Collision and Lane Departure Warning Systems". In: *Traffic Injury Prevention* 16, pp. 109–114. ISSN: 1538957X. DOI: 10.1080/15389588.2015.1063619. URL: <https://www.tandfonline.com/action/journalInformation?journalCode=gcpi20>.
- Lee, Chanho and Ji Hyun Moon (2018). "Robust lane detection and tracking for real-time applications". In: *IEEE Transactions on Intelligent Transportation Systems* 19.12, pp. 4043–4048. ISSN: 15249050. DOI: 10.1109/TITS.2018.2791572.
- Li, Jin and Andrew D Heap (2008). "A Review of Spatial Interpolation Methods for Environmental Scientists". In: *Australian Geological Survey Organisation* 68.2008/23, p. 154. ISSN: 1448-2177. DOI: http://www.ga.gov.au/image_cache/GA12526.pdf.
- Li, Shunxi et al. (2019). "Policy formulation for highly automated vehicles: Emerging importance, research frontiers and insights". In: *Transportation Research Part A: Policy and Practice* 124.May 2018, pp. 573–586. ISSN: 09658564. DOI: 10.1016/j.tratra.2018.05.010. URL: <https://doi.org/10.1016/j.tratra.2018.05.010>.
- Linsley, D. et al. (2017). "What are the Visual Features Underlying Human Versus Machine Vision?" In: *Proceedings - 2017 IEEE International Conference on Computer Vision Workshops, ICCVW 2017*. Vol. 2018-Janua. Venice, Italy, pp. 2706–2714. ISBN: 9781538610343. DOI: 10.1109/ICCVW.2017.331. arXiv: 1701.02704.
- Litman, Todd (2018). *Implications for Transport Planning*. Tech. rep. Victoria, Canada: Victoria Transport Policy Institute. URL: <file:///C:/Users/aned/Downloads/AutonomousVehicleImplementationPredictions.pdf>.
- Lundkvist, Sven-Olof and Carina Fors (2010). *Lane Departure Warning System – LDW Samband mellan LDW:s och vägmarkeringars funktion VTI notat 15-2010*. Tech. rep. Linköping, Sweden: VTI. URL: www.vti.se/publikationer.

- Lutin, Jerome M, A Kornhauser, and Eva Lerner-Lam (2013). "The Revolutionary Development of Self-Driving Vehicles and Implications for the Transportation Engineering Profession". In: *ITE Journal - Institute of Transportation Engineers* 88. URL: [ENoAVsupportConventionalinfrastructure,nodigitalinformation.AVsneedtorecognizeroadgeometryandsignage..](https://doi.org/10.1080/1080/1463922X.2020.1830450)
- Manchon, J. B., Mercedes Bueno, and Jordan Navarro (2020). "From manual to automated driving: how does trust evolve?" In: *Theoretical Issues in Ergonomics Science* 0.0, pp. 1–27. ISSN: 1464536X. DOI: 10.1080/1463922X.2020.1830450. URL: <https://doi.org/10.1080/1463922X.2020.1830450>.
- Matowicki, Michal, Ondrej Pribyl, and Pavel Pribyl (2016). "Analysis of possibility to utilize road marking for the needs of autonomous vehicles". In: *2016 Smart Cities Symposium Prague, SCSP 2016* May. DOI: 10.1109/SCSP.2016.7501026.
- Michon, John A. (1985). "Critical View of Driver Behavior Models: What Do We Know, What Should We Do?" In: *Human behavior and traffic safety*. Ed. by Leonard Evans and Richard C. Schwing. Springer, Boston, MA. Chap. A Critical, pp. 485–524. ISBN: 978-1-4613-2173-6.
- Migletz, J, Joseph K. Fish, and Jerry L. Graham (1994). *Roadway Delineation Practices Handbook*. Tech. rep. Washington DC, USA: Federal Highway Administration.
- Migletz, James et al. (1999). "Field Surveys of Pavement-Marking Retroreflectivity". In: *Transportation Research Record* 1657. URL: <https://journals.sagepub.com/doi/pdf/10.3141/1657-10>.
- Nathanson, Brian H. and Thomas L. Higgins (2008). "An introduction to statistical methods used in binary outcome modeling". In: *Seminars in Cardiothoracic and Vascular Anesthesia* 12.3, pp. 153–166. ISSN: 10892532. DOI: 10.1177/1089253208323415.
- Nayak, Abhishek et al. (2020). "Reference Test System for Machine Vision Used for ADAS Functions". In: *SAE Technical Papers* 2020-April. April, pp. 1–8. ISSN: 01487191. DOI: 10.4271/2020-01-0096.
- Nitsche, Philippe, Isabela Mocanu, and Martin Reinthaler (2014). "Requirements on tomorrow's road infrastructure for highly automated driving". In: *2014 International Conference on Connected Vehicles and Expo, ICCVE 2014 - Proceedings*. Shenzhen, China: IEEE, pp. 939–940. ISBN: 9781479967292. DOI: 10.1109/ICCVE.2014.7297694.
- OECD Road Research Group (1975). *Road Marking and Delineation*. Paris, France: Organization for Economic Co-operation and Development.
- Oregon Department of Transportation (2017). *Mobile LiDAR - Uses at Oregon DOT*. URL: https://www.gis.fhwa.dot.gov/webinars/webinar33_Uses_of_Mobile_LiDAR_at_ODOT.aspx (visited on 01/14/2021).
- Osichenko, Denitsa and Roland Spielhofer (2018). "Monitoring and inventory of road signs and road markings State of the art – a review of existing methods and systems". In: *Transport Research Arena*. Vienna, Austria, pp. 1–9. DOI: 10.5281/zenodo.1320919. URL: <https://zenodo.org/record/1320920#.X8DYaShKguU>.
- Östling, Martin et al. (2019). "Passenger Car Safety Beyond ADAS: Defining Remaining Accident Configurations as Future Priorities". In: *The 26th International Technical Conference on the Enhanced Safety of Vehicles*. Vol. Paper No. Eindhoven, Netherlands, pp. 19–0091. URL: https://www.researchgate.net/profile/Nils_Lubbe2/publication/333748876_Passenger_Car_Safety_Beyond_ADAS_Defining_Remaining_Accident_Configurations_As_Future_Priorities/links/5d03758a2

- 99bf13a3853f4bd/Passenger-Car-Safety-Beyond-ADAS-Defining-Remaining-Acci.
- Piksen, Johan Tobias (2018). "Physical Infrastructure Needs for Autonomous and Connected Trucks An Exploratory Study". PhD thesis. Norwegian University of Science and Technology.
- Pike, Adam, Paul Carlson, and Timothy Barrette (2018). *Evaluation of the Effects of Pavement Marking Width on Detectability By Machine Vision : 4-Inch vs 6-Inch Markings*. Tech. rep. January. Virginia, USA: American Traffic Safety Services Association. URL: https://www.researchgate.net/publication/330545262_Evaluation_of_the_Effects_of_Pavement_Marking_Width_on_Detectability_By_Machine_Vision_4-Inch_vs_6-Inch_Markings.
- Pike, Adam M., Timothy P. Barrette, and Paul J. Carlson (2019). "Machine Vision Detection of Pavement Markings". In: *TRB 2019 Annual Meeting*. Washington DC, USA: TRB. ISBN: 0963-8199. DOI: 10.1080/09638190500372404.
- Pike, Adam M. and Bharadwaj Bommanayakanahalli (2018). "Development of a Pavement Marking Life Cycle Cost Tool". In: *Transportation Research Record 2672.12*, pp. 148–157. ISSN: 21694052. DOI: 10.1177/0361198118758012.
- Podpora, Michal, Grzegorz Paweł Korbaś, and Aleksandra Kawala-Janik (2014). "YUV vs RGB—Choosing a Color Space for Human-Machine Interaction". In: *Position Papers of the 2014 Federated Conference on Computer Science and Information Systems 3*. September, pp. 29–34. ISSN: 2300-5963. DOI: 10.15439/2014f206.
- Rezwanul Haque, Md. et al. (2019). "A Computer Vision based Lane Detection Approach". In: *International Journal of Image, Graphics and Signal Processing 11.3*, pp. 27–34. ISSN: 20749074. DOI: 10.5815/ijigsp.2019.03.04.
- SAE International (2018). *SAE J3016 Surface Vehicle Recommended Practice*. Tech. rep. 724. Warrendale, PA, USA: SAE International, pp. 1–5. URL: http://standards.sae.org/J2016_201806.
- Satterfield, Cathy (2014). *Methods for Maintaining Pavement Marking Retroreflectivity*. Tech. rep. URL: https://safety.fhwa.dot.gov/roadway_dept/night_visib/fhwasa14017/fhwasa14017.pdf.
- Shladover, Steven E. (2018). "Connected and automated vehicle systems: Introduction and overview". In: *Journal of Intelligent Transportation Systems: Technology, Planning, and Operations 22.3*, pp. 190–200. ISSN: 15472442. DOI: 10.1080/15472450.2017.1336053.
- Snyder, James et al. (2018). "Invisible" 2D Bar Code to Enable Machine Readability of Road Signs—Material and Software Solutions. Tech. rep. St. Paul, MN, USA: 3M. URL: <https://multimedia.3m.com/mws/media/15840510/2d-barcode-whitepaper.pdf>.
- Statens vegvesen (2005). *Asfalt 2005-materialer og utførelse Håndbok 246*. Ed. by Sigmund Dørum. Trondheim, Norway: Vegdirektoratet. ISBN: 82-7207-552-0. URL: www.vegvesen.no/handboker.
- (2015). *Håndbok N302 Vegoppmerking - Tekniske bestemmelser og retningslinjer for anvendelse og utforming*. Oslo, Norway: Vegdirektoratet. ISBN: 9788272076855. URL: www.vegvesen.no.
- (2018). *Vegbygging – Håndbok N200*. Oslo, Norway: Statens vegvesen, p. 308. ISBN: 9788272077234.
- (2019a). *Håndbok N100 - Veg- og gateutforming*. Oslo, Norway: Vegdirektoratet. ISBN: 9788272077449. URL: www.vegvesen.no.

- (2019b). *Håndbok V120 Premisser for geometrisk utforming av veger*. Norwegian Public Roads Administration. ISBN: 9788272077456. URL: www.vegvesen.no . .
- (2019c). *Riksvegutredningen 2019*. Tech. rep. Oslo, Norway: Statens vegvesen.
- (2021). *Vegkart*. URL: <https://vegkart.atlas.vegvesen.no/#kartlag:geodata/@600000,7225000,3> (visited on 02/12/2021).
- Sternlund, Simon (2017). “The safety potential of lane departure warning systems—A descriptive real-world study of fatal lane departure passenger car crashes in Sweden”. In: *Traffic Injury Prevention* 18, S18–S23. ISSN: 1538957X. DOI: 10.1080/15389588.2017.1313413. URL: <https://www.tandfonline.com/action/journalInformation?journalCode=gpci20>.
- Storsæter, Ane Dalsnes, Kelly Pitera, and Edward D. McCormack (2020). “The Automated Driver as a New Road User”. In: *Transport Reviews*. DOI: 10.1080/01441647.2020.1861124.
- Teoh, Eric R. and David G. Kidd (2017). “Rage against the machine? Google’s self-driving cars versus human drivers”. In: *Journal of Safety Research* 63, pp. 57–60. ISSN: 00224375. DOI: 10.1016/j.jsr.2017.08.008.
- Thamizharasan, Akila et al. (2003). “A Methodology for Estimating the Lifecycle of Interstate Highway Pavement Marking Retroreflectivity”. In: *Transportation Research Board Annual Meeting* 843. URL: http://www.ltrc.lsu.edu/TRB_82/TRB2003-001867.pdf.
- Transport Research Board (1997). *Determination of Stopping Sight Distances NCHRP Report 400*. Tech. rep. Washington DC, USA: Transportation Research Board.
- Vegdirektoratet (2012). *Opplæring i drift og vedlikehold for operatører*. Tech. rep. 131. Oslo, Norway: Statens vegvesen.
- Vegdirektoratet (2017). *LTA 2011 : Oppfølging av prøvestrekninger 2016*. Tech. rep. Trondheim, Norway: Statens vegvesen, pp. 1–28.
- Wang, Kelvin C.P., Zhiqiong Hou, and Weiguo Gong (2010). “Automated road sign inventory system based on stereo vision and tracking”. In: *Computer-Aided Civil and Infrastructure Engineering* 25.6, pp. 468–477. ISSN: 10939687. DOI: 10.1111/j.1467-8667.2010.00657.x.
- Washburn, Scott S. and Leslie D. Washburn (2018). *Future Highways-Automated Vehicles*. Tech. rep. Wellington, Florida, USA: SunCam. URL: www.SunCam.com.
- Weiss, Brandi A. and William Dardick (2020). “Making the Cut: Comparing Methods for Selecting Cut-Point Location in Logistic Regression”. In: *Journal of Experimental Education* 0.0, pp. 1–21. ISSN: 19400683. DOI: 10.1080/00220973.2019.1689375. URL: <https://doi.org/10.1080/00220973.2019.1689375>.
- Wood, Jonathan S. and Eric T. Donnell (2017). “Stopping sight distance and available sight distance new model and reliability analysis comparison”. In: *Transportation Research Record* 2638.1, pp. 1–9. ISSN: 21694052. DOI: 10.3141/2638-01.
- Xing, Yang et al. (2018). “Advances in Vision-Based Lane Detection: Algorithms, Integration, Assessment, and Perspectives on ACP-Based Parallel Vision”. In: *IEEE/CAA Journal of Automatica Sinica* 5.3, pp. 645–661. ISSN: 23299274. DOI: 10.1109/JAS.2018.7511063.
- Yi, Shu Chung, Yeong Chin Chen, and Ching Haur Chang (2015). “A lane detection approach based on intelligent vision”. In: *Computers and Electrical Engineering* 42.2, pp. 23–29. ISSN: 00457906. DOI: 10.1016/j.compeleceng.2015.01.002. URL: <http://dx.doi.org/10.1016/j.compeleceng.2015.01.002>.

Zwahlen, Helmut T and Thomas Schnell (2000). "Minimum In-Service Retroreflectivity of Pavement Markings". In: *Transportation Research Record 1715*. URL: <https://journals.sagepub.com/doi/pdf/10.3141/1715-09>.

Appendix A

Paper I



Transport Reviews

ISSN: (Print) (Online) Journal homepage: <https://www.tandfonline.com/loi/ttrv20>

The automated driver as a new road user

Ane Dalsnes Storsæter , Kelly Pitera & Edward D. McCormack

To cite this article: Ane Dalsnes Storsæter , Kelly Pitera & Edward D. McCormack (2020): The automated driver as a new road user, Transport Reviews, DOI: [10.1080/01441647.2020.1861124](https://doi.org/10.1080/01441647.2020.1861124)

To link to this article: <https://doi.org/10.1080/01441647.2020.1861124>



© 2020 The Author(s). Published by Informa UK Limited, trading as Taylor & Francis Group



Published online: 21 Dec 2020.



Submit your article to this journal [↗](#)



View related articles [↗](#)



View Crossmark data [↗](#)

The automated driver as a new road user

Ane Dalsnes Storsæter ^{a,b}, Kelly Pitera ^b and Edward D. McCormack ^{b,c}

^aNorwegian Public Roads Administration, Trondheim, Norway; ^bDepartment of Civil and Environmental Engineering, Norwegian University of Science and Technology (NTNU), Trondheim, Norway; ^cCivil and Environmental Engineering, University of Washington, Seattle, WA, USA

ABSTRACT

Although road infrastructure has been designed to accommodate human drivers' physiology and psychology for over a century, human error has always been the main cause of traffic accidents. Consequently, Advanced Driver Assistance Systems (ADAS) have been developed to mitigate human shortcomings. These automated functions are becoming more sophisticated allowing for Automated Driving Systems (ADS) to drive under an increasing number of road conditions. Due to this evolution, a new automated road user has become increasingly relevant for both road owners and the vehicle industry alike. While this automated driver is currently operating on roads designed for human drivers, in the future, infrastructure policies may be designed specifically to accommodate automated drivers. However, the current literature on ADSs does not cover all driving processes. A unified framework for human and automated driver, covering all driving processes, is therefore presented. The unified driving framework, based on theoretical models of human driving and robotics, highlights the importance of sensory input in all driving processes. How human and automated drivers sense their environment is therefore compared to uncover differences between the two road users relevant to adapt road design and maintenance to include the automated driver. The main differences identified between human and automated drivers are that (1) the automated driver has a much greater range of electromagnetic sensitivity and larger field of view, and (2) that the two road users interpret sensory input in different ways. Based on these findings, future research directions for road design and maintenance are suggested.

ARTICLE HISTORY



Received 26 August 2020
Accepted 1 December 2020

Keywords

Automated driving; road user; mobility innovations; transport and society; road infrastructure; policy; driver models; robotics

1. Introduction

Although roads have been developed to accommodate human physiology and psychology for over a century, human errors have been the main cause of traffic accidents (National Highway Traffic Safety Administration, 2015; Transportavdelingen Trafikksikkerhet, 2018), with driving performance failures being the greatest contributing factor to

CONTACT Ane Dalsnes Storsæter  ane.storsater@ntnu.no, ane.storsater@vegvesen.no  Norwegian Public Roads Administration, Abels gate 5, 7030 Trondheim, Norway

© 2020 The Author(s). Published by Informa UK Limited, trading as Taylor & Francis Group
This is an Open Access article distributed under the terms of the Creative Commons Attribution-NonCommercial-NoDerivatives License (<http://creativecommons.org/licenses/by-nc-nd/4.0/>), which permits non-commercial re-use, distribution, and reproduction in any medium, provided the original work is properly cited, and is not altered, transformed, or built upon in any way.

these accidents. Other errors in human behaviour include falling asleep, intoxication and distraction. Consequently, Advanced Driver Assistance Systems (ADAS) have been developed to mitigate human shortcomings. From the introduction of ADAS to higher levels of automation, automated driving features have evolved rapidly and are now able to take over operating a vehicle under an increasing number of road conditions. Due to this evolution, a new road user has emerged, the *automated driver*.

The automated driver comes with promise and possibilities. For example, in the short term, lower levels of automation represented by ADAS can reduce the number of traffic-related accidents (Eckstein & Zlocki, 2013; Östling, Lubbe, Jeppsson, & Puthan, 2019). Furthermore, the sensors utilised by the ADAS features, e.g. cameras and lidars, provide a way to monitor the road infrastructure. As identified by Osichenko and Spielhofer (2018), this can eventually replace manual and time-consuming processes used for monitoring road infrastructure inventory. Currently, maintenance and design factors remain that hinder the detection of inventory elements, including occlusion of signs, fading or damage to road signs and markings as well as improper installation (Osichenko & Spielhofer, 2018; Wali et al., 2019). Some of these issues can be mitigated by improving the automated detection equipment's hardware and software. The other piece of the puzzle might lie in making certain changes to roadway elements, such as paint type or texture choice, while others could be related to maintenance issues, e.g. trimming vegetation, or repainting road markings.

In the long term, higher levels of automation are widely expected to produce automated drivers that are superior to human drivers. Despite this expectation, little effort has been put into ensuring that the road infrastructure will work for the new automated road user. Consider the example of roadside LED signs and message boards, which have been developed as an improvement over conventional signs for humans, both in terms of visibility and use of dynamic information. On the other hand, LED flicker can adversely affect an automated driver's performance. This occurs because camera-based detection of signage typically uses algorithms to manage exposure, and LED flicker causes oscillations in overall image brightness, leading to automated drivers incorrectly identifying LED traffic signs (IEEE P2020 Working Group, 2018). Automated driving has also been suggested to be a factor that lowers road construction costs (Khoury, Amine, & Saad, 2019). The reasoning behind this claim is the idea that an automated driver is assumed to have different characteristics than humans, including longer sight distances, which might allow for a more flexible road design that better suits the terrain, leading to less earthwork during road construction.

Road authorities and society in general therefore have incentives both in terms of increased safety and higher cost-efficiency to adapt current road design policies to accommodate automated driving. In order to include the automated driver in road design, road authorities need to establish characteristics of these automated drivers that will impact road design and maintenance. SAE International's established definition of an automated driving system (ADS) provides a good taxonomy for describing the role of humans and ADS in driving tasks at different levels of automation (SAE International, 2018). However, it does not include details about these systems' software and hardware that shed light on how the ADS differs from human drivers.

In the following, a unified framework of driving covering both human and automated driver is presented based on existing theoretical models of human driving and mobile

robotics, respectively. The unified framework presents perception or sensing as a fundamental process in all phases of driving. Furthermore, perception/sensing represents the direct interaction between driver and road infrastructure and is therefore a natural starting point for understanding how road infrastructure design can facilitate automated driving. Using human senses (sight, hearing, smell, and sense of equilibrium) as references, the automated driver's sensors will be compared and contrasted with these human senses. Differences between the two road users are discussed, leading to suggestions for road infrastructure design adaptations that could facilitate automated drivers.

2. The driving processes

2.1. Human driving

In order to drive safely, humans need to observe their environment and correctly analyse it. Groeger (2000) and Underwood and Radach (1998) describe this process as an initial assessment made of the scene that is immediately followed by rapid analysis. The next step is establishing regions of potential interest and identifying which parts of the scene require more attention. The understanding of the driving environment created in the driver's mind is referred to as "internal representation" (Van der Molen & Bötticher, 1988). This representation of the environment, along with continued sensory input, forms the information needed for humans to make decisions while driving, such as choosing their driving trajectories, speed, and manoeuvres.

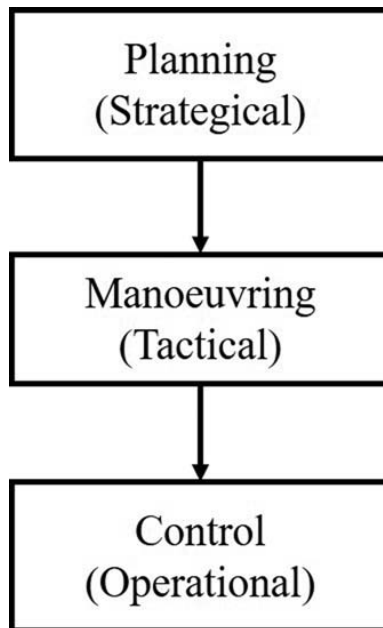


Figure 1. Human driving based on Michon (1985), Van der Molen and Bötticher (1988) and Nääänen and Summala (1974).

As shown in [Figure 1](#), human driving is often separated into three levels: the planning phase, the manoeuvring phase and the control phase (Michon, 1985; Näätänen & Summala, 1974; Van der Molen & Bötticher, 1988). In the planning phase, a human driver performs a strategical assessment of their choice of route, mode of transportation and intended cruising speed, weighing these against the aim of the trip and time available for it, e.g. getting to work on time.

In the manoeuvring phase, the overall plan from the planning phase is turned into tactical, long-term driving behaviour, for instance maintaining a preferred speed and following the intended route. Environmental input can change this process, for example, queues on the originally planned route can cause a change in route, or a slow-moving vehicle can introduce the need to overtake (Van der Molen & Bötticher, 1988).

Lying at the bottom of the hierarchy is the control level, which corresponds to the operations of the vehicle including steering, acceleration, and deceleration. This is also where emergency manoeuvring takes place.

2.2. Automated driving processes

The association SAE International has created a taxonomy for driving automation where the degree of automation is divided into six levels. Level 0 represents no automation, whereas levels 1 and 2 are driving automation levels that support the human driver and are typically ADAS functions. Levels 3–5 differentiate between three levels of ADSs, which are defined as “The hardware and software that are collectively capable of performing the entire DDT [Dynamic Driving Task] on a sustained basis, regardless of whether it is limited to a specific operational design domain (ODD)” (SAE International, 2018).

The dynamic driving task entails the real-time operational and tactical functions required to operate in on-road traffic following the hierarchical structure for human driving presented in [Figure 1](#), yet excluding the strategic function, i.e. trip scheduling. The ODD is the set of conditions for which the automated features are expected to work. For instance, an ADS feature can be designed to operate only on access-controlled freeways with good lane markings in fair weather conditions. As the SAE definition of automated driving neither includes the strategic level nor goes into specifics on how the vehicle works in terms of hardware or software, the framework developed in this paper will introduce automated driving in terms of frameworks taken from the field of robotics. This will allow a more comprehensive definition of automated driving processes, and subsequently the creation of a unified framework for human and automated driving.

Developed half a century ago using Shakey, the first mobile robot, the field of robotics describes the way a machine moves by naming three distinct processes: sense, plan and act (known as *S-P-A architecture*) (Nilsson, 1984). A shortcoming of this architecture is that a robot has to stop and process information before moving, which creates a stop-and-go movement instead of a continuous trajectory (Gat, Bonnasso, & Murphy, 1998). In the mid-eighties, Brooks introduced a reactive alternative known as *subsumption architecture* which, unlike *S-P-A architecture*, did not have to execute movements sequentially. This ability provided more fluid motion as it reacted faster to its surroundings, but had the drawback of not being easily taskable, meaning that it needed to be reprogrammed for new tasks (Brooks, 1986). A third category of robotic architecture is the *hybrid system*, which incorporates the deliberative *S-P-A architecture* in order to obtain the

best high-level control, for instance finding the optimal path, as well as the reactive architecture's superior capability for obstacle avoidance in unknown and dynamic environments (Davies & Jnifene, 2007; Sheikh, Jamil, & Ayaz, 2014). An example of hybrid architecture adapted from Davies and Jnifene (2007) can be seen in Figure 2.

The Defense Advanced Research Projects Agency (DARPA) Urban Challenge of 2007 serves as an example of how hybrid architecture works. In this challenge, self-driving vehicles had to navigate a mock urban setting, while adhering to traffic rules including passing slow-moving vehicles, handling intersections with other vehicles, and parking (Montemerlo et al., 2009). Contestants were given a road network description file containing geometric information on lanes, lane markings, signage, and points of interest, such as check points, as well as an aerial image of the site. These elements constituted the *Global world model* available at the start of the challenge, while data gathered during driving could be used to enhance this model.

In the *Task manager* function, a destination was entered, for instance, reaching a given check point in the Urban Challenge. The desired destination and world model would then be used to calculate a planned path. This path could be implemented in different ways, either by using the fastest route or implementing strategies such as added risk management, for instance, by avoiding left turns. The *Global world model*, *Task manager* and *Path planner* make up the deliberate layer in Figure 2.

The vehicle's trajectory planning and control are in the reactive part of the system, which can handle new events and is dependent on sensory input. Based on the planned path from the deliberate layer and live sensor data, the vehicle finds the free space available and calculates the optimal trajectory. This process involves how the vehicle understands its own location, detecting static and moving objects in addition

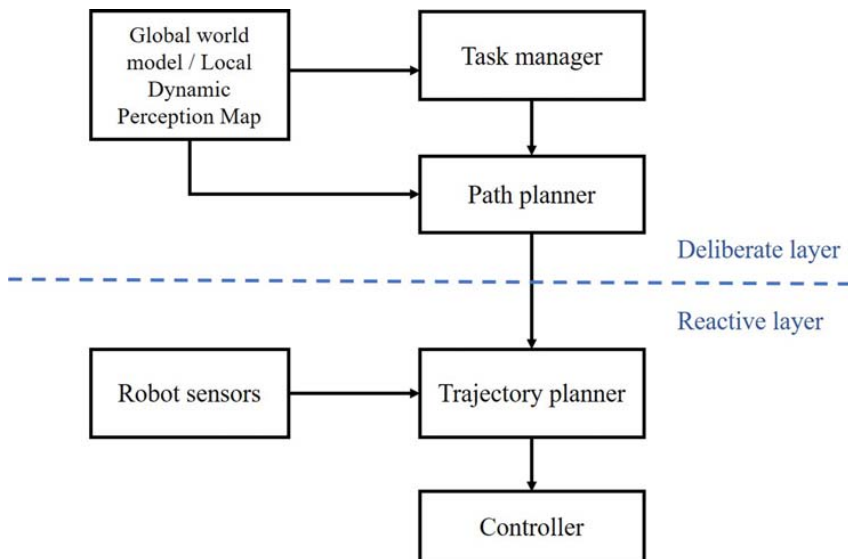


Figure 2. A hybrid robot control architecture adapted from Davies and Jnifene (2007).

to the expected movements of dynamic features, creating what Gruyer et al. (2017) refer to as a local dynamic perception map (LDPM). Trajectories can be altered by dynamic events like an object lying in the road, which imply that the vehicle needs to go around it. The chosen trajectory is translated into commands to control the vehicle's heading and speed and are therefore continually reassessed.

2.3. A unified framework for human and automated driving

As described previously, the processes by which human and automated drivers operate are similar. Thus, a unified framework for both human and automated driving is presented in Figure 3. Human and automated drivers alike use external sources of information to form a global world model based on maps and experience. Driving can be described for both human and automated drivers as starting with a deliberate planning stage where the goal of the trip is turned into a route. Next, the actual trajectories are chosen depending on the driver's local dynamic perception map, e.g. their knowledge of the route in question as well as their dynamic perception while driving. The drivers combine these factors into their actual control of the vehicle, always checking their planned action against their continual sensory input.

While human and automated driver operate in similar fashion on a general level, the way in which they solve their tasks is not the same. For example, in simple cases an automated system can find a suitable path faster than a human (McCourt, Mehta, Doucette, & Curtis, 2016). At the same time, dependent on conditions, path planning can be complex and computationally demanding for automated path planners, giving humans, with their ability to make intuitive decisions based on knowledge and experience, an advantage (Sun, Cai, & Shen, 2015). Due to their different strengths and weaknesses, human and

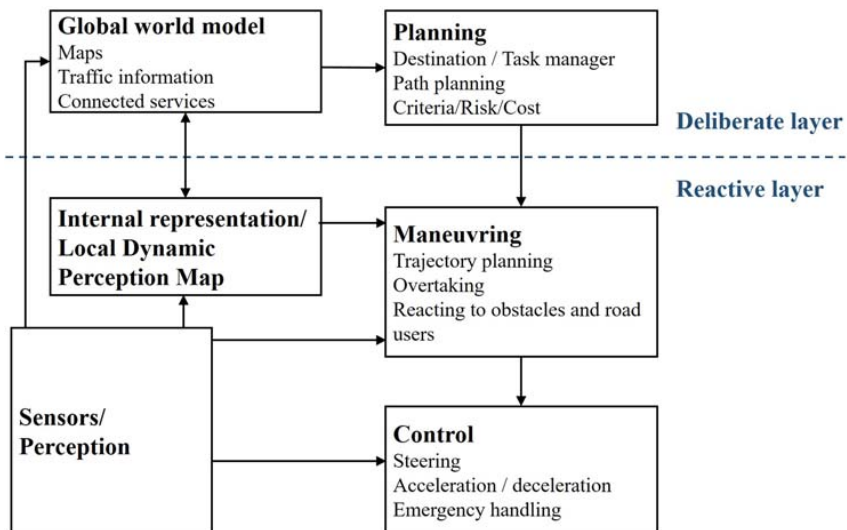


Figure 3. Framework for human and automated driving.

artificial intelligence is sometimes combined. This can be done by humans collaborating with a machine, for instance where they insert way points that are combined with automatic path planning. It may also take place as separate processes where human and machine choices comprised of separate confidence estimates are both inserted into a decision fusion algorithm. The benefit of a combined approach is that a man-machine solution can both realise dynamic threat avoidance and reflect personal preferences in chosen paths (McCourt et al., 2016; Sun et al., 2015).

In [Figure 3](#), the global world model includes external information which can be provided by getting access to positioning services, the internet, or other connected services such as ITS-G5/DSRC. Connectivity is thought to dramatically change the process of driving for automated drivers. Vehicles can first be alerted about objects or incidents that lie outside their sensor ranges and then communicate amongst themselves, theoretically eliminating rear-ending other vehicles, crashing into obstacles and even front-to-front collisions (Shladover, 2018). There are currently three standardisation initiatives for ITS-G5/DSRC (ARIB in Japan, WAVE in USA and ITS-G5 in the EU) based on the IEEE 802.11p protocol. It has been suggested that these communication protocols are not fully developed (Coutinho, Boukerche, & Loureiro, 2018). Insufficient communication quality in terms of packet delivery rate and update delay have been identified in the case of vehicle platooning (Rashdan, Müller, & Sand, 2016), while Zhao, Jing, Hui, Liu, and Khattak (2019) tested a DSRC-based rear-end collision warning system which had an average correct warning rate of 90%. Line of sight remains an issue for ITS-G5/DSRC (Huang, Zhao, & Peng, 2017; Lu, Cheng, Zhang, Shen, & Mark, 2014) as well as privacy (Eckhoff & Sommer, 2014). The alternative, cellular services, would need an unprecedented coverage and level of service to provide reliable vehicle to vehicle communication. The combination of short-range and cellular communication is promising according to Bey & Tewolde (2019) and Yang & Hua (2019). If the issues relating to the quality of communication services are solved, the safety benefit suggested by Shladover (2018) also requires full penetration of communication devices in vehicles. Furthermore, in some situations, such as avoiding crashing into obstacles, it would not be applicable for the first driver to reach the object as it relies on a prior road user to report the obstacle being present. Communication to and between vehicles still provides an external source of information that can provide safety benefits in both the short- and long term but cannot, to date, be assumed to be present at all times or in all cases.

[Figure 3](#) highlights how sensing/perception is essential to all driving processes. The way human and automated drivers alike sense their driving environment is also the most direct interaction between driver and roadway infrastructure: for both these reasons, the sensing processes of human and automated drivers are particularly focused on in the following section.

3. The sensing processes

Similar to humans, an automated driver is dependent on sensing its surroundings to be able to understand the traffic and the surrounding environment. To uncover significant differences between human and automated drivers that might impact road design, the following section compares the sensory system of the automated driver to that of the human.

As shown in [Figure 3](#) sensory input provides necessary input for the global world model, the internal representation, manoeuvring and control processes. In the case of humans, it is easy to only consider vision as the accepted primary sense when it comes to driving ([Macadam, 2003](#)). However, [Sivak \(1996\)](#) evaluated on-road behaviours critical to driving and found that roughly 30% of these were dependent on more than one sense. This finding can be related to the fact that human senses are not used separately, but rather form an understanding of a situation in conjunction with one another ([Guttman, Gilroy, & Blake, 2005](#); [Walker, Stanton, & Young, 2006](#)).

Humans have traditionally been said to have five senses (sight, hearing, taste, smell and touch), but this fails to recognise the kinesthetic system, which provides a human with an awareness of their position and movements ([Farnell & Miller Jr, 2018](#)). In the following, the definition by [Rye et al. \(2013\)](#) is used, where the five senses are defined as sight, hearing, smell, taste and equilibrium (balance and body position). The equilibrium sense includes the sense of touch, vestibular sensation (an organism's sense of spatial orientation and balance), proprioception (position of bones, joints, and muscles), and the sense of limb position that is used to track kinesthesia (limb movement).

Automated drivers have a range of sensors to generate the sensory input needed for driving. The selection and configuration of these vary between vehicles; however, the most commonly used sensors are laser, radar, lidar, ultrasonic and cameras ([Gruyer et al., 2017](#); [Hirz & Walzel, 2018](#); [Steinbaeck, Steger, Holweg, & Druml, 2017](#)). To some extent, these sensors are similar to human sensing as they function by processing the same physical effects and forces. For example, electromagnetic radiation is the basis for human vision and camera-based machine vision. The following section compares the sensory stimulus of human and automated drivers and summarises known differences. The human senses will all be covered with the exception of taste, which has limited use for driving purposes.

3.1. Vision

Human vision can be quantified by visual functions such as acuity, field, contrast, colour and night vision ([Colenbrander & De Laey, 2005](#)). Of these, visual acuity, i.e. the ability to resolve detail, is the only function that is regularly measured, while visual field and contrast sensitivity are only rarely considered ([Colenbrander & De Laey, 2005](#)). Despite its reliance on visual acuity, the relationship between visual acuity and safe driving is found to be weak at best ([Colenbrander & De Laey, 2005](#); [Hills, 1980](#); [Owsley & McGwin, 2010](#)). Rather, visual acuity is most commonly determined by drivers having relatively good vision, for instance, 20/40 ([Colenbrander & De Laey, 2005](#)), while sight distances for road signs in the US assume 20/30 binocular visual acuity ([Owsley & McGwin, 2010](#)).

Merely looking at visual functions does not fully describe human vision, on the contrary, training, experience and familiarity with the driving environment all affect how human drivers see their surroundings, referred to by [Colenbrander and De Laey \(2005\)](#) as functional vision.

Field of view (FOV) determines how much of the surrounding world a human driver can observe. Human binocular vision regarding subjects with no visual impairment is approximately 200° in the horizontal median, and 150° in the vertical ([Wolfe, Dobres, Rosenholtz, & Reimer, 2017](#)). The most widely accepted requirement for visual field is 120° in the horizontal median, although humans are able to rotate their heads to scan more of their

surroundings. Although there is no equivalent vertical requirement, 40° has been suggested (Colenbrander & De Laey, 2005). Rear-view and side mirrors allow human drivers to see the road behind them to some extent; furthermore, ADAS functions, including parking aids, can help human vision. However, while humans are in their cars looking in mirrors or at screens, they lose their forward vision. Drivers having visual field defects, yet who are still deemed to be safe drivers, were found to engage in more scanning behaviour (head movement) compared to unsafe drivers having field defects (Owsley & McGwin, 2010). The area where humans can see clearly is called the Useful Field of View (UFOV), which is often defined in the region of only 20–30°; however, information from the peripheral vision is also important for driving (Wolfe et al., 2017).

The range of electromagnetic radiation that humans can detect is from 380 to 750 nanometer (nm) (Best and Textile Institute, 2012), although the range can be as great as 310 to 1100 nm depending on age and the brightness of the light source (Sloney, 2016).

3.1.1. The equivalent to sight for the automated driver

Vision for an automated driver is herein defined as the sensors that utilise electromagnetic radiation, i.e. cameras, radars and lidars. Automotive imaging consists of many different types of cameras where the optics are different for differing applications, e.g. the lens type can be close to either human vision or a wide-angle lens. The sensitivities of cameras also differ: some cameras utilise visible light, some in UV, while others operate in the infrared (IR) band. Moreover, there are hyperspectral cameras that cover several bands (Uzkent, Hoffman, & Vodacek, 2016). The main differences between human and automotive vision are that the vehicle has a greater FOV and is sensitive to a greater range of electromagnetic radiation depending on the sensor set-up. A vehicle can have sensors that cover up to a 360° FOV in the horizontal median, or sensor input can even form a spherical cap engulfing the vehicle.

To date, there has not been a consistent approach to measuring image quality for the automotive industry (IEEE P2020 Working Group, 2018). Machine vision for automotive use is based on a charge-coupled device (CCD) or complementary metal-oxide semiconductor (CMOS) image sensors (Sloney, 2016; Stemmer Imaging, 2019). CMOS is most widely used due to its better performance at higher temperatures as well as its superior dynamic range (Hosticka et al., 2003). Cameras for automated driving applications have sensitivities ranging from the near ultraviolet (UV) through the visible spectrum and up to about 1000 nm depending on the sensor in question (Stemmer Imaging, 2019; Zhang & Niu, 2016). They can also have superior night vision to humans through their use of infrared (IR) imaging (Mahlke, Rösler, Seifert, Krems, & Thüring, 2007). Night vision enhancement systems (NVES) based on IR radiation come in two categories: near IR NVES uses active infrared headlights for 750–3000 nm, while far IR NVES are passive sensors for 6000–30,000 nm (Mahlke et al., 2007). Cameras are used for the ADAS function Lane Departure Warning, and there has been a fair amount of research completed on how varying light and weather conditions affect automated detections of road markings. In general, wet conditions are challenging for camera-based detection (A. Pike, Carlson, & Barrette, 2018). Successful detection of markings by LDW has been linked to contrast (A. M. Pike, Barrette, & Carlson, 2018; A. Pike, Carlson, et al., 2018; Hadi & Sinha, 2011; Pike & Songchitruksa, 2015) and edge smoothness has been suggested as being relevant to machine-vision detection (Lin, Wu, & Wang, 2016).

While the camera passively registers light, lidars emit laser light with wavelengths of typically 850, 905, 940 or 1550 nm (Hecht, 2018; Rablau, 2019); consequently, the camera detects its surrounding environment in terms of the time it takes for the light to return. Lidars can use rotating or stationary laser light, pulses, or continuous waves, but all lidars produce point clouds. Because laser emission at visible wavelengths, 400 nm to 780 nm, and near infrared wavelengths, 780–1400 nm, can cause eye damage (Douplik, Saiko, Schelkanova, & Tuchin, 2013), lidars can either use pulsing at 905 nm or wavelengths above 1400 nm for safe operation. The latter option, commonly 1550 nm (Hecht, 2018), produces a longer range, and with this range, a longer time for the signal to return. The slower response time can be mitigated by using multiple beams concurrently (Hecht, 2018). FOV differs for diverse lidars, and while a greater FOV provides coverage for a larger area, it is more susceptible to interference for instance from sunlight or headlights (Hecht, 2018). The angular resolution determines the lidar's ability to detect smaller objects, such as motorcycles or light poles. The resolution will depend on the lidar, i.e. the number of laser sources and how they are configured, as well as the distance to the object. The detection distance also depends on the characteristics of the object that reflect the light. The roughness, colour and reflectivity of the objects determine how much light is reflected back to the lidar rather than absorbed or transmitted (Yang & Wang, 2011). Lighter colours absorb less light than darker colours, and smooth surfaces reflect the light as a specular reflection, while rough surfaces create diffuse reflection. While higher levels of reflection generally produce longer detection rates (Hecht, 2018), highly reflective surfaces can also be difficult for lidars to register (Leonard et al., 2014). Some surfaces are particularly challenging, for instance glass where the light is transmitted through the glass and mirrors and where the light is refracted through the glass and hits the material behind the glass. Surface properties and the ability to detect objects in the road environment is worth noting for road infrastructure design, as surfaces of road elements could be optimised to be more prominent for automated drivers.

Radars operate similarly to lidars using radio waves at 24 GHz (1.25×10^{-2} nm) for short-range and 76–80 GHz (3.95×10^{-3} to 3.75×10^{-3} nm) for long-range (Hecht, 2018). This capability gives them longer range, lower angular resolution and better performance in poor weather compared to lidars (Van Brummelen, O'Brien, Gruyer, & Najjaran, 2018). Although not commonly used in automated vehicles at the present time, ground penetrating radars (GPR) are also worth noting. Traditional GPR technology used for infrastructure inspections, through mapping the subsurface profile of road- and railways, operate in the 1–3 GHz band; in general these provide excellent resolution but poor penetration depth (Cornick, Koechling, Stanley, & Zhang, 2016; Lalagüe, 2015). In recent years the use of GPR for localisation has become more common, with an operating range of 100–400 MHz, providing deeper penetration at the cost of resolution (Cornick et al., 2016; Kuutti et al., 2018) and making them suitable for navigation purposes.

The ranges of electromagnetic sensitivities and FOVs for automated driver and human driver is summarised in Figure 4.

3.2. Hearing

Auditory information has been found to improve human driving performance as it reinforces information received from the visual channel (Guttman et al., 2005; Macadam, 2003). Estimation of speed performed by humans becomes more accurate

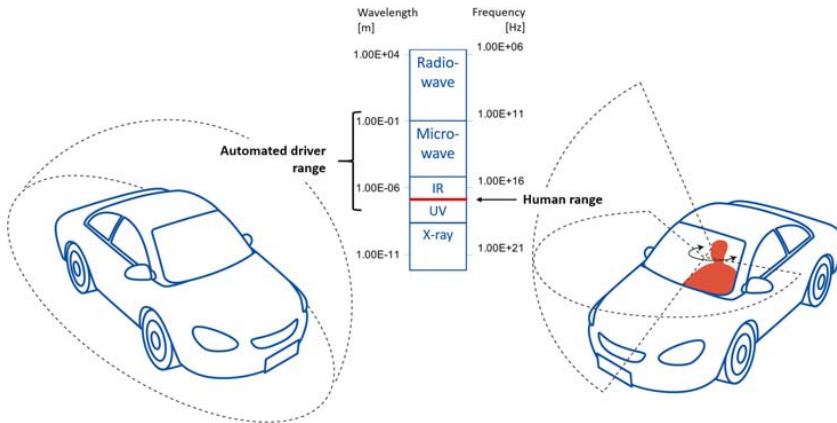


Figure 4. Automated driver vs human driver electromagnetic sensitivity and field of view.

with auditory information (Hellier, Naweed, Walker, Husband, & Edworthy, 2011; Macadam, 2003; Walker et al., 2006), and conversely, a lack of environmental noise can increase driving speed, reduce headways and induce more risky gap acceptance (Hellier et al., 2011; Walker et al., 2006). Recent research has found that when sensory input from two different senses is in conflict, the most reliable sense for a given task takes dominance. So although vision is the most trustworthy sense for spatial information, audition is dominant for temporal input (Guttman et al., 2005).

Auditory feedback in vehicles provides information on the engine, transmission, tyres and aerodynamics (Walker et al., 2006) as well as warnings of disruptive events such as the proximity of emergency vehicles (Macadam, 2003). Whether a sound is audible to humans depends both on the power of the sound, measured in decibels (dB), and the frequency of the vibration (Hz). Humans hear above 0 dB and feel discomfort from 110 dB and up (Institute for Quality and Efficiency in Health, 2008). Normal hearing detects frequencies of sound between 20 and 20,000 Hz (Bagai, 2006). Humans are excellent at localising the sources of sounds, i.e. determining the range, elevation and azimuth angles of a sound's source (Duraiswami & Raykar, 2005). Hearing is also used to determine the movement of objects that are not immediately in view, and it is therefore vital for safe and effective orientation (Gatehouse & Noble, 2004). The distance range of hearing is dependent on the loudness of the sound (Pasnau, 1999) as well as environmental factors including temperature and humidity (Harris, 1966).

3.2.1. The equivalent to hearing for the automated driver

The most common sensor relying on sound waves for vehicles is the ultrasonic sensor (Gruyer et al., 2017; Hirz & Walzel, 2018). Commercial ultrasonic sensors for automotive parking applications typically operate in the region of 40–60 kHz, and have a range of 30–450 cm (Nordevall, 2015). They provide distance measurements to objects at low speeds, which is beneficial for parking aids (Alonso et al., 2011), preventing car crashes (Alonso, Oria, Fernández, & Rodríguez, 2009), measuring characteristics of road surfaces (Hirata, Sun, Ueda, & Hachiyay, 2016), detecting moving obstacles (Ohya, Kosaka, & Kak,

1998), and detection of ice by friction analyses based on noise produced by tyre–road interaction (Gailius & Jacenas, 2007).

Microphones can also be used to interpret acoustic sensory input. Fazenda, Atmoko, Gu, Guan, and Ball (2009) used these to warn human drivers of nearby emergency vehicles as modern cars can be highly insulated against external noise. Such a system could also be used for automated drivers to make use of external sound signals to help interpret the driving situation.

3.3. Smell

The car cabin is exposed to several toxic gases, some of which can cause drowsiness, headaches, nausea, and dizziness. Humans' natural breathing can also cause oxygen deficiencies (Galatsis & Wlodarski, 2006). Smell can provide drivers with an early warning of problems with their vehicle, e.g. the smell of rotten eggs from a failed catalytic converter (Allen, 2006) or the smell of car parts becoming overheated (Pisaturo & Senatore, 2016), which is similar to how humans rely on smell to detect general dangers and identify edible food (Bordegoni, Carulli, & Shi, 2016). In addition to harmful gases in the car acting as a safety factor for human operation, smell can also be used to support driving in a more direct manner by increasing drivers' attention or providing them with feedback about their driving behaviour. Bordegoni et al. (2016) performed experiments on the sense of smell (olfaction) and driver attention, arguing that the visual and auditory stimuli are already subject to high demands. Olfactory stimuli were found to be more effective at increasing the subjects' attention level than auditory stimuli. Furthermore, the subjects found smell to be a more pleasant type of feedback than sounds (Bordegoni et al., 2016). Dmitrenko, Maggioni, and Obrist (2018) reported that olfactory notifications telling drivers to slow down or change lanes was less distracting, more comfortable, and more helpful than visual feedback.

3.3.1. The equivalent to smell for the automated driver

Machine olfaction devices have been utilised for the past 30 years in a wide variety of commercial industries, and work similarly on humans by converting chemicals to electrical signals (Li et al., 2014). There are a number of different sensors available that cover various gases and pollutants (Galatsis & Wlodarski, 2006), but they are currently not being used in vehicles for other purposes than to assess the presence of hazardous fumes, or the pleasant smell of new cars (Li et al., 2014). However, the use of machine olfaction is being researched to provide indications of car problems. Similar to how a human can learn to associate the smell of rotten eggs with a failed catalytic converter (Allen, 2006), machines can be trained to detect unwanted odours. In higher levels of automation, a car would need to be able to self-diagnose errors and evaluate its own fitness for driving. Furthermore, olfaction is being researched as a valuable sensory input for automated driving due to potential customers' expectations. Humans prefer a clean ride; therefore, there might be a need to use artificial noses to detect spills or if the latest customer was a smoker (Walsworth, 2019).

3.4. Sense of equilibrium

Equilibrium senses provide input that human drivers rely on to understand the forces acting on the vehicle correlated to their own movements. They include temperature,

pain, pressure and vibration, sense of spatial orientation and balance as well as the position of bones, joints, and muscles (Rye et al., 2013). Macadam (2003) discovered that humans rely on information obtained from the vestibular (inner ear) and kinesthetic (body distributed) channels for controlling vehicles. Direct contact with the vehicle through the seat, steering wheel, gear shift and foot pedals provide information on lateral forces, vehicular changes in stiffness and vibration, and feedback on roadway conditions, for example, changes in the friction level between tyres and road or wind gusts (Jensen, Tolbert, Wagner, Switzer, & Finn, 2011; Macadam, 2003).

Although there is evidence that humans are sensitive to these stresses, both in terms of assessing vehicular characteristics such as a car's size or weight, as well as aligning torque (i.e. how much force is needed to steer through a curve) (Walker et al., 2006), stimuli to the equilibrium sense remain relatively unexplored in literature compared to audio and visual feedback (Kammermeier, Kron, Hoogen, & Schmidt, 2004; Riener, Jeon, Alvarez, & Frison, 2017; Walker et al., 2006).

3.4.1. The equivalent of equilibrium for the automated driver

Accelerometers and gyroscopes are widely used in the automotive industry to obtain information about the vehicle's velocity, position and heading by measuring forces and rotations (Elkaim, Lie, & Gebre-Egziabher, 2015; Salychev, 2017). Often found as a set of three accelerometers and three gyroscopes, they produce a six degree of freedom sensor system used in the inertial measurement unit (IMU), the output of which is converted to navigation parameters by the inertial navigation system (INS) (Elkaim et al., 2015). INSs are self-contained non-jammable systems, but suffer errors that have an exponential growth over time and GPS-measurements are used to correct this issue (Spangenberg, Calmettes, & Tourneret, 2007). In the absence of GPS or other external sources of positioning, the vehicle relies on so-called dead-reckoning navigation. Dead-reckoning uses the initial position and calculates the following positions with the use of the IMU, the errors of which can be counteracted with the use of additional sensors such as odometers which alleviates drift, and magnetometers that provide heading and inclination data (Barbour, 2004). Another way to improve localisation performance is by using map-matching techniques (Spangenberg et al., 2007).

3.5. Cognition

The focus thus far has been on the sensors of the automated driver, compared to the human sensory system. The sensory inputs are turned into information and understanding through cognition. As Groeger (2002, p. 242) so eloquently puts it:

“Statements to the effect that driving is a largely visual task ... are as meaningless as the assertion that reading is a visual task. Both are obviously heavily dependent on visual perception. However, it is the further processing of that information which underpins our interpretation, comprehension, memory and non-reflex reactions to what we see”

Human drivers depend heavily on their ability to judge positions and movements of other road users, and to predict where these will be in the next few seconds (Hills, 1980). The driving skill has been found to increase with experience. Macadam (2003) linked this to the understanding of vehicle dynamics. Mourant and Rockwell (1972) found that

responding to stimuli, especially beyond the visual channel, required experience. While Hills (1980) concluded that part of the art of driving may be “in developing the skill of looking in the right place at the right time. It may also involve the ability to predict accurately where the critical points in the scene will be in the next few seconds ahead”.

Hollnagel, Nåbo, and Lau (2003) describe the study of driving as traditionally being viewed as either as a problem of guidance and control or as a human factors problem, neither of which is fully adequate to face the challenges of modern and future cars. They further emphasise that the introduction of ADAS, the human is no longer in direct control of the vehicle, but rather in co-operation with an automated driving system.

Cognition is connected to response time, a parameter widely used in road geometry design. Humans have response times as low as 180 milliseconds (ms) for visual stimuli, and about 140 ms for auditory and tactile stimuli when performing simple tasks (Macadam, 2003). The American Association of State Highway and Transportation Officials (2011) state that the reaction time of humans can be from almost negligible to over 1.64 s. Fuller (2005) found that experienced drivers showed anticipatory avoidance of hazard, while inexperienced drivers had a reactive mode of dealing with hazards, i.e. that response time is dependent on experience.

3.5.1. The equivalent of cognition for the automated driver

For the automated driver to outperform humans, they need to correctly understand a given driving situation, and anticipate the actions of other road users. The automated driver’s capability to make fast decisions in complex situations, like humans are innately able to, can, per today’s technological advances, be questioned (Pütz, Murphy, & Mullins, 2019).

Machines need to interpret sensory input, e.g. turning sensor data from the IMU into the position, heading and velocity in the INS. Although it is often assumed that vehicles will have shorter reaction times than humans (Farah, Erkens, Alkim, & van Arem, 2018) this depends on how much data needs to be analysed. The DARPA Urban Challenge in 2007 provides two examples of reaction times. Junior, the Stanford entry which placed second, had a time delay from entry of sensor data to action of approximately 300 ms (Montemerlo et al., 2009). Another participant, Little Ben from the Ben Franklin Racing Team, used 200 milliseconds as the worst-case scenario for its car’s detection and reaction time (Benjamin, Leonard, Schmidt, & Newman, 2008). In the challenge, speed was limited to 30 mph or roughly 50 km/h, with lower speed limits in many places (Montemerlo et al., 2009), and there was no requirement for cars to detect traffic lights or signs (Berger & Rumpel, 2012). Although a technical feat, the challenge is still a long way from real-world driving. On the other hand, over a decade has passed since the DARPA 2007 challenge under which time hardware and software has been improved. Collin et al. (2020) published a study where all driving functions were defined by 24 tasks which were connected by 32 messages. They then simulated the latency of the system at different architectures with different safety levels, for instance with regard to redundancy. Their simulation suggested system latencies, or reaction times, of between 0.34 and 0.38 s.

Central to cognition is object recognition. There are several ways to detect objects such as vehicles and pedestrians through automated features. Vision-based detection can be made based on the recognition of objects directly from the pixels in images or by

analysing subsequent frames (Sivaraman & Trivedi, 2013). Sensor fusion techniques allows for combining the strengths of different sensor types, e.g. cameras and radars (Wang, Xu, Sun, Xin, & Zheng, 2016) and machine learning techniques can be applied to teach the machine to discern different elements of the traffic scenario even in challenging lighting conditions and when the objects are partially occluded (Ohn-bar & Trivedi, 2015). Machines are generally found to be considerably worse than humans at broad categorisation, e.g. identifying an animal (Branson, Van Horn, Wah, Perona, & Belongie, 2014; Fleuret et al., 2011; Linsley, Eberhardt, Sharma, Gupta, & Serre, 2018), but superior in finding small distinctions, e.g. the species of bird in an image. Even when the human and machine reach the same conclusion, they do this based on different visual markers (Linsley et al., 2018). Differences in how humans and machines operate are worth noting, both to ensure safe co-existence on the road, but also to leverage the strengths of machine sensors and cognition.

Infrastructure design could also impact how fast and successful the processing of sensor input is. Road marking detection can again serve as an example. Beyond the problems of capturing the lane markings on camera, lie the problems of correctly analysing them. Issues have been identified with relation to old markings, worn markings and asphalt cracks (Chen, Seff, Kornhauser, & Xiao, 2015; A. Pike, Carlson, et al., 2018), but also problems were other parts of the infrastructure are mistaken for lane markings such as road marking arrows or guardrails (Borkar, Hayes, Smith, & Pankanti, 2009; Chen et al., 2015).

4. Discussion

In order for the automated driver to be considered in future road design and maintenance, its characteristics must first be established. Understanding the differences between human and automated drivers can provide insight into how to ensure the safety benefits expected by automated driving. The current definitions of automated drivers, including the SAE International's ADS, do not provide insight into the unique characteristics of the automated driver. Therefore, a unified framework for driving has been established encompassing all parts of the driving processes. In this framework, how the driver senses their environment was shown to impact all the driving processes. Sensing of the environment also represents the most direct interaction between driver and the road environment. Thus, it is necessary to focus on the sensing processes of both human and automated road users as well how this sensory input is processed (cognition).

As presented in the previous section, there is a significant amount of research on both the different sensors used in driving automation, and the automated driving functions that they make possible. However, these seldom shed light on what changes are needed to make the road infrastructure easier to interpret for automated drivers. The unified framework and analysis of differences between human and automated drivers presented in this paper provide guidance on how to close this research gap.

The main differences identified between humans and automated drivers are that the automated driver has a much greater range of electromagnetic sensitivity and field of view (related to sight), and that the two road users interpret and act on sensory input in different ways (related to cognition).

Given the increased electromagnetic sensitivities, there is potential to use colours and contrasts to aid sensors that depend on available light, e.g. cameras, and use surface textures (roughness, transparency and reflective properties) to improve detection by sensors that actively emit radiation, e.g. radars and lidars.

Road design and road maintenance strategies both play a role in the success of automated driving features. Longitudinal road elements can be hard to distinguish in image processing, e.g. lane markings, cracks in the road and safety rails. Research on how different materials and finishes can help automated drivers correctly classify road infrastructure elements is encouraged. Regarding road maintenance, strategies will need to be updated to ensure the success of automated drivers, e.g. in relation to road damage repairs and maintenance of road markings.

Characteristics of the automated driver also have implications for existing road infrastructure. As mentioned previously, LED signs are hard to read for cameras due to flicker; for this reason, they might not be a cost-effective investment for the future. Glass and mirrors can cause lidars to misinterpret distances to objects. The way objects reflect laser light also impacts lidars' accuracy of object detection. These mechanisms should be considered both in the design of the road infrastructure and for the vehicles themselves. For example, using car paints that are easily detectable by an automated driver, and, if possible, distinguishable from static parts of the road environment, could also increase safety and lower reaction times.

Although it depends on the sensors' set-up on the vehicle, the automated driver usually has some sort of perception in all directions. The greater FOV of automated drivers has the potential to increase safety in traffic but depends on the correct interpretation of sensor data. Placement of sensors will have a specific impact on the eye height parameter which determines sight distance in geometric road design. To include the automated driver in road design, the current design parameters will need to be reevaluated. Definitions used for human drivers might not be directly transferrable to the automated driver. For instance, sensor placements are likely to be both higher and lower than the design criteria of eye height used in current design standards. Sensor fusion, which involves combining sensor input from different sensors, further complicates this definition.

Safe driving is dependent not only on what data is collected by sensors, but also how it is analysed. The amount of sensory data being processed, as well as the processing algorithms themselves, impacts the reaction time of the automated driver. Lower reaction times are expected to be a notable benefit from automated driving; however, in the current stages of development, it will be beneficial to process more sensory data for greater safety and redundancy. An understanding of trade-offs such as this one is important as road authorities will find themselves in a position where they need to develop policies to certify the automated driver for different uses. To better understand how the automated driver operates, one approach is to require programming that explains how automated drivers interpret their surroundings and how they reach their decisions, often referred to as *explainable AI*. The analyses of sensor data, or cognition of the automated driver, is also related to object detection. The differences in cognition for human and automated drivers suggest revising parameters (such as object height and reaction time) that are used to determine stopping sight distance in road design.

Despite the uncertainty surrounding what sensors the automated driver can be expected to have, and how the data from these will be interpreted, the findings of this study suggest areas for future research efforts. The following steps are suggested to identify concrete measures for including the automated driver in the design and maintenance of road infrastructure:

1. Parameters for geometric road design needs reevaluating based on the automated driver's development. Eye height and object height are examples of parameters that require a new definition. Reaction time will likewise need to be defined for automated drivers and monitored as vehicles and systems evolve.
2. The suite of sensors used by the automated driver detects a range of electromagnetic radiation considerably larger than the range visible to human drivers. This should be explored to optimise the design of road infrastructure elements. For example, research can uncover how colours, textures and materials can be used to help machine drivers separate roadway from safety railings or curbs.
3. Maintenance policies need revision as more knowledge about how wear and damages to the road infrastructure affect automated driving is generated.
4. Successful automated driving will require co-operation between road authorities, researchers, and vehicle manufacturers. Transparency with respect to how the infrastructure is sensed and interpreted should be encouraged, including trade-offs of latency versus redundancy and classification of objects.

5. Conclusion

As automated driving features continue to develop, a new road user, *the automated driver*, has emerged. To build infrastructure suited for this automated driver, more knowledge about the automated driver combined with a solid understanding of how the roadway is sensed and interpreted by the automated driver is needed. Current literature lacks a framework for automated driving that covers all driving processes. This paper has established a unified framework for human and automated driving based on theoretical models of human driving and robotics. The unified framework of driving provides an approach to relate the sensor technology used in automated driving to existing human senses to which the roadway infrastructure is currently adapted. The sensing processes of automated and human drivers have been reviewed to identify differences between the two road users. The understanding of these differences provides research directions that can enable inclusion the new automated driver as a road user in road design and maintenance policies.

Acknowledgements

Author contributions: Conceptualisation; Ane Dalsnes Storsæter, Data curation; Not applicable, Formal analysis; Ane Dalsnes Storsæter, Funding acquisition; Ane Dalsnes Storsæter, Investigation; Ane Dalsnes Storsæter, Methodology; Ane Dalsnes Storsæter, Kelly Pitera, Edward McCormack, Project administration; Ane Dalsnes Storsæter, Resources; Ane Dalsnes Storsæter, Software; Not applicable, Supervision; Kelly Pitera, Edward McCormack, Validation; Ane Dalsnes Storsæter, Visualisation; Ane Dalsnes Storsæter, Roles/Writing – original draft; Ane Dalsnes Storsæter Writing – review & editing: Ane Dalsnes Storsæter, Kelly Pitera, Edward McCormack.

Disclosure statement

No potential conflict of interest was reported by the author(s).

Funding

This work was supported by the Norwegian Public Roads Administration.

ORCID

Ane Dalsnes Storsæter  <http://orcid.org/0000-0003-4637-5695>

Kelly Pitera  <http://orcid.org/0000-0001-5621-2828>

Edward D. McCormack  <http://orcid.org/0000-0002-2437-9604>

References

- Allen, M. (2006). *Auto diagnosis - What's that smell?* [WWW Document]. Popular Mechanics. Retrieved from <https://www.popularmechanics.com/cars/how-to/a536/2423551/>
- Alonso, L., Milanés, V., Torre-Ferrero, C., Godoy, J., Oriá, J. P., & de Pedro, T. (2011). Ultrasonic sensors in urban traffic driving-aid systems. *Sensors*, 11, p. 661–673. doi:10.3390/s110100661
- Alonso, L., Oriá, J. P., Fernández, M., & Rodríguez, C. (2009). Car crash prevention expert system in urban traffic based on ultrasounds. *IFAC Proceedings*, 2. doi:10.3182/20090921-3-TR-3005.00024
- American Association of State Highway and Transportation Officials. (2011). *A policy on geometric design of highways and streets* (6th ed). Washington, DC: Author.
- Bagai, A. (2006). Does this patient have hearing impairment? *JAMA*, 295, 416–428.
- Barbour, N. (2004). *Inertial navigation sensors*. NATO RTO Lecture Series. Cambridge, MA: Charles Stark Draper Laboratory. [https://www.sto.nato.int/publications/STO%20Educational%20Notes/RTO-EN-SET-116-2011/EN-SET-116\(2011\)-02.pdf](https://www.sto.nato.int/publications/STO%20Educational%20Notes/RTO-EN-SET-116-2011/EN-SET-116(2011)-02.pdf)
- Benjamin, M. R., Leonard, J. J., Schmidt, H., & Newman, P. M. (2008). Little Ben: The Ben Franklin racing team's entry in the 2007 DARPA urban challenge. *Journal of Field Robotics*, 25, 598–614. doi:10.1002/rob20260
- Berger, C., & Rumpel, B. (2012). *Autonomous driving—5 years after the urban challenge: The anticipatory vehicle as a cyber-physical system*. Proceedings of the 27th IEEE/CAM International Conference on Automated Software Engineering (ASE 2012), Essen, Germany.
- Best, J., & Textile Institute. (2012). *Colour design: Theories and applications*. Manchester: Woodhead Publishing.
- Bey, T., & Tewolde, G. (2019). *Evaluation of DSRC and LTE for V2X*. IEEE 9th Annual Computing and Communication Workshop and Conference (CCWC) 2019, Las Vegas, NV, pp. 1032–1035. doi:10.1109/CCWC.2019.8666563
- Bordegoni, M., Carulli, M., & Shi, Y. (2016). *Investigating the use of smell in vehicle-driver interaction*. Proceedings of the ASME 2016 International Design Engineering Technical Conferences and Computers and Information in Engineering Conference. Volume 1A: 36th Computers and Information in Engineering Conference, Charlotte, NC, August 21–24, 2016. V01AT02A053. ASME. doi:10.1115/DETC2016-60541
- Borkar, A., Hayes, M., Smith, M. T., & Pankanti, S. (2009). *A layered approach to robust lane detection at night*. 2009 IEEE Workshop on Computational Intelligence in Vehicles and Vehicular Systems (CIVVS) 2009, pp. 51–57. doi:10.1109/CIVVS.2009.4938723
- Branson, S., Van Horn, G., Wah, C., Perona, P., & Belongie, S. (2014). The ignorant led by the blind: A hybrid human-machine vision system for fine-grained categorization. *International Journal of Computer Vision*, 108, 3–29. doi:10.1007/s11263-014-0698-4
- Brooks, R. A. (1986). A robust layered control system for a mobile robot. *IEEE Journal on Robotics and Automation*, 2, 14–23.

- Chen, C., Seff, A., Kornhauser, A., & Xiao, J. (2015). *DeepDriving: Learning affordance for direct perception in autonomous driving*. 2015 IEEE International Conference on Computer Vision (ICCV), Santiago, pp. 2722–2730. doi:10.1109/ICCV.2015.312.8
- Colenbrander, A., & De Laey, J.-J. (2005). *Vision requirements for driving safety with emphasis on individual assessment*. International Council of Ophthalmology.
- Collin, A., Siddiqi, A., Imanishi, Y., Rebentisch, E., Tanimichi, T., & Weck, O. L. (2020). Autonomous driving systems hardware and software architecture exploration: Optimizing latency and cost under safety constraints. *Systems Engineering*, 23, 327–337. doi:10.1002/sys.21528
- Cornick, M., Koehling, J., Stanley, B., & Zhang, B. (2016). Localizing ground penetrating RADAR: A step toward robust autonomous ground vehicle localization. *Journal of Field Robotics*, 33, 82–102. doi:10.1002/rob.21605
- Coutinho, R. W. L., Boukerche, A., & Loureiro, A. A. F. (2018). Design guidelines for information-centric connected and autonomous vehicles. *IEEE Communications Magazine*. doi:10.1109/MCOM.2018.1800134
- Davies, T., & Jnifene, A. (2007). *Path planning and trajectory control of collaborative mobile robots using hybrid control architecture*. CITSA 2007 - International Conference on Cybernetics and Information Technologies, Systems and Applications and CCCT 2007 - International Conference on Computing, Communications and Control Technologies, Proceedings, Orlando, FL.
- Dmitrenko, D., Maggioni, E., & Obrist, M. (2018). *I smell trouble*. International Conference on Multimodal Interaction, Boulder, CO, pp. 234–238. doi:10.1145/3242969.3243015
- Douplik, A., Saiko, G., Schelkanova, I., & Tuchin, V. V. (2013). The response of tissue to laser light. In H. Jelinkova (Ed.), *Lasers for medical applications: Diagnostics, therapy and surgery* (pp. 47–109). Cambridge: Woodhead Publishing Series in Electronic and Optical Materials.
- Duraiswami, R., & Raykar, V. C. (2005). *The manifolds of spatial hearing*. ICASSP, IEEE International Conference on Acoustics, Speech, and Signal Processing – Proceedings III, Philadelphia, PA, Vol. 3, pp. iii/285–iii/288. doi:10.1109/ICASSP.2005.1415702
- Eckhoff, D., & Sommer, C. (2014). Driving for big data? Privacy concerns in vehicular networking. *IEEE Security & Privacy*, 12, 77–79. doi:10.1109/MSP.2014.2
- Eckstein, L., & Zlocki, A. (2013, May 27–30). *Safety potential of ADAS: Combined methods for an effective evaluation*. The 23rd International Technical Conference on the Enhanced Safety of Vehicles (ESV) Seoul, Republic of Korea, 13-0391-W.
- Elkaim, G. H., Lie, F. A. P., & Gebre-Egziabher, D. (2015). Principles of guidance, navigation, and control of UAVs. In K. P. Valavanis & G. J. Vachtsevanos (Eds.), *Handbook of unmanned aerial vehicles* (pp. 347–380). Dordrech: Springer Science+Business Media. doi:10.1007/978-90-481-9707-1
- Farah, H., Erkens, S. M. J. G., Alkim, T., & van Arem, B. (2018). Infrastructure for automated and connected driving: State of the art and future research directions. *Road Vehicle Automation*, 4, 187–197. doi:10.1007/978-3-319-60934-8
- Farnell, B. M., & Miller Jr, H. L. (2018). The kinesthetic system. In H. Miller (Ed.), *The SAGE encyclopedia of theory in psychology* (pp. 483–485). Thousand Oaks, CA: SAGE Publications.
- Fazenda, B., Atmoko, H., Gu, F., Guan, L., & Ball, A. (2009). *Acoustic based safety emergency vehicle detection for intelligent transport systems*. ICCAS-SICE 2009 - ICROS-SICE International Joint Conference 2009, Fukuoka, Japan, pp. 4250–4255.
- Fleuret, F., Li, T., Dubout, C., Wampler, E. K., Yantis, S., & Geman, D. (2011). Comparing machines and humans on a visual categorization test. *Proceedings of the National Academy of Sciences*, 108, 17621–17625. doi:10.1073/pnas.1109168108
- Fuller, R. (2005). Towards a general theory of driver behaviour. *Accident Analysis & Prevention*, 37, 461–472. doi:10.1016/j.aap.2004.11.003
- Gailius, D., & Jacenas, S. (2007). Ice detection on a road by analyzing tire to road friction ultrasonic noise. *Ultragarsas*, 62, 17–20.
- Galatsis, K., & Wlodarski, W. (2006). Car cabin air quality sensors and systems. In C. A. Grimes, E. C. Dickey, & M. V. Pishko (Eds.), *Encyclopedia of sensors* (pp. 1–11). Valencia, CA: American Scientific Publishers.

- Gat, E., Bonasso, R. P., & Murphy, R. (1998). On three-layer architectures. In D. Kortenkamp, R. P. Bonasso, & R. R. Murphy (Eds.), *Artificial intelligence and mobile robots* (pp. 195–210). Cambridge, MA: AAAI Press.
- Gatehouse, S., & Noble, I. (2004). The speech, spatial and qualities of hearing scale (SSQ). *International Journal of Audiology*, *43*, 85–99. doi:10.1080/14992020400050014
- Groeger, J. A. (2002). Trafficking in cognition: Applying cognitive psychology to driving. *Transportation Research Part F: Traffic Psychology and Behaviour*, *5*, 235–248. doi:10.1016/S1369-8478(03)00006-8
- Groeger, J. (2000). *Understanding driving, applying cognitive psychology to a complex everyday task*. Hove: Psychology Press.
- Gruyer, D., Magnier, V., Hamdi, K., Claussmann, L., Orfila, O., & Rakotonirainy, A. (2017). Perception, information processing and modeling: Critical stages for autonomous driving applications. *Annual Reviews in Control*, *44*, 323–341. doi:10.1016/j.arcontrol.2017.09.012
- Guttman, S. E., Gilroy, L. A., & Blake, R. (2005). Hearing what the eyes see: Auditory encoding of visual temporal sequences. *Psychological Science*, *16*, 228–235. doi:10.1111/j.0956-7976.2005.00808.x
- Hadi, M., & Sinha, P. (2011). Effect of pavement marking retroreflectivity on the performance of vision-based lane departure warning systems. *Journal of Intelligent Transportation Systems*, *15*, 42–51. doi:10.1080/15472450.2011.544587
- Harris, C. M. (1966). Absorption of sound in air versus humidity and temperature. *The Journal of the Acoustical Society of America*, *40*, 148. doi:10.1121/1.1910031
- Hecht, J. (2018). Lidar for self-driving cars. *Optics and Photonics News*, *29*, 26–33.
- Hellier, E., Naweed, A., Walker, G., Husband, P., & Edworthy, J. (2011). The influence of auditory feedback on speed choice, violations and comfort in a driving simulation game. *Transportation Research Part F: Traffic Psychology and Behaviour*, *14*, 591–599. doi:10.1016/j.trf.2011.07.004
- Hills, B. L. (1980). Vision, visibility, and perception in driving. *Perception*, *9*, 183–216. doi:10.1068/p090183
- Hirata, S., Sun, Q., Ueda, M., & Hachiyay, H. (2016). Measurement of road surfaces by reflection characteristics of airborne ultrasound. *Acoustical Science and Technology*, *37*, 322–325. doi:10.1250/ast.37.322
- Hirz, M., & Walzel, B. (2018). Sensor and object recognition technologies for self-driving cars. *Computer-Aided Design and Applications*, *15*, 501–508. doi:10.1080/16864360.2017.1419638
- Hollnagel, E., Näbo, A., & Lau, I. V. (2003). *A systemic model for driver-in-control*. Proceedings of Second International Driving Symposium on Human Factors in Driver Assessment, Training, and Vehicle Design, Park City, Utah, pp. 86–91.
- Hosticka, B. J., Brockherde, W., Bußmann, A., Heimann, T., Jeremias, R., Kemma, A., ... Schrey, O. (2003). CMOS imaging for automotive applications. *IEEE Transactions on Electron Devices*, *50*, 173–183. doi:10.1109/TED.2002.807258
- Huang, X., Zhao, D., & Peng, H. (2017). Empirical study of DSRC performance based on safety pilot model deployment data. *IEEE Transactions on Intelligent Transportation Systems*, *18*, 2619–2628. doi:10.1109/TITS.2017.2649538
- IEEE P2020 Working Group. (2018). *IEEE P2020 Automotive Imaging White Paper*, IEEE, New York. <http://www.ieee.org/web/aboutus/whatis/policies/p9-26.html>
- Institute for Quality and Efficiency in Health. (2008). *Hearing loss and deafness: Normal hearing and impaired hearing* [WWW Document]. NCBI Bookshelf. Retrieved from <https://www.ncbi.nlm.nih.gov/books/NBK390300/>
- Jensen, M. J., Tolbert, A. M., Wagner, J. R., Switzer, F. S., & Finn, J. W. (2011). A customizable automotive steering system with a haptic feedback control strategy for obstacle avoidance notification. *IEEE Transactions on Vehicular Technology*, *60*, 4208–4216. doi:10.1109/TVT.2011.2172472
- Kammermeier, P., Kron, A., Hoogen, J., & Schmidt, G. (2004). Display of holistic haptic sensations by combined tactile and kinesthetic feedback. *Presence: Teleoperators and Virtual Environments*, *13*, 1–15. doi:10.1162/105474604774048199
- Khoury, J., Amine, K., & Saad, R. A. (2019). An initial investigation of the effects of a fully automated vehicle fleet on geometric design. *Journal of Advanced Transportation*, *2019*, 1–10. doi:10.1155/2019/6126408

- Kuutti, S., Fallah, S., Katsaros, K., Dianati, M., McCullough, F., & Mouzakitis, A. (2018). A survey of the state-of-the-art localization techniques and their potentials for autonomous vehicle applications. *IEEE Internet of Things Journal*, 5, 829–846. doi:10.1109/JIOT.2018.2812300
- Lalagüe, A. (2015). *Use of ground penetrating radar for transportation infrastructure maintenance* (Dr. theses). NTNU, 2015188.
- Leonard, J., How, J., Teller, S., Berger, M., Campbell, S., Fiore, G., ... Walter, M. (2014). A perception-driven autonomous urban vehicle. *Journal of Field Robotics*, 33, 1–17. doi:10.1002/rob
- Li, J., Hodges, R. D., Schiffman, S. S., Nagle, H. T., Gutierrez-Osuna, R., Luckey, G., ... Crowell, J. (2014). *Odor assessment of automobile cabin air by machine olfaction*. Proceedings of IEEE Sensors 2014, Valencia, Spain, pp. 1726–1729. doi:10.1109/ICSENS.2014.6985356
- Lin, K. L., Wu, T. C., & Wang, Y. R. (2016). An innovative road marking quality assessment mechanism using computer vision. *Advances in Mechanical Engineering*, 8, 1–8. doi:10.1177/1687814016654043
- Linsley, D., Eberhardt, S., Sharma, T., Gupta, P., & Serre, T. (2018). *What are the visual features underlying human versus machine vision?* Proceedings - 2017 IEEE International Conference on Computer Vision Workshops, ICCVW 2017, Venice, Italy, pp. 2706–2714. doi:10.1109/ICCVW.2017.331
- Lu, N., Cheng, N., Zhang, N., Shen, X., & Mark, J. W. (2014). Connected vehicles: Solutions and challenges. *IEEE Internet of Things Journal*, 1(4), 289–299. doi:10.1109/JIOT.2014.2327587
- Macadam, C. C. (2003). Understanding and modeling the human driver. *Vehicle System Dynamics*, 40, 101–134. doi:10.1076/vesd.40.1.101.15875
- Mahlke, S., Rösler, D., Seifert, K., Krems, J. F., & Thüring, M. (2007). Evaluation of six night vision enhancement systems: Qualitative and quantitative support for intelligent image processing. *Human Factors: The Journal of the Human Factors and Ergonomics Society*, 49, 518–531. doi:10.1518/001872007X200148
- McCourt, M. J., Mehta, S. S., Doucette, E. A., & Curtis, J. W. (2016). *Human-machine teaming for effective estimation and path planning*. Micro-Nanotechnology Sensors, Systems, and Applications VIII 9836, 98361W. doi:10.1117/12.2224121
- Michon, J. A. (1985). Critical view of driver behavior models: What do we know, what should we do? In L. Evans, & R. C. Schwing (Eds.), *Human behavior and traffic safety* (pp. 485–524). Boston, MA: Springer.
- Montemerlo, M., Becker, J., Bhat, S., Dahlkamp, H., Dolgov, D., Ettinger, S., ... Thrun, S. (2009). Junior: The Stanford entry in the urban challenge. In M. Buehler, K. Iagnemma, & S. Singh (Eds.), *Springer tracts in advanced robotics* (Vol. 56, pp. 91–123). Berlin: Springer. doi:10.1007/978-3-642-03991-1_3
- Mourant, R. R., & Rockwell, T. H. (1972). Strategies of visual search by novice and experienced drivers. *Human Factors*, 14(4), 325–335. doi:10.1177/001872087201400405
- Näätänen, R., & Summala, H. (1974). A model for the role of motivational factors in drivers' decision-making. *Accident Analysis & Prevention*, 6, 243–261. doi:10.1016/0001-4575(74)90003-7
- National Highway Traffic Safety Administration. (2015). *Traffic safety facts crash stats critical reasons for crashes investigated in the national motor vehicle crash causation survey*. US Department of Transportation, Washington, DC. <https://crashstats.nhtsa.dot.gov/Api/Public/ViewPublication/812115>
- Nilsson, N. J. (1984). *Shakey the Robot, Technical Note 323 [WWW Document]*. Retrieved from <http://ai.stanford.edu/~nilsson/OnlinePubs-Nils/shakey-the-robot.pdf>
- Nordevall, J. (2015). *Method development of automotive ultrasound simulations*. Gøteborg: Chalmers University of Technology.
- Ohn-bar, E., & Trivedi, M. M. (2015). Learning to detect vehicles by clustering appearance patterns. *IEEE Transactions on Intelligent Transportation Systems*, 16, 2511–2521.
- Ohya, A., Kosaka, A., & Kak, A. (1998). Vision-based navigation by a mobile robot with obstacle avoidance using single-camera vision and ultrasonic sensing. *IEEE Transactions on Robotics and Automation*, 14, 969–978. doi:10.1109/70.736780
- Osichenko, D., & Spielhofer, R. (2018). *Monitoring and inventory of road signs and road markings. State of the art – a review of existing methods and systems*. Transport Research Arena, pp. 1–9. doi:10.5281/zenodo.1320919

- Östling, M., Lubbe, N., Jeppsson, H., & Puthan, P. (2019). *Passenger car safety beyond ADAS: Defining remaining accident configurations as future priorities*. The 26th International Technical Conference on the Enhanced Safety of Vehicles, Eindhoven, Netherlands, 19-0091.
- Owsley, C., & McGwin, G. (2010). Vision and driving. *Vision Research*, 50, 2348–2361. doi:10.1016/j.visres.2010.05.021
- Pasnau, R. (1999). What is sound? *Philosophical Quarterly*, 49(196), 309–324. doi:10.1111/1467-9213.00144
- Pike, A. M., Barrette, T. P., & Carlson, P. J. (2018). *Machine vision detection of pavement markings*. TRB 2019 Annual Meeting. doi:10.1080/09638190500372404
- Pike, A., Carlson, P., & Barrette, T. (2018). *Evaluation of the effects of pavement marking width on detectability by machine vision: 4-inch vs 6-inch markings*. American Traffic Safety Services Association.
- Pike, A. M., & Songchitruksa, P. (2015). Predicting pavement marking service life with transverse test deck data. *Transportation Research Record: Journal of the Transportation Research Board*, 2482, 16–22. doi:10.3141/2482-03
- Pisaturo, M., & Senatore, A. (2016). Simulation of engagement control in automotive dry-clutch and temperature field analysis through finite element model. *Applied Thermal Engineering*, 93, 958–966. doi:10.1016/j.applthermaleng.2015.10.068
- Pütz, F., Murphy, F., & Mullins, M. (2019). Driving to a future without accidents? Connected automated vehicles' impact on accident frequency and motor insurance risk. *Environment Systems and Decisions*, 39(4), 383–395. doi:10.1007/s10669-019-09739-x
- Rablau, C. I. (2019). *Lidar: A new self-driving vehicle for introducing optics to broader engineering and non-engineering audiences*. Proc. SPIE 11143, Fifteenth Conference on Education and Training in Optics and Photonics: ETOP 2019, Quebec, Canada.
- Rashdan, I., Müller, F. d. P., & Sand, S. (2016). *ITS-G5 challenges and 5G solutions for vehicular platooning*. WWRF37, Kassel, Germany.
- Riener, A., Jeon, M., Alvarez, I., & Frison, A. K. (2017). *Driver in the loop: Best practices in automotive sensing and feedback mechanisms* (pp. 295–323). Cham: Springer.
- Rye, C., Wise, R., Jurukovski, V., DeSaix, J., Choi, J., & Avissar, Y. (2013). *Biology*. Houston, TX: Rice University. <https://cnx.org/exports/185cbf87-c72e-48f5-b51e-f14f21b5eabd@10.4.pdf/biology-10.4.pdf>
- SAE International. (2018). *SAE J3016 surface vehicle recommended practice*. Warrendale, PA: SAE International. http://standards.sae.org/J2016_201806
- Salychev, O. S. (2017). *Verified approaches to inertial navigation*. Moscow: BMSTU Press. ISBN: 978-5-7038-4625-4
- Sheikh, U. A., Jamil, M., & Ayaz, Y. (2014). *A comparison of various robotic control architectures for autonomous navigation of mobile robots*. 2014 International Conference on Robotics and Emerging Allied Technologies in Engineering, Islamabad, Pakistan, IEEE. doi:10.1109/iCREATE.2014.6828372
- Shladover, S. E. (2018). Connected and automated vehicle systems: Introduction and overview. *Journal of Intelligent Transportation Systems*, 22, 190–200. doi:10.1080/15472450.2017.1336053
- Sivak, M. (1996). The information that drivers use: Is it indeed 90% visual? *Perception*, 25(9), 1081–1089. doi:10.1068/p251081
- Sivaraman, S., & Trivedi, M. M. (2013). Looking at vehicles on the road: A survey of vision-based vehicle detection, tracking, and behavior analysis. *IEEE Transactions on Intelligent Transportation Systems*, 14, 1773–1795. doi:10.1109/TITS.2013.2266661
- Sliney, D. H. (2016). What is light? The visible spectrum and beyond. *Eye*, 30, 222–229. doi:10.1038/eye.2015.252
- Spangenberg, M., Calmettes, V., & Tourneret, J. Y. (2007). *Fusion of GPS, INS and odometric data for automotive navigation*. European Signal Processing Conference, Poznan, Poland, pp. 886–890.
- Steinbaeck, J., Steger, C., Holweg, G., & Druml, N. (2017, December). *Next generation radar sensors in automotive sensor fusion systems*. 2017 Symposium Sensor Data Fusion: Trends, Solutions, and Application (SDF) 2017, December, 1–6. doi:10.1109/SDF.2017.8126389

- Stemmer Imaging. (2019). *Spectral response - Glossary* [WWW Document]. Retrieved from <https://www.stemmer-imaging.com/en-pl/knowledge-base/spectral-response/>
- Sun, X., Cai, C., & Shen, X. (2015). A new cloud model based human-machine cooperative path planning method. *Journal of Intelligent & Robotic Systems*, 79, 3–19. doi:10.1007/s10846-014-0079-9
- Transportavdelingen Trafikksikkerhet, V. (2018). Statens vegvesens rapporter Dybdeanalyser av døds-ulykker i vegtrafikken 2017.
- Underwood, G., & Radach, R. (1998). Chapter 1 - eye guidance and visual information processing: Reading, visual search, picture perception and driving. In G. Underwood (Ed.), *Eye guidance in reading and scene perception* (pp. 1–27). Amsterdam: Elsevier Science.
- Uz kent, B., Hoffman, M. J., & Vodacek, A. (2016). *Real-time vehicle tracking in aerial video using hyper-spectral features*. IEEE Computer Society Conference on Computer Vision and Pattern Recognition Workshops, Las Vegas, NV. doi:10.1109/CVPRW.2016.181
- Van Brummelen, J., O'Brien, M., Gruyer, D., & Najjaran, H. (2018). Autonomous vehicle perception: The technology of today and tomorrow. *Transportation Research Part C: Emerging Technologies*, 89, 384–406. doi:10.1016/j.trc.2018.02.012
- Van der Molen, H., & Bötticher, A. (1988). A hierarchical risk model for traffic participants. *Ergonomics*, 31, 537–555. doi:10.1080/00140138808966698
- Wali, S. B., Abdullah, M. A., Hannan, M. A., Hussain, A., Samad, S. A., Ker, P. J., ... Mansor, M. B. (2019). Vision-based traffic sign detection and recognition systems: Current trends and challenges. *Sensors*, 19(9), 2093. doi:10.3390/s19092093
- Walker, G. H., Stanton, N. A., & Young, M. S. (2006). The ironies of vehicle feedback in car design. *Ergonomics*, 49, 161–179. doi:10.1080/00140130500448085
- Walsworth, J. (2019). *Aryballe's odor sensors help sniff out trouble* [WWW Document]. Automotive News. Retrieved from <https://www.autonews.com/technology/can-odor-sensors-sniff-out-car-trouble>
- Wang, X., Xu, L., Sun, H., Xin, J., & Zheng, N. (2016). On-road vehicle detection and tracking using MMW radar and monovision fusion. *IEEE Transactions on Intelligent Transportation Systems*, 17, 2075–2084. doi:10.1109/TITS.2016.2533542
- Wolfe, B., Dobres, J., Rosenholtz, R., & Reimer, B. (2017). More than the useful field: Considering peripheral vision in driving. *Applied Ergonomics*, 65, 316–325. doi:10.1016/j.apergo.2017.07.009
- Yang, Y., & Hua, K. (2019). Emerging technologies for 5G-enabled vehicular networks. *IEEE Access*, 7, 181117–181141. doi:10.1109/ACCESS.2019.2954466
- Yang, S. W., & Wang, C. C. (2011). On solving mirror reflection in LIDAR sensing. *IEEE/ASME Transactions on Mechatronics*, 16, 255–265. doi:10.1109/TMECH.2010.2040113
- Zhang, F., & Niu, H. (2016). A 75-ps gated CMOS image sensor with low parasitic light sensitivity. *Sensors*, 16. doi:10.3390/s16070999
- Zhao, X., Jing, S., Hui, F., Liu, R., & Khattak, A. J. (2019). DSRC-based rear-end collision warning system – An error-component safety distance model and field test. *Transportation Research Part C: Emerging Technologies*, 107, 92–104. doi:10.1016/j.trc.2019.08.002

Appendix B

Paper II (in progress)

Preparing for Automated Drivers – An Evaluation of Current Road Design Parameters

Ane Dalsnes Storsæter^{a,b*}, Kelly Pitera^b and Edward D. McCormack^{b,c}

^aTransport Development, Norwegian Public Roads Administration, Trondheim, Norway; ^bDepartment of Civil and Environmental Engineering, Norwegian University of Science and Technology, Norway; ^cCivil and Environmental Engineering, University of Washington, Seattle, USA

Ane Dalsnes Storsæter

Senior Engineer

Norwegian Public Roads Administration, 7030 Trondheim, Norway

E-mail : ane.storsater@vegvesen.no

Preparing for Automated Drivers – An Evaluation of Current Road Design Parameters

Geometric road design has evolved over a century based on increased knowledge of the human driver, vehicle performance, and the laws of physics. Recently, a new non-human road user has emerged, the automated driver. Born from driving support systems and becoming increasingly capable of driving on its own, the automated driver senses and acts differently to the roadway environment from a human driver. To capitalize on the expected benefits of automated drivers, e.g. fewer accidents and more flexibility in road design and freight, current human-oriented road design parameters need to be reconsidered.

Within this review, Norwegian geometric road design parameters, as well as their U.S. equivalents, are evaluated considering the transition from human to automated driver. Subsequently, the parameters most likely to be affected by automated drivers are highlighted and the consequences of these effects discussed. Parameters currently in need of revision as well as those needing monitoring for future revisions are indicated. Road design for automated drivers is found to be potentially more flexible, which could allow for more cost-efficient roads. However, human comfort is a limiting factor in road design where humans are drivers or passengers. Development of two sets of road design parameters, one for passenger transport and the other for freight transport (without human occupants), may be considered, as freight movement might be able to take advantage of greater range in roadway design, including smaller radii for roadway curvatures.

Keywords: road design; automated driving; policy; automated driver; design parameters

1. Introduction

Geometric road design is influenced by human physiology and psychology as well as the laws of physics. Human reaction times are used to define parameters such as stopping sight distances; they are then used to determine vertical crest curves. Human comfort also plays a central role in road design. To ensure comfortable driving situations for human drivers and passengers, there are limits on road design elements such as sag curves to prevent accelerations beyond human acceptance levels. An example of how, also, human psychology influences road design is horizontal curvatures, which are designed to help human drivers choose a suitable speed and trajectory when driving through curves. Wider curves are more forgiving in terms of the trajectory chosen; however, this effect is often negated, as the increased width also encourages human drivers to drive faster (Ben-Bassat & Shinar, 2011; Charlton, 2007).

Finally, the physics of driving revolve around a mechanical interaction of tire and road that creates the friction necessary for control, acceleration, and deceleration. It is supported by road characteristics such as banking and gradients, which ensure proper run-off of water while keeping lateral forces low enough for safe driving. Automated driving may also affect vehicle dynamics. For instance, it has been suggested that acceleration and deceleration rates could increase with automation (Washburn et al., 2018).

Some road design parameters have remained unchanged for decades. For instance, current definitions of stopping sight distance (SSD) were developed in the 1940s with minor revisions in the mid-eighties (Khoury et al., 2019) and mid-nineties (Transport Research Board, 1997; Wood & Donnell, 2017), while perception-reaction time road for conditions for drivers back to 1954 (Khoury et al., 2019). Since this, a new road user has emerged, *the automated driver*. The automated driver differs significantly from human drivers in terms of physical attributes (such as eye height) and cognitive characteristics (such as reaction time).

National and international road authorities have developed current road design standards to make safe and efficient roads for humans. It may be argued that developers of automated driving systems need to respond to the roads as they are, and not presuppose that road design will take into consideration automated features. The shift from human to automated driver comes with a promise of fewer accidents on existing roads, as these accidents are mostly due to human error (National Highway Traffic Safety Administration, 2015; Vegdirektoratet, 2018). Yet, some crashes are not due to driver error, but instead can arise from poor roadway design, including inadequate sight distance or intersection configuration (Noy et al., 2018). In Norway, an average of 28 percent of fatal crashes were at least in part due to factors pertaining to the roadway, including road alignment, available sight distance and the state of the road surface (Vegdirektoratet, 2018). So, to reap the expected benefits of automated driving, it is in the interest of the vehicle industry and road authorities alike to a) acknowledge how the automated driver differs from humans and b) determine how that knowledge may be used to optimize road design for both humans and automated drivers. In addition, it is worth investigating whether the new automated driver can allow for road design that is less resource intensive due to factors such

as more flexible road design (e.g., smaller radii curves) and fewer safety features (e.g., design speed buffers).

Literature on how the change from human to automated driving could affect physical road infrastructure is limited, and research on potential changes in geometric road design at different levels of automation is needed (Farah et al., 2018). The existing work most often considers scenarios with full automation. It is suggested that automated drivers can lead to narrower lanes due to their superior positioning (Hayeri et al., 2015; Lumiaho & Malin, 2016; McDonald & Rodier, 2015) and that a need may arise for dedicated lanes and longer ramps to accommodate platooning of vehicles, i.e. several vehicles driving together (Deshpande et al., 1996; Lutin et al., 2013). Based on the assumption that automated drivers have lower reaction times compared to those of human drivers, it is suggested that design speeds be increased (McDonald & Rodier, 2015; Washburn et al., 2018). Full automation could lead to reduced cut and fill volumes for roadway construction due to flexibility caused by using vertical curves with smaller radii (Khoury et al., 2019).

This paper examines how the developing capabilities of automated drivers may be included in an iterative process of updating road design parameters. Through a review of the *Norwegian Handbook of Geometric Road Design* (Statens vegvesen, 2019a), and a comparison to the equivalent U.S. design parameters from the American Association of State Highway and Transportation Officials' (AASHTO) *A Policy on Geometric Design of Highways and Streets*, parameters that are likely to be affected by this change are suggested. The work is aimed at providing transportation engineers and road authorities with a starting point to revise road design parameters to accommodate the increasing levels of automation seen in today's road transportation.

1.1 Geometric Road Design

The design of roadways in Norway is governed by the *Handbook of Road and Street Design N100* (Statens vegvesen, 2019a) and the *Handbook of Geometric Road Design V120* (Statens vegvesen, 2019b). In the following, the road design parameters from the latter, which are used in geometric road design and ultimately roadway construction, will be presented and subsequently reviewed in light of the automated driver. While these guidelines are specific to Norway, they are based on theoretical concepts in physics and geometry that are universally related to road design, and thus show similarities to other international design standards. The parameters used in Norwegian geometric road design are compared to the U.S. equivalents from AASHTO's *A Policy on Geometric Design of Highways and Streets*.

Geometric road design consists of 1) Basic parameters, e.g., eye height and reaction time, and 2) derived Design parameters, including horizontal and vertical curve radii. The parameters are presented in **Figure 1**, where the basic parameters appear in blue and the design parameters in white.

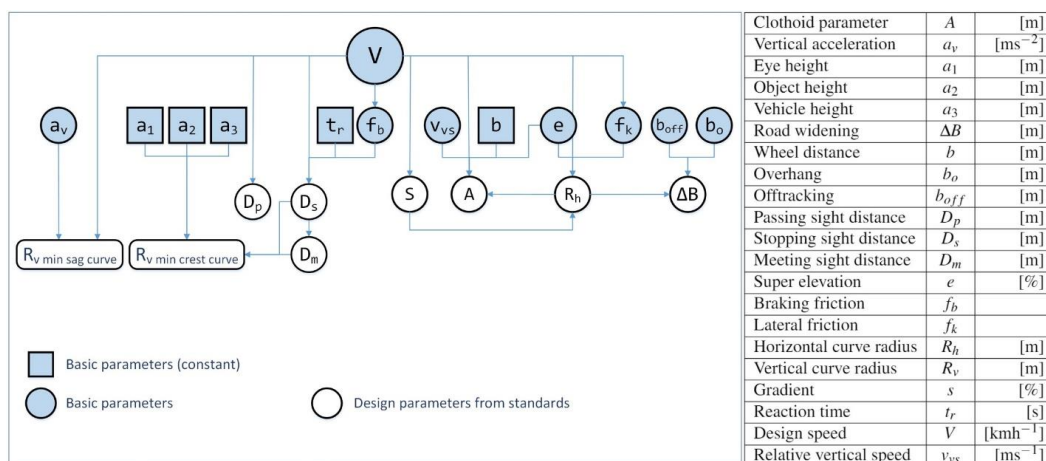


Figure 1 Relationship between basic parameters (blue) and design parameters (white) derived from (Statens vegvesen, 2019b)

Automated driving features are becoming more common on public roads including Advanced driver assistance systems (ADAS) and more advanced systems such as General Motor's *Super Cruise* and Tesla's *Autopilot*. Fully automated driving systems are suggested to be publicly available in two to three decades (Litman, 2018). When a road is planned, it is built to serve the traffic needs in the subsequent 20 years. This indicates that geometric road design needs to be revised to include automated users. The following section defines automated drivers and identifies known characteristics of these new road users. As automated drivers are under development this definition is based on existing driving automation features.

1.2 Defining the automated driver

Today's road design is based on human characteristics, including *Eye height* and *Reaction time*. To reevaluate current road design considering the new road user, the automated driver must be defined. The Society of Automotive Engineers defines six different levels of automated driving as shown in **Table 1**, where level 0 is no automation and level 1 represents ADAS features such as lane departure warning, advanced cruise control and parking assistance.

Driving automation systems like *Autopilot* and *Super Cruise* are at level 2 as they are not able to handle the Object and Event Detection and Response (OEDR) functions, e.g., handling road works. On level 3, the driving automation is capable of OEDR with the human driver ready to take over if needed, i.e., fallback. At level 3 the fallback-ready user can be either a human driver or the driving automation system itself. If fallback is necessary, it means that the automated driver is unable to perform the driving tasks. If a human is the fallback-ready user it may continue to drive if possible, while if the system is the fallback, it will try to achieve a minimal risk condition, e.g., stopping at the side of the road. At level 4 and 5 the driving automation system handles all dynamic driving tasks. Level 4 may have restrictions on the

conditions under which it can operate, known as the operational design domain (ODD), e.g., it may not handle snowy conditions.

Table 1 Levels of driving automation adapted from (SAE International, 2018).

Dynamic Driving Task (DDT)					
Level	Name	Sustained lateral and longitudinal control	Object/Event Detection and Response (OEDR)	Fallback	Operational Design Domain (ODD)
0	No driving automation	Driver	Driver	Driver	N/A
1	Driver assistance	Driver and System	Driver	Driver	Limited
2	Partial driving automation	System	Driver	Driver	Limited
3	Conditional driving automation	System	System	Fallback-ready user	Limited
4	High driving automation	System	System	System	
5	Full driving automation	System	System	System	Unlimited

The levels of automation defined by SAE International define the role of human and automated driving system but do not describe how the automated driver differs from human drivers. Characteristics of automated drivers are related to their sensors, sensor placement and the software that interprets the sensor data and controls the vehicle. Based on commonly used sensors in modern cars some differences between human and automated driver can be identified.

Vehicles with driving automation functionality have sensors that monitor the vehicle itself as well as sensors that sense the driving environment outside it. In relation to road design, the sensors that sense the environment outside the vehicle are the most important. The most commonly used environmental perception sensors are radars, cameras, and sonars (ultrasound) when considering publicly available vehicles. Lidars are widely used for development vehicles and are likely to be used in cars accessible to the public for higher levels of automation in the future (Gruyer et al., 2017; Hirz & Walzel, 2018; Steinbaeck et al., 2017; Van Brummelen et al., 2018).

At any level of automation, the automated driving system's environmental perception is different to a human driver's perception. Humans have one eye height where the value used in road design is based on statistical means of human eye height while sitting in the driver seat of a car. Humans can use mirrors and aids such as rear-facing cameras to increase their field of view but can only look in one direction at a time.

Sensor placement for cars can be lower than human eye height, e.g., parking sensors, at approximately the same height as human eye height, such as cameras in the rear-view mirror

sensor cluster, and higher than human sight, e.g., roof-mounted lidars. Sensors are placed around the vehicle so that automated driving features have perception in all direction at once. From this it is apparent that the *Eye height* parameter used in geometric road design is not applicable to automated drivers.

2. Related Work

2.1 The Impact of Automated Driving on Geometric Road Design

Literature searches were performed in Oria (a database of literature available via Norwegian universities and research institutions) and Google Scholar using the search terms: *geometric road design* AND (*automated* OR *autonomous*) AND (*driving* OR *driver* OR *vehicle*). Farah et al. (2018) pointed out in their state of the art on infrastructure for automated and connected vehicles that adaptations of physical road infrastructure to facilitate automated driving represents a knowledge gap.

Washburn et al. (2018) discussed the impact of automated driving on transport engineering. Related to geometric road design they suggest that automated drivers will have shorter reaction times and potentially higher acceleration and deceleration rates which, in turn, can lead to shorter ramps, steeper upgrades/downgrades and steeper and/or shorter climbing/passing lanes. A shorter reaction time would also lead to shorter stopping and decision sight distances. However, they conclude that vehicle performance as a result of driving automation is not likely to impact on geometric design standards due to 1) limits in acceleration/deceleration due to tire/pavement interface, 2) road design needs to consider drivers and vehicles in the lower end of the performance range, and 3) human comfort considerations.

Khoury et al. (2019) reviewed the road design parameters stopping sight distance (SSD), decision sight distance (DSD), and vertical curve radii. In their analyses they consider only fully automated transport and conclude that the shorter SSDs can be obtained as a result of the expectation of lower reaction time and that radii of vertical curves can be reduced while still being limited by human comfort. They also find that sensor placement, i.e., the automated drivers *eye height* impacts the stopping and decisions sight distances.

Considering reaction time, Khoury et al. suggest 0.5 seconds as the time from an object is detected by an automated driver to the brakes are applied. This is in line with the findings of Collin et al. (2019) who simulated the performance of different system architectures in terms of latency (e.g., the time between identifying an object and a braking action) and cost as defined by the load on the system's processing and communication (i.e. the cost of the computing system's processors and buses). In their simulation they found the latency of the system architectures performing the tasks to be between 0.34 and 0.38 seconds (Collin et al., 2019). Reaction time will be dependent on the amount and type of sensors used as well as the hardware and software architecture of the driving system as well as the complexity of the driving environment. How object detection is defined is also of interest when considering automated drivers. Object detection is also dependent on the hardware and software set-up. An object can be detected as pixels in one or more frames (Sivaraman & Trivedi, 2013), by fusing sensor signals from different sources (Wang et al., 2016) and machine learning can be utilized to help automated drivers discern different elements of the driving environment (Ohn-bar & Trivedi, 2015). There is also the issue of correctly classifying what the sensors detect. In general, machines are not as adept as humans in broad categorization (Branson et al., 2014; Fleuret et al., 2011; Linsley et al., 2017) and they can not be trained on every thinkable driving scenario in advance.

Stopping sight distances are based on designing roads where the driver is able to detect an obstacle and stopping before hitting it. Urmson (2006) found that swerving around an obstacle requires a smaller distance than stopping for it. However, to be able to swerve around an obstacle there needs to be the available free space outside the normal lane. This will not always be the case due to oncoming traffic or safety barriers but may be an option for the future on roads without safety barriers and in instances without oncoming vehicles .

Regarding horizontal curvature, García et al. (2020) used a vehicle with level 2 automation, BMW 520d 2017 model with Active Cruise Control (ACC) and Lane Keeping Assistant (LKA), to investigate the maximum speed this lower level of driving automation could obtain through horizontal curves. They found that this level 2 driving functionality consistently drove below the posted speed limit. This research is based on one specific implementation of level 2 automation which can be assumed also to have been programmed to behave on the cautious side. Higher levels of automation should be able to drive as fast as humans or faster, however, there are limitations on the minimum radii of horizontal curves that relate to the danger of skidding or rollover (Easa & Dabbour, 2003; Harwood & Mason, 1994).

Road design is to a large extent governed by the poorest performers. When considering road design to include automated users, these are largely expected to be human drivers with the exception of level 2 driving automation as identified by García et al. (2020). From this it follows that road design for both human and automated users will be limited by human capabilities. This may be the reason that most of the research on the impact of driving automation on geometric road design considers full automation only. However, there is one other application where the changes to road design as a result of automation can be explored; namely automated freight of goods that excludes human passengers.

In the following, the geometric road design parameters used in Norwegian road design will be assessed considering automated drivers. Norwegian geometric road design is governed by the Handbook of Geometric Road Design V120 (Statens vegvesen, 2019b). These will be discussed and compared to U.S. road design equivalents primarily governed by the American Association of State Highway and Transportation Officials' (AASHTO) guidelines in A Policy on Geometric Design of Highways and Streets (American Association of State Highway and Transportation Officials, 2011). While these guidelines are specific to these countries, they are based on theoretical concepts in physics and geometry that are universally related to road design, and thus have international relevance.

3. Analyses

The analyses will cover what are referred to as basic parameters in Norwegian design standard first as they are used in the remaining design parameters discussed in section 3.2.

3.1 Basic parameters

Vehicle size and dimensions

Several basic parameters used in road design are based on the size of the vehicle, including *Vehicle height*, *Vehicle width* and *Wheel distance*, *Overhang*, and *Off-tracking*. Due to the increasingly precise positioning capabilities expected from automated drivers, some researchers have suggested that lanes will become narrower (Hayeri et al., 2015). If this is true, it seems unlikely that vehicle width will increase. Additionally, increasing the outer dimensions of vehicles would mean less distance to other vehicles, curbs, and dividers within the current

infrastructure, which in turn would yield smaller safety margins for positioning and maneuvering. Moreover, increases in outer size would require that changes be made to supporting infrastructure such as on- and offloading facilities. It has been suggested that fully automated vehicles can be more flexible in design, for instance as small pods for moving passengers or distributing goods in cities (Duarte & Ratti, 2018). In the case of trucks, the outer dimensions at present time cannot be decreased without providing less space for goods which is undesirable in freight application. Platooning has been suggested to introduce a need for longer ramps, shoulders and designated lanes (Farah et al., 2018; Hayeri et al., 2015) will be required, all of which could also allow for longer vehicles.

Although, in time, vehicles may change in size and function due to automation, for now there are no clear trends that indicate a need to change the generalized vehicle dimensions used in road design. Regardless of this situation, the statistical variance of vehicles should continue to be evaluated periodically to check that the parameters relating to vehicle size continue to be representative of the current fleet of vehicles of a given class. This includes basic parameters such as *Vehicle height* (a_3), *Wheel distance* (b), *Overhang* (b_o) and *Offtracking* (b_{off}). Although *Eye height* (a_1) can also be said to be related to a vehicle's outer dimensions, the value will depend more on the placement of sensors than the height or width of the vehicle itself.

Eye height, a_1

For a human driver, Eye height is dependent on the human driver's height and the position of the driver's seat in relation to the road. In the case of an automated driver, "eye height" is dependent on the position of its sensors. Cameras are often placed in the vicinity of the rear-view mirror. This placement may produce a somewhat higher "eye height" than those used in the Norwegian and American road standards of 1.1 or 1.08 meters, respectively (AASHTO, 2011; Statens vegvesen, 2019b). Radars and ultrasound are normally placed below the windows on the vehicle's body. In this case, the "eye height" of the vehicle is lower than that of a human. The use of multiple sensors therefore allows the automated driver to obtain visibility far beyond the human driver. A low sensor placement can give vision below vehicles or other obstacles, sensor placement above the standardized human eye height allow for longer sight lines for example in the case of crest curves. Furthermore, placing sensors in the extremes of the width of the vehicle can give superior sight lines in horizontal curves. The *Eye height* parameter is not applicable to automated driving systems and should therefore be revised.

Eye height is used in the design of crest curves (**Figure 2**).

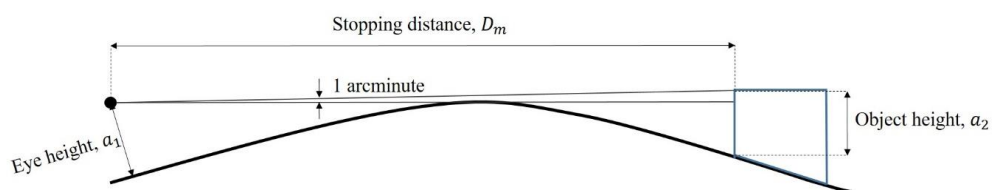


Figure 2 Crest curve and the use of eye height and object height

The requirement for the smallest vertical crest curve in the *Norwegian Handbook of Geometric Road Design* is based on securing an adequate stopping distance before an object on the other side of the crest curve.

Object height, a_2

Object height is defined as the height of an object that a driver can detect and stop for. The detection of an object by a human in the Norwegian road design standard is defined as seeing a sector of the object covered by an angle of one arcminute (as shown in **Figure 2**). *Object height* is set at 0.25 m (Statens vegvesen, 2019b). The U.S. value is 0.60 m, based on the finding that objects with heights less than this are not likely to be involved in crashes (AASHTO, 2011). If a crest curve were to be designed for meeting sight distance, for example on a one-lane road, values of vehicle height (a_3) measuring 1.25 m and 1.08 m would be used in Norway and the US, respectively (AASHTO, 2011; Statens vegvesen, 2019b).

The detection of an object by an automated driver may be done by many different sensors; therefore, it can be defined in different ways. For example, for a camera it can be based on the number of pixels at a given distance; however, the number of pixels seen at a given distance does not indicate a quality of perception without the viewer knowing something about the size of the object. Regarding other sensors, such as radars and lidars, the detection of an object could be defined by a defined signal response. The signal that is transmitted and reflected depends on the hardware and software used. Furthermore, the reflected signal depends on the surface characteristics as well as the size and movement of the object in question (Yang & Wang, 2011). Thus, it might be more reasonable to define object detection by an automated driver as correct identification based on its software. This detection relies on input from either the automated driver's own sensors or a trusted external source, for instance via communication with another vehicle or roadside sensors. The software must be able to both identify an object's existence and determine if this object must be avoided. The *Object height* parameter should be revised in conjunction with eye height. For automated users parameter(s) describing the sight lines and object detection capabilities are suggested in place of the eye height and object height parameters used in human-oriented road design.

Reaction time, t_r

Reaction time is a crucial parameter when considering any type of driving, as it impacts the distance needed to stop at a given speed. The parameter is used to find stopping and meeting sight distance, where a shorter reaction time can theoretically allow for a higher speed limit on an existing roadway or reduce sight distance design requirements for a new roadway.

It is challenging to estimate the *Reaction time* for an automated driver because it is a systemic response, and the system has not yet been fully defined. Humans' reaction times may span from almost negligible to over 1.64 seconds (AASHTO, 2011) depending on the complexity of the situation, attention of the driver and individual performance. The recommended design criteria for reaction time is 2.5 seconds in the U.S. (AASHTO, 2011), while the Norwegian standard uses 2.0 seconds (Statens vegvesen, 2019b). It is generally

expected that automated drivers will have shorter reaction times than human drivers (Farah et al., 2018; Teoh & Kidd, 2017). The automated driver's *Reaction time* depends on vehicle characteristics and driving situations. The more sensors the vehicle has, the more information it has to create an understanding of its surroundings while adding to the data load. Hardware, (e.g. sensors and processing power) and software determine the system's processing speed (Katrakazas et al., 2015). The automated driver's *Reaction time* also depends on the complexity of the situation it is interpreting.

The push for low reaction times and long detection ranges conflict with high resolution and sample rates, limiting the overall amount of data processed. Robust and accurate algorithms that turn the sensor data into correct decisions might increase the computational complexity of driving (Shi et al., 2017). For instance, automated drivers are often developed using machine learning, and the training set contains a large number of scenarios where there is nothing out of the ordinary happening, e.g., driving on a freeway. This means that the automated driver trains mostly on dealing with easy scenarios; as a result, it does not become as accomplished at handling extraordinary events, referred to as *corner cases* (Bolte et al., 2019). More complex software thus requires more advanced hardware to obtain acceptable reaction times (Collin et al., 2019; Shi et al., 2017). The artificial intelligence behind the decision-making process will continue to evolve, which means that the automated drivers' choices and latencies can change over time (Shi et al., 2017). *Reaction time*, therefore, also needs to be revised to include automated drivers where the ability to correctly interpret driving situations and make correct decisions must be assured when the *Reaction time* of a driving automation system is considered.

Design speed, V.

The design speed is used to determine elements of the horizontal alignment, vertical alignment, and cross-sectional design. Furthermore, design speed (along with braking friction) affect stopping and meeting distances, which will be covered in section 2.2.

The *Design speed* is the speed limit plus a buffer that depends on the road standard. The added buffer considers measured operating speeds and accounts for risks associated with driving on the road, increasing with higher speed limits and the average annual daily traffic rate (Statens vegvesen, 2019a). The *Design speed* also impacts the basic parameters of lateral and braking friction, as tire/road friction decreases non-linearly with increasing speed (Fan et al., 2010; Heinrichs et al., 2004).

Design speed may be affected by automated driving in two ways. First, automated drivers can be programmed to adhere to speed limits. This would make speed limits equivalent to operating speeds and reduce the need for safety buffers in design speeds, which would not impact geometric design, as the *Design speed* does not change. Secondly, if automated drivers can be assumed to have lower *Reaction times* than humans, it could allow higher *Design speeds* for existing infrastructures (McDonald & Rodier, 2015; Washburn et al., 2018). Indeed, in the short term, speed limits could be set equivalent to the design speed for automated drivers. If lower reaction times and safe operations can be consistently demonstrated by automated drivers

under challenging conditions, then it may be considered if established speed limits and design speed could be increased. However, *Design speed*, as well as other design parameters such as minimum curve radii, are also limited by human comfort. The road design developed over the last century considers the forces acting on the human body due to inertia to ensure that driving feels comfortable for humans.

Vehicle dynamics

Vehicle dynamics such as *Acceleration*, a , and *Retardation (Deceleration)*, r , are dependent on vehicle characteristics and road conditions, including the available friction of the road surface. Both parameters are used in Norway to determine the length of road sections where active acceleration or deceleration takes place, i.e., ramps for entering or exiting highways. It has been suggested that automated drivers are more effective at braking than human drivers (Washburn et al., 2018), yet there is no data or information on vehicle dynamics associated with automated drivers providing insight into how acceleration and retardation may change. Additionally, advances in rates of acceleration and deceleration may find themselves limited by human comfort. These parameters should therefore be reassessed as more information on automated drivers emerges, and they should also be considered more specifically in transport cases without human passengers.

Vertical acceleration (a_v)

The limit on *Vertical accelerations* (0.3 ms^{-2}) is used to ensure the comfort of the human driver or passenger (Statens vegvesen, 2019a) and factors into the minimum *Vertical curve radius* in sag curves. During automated driving, this means that if there are human passengers in the vehicle, this parameter is likely to remain the same. In the event of automated driving without humans, e.g., freight, the maximum *Vertical acceleration* might be relaxed, if the goods transported would not be negatively affected.

Relative vertical speed (v_{vs})

The *Relative vertical speed* is the difference in vertical speeds of wheels located on the same axle, for instance due to turning motions caused by the outer and inner wheel following radii of different sizes. In road design *Relative vertical speed* is used to determine the lengths required to achieve a certain superelevation. As with vertical acceleration, the parameter limit (0.05 ms^{-1}) is set due to human comfort (Statens vegvesen, 2019a) and could be altered for transportation without humans.

Total available friction (f_t)

Drivers need friction to brake and avoid unwanted lateral movement while moving through a horizontal curve. The design values for available friction levels are based on empirical findings. The values used in Norway are assumed to be valid for 95% of the road surface under wet conditions when measured at 60 km/h and adjusted for other speeds (Statens vegvesen, 2019b). Although total friction values are not used in road design, they may be broken down to obtain braking friction, f_b , and lateral friction, f_k , as seen below in Equation 1.

$$f_t^2 = f_k^2 + f_b^2 \quad (1)$$

The *Braking friction* is not expected to change when an automated driver is behind the steering wheel, as the total friction required to halt the vehicle from its current speed is not dependent on the driver. Similarly, as previously mentioned, while *Lateral friction* is assumed to remain unaffected, any increases made to design speed will decrease tire/road friction levels.

Superelevation (e)

Superelevation helps keep vehicles on the road while they are moving through horizontal curves by increasing the lateral friction, thereby affecting horizontal radii. The maximum value of superelevation, e_{\max} , in Norway (8%) is limited by winter conditions, which results in slow-moving vehicles not being able to slide inwards on the curve in icy conditions. Higher Superelevations also increase the probability of rollover for larger vehicles (Easa & Dabbour, 2003; Harwood & Mason, 1994). The corresponding value for e_{\max} in the U.S. is 12% (AASHTO, 2011). Superelevation also impacts the length of clothoids (also known as spiral transition curves), allowing for safe and comfortable transitions between cross-sloped and superelevated road segments. Because of these winter driving conditions, it is unlikely that any change will be made to these requirements.

3.2 Implications for Design Parameters

This section discussed the impact of automated drivers on design parameters.

Stopping sight distance (D_s)

The *Stopping sight distance* is the distance drivers need to stop for an object in the road and is equal to the sum of the reaction distance, D_r , and braking distance, D_b , i.e.:

$$D_s = D_r + D_b = 0.278 * t_r * V + \frac{V^2}{254.3*(f_b+s)} \quad (2)$$

It is dependent on *Design speed*, V (kmh^{-1}), and *Reaction time*, t_r (s), as well as *Braking friction*, f_b , and *Gradient*, s . In the formula used in Norwegian design, the constant value 0.278 accounts for unit conversion, and the constant value 254.3 accounts for gravitational acceleration and unit conversion. Given the expected changes to reaction times (and possibly design speeds), this distance is likely to be affected by changing to an automated driver because a lower reaction time will have the potential to reduce the stopping distance considerably, even when applying a higher design speed.

To illustrate, **Figure 3** shows how the SSD is affected by changes in reaction time and design speed. For instance, given a design speed of 80 kmh^{-1} , a reduction in the reaction time from 2 seconds to 1 second produces a 22.4 percent lower stopping sight distance.



Figure 3 The effect of reductions in reaction time (t_r) and increases in design speed (V) on stopping sight distances

Meeting sight distance (D_m)

The Meeting sight distance is defined by **Equation 3**:

$$D_m = 2D_s + 10 \quad (3)$$

The Meeting sight distance is directly related to the Stopping sight distance, which means that the effects of having an automated driver would be similar, i.e. a lower Reaction time will yield lower meeting sight distances, even when considering higher design speeds.

Passing sight distance (D_p)

The passing sight distance is calculated by a model for overtaking, as shown in **Figure 4** (Statens vegvesen, 2019a). The model is based on three vehicles, an active vehicle that is trying to overtake another vehicle, a passive vehicle, and an oncoming vehicle.

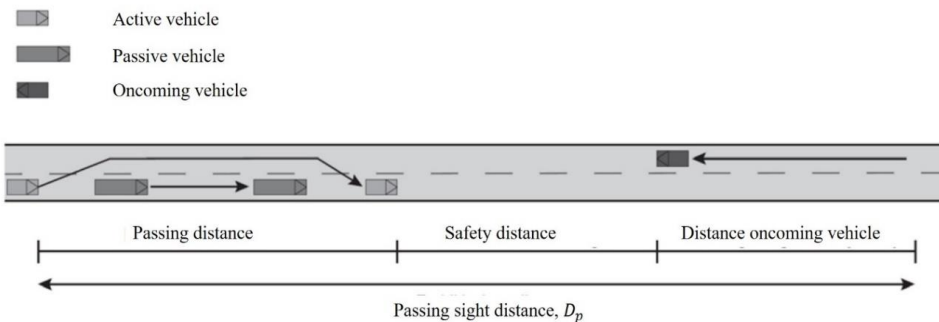


Figure 4 Passing sight distance (Statens vegvesen, 2019b)

The speeds of the vehicles are found in **Equations 4-6**:

$$V_{active} = 1.19 * V_{passive} + 3.87 \quad (4)$$

$$V_{passive} = Speed\ limit - 5\ kmh^{-1} \quad (5)$$

$$V_{oncoming} = Speed\ limit + 5\ kmh^{-1} \quad (6)$$

The passing sight distance is the sum of the passing distance, safety distance and distance covered by the oncoming vehicle, as illustrated by **Figure 4**.

The three individual distances that make up the passing sight distance are all related to one or more of the three vehicle speeds found in the model. The potential increase in speed following the automation of driving would therefore increase passing sight distances.

Vertical curve radius (R_v)

The minimum *Vertical curve radius* for crest curves is determined by the *Stopping sight distance* (D_s), as well as the *Eye height* (a₁) and *Object height* (a₂), or *Meeting sight distance* (D_m), *Eye height*, *Vehicle height* (a₃) for one-lane roadways, as shown in **Equation 7**.

$$R_{v,min} = \frac{1}{2} * \left(\frac{D_{s(m)}}{\sqrt{a_1} + \sqrt{a_{2(3)}}} \right)^2 \quad (7)$$

As described above, the sight distance is linked to speed and reaction times. A higher *Design speed* alone will therefore result in a larger radii vertical curve, while a lower *Reaction time* will reduce the radius, even at a higher design speed.

Vertical crest curve radii are also affected by the vehicle characteristics of the automated driver that are equivalent to human eye height. An *Eye height* that is higher above the road than the values currently used for human *Eye height* will allow for a smaller *Vertical curve radius* (Khoury et al., 2019). *Object height* is also central to the determination of crest curve radii, and, as previously stated, should be revised for automated drivers given that there are differences in the way automated vehicles identify objects in the roadway. *Vehicle height* is not considered to be affected by automated drivers at present time. While sight distance currently controls the design of crest curves, if reductions to sight distance requirements were great enough, a limiting factor might still be comfort, i.e., whether it is possible to increase speed or make curvatures smaller without compromising on the human comfort factor.

For vertical sag curves, R_{vmin} is defined by **Equation 8**:

$$R_{v,min} = \frac{v^2}{12.96 * a_v} \quad (8)$$

In the formula, the constant value 12.96 accounts for unit conversion.

Sag curves are designed for daylight conditions in Norway; thus, they inherently have less sight distance concerns and are designed to ensure the comfort of the driver/passenger. The

limitation is therefore in the *Vertical acceleration*, a_v , which in Norwegian and U.S. design requirements is set to 0.3 ms^{-2} . As a result, roads designed without human comfort in mind could use smaller radii for both crest and sag curves.

Horizontal curve radius (R_h)

$R_{h,min}$ is related to *Design speed*, V (kmh^{-1}), *Superelevation* (e), and *Lateral friction* (f_k) as shown in **Equation 9**. In the formula, the constant value 127 accounts for gravitational acceleration and unit conversion.

$$R_{h,min} = \frac{V^2}{127*(e_{max}+f_k)} \quad (9)$$

An increased *Design speed* would lead to a larger minimum curvature. While the *Superelevation* e_{max} is not likely to change due to danger of skidding or rollover issues.

Tunnels comprise a unique case in road design since the tunnel walls restrict the available sight distance through curves. Thus, the minimum horizontal curvature in tunnels is controlled by sight distance and is determined by **Equation 10**:

$$R_{h,min} = \frac{D_s^2}{8*B} \quad (10)$$

In this equation, D_s is the required *Stopping sight distance*, and B is the distance from the center of the lane to the tunnel wall. A lower *Reaction time* would have the potential to reduce the minimum horizontal curvatures due to its relation to the stopping distance.

Clothoid parameter (A)

A *Clothoid* is a spiral curve used to transition between different horizontal curve radii. The minimum *Clothoid parameter*, A_{min} , is related to the minimum *Horizontal curve radius*, $R_{h,min}$, and length, as shown by **Equations 10 and 11**:

$$A_{min} = \sqrt{R_{h,min} * L_{o,min}} \quad (10), \text{ where } L_{o,min} = \frac{b*V*e_{max}}{3,6*v_{ps}} \quad (11)$$

$L_{o,min}$ is the distance needed to achieve the maximum *Superelevation*, and it increases at higher speeds, while the *Superelevation* and *Wheel distance*, b , are assumed to remain the same. A reduction in length could result from a greater relative vertical speed that could be considered for human-free movement, which is again due to relaxing comfort restraints.

Road widening (ΔB)

Road widening is necessary in small horizontal curves (less than 500m in radius) and increases with larger vehicle types. Based on arguments pertaining to the size and dimension of vehicles with the evolution of the automated driver, the parameters related to vehicle size are assumed to stay the same. As *Road widening* is related to the *Horizontal curve radii*, significant decreases in minimum *Horizontal curve radii* would increase the design needs for *Road widening*; however, this would not change the widening width itself.

4. Discussion

The parameters for geometric road design were evaluated in light of the automated driver. The results of the analyses in section 3.1 and 3.2 are summarized in **Figure 5**.

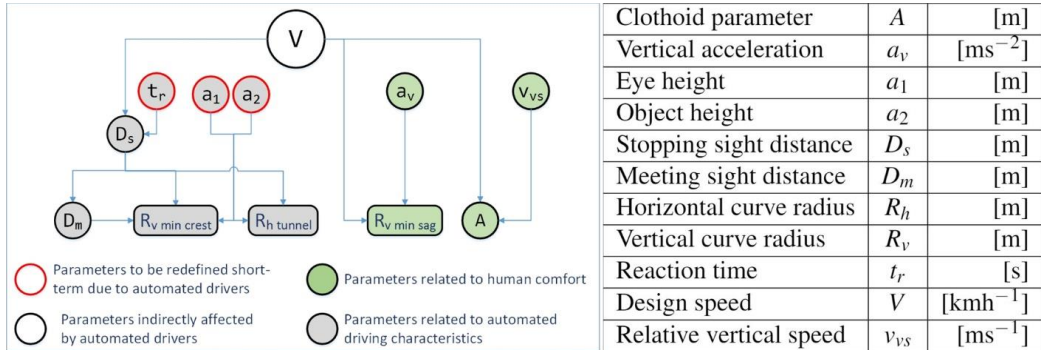


Figure 5 Parameters of geometric road design affected by the automated driver

Eye height, *Object height* and *Reaction time* are basic parameters that differ significantly from human to automated driver, as these depend on the automated driver's hardware (i.e., sensors) and software. The concept of *Eye height* is a direct consequence of human anatomy and as such is not applicable to an automated driver. An automated vehicle is likely to be surrounded by sensor perception located at different heights. This means that the concept of *Eye height* and design parameters linked to eye height, i.e., the minimum vertical crest curve, should be revised.

Similarly, *Object height* (i.e. detecting objects ahead in the road) is a fundamentally different concept when considering an automated rather than a human driver. Like *Eye height*, *Object height* is currently used in the calculation of minimum crest curves. It might be more relevant to look at the processing and classification of sensory input to establish criteria on object height detection for automated drivers. As automated driving is under development, perception and classification by automated systems should continue to be investigated while encouraging developers of automated vehicles to design vehicles that can explain what they sense and why they choose the actions that they do, e.g., through explainable artificial intelligence.

Design speed can be considered a redundant parameter when exclusively considering automated drivers as they can be programmed to adhere to the maximum operating speed. While this fact alone does not change the geometric design parameters, as automated drivers increase in number and potential safety effects are realized, policies concerning design speed versus operating speed may be considered.

If automated drivers can be expected to have lower *Reaction times* than humans, it could have significant implications for road design. *Reaction time* and *Design speed* feature jointly in *Stopping sight distance* (D_s), *Meeting sight distance* (D_m), *Horizontal curve radius* (R_h) and *Vertical crest curve radius* ($R_{v,crest}$). In these instances, lower *Reaction times* allow for greater

Design speeds while still reducing distances and curve radii. This is not the case for passing distances (given the current Norwegian definition) or for vertical sag curve radii ($R_{v,sag}$) which are only related to *Design speed* and not to *Reaction time*. While *Reaction time* is expected to be lower for automated drivers than for human drivers; at the same time, this will require further monitoring in relation to how *Reaction times* for automated drivers are defined and under which circumstances this lower *Reaction time* occurs.

Although lane width is not part of the Norwegian geometric design parameters as described within this study, it is relevant to the discussion of how automated drivers can change road design. As mentioned, it has been suggested that lane widths could be made narrower due to the superior positioning of automated vehicles (Hayeri et al., 2015; Lumiaho & Malin, 2016; McDonald & Rodier, 2015), which could in turn either increase capacity by adding lanes to existing multilane roads or reduce the cost of building new roads. At present time, however, the accuracy of positioning is not high enough to warrant decreasing lane width (Cui et al., 2016), so mixed traffic will have to be assumed. Lane width reduction could be relevant for roads designed specifically for automated drivers.

4.1 Comfort

When considering the changes that could be made possible by automated drivers, including smaller horizontal and vertical curve radii, there might still be restrictions related to human comfort factors. The parameters linked to human comfort are indicated by green in **Figure 5**. The physical forces acting on the body are the foundation of how human comfort is currently factored into current geometric road design parameters. However, the term *comfort* may be perceived differently when it concerns an automated driver compared to a human driver. Research shows that the preferred driving style of an automated driver does not necessarily correspond to how humans would drive the vehicle themselves (Bellem et al., 2018). Humans indicated that they preferred the automated driver to perform distinct and observable movements (i.e., change speed or direction, or both), to signal that a maneuver was initiated in situations in which a critical element might arise, and provide a more flexible onset of actuators when the situation was not critical.

While accelerations associated with smaller radii curves might be problematic in terms of human comfort, they are of less concern if considering roads which serve only non-human transport. This type of road project has been suggested to take place between Detroit and Ann Arbor, Michigan (Roberts, 2020). In such a situation, automated drivers could potentially use a more flexible road design where narrower curves could be combined with wider curves to better suit the terrain (Khoury et al., 2019). Yet if considering roads designed specifically for freight vehicles, smaller radii curves may be problematic for trucks in terms of forces acting on the vehicle and cargo. Today, successive radii have similar sizes, a factor that makes the road predictable for humans and supports steady speeds. In Norwegian road design, long stretches of straight roads are also avoided to mitigate human drivers' drowsiness. Removing the comfort-

related aspects of predictability and variability needed for human drivers and passengers could thus make possible road alignments that are more cost-efficient to build.

4.2 Connectivity

If vehicles can communicate with each other, then theoretically, vehicles could be notified of obstacles in the road well in advance of reaching them (Farah et al., 2018), giving an altogether different meaning to reaction time and sight distances. However, this implies flawless coverage and communication services, which is unlikely to occur; furthermore, it would require that a previous vehicle would pass on this information. As the latter cannot be assumed to be true, connectivity is no substitute for needing a reaction time generated by the system. 5.

5. Conclusion

Road design parameters must be updated to accommodate the new road user, the automated driver. As a starting point for making way for the automated driver in road design, after a review of the current Norwegian road design standards, the following action points are suggested.

Short-term recommendations are to redefine the following road geometry parameters:

- *Eye height*
- *Object height*
- *Reaction time*

These parameters are the ones most impacted by the introduction of the automated driver, affecting road design parameters such as sight and stopping distances as well as horizontal and vertical curvatures. Given the way automated drivers identify and react to obstacles in the roadway, traditional considerations of these parameters need to be revisited and likely revised.

Long-term recommendations are to evaluate the possibility of a geometric road design standard for automated freight where the following design parameters are found to be promising candidates for increasing the flexibility of road design:

- *Vertical acceleration*
- *Relative vertical speed*
- *Clothoid parameter*
- *Minimum vertical curve radii (crest)*
- *Minimum vertical curve radii (sag)*
- *Horizontal curve radii*

Current road geometry parameters are closely linked to human comfort. Redefining standards of road design to incorporate the automated driver could include designing freight roads without human passengers, allowing for a more flexible design through smaller radii curves and shorter transition elements, for instance ramps or clothoids. Additionally, if higher *Acceleration/Deceleration* rates can be ensured, *Stopping*, *Meeting*, and *Passing sight distances* can be decreased.

Vehicle characteristics relating to both the physical dimensions of AVs, e.g., vehicle width or wheelbase, as well as vehicle dynamics, should be monitored so that changes to the assumptions used in the road design standards are aligned with the vehicle fleet. Additionally, consideration of whether design speed can be increased based on the performance of AVs is required.

Within this study, the need to revise current geometric road design parameters with the introduction of the automated driver has been highlighted, and recommendations on starting points for this iterative process have been presented. The greatest potential advantages with respect to freedom of road design are for automated freight transportation on designated roads. Building roads for these purposes might be worth the investment for specific cases, e.g., transporting goods from a production to a distribution site in challenging terrain. This could be met by a specific geometric road design standard for roads operated by solely automated drivers. The possibility of reducing the horizontal and vertical curvatures should be assessed with the risk of unintended effects in mind, e.g., inducing unwanted forces acting to move the cargo away from the vehicle. Increases in fuel consumption should also be considered. In the case of mixed traffic, more research is needed on how automated driving affects human comfort.

ACKNOWLEDGMENTS

This research has been funded by the Norwegian Public Roads Administration.

References

- American Association of State Highway and Transportation Officials. (2011). *A Policy on Geometric Design of Highways and Streets* (6th ed.). American Association of State Highway and Transportation Officials.
- Bellem, H., Thiel, B., Schrauf, M., & Krems, J. F. (2018). Comfort in automated driving: An analysis of preferences for different automated driving styles and their dependence on personality traits. *Transportation Research Part F: Traffic Psychology and Behaviour*, 55, 90–100. <https://doi.org/10.1016/j.trf.2018.02.036>
- Ben-Bassat, T., & Shinar, D. (2011). Effect of shoulder width, guardrail and roadway geometry on driver perception and behavior. *Accident Analysis and Prevention*, 43(6), 2142–2152. <https://doi.org/10.1016/j.aap.2011.06.004>
- Bolte, J. A., Bar, A., Lipinski, D., & Fingscheidt, T. (2019). Towards corner case detection for autonomous driving. *IEEE Intelligent Vehicles Symposium, Proceedings, 2019-June*, 438–445. <https://doi.org/10.1109/IVS.2019.8813817>
- Branson, S., Van Horn, G., Wah, C., Perona, P., & Belongie, S. (2014). The ignorant led by the blind: A hybrid human-machine vision system for fine-grained categorization. *International Journal of Computer Vision*, 108(1–2), 3–29. <https://doi.org/10.1007/s11263-014-0698-4>
- Charlton, S. G. (2007). The role of attention in horizontal curves: A comparison of advance warning, delineation, and road marking treatments. *Accident Analysis and Prevention*, 39(5), 873–885. <https://doi.org/10.1016/j.aap.2006.12.007>
- Collin, A., Siddiqi, A., Imanishi, Y., Rebentisch, E., Tanimichi, T., & de Weck, O. L. (2019). Autonomous driving systems hardware and software architecture exploration: optimizing latency and cost under safety constraints. *Systems Engineering, October 2018*, 327–337. <https://doi.org/10.1002/sys.21528>
- Cui, D., Xue, J., & Zheng, N. (2016). Real-Time Global Localization of Robotic Cars in Lane Level via Lane Marking Detection and Shape Registration. *IEEE Transactions on Intelligent Transportation Systems*, 17(4), 1039–1050. <https://doi.org/10.1109/TITS.2015.2492019>
- De Santos-Berbel, C., & Castro, M. (2020). Effect of vehicle swiveling headlamps and highway geometric design on nighttime sight distance. *Mathematics and Computers in Simulation*, 170, 32–50. <https://doi.org/10.1016/j.matcom.2019.08.012>
- De Santos-Berbel, C., Castro, M., & Iglesias, L. (2016). Influence of headlamp lighting parameters on nighttime sight distance. *Proceedings of the 3rd International Conference on Traffic and Transport Engineering (ICTTE), November*, 88–94.
- Deshpande, A., Godbole, D., Göllü, A., & Varaiya, P. (1996). Design and evaluation tools for automated highway systems. In *Lecture Notes in Computer Science (including subseries Lecture Notes in Artificial Intelligence and Lecture Notes in Bioinformatics)* (Vol. 1066). <https://doi.org/10.1007/BFb0020941>

- Duarte, F., & Ratti, C. (2018). The Impact of Autonomous Vehicles on Cities: A Review. *Journal of Urban Technology*, 25(4), 3–18.
<https://doi.org/10.1080/10630732.2018.1493883>
- Easa, S. M., & Dabbour, E. (2003). Design radius requirements for simple horizontal curves on three-dimensional alignments. *Canadian Journal of Civil Engineering*, 30(6), 1022–1033.
<https://doi.org/10.1139/103-022>
- Fan, S., Zhang, L., Cheng, L., Tian, G., & Yang, S. (2010). Effect of braking pressure and braking speed on the tribological properties of C/SiC aircraft brake materials. *Composites Science and Technology*, 70(6), 959–965.
<https://doi.org/10.1016/j.compscitech.2010.02.012>
- Farah, H., Erkens, S. M. J. G., Alkim, T., & van Arem, B. (2018). Infrastructure for Automated and Connected Driving: State of the Art and Future Research Directions. In *Road Vehicle Automation 4* (pp. 187–197). <https://doi.org/10.1007/978-3-319-60934-8>
- Fleuret, F., Li, T., Dubout, C., Wampler, E. K., Yantis, S., & Geman, D. (2011). Comparing machines and humans on a visual categorization test. *Proceedings of the National Academy of Sciences of the United States of America*, 108(43), 17621–17625.
<https://doi.org/10.1073/pnas.1109168108>
- García, A., Camacho-Torregrosa, F. J., & Padovani Baez, P. V. (2020). Examining the effect of road horizontal alignment on the speed of semi-automated vehicles. *Accident Analysis and Prevention*, 146(March), 105732. <https://doi.org/10.1016/j.aap.2020.105732>
- Gruyer, D., Magnier, V., Hamdi, K., Claussmann, L., Orfila, O., & Rakotonirainy, A. (2017). Perception, information processing and modeling: Critical stages for autonomous driving applications. *Annual Reviews in Control*, 44, 323–341.
<https://doi.org/10.1016/j.arcontrol.2017.09.012>
- Harwood, D. W., & Mason, J. M. (1994). Horizontal curve design for passenger cars and trucks. *Transportation Research Record*, 1445, 22–33.
- Hayeri, Y. M., Hendrickson, C. T., & Biehler, A. D. (2015). Potential impacts of vehicle automation on design, infrastructure and investment decisions - A State DOT perspective. *Transportation Research Board 93rd Annual Meeting. January 12-16, Washington, D.C.*, 301, 1–18.
- Heinrichs, B. E., Allin, B. D., Bowler, J. J., & Siegmund, G. P. (2004). Vehicle speed affects both pre-skid braking kinematics and average tire/roadway friction. *Accident Analysis and Prevention*, 36(5), 829–840. <https://doi.org/10.1016/j.aap.2003.08.002>
- Hirz, M., & Walzel, B. (2018). Sensor and object recognition technologies for self-driving cars. *Computer-Aided Design and Applications*, 15(4), 501–508.
<https://doi.org/10.1080/16864360.2017.1419638>
- Katrakazas, C., Quddus, M., Chen, W. H., & Deka, L. (2015). Real-time motion planning methods for autonomous on-road driving: State-of-the-art and future research directions.

Transportation Research Part C: Emerging Technologies, 60, 416–442.
<https://doi.org/10.1016/j.trc.2015.09.011>

- Khoury, J., Amine, K., & Saad, R. A. (2019). An Initial Investigation of the Effects of a Fully Automated Vehicle Fleet on Geometric Design. *Journal of Advanced Transportation*, 2019(May), 1–10. <https://doi.org/10.1155/2019/6126408>
- Linsley, D., Eberhardt, S., Sharma, T., Gupta, P., & Serre, T. (2017). What are the Visual Features Underlying Human Versus Machine Vision? *Proceedings - 2017 IEEE International Conference on Computer Vision Workshops, ICCVW 2017, 2018-Janua*, 2706–2714. <https://doi.org/10.1109/ICCVW.2017.331>
- Litman, T. (2018). Implications for Transport Planning. In *Autonomous Vehicle Implementation Predictions*.
 file:///C:/Users/aned/Downloads/AutonomousVehicleImplementationPredictions.pdf
- Lumiaho, A., & Malin, F. (2016). *Road Transport Automation Road Map and Action Plan 2016–2020*. https://julkaisut.liikennevirasto.fi/pdf8/lts_2016-19eng_road_transport_web.pdf
- Lutin, J. M., Kornhauser, A., & Lerner-Lam, E. (2013). The Revolutionary Development of Self-Driving Vehicles and Implications for the Transportation Engineering Profession. *ITE Journal - Institute of Transportation Engineers*, 88.
https://orfe.princeton.edu/~alaink/SmartDrivingCars/Papers/ITE_Journal_The_Revolutionary_Development_of_Self-Driving_Vehicles_and_Implications_for_the_Transportation_Engineering_Profession.pdf
- McDonald, S. S., & Rodier, C. (2015). Envisioning Automated Vehicles within the Built Environment: 2020, 2035, and 2050. In G. Meyer & S. Beiker (Eds.), *Road Vehicle Automation 2* (pp. 225–233). Springer International Publishing. https://doi.org/10.1007/978-3-319-19078-5_20
- National Highway Traffic Safety Administration. (2015). *Traffic safety facts Crash Stats Critical Reasons for Crashes Investigated in the National Motor Vehicle Crash Causation Survey*. <https://crashstats.nhtsa.dot.gov/Api/Public/ViewPublication/812115>
- Noy, I. Y., Shinar, D., & Horrey, W. J. (2018). Automated driving: Safety blind spots. *Safety Science*, 102(July 2017), 68–78. <https://doi.org/10.1016/j.ssci.2017.07.018>
- Ohn-bar, E., & Trivedi, M. M. (2015). Appearance Patterns. *IEEE Transactions on Intelligent Transportation Systems*, 16(5), 1–11.
- Papadimitriou, E., Mavromatis, S., & Psarianos, B. (2018). Stopping sight distance adequacy assessment on freeways: the case of left horizontal curves over crest vertical curves. *Transportation Letters*, 10(5), 269–279. <https://doi.org/10.1080/19427867.2016.1259759>
- Roberts, J. J. (2020, August 13). “Road of the Future” to link Detroit and Ann Arbor with 40 miles of driverless cars and shuttles | *Fortune*. <https://fortune.com/2020/08/13/road-of-the-future-detroit-ann-arbor-driverless-cars-autonomous-vehicles/>
- SAE International. (2018). SAE J3016 Surface Vehicle Recommended Practice. In *SAE*

International (Issue 724). http://standards.sae.org/J2016_201806

- Shi, W., Alawieh, M. B., Li, X., & Yu, H. (2017). Algorithm and hardware implementation for visual perception system in autonomous vehicle: A survey. *Integration, the VLSI Journal*, 59(May), 148–156. <https://doi.org/10.1016/j.vlsi.2017.07.007>
- Sivaraman, S., & Trivedi, M. M. (2013). Looking at vehicles on the road: A survey of vision-based vehicle detection, tracking, and behavior analysis. *IEEE Transactions on Intelligent Transportation Systems*, 14(4), 1773–1795. <https://doi.org/10.1109/TITS.2013.2266661>
- Statens vegvesen. (2019a). *Håndbok N100 - Veg- og gateutforming*. Vegdirektoratet. www.vegvesen.no.
- Statens vegvesen. (2019b). *Håndbok V120 Premisser for geometrisk utforming av veger*. Norwegian Public Roads Administration. www.vegvesen.no.
- Steinbaeck, J., Steger, C., Holweg, G., & Druml, N. (2017). Next generation radar sensors in automotive sensor fusion systems. *2017 Symposium on Sensor Data Fusion: Trends, Solutions, Applications, SDF 2017, 2017-Decem*, 1–6. <https://doi.org/10.1109/SDF.2017.8126389>
- Teoh, E. R., & Kidd, D. G. (2017). Rage against the machine? Google's self-driving cars versus human drivers. *Journal of Safety Research*, 63, 57–60. <https://doi.org/10.1016/j.jsr.2017.08.008>
- Transport Research Board. (1997). *Determination of Stopping Sight Distances NCHRP Report 400*. National Academy Press.
- Urmson, C. (2006). Driving beyond stopping distance constraints. *IEEE International Conference on Intelligent Robots and Systems*, 1189–1194. <https://doi.org/10.1109/IROS.2006.281852>
- Van Brummelen, J., O'Brien, M., Gruyer, D., & Najjaran, H. (2018). Autonomous vehicle perception: The technology of today and tomorrow. In *Transportation Research Part C: Emerging Technologies* (Vol. 89, pp. 384–406). Elsevier Ltd. <https://doi.org/10.1016/j.trc.2018.02.012>
- Vegdirektoratet. (2018). *Statens vegvesens rapporter Dybdeanalyser av døds-ulykker i vegtrafikken 2017*. https://www.vegvesen.no/_attachment/2346577/binary/1267249?fast_title=Dybdeanalyser+av+dødsulykker+i+vegtrafikken+2017.pdf
- Wang, X., Xu, L., Sun, H., Xin, J., & Zheng, N. (2016). On-Road Vehicle Detection and Tracking Using MMW Radar and Monovision Fusion. *IEEE Transactions on Intelligent Transportation Systems*, 17(7), 2075–2084. <https://doi.org/10.1109/TITS.2016.2533542>
- Washburn, S. S., Leslie, P. E., & Washburn, D. (2018). *Future Highways-Automated Vehicles*. www.SunCam.com
- Wood, J. S., & Donnell, E. T. (2017). Stopping sight distance and available sight distance new

model and reliability analysis comparison. *Transportation Research Record*, 2638(1), 1–9.
<https://doi.org/10.3141/2638-01>

Wood, J. S., & Zhang, S. (2020). Evaluating Relationships between Perception-Reaction Times, Emergency Deceleration Rates, and Crash Outcomes using Naturalistic Driving Data. *Transportation Research Record: Journal of the Transportation Research Board*, 036119812096660. <https://doi.org/10.1177/0361198120966602>

Yang, S. W., & Wang, C. C. (2011). On solving mirror reflection in LIDAR sensing. *IEEE/ASME Transactions on Mechatronics*, 16(2), 255–265.
<https://doi.org/10.1109/TMECH.2010.2040113>

Appendix C

Paper III

Article

Using ADAS to Future-Proof Roads—Comparison of Fog Line Detection from an In-Vehicle Camera and Mobile Retroreflector

Ane Dalsnes Storsæter ^{1,2,*} , Kelly Pitera ²  and Edward McCormack ^{2,3}

¹ Norwegian Public Roads Administration (NPRA), Directorate of Public Roads, 7030 Trondheim, Norway

² Department of Civil and Environmental Engineering, Norwegian University of Science and Technology (NTNU), 7491 Trondheim, Norway; kelly.pitera@ntnu.no (K.P.); edm@uw.edu (E.M.)

³ Civil and Environmental Engineering, University of Washington, Seattle, WA 98195, USA

* Correspondence: ane.storsater@ntnu.no; Tel.: +47-9775-9903

Abstract: Pavement markings are used to convey positioning information to both humans and automated driving systems. As automated driving is increasingly being adopted to support safety, it is important to understand how successfully sensor systems can interpret these markings. In this effort, an in-vehicle lane departure warning system was compared to data collected simultaneously from an externally mounted mobile retroreflector. The test, performed over 200 km of driving on three different routes in variable lighting conditions and road classes found that, depending on conditions, the retroreflector could predict whether the car's lane departure systems would detect markings in 92% to 98% of cases. The test demonstrated that automated driving systems can be used to monitor the state of pavement markings and can provide input on how to design and maintain road infrastructure to support automated driving features. Since data about the condition of lane marking from multiple lane departure warning systems (crowd-sourced data) can provide input into the pavement marking management systems operated by many road owners, these findings also indicate that these automated driving sensors have an important role in enhancing the maintenance of pavement markings.

Keywords: lane detection; retroreflector; road asset management; road maintenance; ADAS; automated driving; road infrastructure



Citation: Storsæter, A.D.; Pitera, K.; McCormack, E. Using ADAS to Future-Proof Roads—Comparison of Fog Line Detection from an In-Vehicle Camera and Mobile Retroreflector. *Sensors* **2021**, *21*, 1737. <https://doi.org/10.3390/s21051737>

Academic Editors: Dominique Gruyer and Rupak Kharel

Received: 27 January 2021

Accepted: 25 February 2021

Published: 3 March 2021

Publisher's Note: MDPI stays neutral with regard to jurisdictional claims in published maps and institutional affiliations.



Copyright: © 2021 by the authors. Licensee MDPI, Basel, Switzerland. This article is an open access article distributed under the terms and conditions of the Creative Commons Attribution (CC BY) license (<https://creativecommons.org/licenses/by/4.0/>).

1. Introduction

Road authorities around the world face the challenges of maintaining visible road markings under varying conditions. There are a number of factors that affect the degradation of road markings, including the material (thermoplastic, spray plastic, paint, etc.), location/climate (coastal, inland, etc.), share of studded tires usage, annual average daily traffic (AADT), pavement surface characteristics and conditions, heavy vehicle percentages, quality control in applying the marking material and the use of salts, abrasives or mechanical snow removal [1–3].

Gathering data to keep an updated status and inventory of road marking quality is a time-consuming process using specialized equipment and personnel [4]. Road asset management systems are being developed to help with these tasks. A Nordic certification system for road marking materials was introduced in 2015 and adopted by Norway, Sweden, and Denmark [5]. The certification system is based on the European standards EN 1824 Road marking materials—Road trials, EN 436 Road marking materials—Road marking performance for road users, and EN 12,802 Road marking materials—Laboratory methods for identification. Documented performance measurements of material samples applied on test fields on public roads are the basis for the certification system. Performance requirements include the coefficient of retroreflected luminance (R_L), under wet and dry

conditions, luminance coefficient under diffuse illumination (Q_d) as well as friction and color coordinates. Approval is granted in relation to the number of wheel passages the material will withstand [5].

In the United States, the Missouri Department of Transportation developed a Pavement Marking Management System (PMMS) as “the only practical method to allow state highway agencies to track the materials, age, cumulative traffic exposure, and retroreflectivity level of existing pavement markings and to enable systematic decisions concerning when, and with what materials, existing markings should be renewed or replaced.” [6]. Likewise, between June 2001 and December 2002 a maintenance management program for the North Dakota Department of Transportation was developed. The program investigated the use of technology such as cameras and positioning devices, along with new software, to allow for more efficient registration of road signs in the field [4].

Advanced driver assistance systems (ADAS) have been developed to support human drivers. Lane departure warning (LDW) systems, a form of ADAS, have the potential to decrease the number of accidents but typically rely on road markings to do so [7,8]. The increasing use of cameras and automation in ADAS introduces a possibility to gain access to data for road asset management systems through crowdsourcing [9]. ADAS could thus provide quality assurance systems such as the PMMS with the data to successfully predict maintenance needs.

A report from the European Road Assessment Programme (EuroRAP) has suggested that inadequate road maintenance and the lack of marking consistency across Europe negatively influence the efficacy and implementation of advanced driver assistance systems [10]. ADAS functionality is a step toward increasing driving automation, introducing a new road user: the automated driving system (ADS). However, little effort has thus far been spent on understanding the implications of changing from a human driver to an ADS for the physical road infrastructure and vice versa [11]. ADSs are expected to contribute to safer roads. To ensure this outcome, the design and maintenance of road infrastructure must be correctly interpreted by both humans and machines. To evaluate existing quality parameters such as the visibility of road markings considering automated driving systems can help future-proof road infrastructure.

Lane detection is considered to be important for any ADS [12–15] and is dependent on the visibility and consistency of lane markings [16,17]. Identification of lanes via longitudinal road markings is usually done with cameras, in either monocular or stereo vision [13,14,18]. Lane detection systems need to overcome several challenges, including knowing which lane a vehicle is in on a multilane road, separating road markings from other longitudinal lines such as asphalt surface cracks and guardrails, and accurately detecting worn markings, even in challenging light and weather conditions [12]. Worn markings pose a similar safety concern for human drivers [19,20].

Given the continuing development of vehicle technology, ADAS is a promising source of data on both the condition of road infrastructure elements and how to facilitate automated detection of such elements. This data is valuable input for road asset management systems and can facilitate safer roads through design and management that play to the strengths of driver support systems. The aim of this study was to determine whether conventional methods of assessing road marking quality through retroreflectivity are consistent with lane marking detection systems found in cars that typically rely on cameras. The conventional method utilizes a retroreflectometer, and those results were then compared to results from a lane departure warning system. A similar comparison was made by [18]. In their study, they used two different vehicles to cover a 100 km stretch of highway outside Prague, one with a lane departure warning system and another with a retroreflectometer attached. In contrast, this study used a mobile retroreflectometer on the same vehicle that had the lane departure warning system. In this way, the data collected were known to be consistent for the two sources. Moreover, this study investigated the differences between freeways and county roads, as well as both daytime and night-time conditions. Another effort to relate the quality of road markings to the success of automated camera-based

lane detection was presented in [19]. The research compared the retroreflection measured by a roof-mounted Automatic Road Analyzer to the results of a Mobileye lane detection system. The Mobileye system was mounted on the vehicle equipped with the Automatic Road Analyzer and results suggest that a Q_d higher than 135 mcd/m²/lux improves the detection of lane markings using a Mobileye lane detection system. A reference test system for camera-based lane detection was developed in [15]. In this research, it is stated that there are no available standards or benchmarks to assess the quality of either road markings or perception algorithms associated with these. While it could be argued that there are benchmarks for road markings, e.g., there are both European [20] and Nordic standards for evaluating the quality of road markings [5], it highlights the need for similar standards for machine-vision applications. Where the work in [15] compares videos annotated with additional data by mobile retroreflectometer, the video and reference data were not gathered simultaneously. There is no information on the retroreflectometer readings in terms of how it logged data (time-based versus distance-based) or whether the readings were averaged over some time or distance. Due to these two reasons, there are unknown sources of errors in the use of the mobile retroreflectometer as a reference. While the study in [15] investigates different lane detection algorithms used on annotated videos, the research described in this paper shows how the output from the LDW system could be used directly by road owners and operators (ROOs). This is an important difference as the video on which the LDW system relies is generally not available while the output of the LDW system is a binary output that could easily be shared between vehicles and ROOs.

Two of the most commonly used properties to assess the quality of road markings are the luminance factor under diffuse illumination, Q_d , and the coefficient of retroreflected luminance, R_L . Q_d is a measure for visibility under daylight conditions, during which natural light hits the marking and is dispersed in all directions. R_L is used under night-time or otherwise dark conditions, during which an active light source is directed toward the marking and reflection is measured. Mobile retroreflectometers have been developed that can measure the night-time retroreflectivity of road markings using a laser beam to simulate vehicle headlights, and these measurements are independent of ambient light levels. Retroreflectometers are designed to match the entrance and observation angles from a driver's eye to the road marking [21]. The coefficient of retroreflected luminance, R_L , measured in millicandelas per lux per square meter (mcd/m²/lux), is defined by the American Society for Testing and Materials as the ratio of the luminance of a projected surface to the normal illuminance at the surface on a plane normal to the incident light [22].

Today, it is common for road agencies to use reflectorized pavement markings that contain glass or ceramic beads. Nonreflectorized markings also have reflectivity based on the type of material, but reflectorized markings are generally preferred because of their higher reflectivity at night [23]. Experts have highlighted the need for a minimum requirement for retroreflectivity [24]. In Europe, a minimum retroreflectivity of 150 (mcd/lux/m²) has been suggested for dry conditions, which is in line with the minimum requirement already in effect in several European countries [10]. In the US, a supplemental notice of proposed amendment (SNPA) establishes a revised set of standards to be incorporated in the American Manual on Uniform Traffic Control Devices [25]. The SNPA suggests a minimum retroreflectivity level of 50 mcd/lux/m² for speed limits of greater than 35 mph. For speed limits above 70 mph, the minimum retroreflectivity level suggested is 100 mcd/lux/m².

Contrast has been identified as important for humans to be able to detect road markings [26,27] and stay in their lanes [28]. For ADSs, the need for contrast has likewise been identified [8,19,29,30].

Retroreflectometers, like the equipment used in this study, provide only R_L and contrast values. These were also crucial in the study by Lundkvist and Fors [31] to determine whether current Swedish requirements for road markings were sufficient for the LDW system of a Volvo S80. They used a mobile retroreflectometer to obtain the retroreflective value of the marking, $R_{L, dry}$, and contrast, along with an optocator to provide macrotex-

ture readings of the road surface. Tests were performed on roads of different classes and under varying conditions (wet, dry, day, and night). Their study showed that the LDW system worked well on primary roads during daytime conditions (wet and dry), with a detection rate of about 99%. While the same was true for night-time dry conditions, for night-time wet conditions the rate dropped to 92%. For secondary roads, the detection rate for daytime was 80%, and the lower detection rate was accredited to worn or dirty markings. Lundkvist and Fors stated that the detection rate for secondary roads during night-time wet conditions was very low on some roads, and no overall rate of detection for this case was given. The reason for the lack of detection was thought to be the low contrast between the markings and pavement as well as the fact that the secondary roads did not have retroreflective markings. Another case that proved difficult for the LDW system was when the sun was low on the horizon, which caused detection rates as low as 50%. The study identified lower limits for R_L , Q_d , and their respective contrasts. The contrast for Q_d was calculated by using Equation (1) and equivalently calculated for C_{RL} . The lower limits are presented in Table 1.

$$C_{QD} = \left| \frac{Q_{\text{marking}} - Q_{\text{road surface}}}{Q_{\text{road surface}}} \right| \quad (1)$$

Table 1. Estimated lower limits for detection by LDW [31].

Condition	Lowest Q_d [mcd/m ² /lux]	Lowest R_L [mcd/m ² /lux]	Lowest C_{QD}	Lowest C_{RL}
Daytime, dry	≈65		≈0.08	
Daytime, wet	≈65		≈0.08	
Night-time, dry		≈70		≈3.7
Night-time, wet		≈20		≈3.0

The visibility of markings is affected by the available ambient light. Night-time light conditions provide lower visibility for both humans and machines [8,21], although some machine vision systems have shown better results during wet night-time conditions than during wet daytime conditions [29]. Bright illumination in low light conditions, for instance from street lights or headlights, can saturate the image and make the detection of lane markers challenging, especially if the road marking is aged and worn [32].

Lin et al. [33] proposed edge smoothness as a new quality indicator specifically for machine vision systems. Algorithms detect road markings in images by using lines, edges, and rectangular shapes; therefore, their research has suggested that road markings with smooth edges would be easier to identify, as they resemble the straight lines used in the algorithms' computations. Edge smoothness has not traditionally been measured in the field: to do so, both the measurement device and relevant thresholds would need to be determined. Edge smoothness was not evaluated in this study, as relevant data for this type of analysis were not available from the equipment used.

Finally, speed impacts the ability to identify markings, as speed determines the amount of time the driver has to detect markings. Zwahlen and Schnell [26] performed numerous simulator studies using human drivers. Their studies showed that an increase in vehicle speed required a considerable increase in minimum retroreflectivity levels to attain the same preview time. For a machine vision system, higher speeds would mean fewer frames for analysis and less time for processing.

This paper investigates if ADAS functionality, represented by the case of LDW, provides an efficient way to monitor the road infrastructure and assesses how traditional measures of quality, for example, retroreflection, affect the outcome of lane detection by the LDW. The following section describes the design of the experiment and the data collected. Section 3 describes the results of the data analyses, while the implications and future research avenues are discussed in the fourth and final section.

2. Methods

In May 2019, a test was performed by the paper's authors to compare the measurements of a retroreflectometer with the lane detection results from a car with LDW functionality. A car with a built-in lane detection camera was outfitted with a retroreflectometer and driven on three routes between the locations of Oslo, Moss, and Drøbak in Norway (Figure 1). Route 1 was on freeways (E-road 6), and routes 2 (daytime driving on county roads 152, 155, 156, and 1386) and 3 (night-time driving on county roads 51, 60, 152, 316, and 1422) were on county roads. The higher maintenance level of the freeway meant that those road markings were subject to stricter requirements, although this does not always guarantee that freeways have higher levels of retroreflectivity and contrast [34].

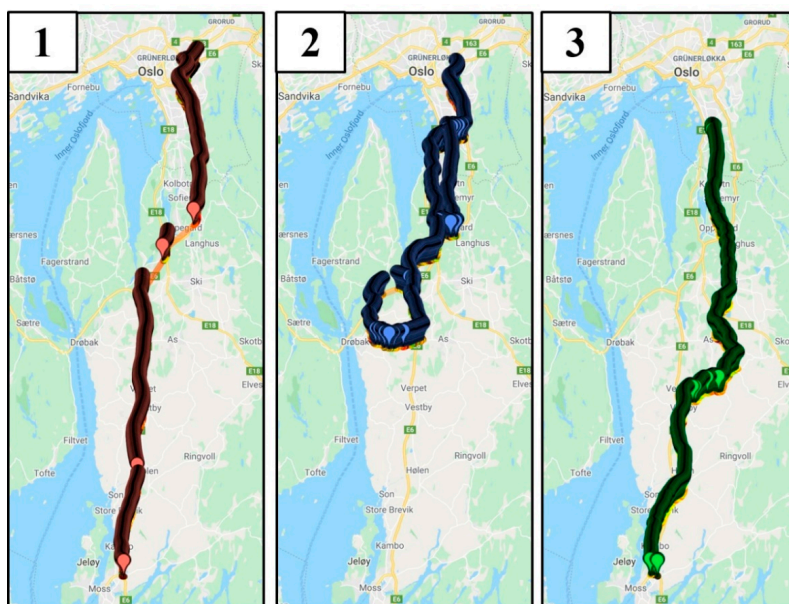


Figure 1. Routes driven: (1) freeway route for both day and night cases, (2) county roads daytime route, (3) county road night-time route. Visualization: <http://geojsonviewer.nsspot.net/> (accessed on 20 February 2021).

The requirements for retroreflection from the Norwegian road manual are dependent on winter maintenance classes, which are divided into five levels. Freeways require the highest level of winter maintenance, class DkA, while county roads call for the second-highest level, the DkB class. For both the DkA and DkB classes, the minimum required RL is dependent on the average annual daily traffic (AADT). If AADT is below 5000, as seen along parts of county roads, the minimum R_L is $100 \text{ mcd/m}^2/\text{lux}$. For AADTs greater than 5000, which includes the freeways and remaining sections of county roads, the requirement is $150 \text{ mcd/m}^2/\text{lux}$ [35].

The conditions during the test were dry asphalt, and data were recorded for both daytime and night-time. In the freeway case, the data were recorded along the same route for both day and night (route 1 in Figure 1). For the county roads, the data captured for day and night did not follow the same route, as a malfunction in the retroreflectometer caused by low temperatures at night prevented the logging of data. For the county road, daylight data were from route 2, and night-time data were from route 3 (Figure 1). A visual

comparison of routes 2 and 3 indicated that there were no large differences in the standards of the roads or road markings.

The daytime measurements were taken on a generally overcast day, with the car reporting a lux value for ambient light of around 10,000. For reference, bright sunlight produces lux values of between 50,000 to 100,000 [36]. The night-time measurements were performed from approximately 9:30 pm to midnight, with most lux readings taken between 0 and 11.

The test was performed by using a single 2018-model car with an LDW system. The data from the car were made available from the manufacturer. The LDW system produced data in four discrete values, indicating whether the system registered no detection, left-hand detection, right-hand detection, or detection on both sides. The LDW system used a mono camera mounted behind the rear-view mirror, a height similar to the eye height of humans. It also used data from an odometer and an inertial measurement unit; the latter indicated the forces acting on the car and its heading.

A Laserlux G7 retroreflector from RoadVista was used to register the retroreflection and contrast of the longitudinal road marking. It was attached to the car with the LDW system as shown in Figure 2. The retroreflector measured the quality of road markings while driving at highway speeds, registering data averaged over 30 m. The distance was set to 30 m as this setting gave a consistent flow of registered data; smaller values often resulted in improperly recorded data. A secondary reference camera was installed within the vehicle to capture video logs of the test conditions.

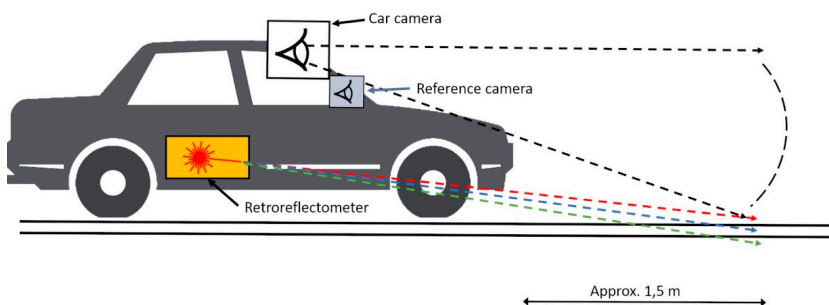


Figure 2. Illustration of the test set-up.

The Laserlux retroreflector can only measure road markings on one side of the car at a time. Zwahlen and Schnell [37] found in their research that the distance at which humans can see road markings is mainly governed by the visibility of the right edge line in the case of a fully marked road. The retroreflector was therefore attached to the right side of the car with respect to the driving direction, and the car was driven in the rightmost lane throughout the test, thus detecting the fog line. The retroreflector's laser beams hit the road at approximately 1.5 m in front of the car on the fog line (Figure 2).

The laser beams had an impact width of about three times the width of the freeway markings and about five times the width of the county road markings (because of the difference in road marking widths). The data were collected by driving so that the retroreflector's lasers hit the fog line; given the impact width, the laser was therefore thought to have hit the markings throughout most of the experiment. Some discrepancies were expected, as the car was driven manually.

The differences in lane marking detection by a camera and a retroreflector are worth noting. In comparison to retroreflectometers, a car's camera has a relatively high position, which provides a much greater vision angle and viewing distance (Figure 2). In addition to the different positions of the sensing media, the camera is more dependent on ambient light than the retroreflector. This is because the latter has active lighting

in the form of laser beams, which hit the markings so their reflection can be measured, making the system insensitive to ambient light. Because of these differences, it was of interest to determine whether detection by the retroreflector, an established quality assessment tool for road markings, would be comparable to detection by a typical lane departure warning system. Table 2 shows the data collected.

Table 2. Data used for analysis.

Retroreflector Laserlux G7			Car with Lane Departure Warning		
Data	Sample rate	Unit	Data	Sample rate	Unit
Latitude, longitude	30 m	WGS84	Latitude, longitude	12.5 Hz	WGS84
Vehicle speed	30 m	km/h	Vehicle speed	200 Hz	m/s
Retroreflection average	30 m	mcd/lux/m ²	Ambient light	100 Hz	lux
Contrast	30 m	Contrast (Equation (1))	Lane detection	50 Hz	Yes/No

The mobile retroreflector reported contrast values based on Equation (2):

$$C = 1 - \frac{\text{return signal (pavement)}}{\text{return signal (marking)}} \quad (2)$$

This value can be converted to a contrast ratio by Equation (3):

$$CR = \frac{-1}{C - 1} \quad (3)$$

The retroreflector collects data based on distance, whereas the car's data capture is based on time. These differences resulted in different data densities for different speeds. The car had a high data sample rate, 12.5200 Hz (Table 2). The retroreflector collected data and averaged them over 30 m. This provided low data densities at low speed and denser data at higher speeds.

The four previously described categories of lane detection were converted to a binary set in which values for *None* and *Left-hand* detection were set at 0, and values for *Both* and *Right-hand* detection were set at 1 to identify when the right-side marking was detected. The other data were resampled with interpolation to match the sample rate of the *Lane detection* values by using the Python data analysis library *Pandas*. The reason for choosing *Lane detection* values as the sampling reference was their binary nature. Resampling the lane detection values would change them from discrete to an artificial continuous set of values and make the analyses less meaningful. The data were time-series data which are classified as ordered data. They could therefore be merged on the time variables using *Pandas* function *pdmerge_ordered* with forward fill. Forward fill propagates the last valid observation forward in the case of missing values.

Binary logistic regressions were performed in SPSS to investigate whether the data from the retroreflector could predict the outcome of the lane detection. Binary regression was used since the predicted outcome, whether the LDW function detected the road marking, was a binary outcome. The binary logistic regression is expressed as the estimated probability that Y equals 1 given input X , where $Y \in \{0,1\}$:

$$\text{Prob}\{Y = 1 | X\} = [1 + \exp(-X\beta)]^{-1} \quad (4)$$

The regression parameters β are estimated by the method of maximum likelihood [38]. Four cases were considered: two sets of data from the freeway between Oslo and Moss (route 1), one for daytime, and another for night-time. Another two sets were from the county roads. The day case covered roads between Drøbak and Oslo (route 2, Figure 1), and the night case involved roads between Moss and Oslo (route 3, Figure 1). Regarding the binary logistic regression, the predictors were *Retroreflection*, *Contrast*, *Vehicle speed*, and *Ambient light*, and the dependent variable was *Lane detection*. *Retroreflection* was chosen

as a predictor since it is the most common measure of road marking quality and *Contrast* was chosen due to the body of research indicating its importance for both human and machine perception of lanes. The *Vehicle speed* was selected as a predictor because the retroreflector logged data based on distance while the vehicle logged based on time, and *Ambient light* was chosen as visibility is related to available light.

3. Results

The binary logistic regression model determined to what extent the *Retroreflection*, *Contrast*, *Vehicle speed*, and *Ambient light* could be used to predict whether the LDW system in the vehicle detected the fog line.

Examples of daytime situations are shown in Figure 3. Please note that these are from the reference camera and not from the car's camera.



Figure 3. Light conditions for daytime driving for freeway (left) and county road (right).

Figure 4 shows images from the freeway (left) and county road (right), both with and without street lighting, also taken from the reference camera. The retroreflector's lasers is visible in the images in Figure 4 and, as previously stated, was not dependent on ambient light (unlike the camera). In the lower right image, the headlights saturate the image to the extent that the road marking is difficult to discern from the pavement, highlighting the challenges of camera detection with low ambient light.

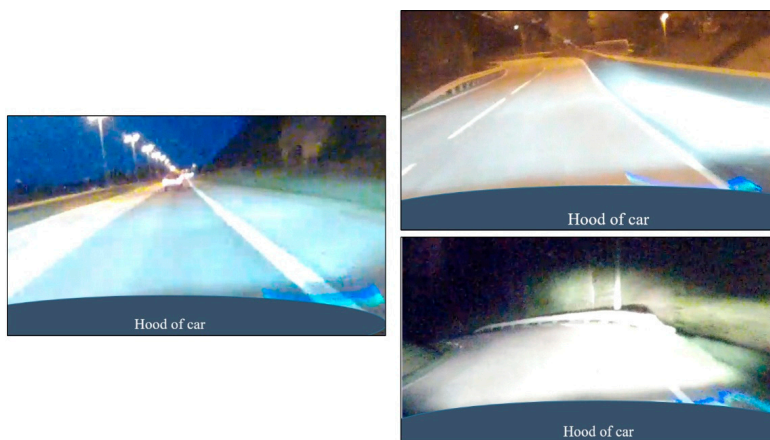


Figure 4. Light conditions for night-time driving for freeway (left), county road with street lighting (upper right), and county road without street lighting (lower right).

3.1. Binary Regression for Freeway and County Road in Daytime and Night-Time Conditions

The results of the binary regression analysis are presented in Table 3. The cut value was set to 0.5 for the analysis in Table 3, meaning that if the probability of lane marking being detected was greater than 50%, it would be classified as a positive detection (=1).

Table 3. Classification of all cases: freeway and county roads in daytime and nighttime.

Freeway Daytime (Lux Values: Mean = 9663, Median = 10,000), (Cut Value is 0.5)					Freeway Night-Time (Lux Values: Mean = 10, Median = 7), (Cut Value is 0.5)				
Observed	Predicted			Correct (%)	Observed	Predicted			Correct (%)
	0	Lane detection	1			0	Lane detection	1	
Lane detection by car	0	959,887	55,543	94.5	Lane detection by car	0	369,022	28,771	92.8
	1	60,635	401,120	86.9		1	35,314	461,956	92.9
Overall (%)				92.1	Overall (%)				92.8
County road daytime (lux values: mean = 9,726, median = 10,000), (cut value is 0.5)					County road night-time (lux values: mean = 6, median = 3), (cut value is 0.5)				
Observed	Predicted			Correct (%)	Observed	Predicted			Correct (%)
	0	Lane detection	1			0	Lane detection	1	
Lane detection by car	0	1,256,579	55,058	95.8	Lane detection by car	0	1,064,740	17,027	98.4
	1	67,802	401,812	85.6		1	7,020	202,021	96.6
Overall (%)				93.1	Overall (%)				98.1

In the table, 0 indicates that no lane marking was detected, while 1 indicates that the road marking was found. Table 3 shows that the outcome of the lane detection's functionality was correctly predicted by the model in 92.1% of cases for the freeway and 92.8% of cases for county roads in the daytime. Regarding night-time, the results were 93.1% for the freeway and 98.1% for county roads. There was a higher accuracy level for no detection of lane markings on the freeway in both daytime and night-time. The same was true for the county roads at night-time, although the difference was not as distinct. With respect to the county road daytime case, the accuracy was similar between no marking detected and a marking found. There was a considerable difference between the freeway and county roads in the share of cases concerning where markings were detected versus where they were not. The county roads had higher rates of unmarked roads than the freeway. This was expected because of the county roads' lower maintenance level.

3.2. Significance of the Predictor Variables

In the case of binary logistic regression, it is assumed that observations are independent and that the explanatory variables are not linear combinations of each other. This ensures that multicollinearity is not introduced into the analysis. In this model, the two predictor variables *Retroreflection* and *Contrast* were related by Equation (2). According to Midi et al. [39], "Multicollinearity does not reduce the predictive power or reliability of the model as a whole; it only affects calculations regarding individual predictors." To investigate the impacts of the four individual predictors without multicollinearity issues, the binary regression analyses were performed using the *Retroreflection* and *Contrast* predictors separately, keeping the other two predictor variables. As the values for *Vehicle speed* and *Ambient light* remained almost identical in the analyses with *Retroreflection* and *Contrast*, respectively, their values were averaged, as shown in Table 4. In Table 4, B represents the regression weights, that is, the β s from Equation (4), S.E. is an abbreviation for Standard Error, Sig. is an abbreviation for statistical significance, and the Exp(B) is the exponential of B also known as the odds ratio which signifies how the odds change with respect to changes in the associated predictor variable.

Table 4. Significance of predictor variables.

	County Road Daytime					County Road Nighttime			
	B	S.E.	Sig.	Exp(B)		B	S.E.	Sig.	Exp(B)
Retroreflection	0.003	0.000	0.000	1.003	Retroreflection	−0.010	0.012	0.000	0.990
Contrast	0.538	0.000	0.000	1.712	Contrast	0.514	0.067	0.000	1.672
Vehicle Speed	1.127	0.002	0.000	3.087	Vehicle Speed	3.097	0.012	0.000	22.127
Ambient Light	0.000	0.000	0.000	1.000	Ambient Light	0.003	0.001	0.000	1.003
Constant	−19.30	0.043	0.000	0.000	Constant	−50.89	0.207	0.000	0.000
	Freeway daytime					Freeway nighttime			
	B	S.E.	Sig.	Exp(B)		B	S.E.	Sig.	Exp(B)
Retroreflection	0.003	0.000	0.000	1.003	Retroreflection	0.004	0.000	0.000	1.004
Contrast	0.538	0.008	0.000	1.713	Contrast	0.495	0.017	0.000	1.640
Vehicle Speed	1.076	0.002	0.000	2.932	Vehicle Speed	0.429	0.001	0.000	1.536
Ambient Light	0.000	0.000	0.000	1.000	Ambient Light	−0.011	0.000	0.000	0.989
Constant	−18.39	0.043	0.000	0.000	Constant	−8.100	0.023	0.000	0.000

In all cases, *Ambient light* had no impact on a successful prediction, as indicated by the exponential(B) or odds ratio ≈ 1 in Table 4. It is possible that the scenarios used in this study did not provide a wide enough range of ambient light values to correctly identify its significance in camera-based lane detection. However, the results were in line with Table 2, which showed that the best prediction of road marking detection occurred at night, suggesting that the LDW system was not dependent on ambient light. These results indicate that the combination of low ambient light and headlights, as shown in Figure 4, does not pose a problem for machine vision lane detection. In fact, the model performed overall better at night, which was contrary to findings by Lundkvist and Fors [31] and Borkar et al. [32].

Similarly, regarding *Retroreflection*, the odds ratio was close to 1.0 in all four cases, meaning it had very little effect on predicting a correct outcome. As retroreflection is the most common indicator of quality in traditional road marking evaluation, this is of interest and suggests that other parameters (e.g., contrast and edge smoothness) might be needed to evaluate the quality of road markings for machine vision-based systems.

Vehicle speed proved to be the most influential predictor of the analysis. That was not surprising, as the data collection used as input was directly dependent on speed. When a vehicle travels faster, more distance is covered, providing more data points from the input data generated by the retroreflectometer. This means that the faster the vehicle with the retroreflectometer travels, the more data points the retroreflectometer has on which to base its prediction of the LDW system's outcome, relative to the time constant machine vision. In both daytime conditions, the analyses yielded an odds ratio of approximately 3, meaning that a one-point increase in speed would produce a threefold increase in successful predictions. Under night-time conditions, the results showed a clear difference between road types. On the freeway, the effect of speed was lower, at an odds ratio of about 1.5, whereas on the county road, the odds ratio for speed was about seven times higher than for day, at 22.1. To interpret these results, the difference between road types must be considered. For instance, vehicle speeds on the freeway had a smaller range and higher mean, as driving at the speed limit on the freeway resulted in a consistent speed of about 80 km/h. On the county roads, speeds varied more, from low speeds in corners and roundabouts to about 60 km/h in straight sections. The freeway case, therefore, produced a higher and more consistent rate of data from the retroreflectometer, the input data. Regarding the county roads, the range in speed meant that at low speeds the input data were very scarce in comparison to the output they were meant to predict, while at higher speeds the input data were denser than the time constant LDW data.

To further understand the great difference in odds ratios for the *Vehicle speed* on county roads given the time of day, an overlapping section on route 2 (daytime) and route 3 (night-time) was isolated. The overlapping segment is shown in Figure 5.

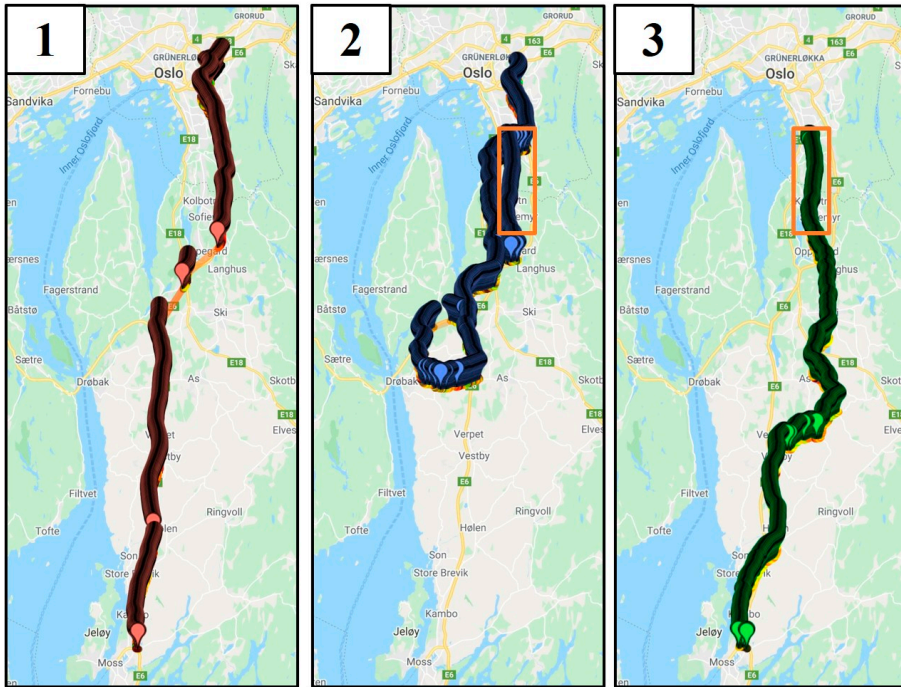


Figure 5. Overlapping road sections on county roads for daytime (2) and night-time (3) driving.

In this section, no positive identifications of lane marking could be found in the night-time case, yet there are numerous positive identifications for the daytime case (Figure 6).

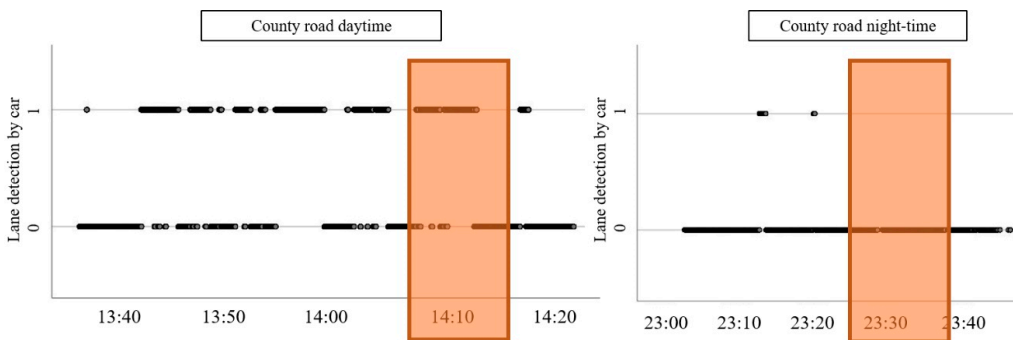


Figure 6. Overlapping segment on county roads for daytime vs. night-time.

The data were collected on consecutive days and under the same weather conditions, which means that the main difference was the amount of ambient light available. The videos from the stretch of road were reviewed to find causes for the lack of detections. Some on-coming traffic was noted, which can be problematic for the LDW [31], but this would not have accounted for the complete lack of detections at night. The type of marking used, that is, paint or thermoplastic, was rudimentarily checked by manually comparing the stretches of road for the day and night scenario, respectively, where information on what

material was used was available. The night route had more spray thermoplastics (1–1.5 mm thickness) than the day route, which had almost entirely preformed thermoplastics (3 mm). This could explain the overall trend of much fewer successful lane detection for night versus day. For the overlapping segment, however, the marking was thermoplastic marking in both cases. The marking used on county road was 2 mm thick thermoplastic compared to the 3mm thick thermoplastic used on the freeway. In addition to thickness, application and wear can factor into the marking's visibility. As ambient light was shown not to be a predictor for the outcome of the LDW, the material and thickness used for road marking could be investigated as a predictor for automated lane detection in future studies.

Contrast was the second most influential predictor, contributing in the range of 1.64 to 1.71 for the different scenarios, with slightly higher values for daytime conditions. This means a unit change in contrast would result in 1.64–1.71 times the odds of getting a correct prediction. Lundkvist and Fors [31] found that the successful detection of road markings by an LDW system in daytime did not require high contrast, and the results of binary logistic regression indicated that contrast was a better indicator of whether the LDW system detected markings than the more widely used Q_d or R_L . *Contrast* has been identified as an important parameter for both human and machine detection [8,34], a finding supported by these results. The level to which it contributed was modest but consistent across all scenarios.

3.3. Evaluation of Possible Threshold Values

Receiver operating characteristic (ROC) curves can be used to look for threshold values for successful detection. The ROC curve summarizes the trade-off between the true positive rate and false-positive rate for a predictive model and is used as a diagnostic tool for the model. The four predictor parameters were used as test variables, and the positive lane detection was set as the state variable. Figure 6 shows the ROC curves for the four cases, with sensitivity plotted on the y -axis and 1-specificity on the x -axis, as per convention. The sensitivity and specificity are defined by Equations (5) and (6) [40]:

$$\text{Sensitivity} = \frac{\text{True positives}}{\text{True positives} + \text{False negatives}} \quad (5)$$

$$\text{Specificity} = \frac{\text{True negatives}}{\text{True negatives} + \text{False positives}} \quad (6)$$

In the figure, the larger the area under the curve (AUC) for a given line, the more accurate the variable is at predicting the outcome. Threshold values for the variables are located at points as far upward and to the left on the curve being analyzed as possible. The higher up on the y -axis, the more true positives are included. However, as the x values increases, so does the rate of false positives.

A curve close to the diagonal reference line indicates that the test variable is not useful for distinguishing between a positive or negative outcome. In Figure 7, ambient light lies close to the diagonal in all cases except for the freeway night-time case, which has a slight distinction. The ROC curves indicate that ambient light is not a good indicator of whether the lane is detected, as was seen in the regression analyses.

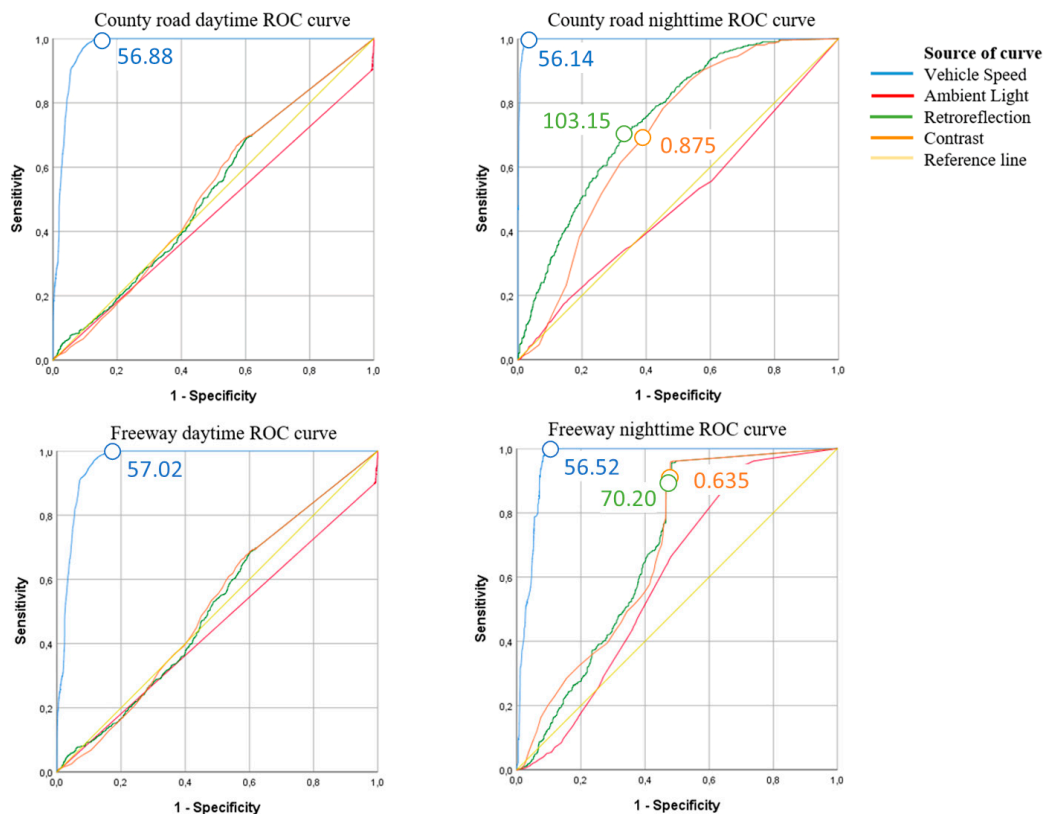


Figure 7. Receiver operating characteristics curves and suggested threshold values for the predictor variables.

Figure 6 shows that with respect to daytime driving, *Retroreflection* and *Contrast* also seemed to have little predictive quality. Under night-time conditions, the AUC is larger for these two variables, and within these two cases, the curves for the county road are the best in terms of establishing a threshold cut-off. Resulting in a high level of sensitivity and relatively low value for 1-specificity.

In the tables that accompanied the ROC curves, the value of the test variable that corresponded to an identified threshold point on the curve (high y-coordinate, low x-coordinate) could be extracted. These threshold values are indicated in Figure 7.

The ROC curves for *Vehicle speed* have large AUCs, indicating that a high level of sensitivity and specificity can be obtained without introducing too many false positives or negatives. As with the binary logistic regression analysis, they have the largest impact on predicting the outcome. Additionally, Figure 7 shows the chosen threshold points and values for the test variables. With respect to *Vehicle speed*, the threshold values lie between 56.14 and 57.02 km/h.

The night-time contrasts thresholds reported were converted to contrast ratios by Equation (3), and county roads were associated with a threshold contrast ratio of 8, whereas for the freeway the threshold equated to a contrast ratio of 2.74. The required contrast for detection of road markings by LDW identified by Lundkvist and Fors (2010), C_{RL} , was 3 (Table 1). Unfortunately, as the retroreflectometer used was not the same, and data were not derived in the same manner, it is difficult to compare the results of the two studies. Substituting Equation (2) for C in Equation (3) would give Equation (7) for determining CR

within this study, while Lundkvist and Fors used Equation (8). The equipment used in this work did not report R, therefore, it was not possible to calculate the contrast in the same way as in Equation (8).

$$CR = \frac{\text{return signal}_{\text{marking}}}{\text{return signal}_{\text{pavement}}} \quad (7)$$

$$C_{RL} = \left| \frac{R_{\text{marking}} - R_{\text{road surface}}}{R_{\text{road surface}}} \right| \quad (8)$$

4. Discussion

This study compared data from a conventional performance measure for longitudinal road marking, a retroreflector, to those from a modern ADAS feature, LDW, which utilizes a camera within the vehicle. The aim was to determine to what extent the conventional retroreflector could predict the outcome of the LDW's ability to detect lane markings. The results give insight into both whether the established quality parameters for road markings are suitable for automated detection systems and whether crowdsourced data from vehicles can be used to monitor pavement marking conditions.

The binary regression analyses showed that the model, correctly predicts the result of the car's lane detection in 92.1% to 98.1% of cases, depending on driving conditions.

The results indicate that the in-vehicle camera's ability to detect lane markings could potentially be used as a surrogate for conventional methods of assessing the status of pavement markings. The impact of the specific input variables on the model was also considered to better understand how traditional metrics associated with the assessment of lane markings impact the LDW predictions.

Ambient light and *Retroreflection* were found to have minimal impact on the success of predictions. The lack of impact of ambient light might be due to the limited range of input values, as the measurements were taken in either high or very low ambient light conditions and did not cover the middle ground. Another possibility is that the LDW system is not dependent on ambient light and that headlights provide sufficient lighting to detect markings. Additional investigations are likely needed, but these results indicate that the LDW system is not dependent on street lighting which is a useful input towards facilitation for driving automation in road design.

Retroreflection is the most common parameter for the quality assessment of road markings today. This work indicates that the retroreflection value in itself is not important for the successful identification of road marking by machine vision. The algorithms used to detect markings search for lines, edges, and rectangular shapes, making the contrast between the road surface and road marking more critical than solely the amount of light reflected from the marking. Threshold values for *Contrast* could only be suggested in nighttime driving, and for these limited tests, the contrast ratio thresholds were found to be 2.74 for the freeway and 8 for the county roads. Contrast, as well as edge smoothness, are suggested as quality parameters for machine vision detection of lane markings. Yet, as contrast is calculated differently depending on the method used, it may be difficult to specify a universal threshold value.

The analysis showed that *Vehicle speed* had the strongest impact on the success of predictions. This is because of its direct relation to the amount of data captured. The speed of the vehicle carrying the retroreflector should be 57 km/h or higher for best results.

The high probability of predicting the outcome of the lane detection feature, despite relying on few input variables (*Retroreflectivity* and the derived *Contrast*) suggests that the LDW system is more dependent on longitudinal road markings than other elements of the road geometry such as the road's width, edge, or centerline.

Further investigations should be performed to affirm the indication that LDW functionality can be used to monitor the state of road markings. This could include using different makes of cars and collecting data from more roads. The indication that ambient light does not affect the success of the LDW system could be researched further by driving

in different conditions of natural and artificial light. The effect of road marking material and thickness on lane detection by the LDW is encouraged as it could be particularly useful for adapting design and maintenance of roads to support automated driving features. Harmonization of measurement techniques would be beneficial in supporting earlier findings. For instance, the contrast measurement in [31] is not directly comparable to the contrast measurement in this paper. Likewise, the retroreflectivity in [19] is of Q_d which is dependent on ambient light, while this paper used an active laser measuring R_L .

This research has shown that ADAS functionality such as LDW provides an efficient way to monitor the road infrastructure. The work identified that contrast between the road marking and the adjacent road surface is of more importance than the retroreflectivity of the road marking material, suggesting that contrast should be a metric for quality of road marking to start including automated driving functions in the design and maintenance of roads. Gaining knowledge about how well infrastructure designed for humans also supports automated driving systems will be useful for future-proofing roads. It will help reap the promised safety benefits of automated driving features, from today's ADAS to more comprehensive future ADS. Additionally, crowdsourcing is an efficient way of monitoring the state of road infrastructure and can provide systems for predicting road maintenance, such as the PMMS, with highly valuable data. Understanding how infrastructure is "seen" by both humans and ADSs will allow engineers to prepare for higher levels of automation by taking incremental steps in which road infrastructure design and maintenance can be developed in parallel with vehicle automation.

Author Contributions: Conceptualization; A.D.S., Data curation; A.D.S., Formal analysis; A.D.S., Funding acquisition; A.D.S., Investigation; A.D.S., Methodology; A.D.S., K.P., E.M., Project administration; A.D.S., Resources; A.D.S., Software; A.D.S., Supervision; K.P., E.M., Validation; A.D.S., Visualization; A.D.S., Roles/Writing—original draft; A.D.S. Writing—review and editing; A.D.S., K.P., E.M. All authors have read and agreed to the published version of the manuscript.

Funding: This research was funded by the Norwegian Public Roads Administration.

Institutional Review Board Statement: Not applicable.

Informed Consent Statement: Not applicable.

Data Availability Statement: The data presented in this study are available at <https://github.com/ResearchAne/DataAnalysesLDW> (accessed on 5 February 2021).

Conflicts of Interest: The authors declare no conflict of interest.

References

1. Lundkvist, T.C.; Johansen, S.-O.; Johansen, S.-O.L.T.C. Road Marking Management System A Pre-Study. 2009. Available online: www.vti.se/publications (accessed on 20 March 2019).
2. Shahata, K.; Fares, H.; Zayed, T.; Abdelrahman, M.; Chughtai, F. Condition rating models for sustainable pavement marking. In Proceedings of the Transportation Research Board 87th Annual Meeting, Washington, DC, USA, 13–17 January 2008; pp. 8–18.
3. Thamizharasan, A.; Sarasua, W.A.; Clarke, D.B.; Davis, W.J. A Methodology for Estimating the Lifecycle of Interstate Highway Pavement Marking Retroreflectivity. In Proceedings of the 82nd Annual Meeting of the Transportation Research Board of the National Academies, Washington, DC, USA, 12–16 January 2003; Available online: http://www.ltrc.lsu.edu/TRB_82/TRB2003-001867.pdf (accessed on 25 February 2021).
4. Kruse, K.B.; Simmer, T. *Asset Management of Roadway Signs through Advanced Technology*; Upper Great Plains Transportation: Fargo, ND, USA, 2003.
5. Fors, C.; Johansen, C.; Lundkvist, S.-O.; Nygårdhs, S. Nordic Certification System for Road Marking Materials. 2018. Available online: www.vti.se/en/publications (accessed on 20 March 2019).
6. Missouri Department of Transportation. *Pavement Marking Management System Phase I*; MoDOT: Jefferson City, MO, USA, 2000.
7. KKusano, K.D.; Gabler, H.C. Comparison of Expected Crash and Injury Reduction from Production Forward Collision and Lane Departure Warning Systems. *Traffic Inj. Prev.* **2015**, *16*, S109–S114. [[CrossRef](#)] [[PubMed](#)]
8. Hadi, M.; Sinha, P. Effect of Pavement Marking Retroreflectivity on the Performance of Vision-Based Lane Departure Warning Systems. *J. Intell. Transp. Syst.* **2011**, *15*, 42–51. [[CrossRef](#)]

9. Osichenko, D.; Spielhofer, R. Monitoring and inventory of road signs and road markings State of the art—A review of existing methods and systems. In Proceedings of the Transport Research Arena Vienna, Vienna, Austria, 16–19 April 2018; pp. 1–9. [CrossRef]
10. European Road Assessment Program. Roads that cars can read A Quality Standard for Road Markings and Traffic Signs on Major Rural Roads Proposals for Consultation. 2013. Available online: <http://www.eurorap.org/media/93768/20110629-RoadsThatCarsCan> (accessed on 28 August 2019).
11. Farah, H.; Erkens, S.M.; Alkim, T.; van Arem, B. Infrastructure for Automated and Connected Driving: State of the Art and Future Research Directions. In *Road Vehicle Automation 4*; Meyer, G., Beiker, S., Eds.; Springer: Cham, Switzerland; San Francisco, CA, USA, 2018; pp. 187–197. [CrossRef]
12. Chen, C.; Seff, A.; Kornhauser, A.; Xiao, J. DeepDriving: Learning Affordance for Direct Perception in Autonomous Driving. In Proceedings of the 15th IEEE International Conference on Computer Vision (ICCV2015), Santiago, Chile, 11–18 December 2015. [CrossRef]
13. Aly, M. Real time detection of lane markers in urban streets. In Proceedings of the IEEE Intelligent Vehicles Symposium, Eindhoven, The Netherlands, 4–6 June 2008; pp. 7–12. [CrossRef]
14. Yi, S.-C.; Chen, Y.-C.; Chang, C.-H. A lane detection approach based on intelligent vision. *Comput. Electr. Eng.* **2015**, *42*, 23–29. [CrossRef]
15. Nayak, A.; Rathinam, S.; Pike, A.; Gopalswamy, S. Reference Test System for Machine Vision Used for ADAS Functions. *SAE Tech. Paper Ser.* **2020**, 1–8. [CrossRef]
16. Nitsche, P.; Mocanu, I.; Reinthaler, M. Requirements on tomorrow’s road infrastructure for highly automated driving. In Proceedings of the 2014 International Conference on Connected Vehicles and Expo ICCVE, Vienna, Austria, 3–7 November 2014; pp. 939–940. [CrossRef]
17. Fares, H.; Shahata, K.; Elwakil, E.; Eweda, A.; Zayed, T.; Abdelrahman, M.; Basha, I. Modelling the performance of pavement marking in cold weather conditions. *Struct. Infrastruct. Eng.* **2010**, *6*, 1–13. [CrossRef]
18. Matowicki, M.; Pribyl, O.; Pribyl, P. Analysis of possibility to utilize road marking for the needs of autonomous vehicles. In Proceedings of the 2016 Smart Cities Symp, Prague, Czech Republic, 26–27 May 2016. [CrossRef]
19. Pappalardo, G.; Cafiso, S.; Di Graziano, A.; Severino, A. Decision Tree Method to Analyze the Performance of Lane Support Systems. *Sustainability* **2021**, *13*, 846. [CrossRef]
20. European Committee for Standardization. CEN—EN 1824—Road Marking Materials—Road Trials | Engineering 360. 2011. Available online: <https://standards.globalspec.com/std/1387919/en-1824> (accessed on 7 May 2019).
21. Migletz, J.; Graham, J.L.; Harwood, D.W.; Bauer, K.M. Service Life of Durable Pavement Markings. *Transp. Res. Rec. J. Transp. Res. Board* **2001**, *1749*, 13–21. [CrossRef]
22. ASTM E1710-05. *Standard Test Method for Measurement of Retroreflective Pavement Marking Materials with CEN-Prescribed Geometry Using a Portable Retroreflector*; ASTM: West Conshohocken, PA, USA, 2005. [CrossRef]
23. Mull, D.M.; Sitzabee, W.E. Paint Pavement Marking Performance Prediction Model. *J. Transp. Eng.* **2012**, *138*, 618–624. [CrossRef]
24. Rasdorf, W.J.; Zhang, G.; Hummer, J.E. The Impact of Directionality on Paint Pavement Marking Retroreflectivity. *Public Work. Manag. Policy* **2008**, *13*, 265–277. [CrossRef]
25. Satterfield, C. National Standards for Traffic Control Devices; the Manual on Uniform Traffic Control Devices for Streets and Highways; Maintaining Pavement Marking Retroreflectivity SNPA. Available online: <http://www.regulations.gov> (accessed on 10 July 2019).
26. Zwahlen, H.T.; Schnell, T. Minimum In-Service Retroreflectivity of Pavement Markings. *Transp. Res. Rec. J. Transp. Res. Board* **2000**, *1715*, 60–70. [CrossRef]
27. Hills, B.L. Vision, Visibility, and Perception in Driving. *Perception* **1980**, *9*, 183–216. [CrossRef] [PubMed]
28. Allen, R.W.; O’hanlon, J.F. Effects of Roadway Delineation and Visibility Conditions on Driver Steering Performance. 1991. Available online: <https://pdfs.semanticscholar.org/eb04/84614672f1b84c2db3a5f70e46e075cff8b4.pdf> (accessed on 14 August 2019).
29. Pike, A.; Carlson, P.; Barrette, T. Evaluation of the Effects of Pavement Marking Width on Detectability By Machine Vision: 4-Inch vs. 6-Inch Markings, Virginia, USA. 2018. Available online: https://www.researchgate.net/publication/330545262_Evaluation_of_the_Effects_of_Pavement_Marking_Width_on_Detectability_By_Machine_Vision_4-Inch_vs_6-Inch_Markings (accessed on 25 February 2021).
30. Hertel, T.W.; Reimer, J.J. Predicting the poverty impacts of trade reform. *J. Int. Trade Econ. Dev.* **2005**, *14*, 377–405. [CrossRef]
31. Lundkvist, S.-O.; Fors, C. Lane Departure Warning System—LDW Samband mellan LDW:s och Vägmarkeringars Funktion VTI notat 15–2010, Linköping, Sweden. 2010. Available online: www.vti.se/publikationer (accessed on 19 December 2019).
32. Borkar, A.; Hayes, M.; Smith, M.T.; Pankanti, S. A layered approach to robust lane detection at night. In Proceedings of the 2009 IEEE Workshop on Computational Intelligence in Vehicles and Vehicular Systems CIVVS 2009, Nashville, TN, USA, 30 March–2 April 2009; pp. 51–57. [CrossRef]
33. Lin, K.-L.; Wu, T.-C.; Wang, Y.-R. An innovative road marking quality assessment mechanism using computer vision. *Adv. Mech. Eng.* **2016**, *8*, 1–8. [CrossRef]
34. Migletz, J.; Graham, J.L.; Bauer, K.M.; Harwood, D.W. Field Surveys of Pavement-Marking Retroreflectivity. *Transp. Res. Rec. J. Transp. Res. Board* **1999**, *1657*, 71–78. [CrossRef]

35. Statens Vegvesen and Vegdirektoratet. *Håndbok R610 Standard for driFt og Vedlikehold av Riksveger*; no. R610; Statens Vegvesen: Oslo, Norway, 2014.
36. Kandilli, C.; Ülgen, K. Solar Illumination and Estimating Daylight Availability of Global Solar Irradiance. *Energy Sources Part A Recover. Util. Environ. Eff.* **2008**, *30*, 1127–1140. [[CrossRef](#)]
37. Zwahlen, H.T.; Schnell, T. Visibility of New Centerline and Edge Line Pavement Markings. *Transp. Res. Rec. J. Transp. Res. Board* **1997**, *1605*, 49–61. [[CrossRef](#)]
38. Harrell, F.E. Binary Logistic Regression. In *Regression Modeling Strategies: With Applications to Linear Models, Logistic and Ordinal Regression, and Survival Analysis*; Springer International Publishing: Cham, Switzerland, 2015; pp. 219–274.
39. Midi, H.; Sarkar, S.; Rana, S. Collinearity diagnostics of binary logistic regression model. *J. Interdiscip. Math.* **2010**, *13*, 253–267. [[CrossRef](#)]
40. Habibzadeh, F.; Habibzadeh, P.; Yadollahie, M. On determining the most appropriate test cut-off value: The case of tests with continuous results. *Biochem. Med.* **2016**, *26*, 297–307. [[CrossRef](#)] [[PubMed](#)]

Appendix D

Paper IV (preprint)

Camera-Based Lane Detection - Can Yellow Road Marking Facilitate Automated Driving in Snow?

Ane Dalsnes Storsæter

Senior Engineer

Norwegian Public Roads Administration, 7030 Trondheim, Norway

E-mail: ane.storsater@vegvesen.no

Kelly Pitera

Associate Professor

Department of Civil and Environmental Engineering

Norwegian University of Science and Technology (NTNU), 7491 Trondheim, Norway

Email: kelly.pitera@ntnu.no

Edward D. McCormack

Research Associate Professor

Civil and Environmental Engineering

University of Washington, Seattle, WA-98195-2700, USA

Email: edm@uw.edu

Acknowledgements

This work was funded by the Norwegian Public Roads Administration

Abstract

Road markings are beneficial to human drivers, advanced driver assistance systems (ADAS) and automated driving systems (ADS). Snow coverage on roads provides a challenging case for lane detection as the white road marking is hard to distinguish from the snow. For human drivers, yellow road markings provide a visual contrast to the snow that can increase visibility. Yet, yellow road markings are becoming increasingly rare due in Europe due to the cost of installing and maintaining two road marking colors. With increased reliance on automated driving, the question of whether yellow road markings can be of value to automatic lane detection functions arises.

To answer this question, images from snowy conditions are assessed to see how different representations of colors in images (color spaces) affect the visibility of white and yellow road markings. The results indicate that images represented by RGB chrominance and grayscale images provide poor contrast between road markings and snow. Color spaces HSL, HSV and YUV show promise in creating images where road markings have higher visibility for machine vision in snowy conditions.

The results presented in this paper suggest that yellow markings have benefit for automated driving and gives recommendations on the most appropriate color spaces for lane detection in snowy conditions. To obtain the safest and most cost-efficient roads for the future, both human and automated drivers must be considered. Road authorities and car manufacturers have a shared interest in discovering how road infrastructure design, including road marking, can be adapted to support automated driving.

Keywords: Automated driving, road infrastructure, computer vision, lane detection, lane marking

1 INTRODUCTION

Driving is becoming increasingly automated. Advanced driver assistance systems (ADAS) have become ubiquitous, providing driver support such as lane departure warning (LDW) for lateral control and adaptive cruise control (ACC) for longitudinal control. These ADAS functions are evolving into automated driving systems (ADSs) that perform increasingly advanced driving tasks. ADSs represent a new type of road user (Storsæter et al., in press), and, like ADAS systems, they rely on sensors to sense their surroundings as well as software to interpret the data these create. The sensory system of an automated driver is different to that of a human, thus, it is essential that roads are designed and maintained to facilitate the sensory apparatus of both human and automated road users during the transition to higher levels of automation in driving.

To investigate the requirements for road infrastructure for highly automated driving, Nitsche et al. (2014) used a literature review and a web questionnaire with participants from research and development, academia, automotive or supplier industry and public authorities. They conclude that the visibility and quality of lane markings are of particular importance, specifically in adverse weather. Shladover (2018) further suggests that road authorities need guidance about possible modifications to road markings in response to automated drivers.

Road markings have the following main functions (Carlson et al., 2009; Statens Vegvesen, 2015):

1. Leading traffic; through enhancing the road geometry, road delineation and lanes.
2. Notifying drivers; through information on specific stretches of road that require more attention, or adaption of driving.
3. Regulating traffic; through road markings that assign rules to the use of the road.

Lane detection, i.e. identifying road marking, is considered to be important for any autonomous driving system (Aly, 2008; Chen et al., 2015; Yi et al., 2015) and ADAS functionality such as LDW has been found to increase traffic safety (Kusano and Gabler, 2015; Sternlund, 2017). Lane detection can be accomplished by using different sensors, e.g. camera, lidar or radar. However, the most widely used method is camera-based (Bar Hillel et al., 2014; Chetan et al., 2020; Gruyer et al., 2017; Xing et al., 2018). Adverse weather, e.g. rain, fog and snow, can be challenging for vision-based lane detection (Bar Hillel et al., 2014; Huang et al., 2009; Stevic et al., 2020; Xuan et al., 2017; Yinka et al., 2014; Zhang et al., 2020). Gruyer et al. (2017) establishes that fog and snow are particularly problematic for camera-based driving features.

Several studies consider how road marking design and quality influences detection rates of camera-based LDW systems (Lundkvist and Fors, 2010; Pike et al., 2018), which shed light on how road design and maintenance can support automated driving. However, there is a lack of research on how design and maintenance of road markings can increase lane detection in snowy conditions. Facilitating automated recognition of road infrastructure elements can be beneficial to traffic safety both to increase the probability of correct identification of road features, and to help attain low reaction times for automated driving features. Algorithms for lane detection are continually improving and, consequently, adverse weather issues are more frequently addressed.

For instance, algorithms that can detect lane markings in rain and snow have been developed (Lee and Moon, 2018; Yinka et al., 2014). They are useful contributions to lane detection software development, but do not give the information needed for road authorities to know whether road markings should be modified, or snow removal procedures changed. Furthermore, the amount of snow considered in the aforementioned research is limited, suggesting further research is needed on lane detection with a deeper cover of snow. For guidance on future-proofing road marking design and snow removal procedures, there is a need to know when the LDW systems work or not, as well as why.

While not snow, Blake et al. (2016) performed experiments to see how volcanic ash covering reduced visibility of white road markings. The results found that “very small accumulations of ash are responsible for road marking coverage and suggest that around 8 % visible white paint or less would result in the road markings being hidden.” Furthermore, they report that road markings are more easily covered by fine-grained ash, and that the color of the ash influences detection. The study used image processing as well as visual inspection in their research, which both concluded that white road markings covered by light-colored deposits were especially detrimental to lane detection. White ash on white markings can be compared to snow on white markings when considering camera-based lane detection. The fundamental task, finding lane markings on the road, is a question of contrast. Although white generally produces the greatest contrast to the road surface, it is also similar in color to naturally occurring elements in nature that can hinder detection including ash and snow. Vehicles will typically have redundancy of sensors and not rely on cameras alone. However, in the case of sensors that actively send out light and read their reflection (e.g. lidar), snow coverage may make lane detection even more challenging (Aldibaja et al., 2017; Razmi Rad et al., 2020).

In the interest of creating the safest and most cost-efficient road infrastructure for the future the issue of lane detection in snow also intersects with another road marking design choice, whether to use yellow road markings. Road markings are a major expense for road agencies (Pike and Bommanayakanahalli, 2018). While still in use in the U.S., yellow road markings are disappearing in Europe. The European Union does not require it to be used (European Union Road Federation, 2012) and there are significant cost savings in using solely white road markings. In the Nordic countries, Finland is in the process of phasing out yellow markings, leaving Norway as the only country using yellow center road markings (Finnish Transport and Communications Agency, 2020; Vadeby et al., 2018). In Iceland, yellow road markings are still in use, though not as center line markings but rather to inform drivers that parking or stopping is illegal.

In the U.S. and Norway, yellow longitudinal markings separate traffic traveling in opposite directions and are used on the left-hand edge of the roadways of divided highways and one-way streets or ramps (Statens Vegvesen, 2015; U.S. Department of Transportation, 2009). Yellow markings, thus, give the driver additional information on the characteristics of adjacent lanes which is thought to be beneficial for driving safety for humans (Schnell and Zwahlen, 2000).

For both road authorities and vehicle manufacturers to be able to make informed decisions, there is a need to know whether yellow road markings can be beneficial for camera-based lane

detection in snowy conditions. It has been shown that yellow markings are less visible in grayscale images than white markings (Lee and Moon, 2018; Lin et al., 2010). However, in challenging condition such as snow, yellow road marking may offer higher visibility in color images. The purpose of this paper is to compare the visibility and contrast of white and yellow road markings compared to adjacent surfaces in snowy conditions. Color images can be represented by several different mathematical representations known as color spaces. To compare white and yellow road markings, images of lane marking in a set of snowy conditions are converted to different color spaces and the visibility and contrast of the lane marking are assessed by visual assessment and histogram plots of the pixel intensities. Furthermore, at what depth of snow automated lane detection becomes unfeasible is discussed.

2 IMAGE-BASED LANE DETECTION

The process of lane detection in images typically includes camera calibration, correction of image distortions, conversions of color space (if needed), application of a mask to set the region of interest, noise-filtering, and edge detection. In this research, camera calibration and correction of distortions will not be applied as the focus is on how color space representations affect the visibility of markings.

Lane detections in images are mainly based on changes in colors and patterns between the road surface and road marking (Hernández et al., 2016). The representation of a road marking adjacent to the road surface in images (under most conditions) provide a significant change in the intensity and contrast of pixels, i.e. an edge. Edge detection is thus based on identifying the greatest changes in image intensity or contrast in an image (Acharjya et al., 2012; Samuel et al., 2018).

The simplest form of edge detection is simply by using thresholds. In many cases, a threshold at a certain pixel intensity can be enough to separate an object from the background (Kaur et al., 2012). However, a more robust approach is found in traditional edge detector algorithms, e.g. Sobel, Prewitt, Laplacian of Gaussian (LOG) and Roberts, that use kernels, i.e. small matrices, to calculate gradients of the pixel intensities along rows and columns of images.

The difference in the way humans see and extract information from images and how an automated driver, a machine, does it, is shown in **Figure 1**. Humans view an image and identify the lane markings directly, but a machine does not interpret the image in the same way. An automated driving system will look at the information contained in the pixels that make up an image. In a black and white image, the intensity value of the pixels typically varies from black (0) to white (255). To identify features, the automated system scans the rows and columns to look for trends that can help it pick out features. In **Figure 1**, the left hand side shows the lane markings as humans see them, where on the right is one way for an automated system to see the road markings. The histogram is plotted by adding the pixel values for each column, then plotting the result with the sum of the pixel intensities on the y-axis and the column number on the x-axis. The histogram plot shows very distinct peaks with high gradients which identifies and positions the lane marking in the image. The dashed lane marking produces a lower sum of pixel values than the continuous line, resulting in a slightly lower peak height.

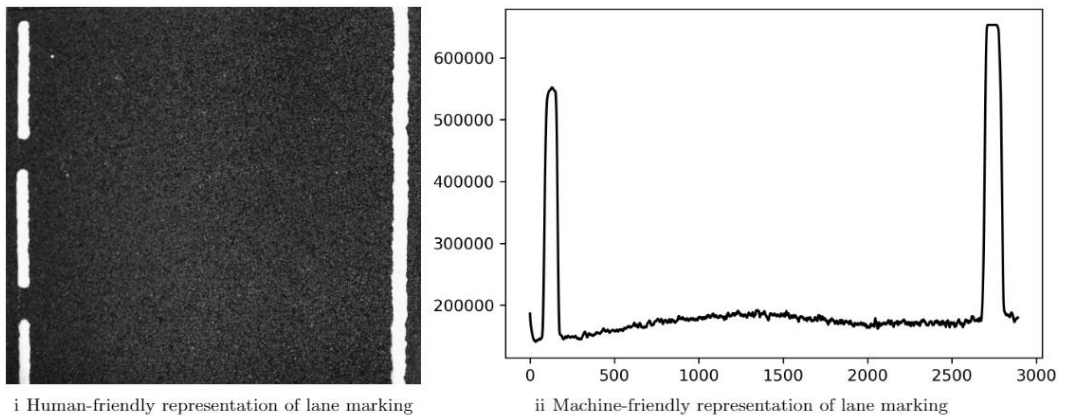


Figure 1 Representing lane marking for human drivers versus for automated drivers

2.1 COLOR SPACES

Different color spaces are ways of mathematically expressing color that have their advantages and limitations depending on the application. Grayscale images consist of a single channel indicating brightness, compared to three channels for color images, and are the most commonly used image representation in lane detection (Aly, 2008; Huang et al., 2009; Li et al., 2018; Narote et al., 2018; Xuan et al., 2017). Grayscale images provide an effective approach as some cameras used in automotive applications are grayscale cameras, but also as lane detection algorithms typically use a single channel as input. How colors appear in an image is dependent on the ambient light, i.e. the same color will give different pixel values in different lighting conditions. This makes grayscale images attractive to use as white road marking will appear as some of the brightest pixels in a grayscale image in a variety of conditions. The software performing the lane detection will search for contrast, i.e. bright pixels identifying lane lines adjacent to darker pavement pixels. This also implies that the color and texture of the road surface affects lane detection by cameras, where a darker road surface creates a greater contrast to lane markings.

The most common way of depicting color images is using red (R), green (G) and blue (B) chromaticities, known as the RGB color space (Wang et al., 2014). In RGB, a color is represented as the additive combination of the three separate color channels, for instance, white would be given as $R = 255$, $G = 255$ and $B = 255$, i.e. the maximum value for the red, green and blue color channels, respectively.

Colors are a vital part of image and video processing. They are, for instance, used to identify objects, and from these, segment an image into meaningful elements such as roadway, vehicles, and signs. Depending on the goal of the image processing, different approaches are used; clusters of similar pixels can represent as an object, other times edge detection can be more relevant such as for lane detection.

Given the application of lane marking detection, yellow markings are less visible in grayscale images than white markings, prompting some researchers to use color images to achieve better lane detection rates (for roads with both white and yellow markings) in challenging weather and light conditions (Lee and Moon, 2018; Lin et al., 2010). This is also seen in research by Yinka et al. (2014) who suggested an approach for finding the drivable path for a vehicle in snow and rain using computer vision. They introduced a filter to remove the snow or rain in the imagery, based on the difference in intensity of pixels representing snow or rain particles with respect to the background. Such an approach supports the use of colored road marking, as yellow road marking would have a color and intensity profile that would be different to rain and snow particles.

There are many ways to depict color for images. The RGB color space use three channels (red, green and blue) to make color images and was used by Yinka et al. (2014) in their work when filtering out rain and snow. However, research suggests that the color space YUV is better suited both for computer and human vision (Lee and Moon, 2018; Podpora et al., 2014). In the YUV color space, the first channel, Y, refers to luminance independent of color. The next two channels are color channels that can be defined in various ways; however, “U” is often the blue-luminance and “V” the red-luminance (this instance of YUV is referred to as YCbCr). This separation of black and white information, or luminance, from color is thought to be similar to how the human eye works as humans are unable to differentiate colors in low lighting settings (Podpora et al., 2014). YUV color space was selected by Lee and Moon (2018) and Lin et al. (2010) in their respective works. Another color space; Hue, Saturation and Lightness (HSL) has also been shown to be well-suited for lane detection, particularly in images with lighter road surface colors (Haque et al., 2019). *Hue* is a representation of color described in a 360° spectrum as shown in **Figure 2**.

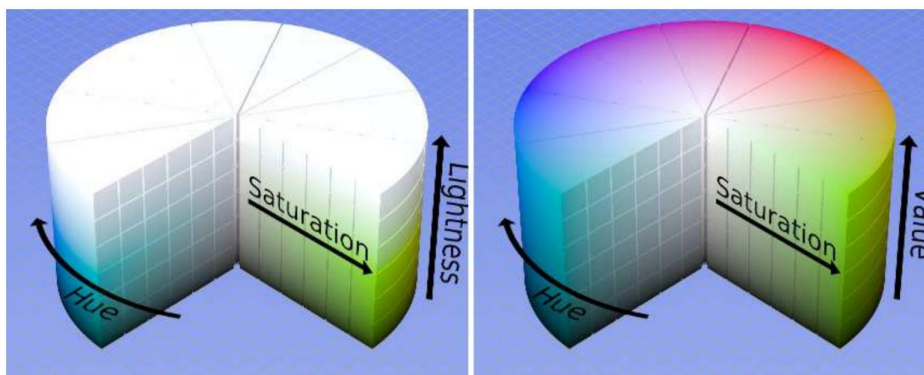


Figure 2 Graphical illustration of the HSL (left) and HSV (right) color spaces (Anisetti, 2009)

It can be thought of as a disk where the radial value indicates the *Saturation*, i.e. the difference between the color and a grayscale value of equal intensity of the color in question (Wang et al., 2014). Finally, *Lightness* forms the height of the column, indicating how white a color is. Another color space similar to HSL is the Hue, Saturation and Value (HSV) color space. It consists of the same first two channels, but the third, *Value*, indicates the brightness of a color. An illustration of the HSL and HSV color spaces are shown in **Figure 2**.

3 METHOD

To investigate if using color images will enhance the visibility of yellow and white markings in snowy conditions, a range of images from three scenarios: a laboratory, a test track, and public roads, were collected. The images were analyzed in grayscale, RGB, HSL, HSV and YUV color spaces. Images of white and yellow road markings from seven different cases shown in **Figure 3** and described in **Table 1**.

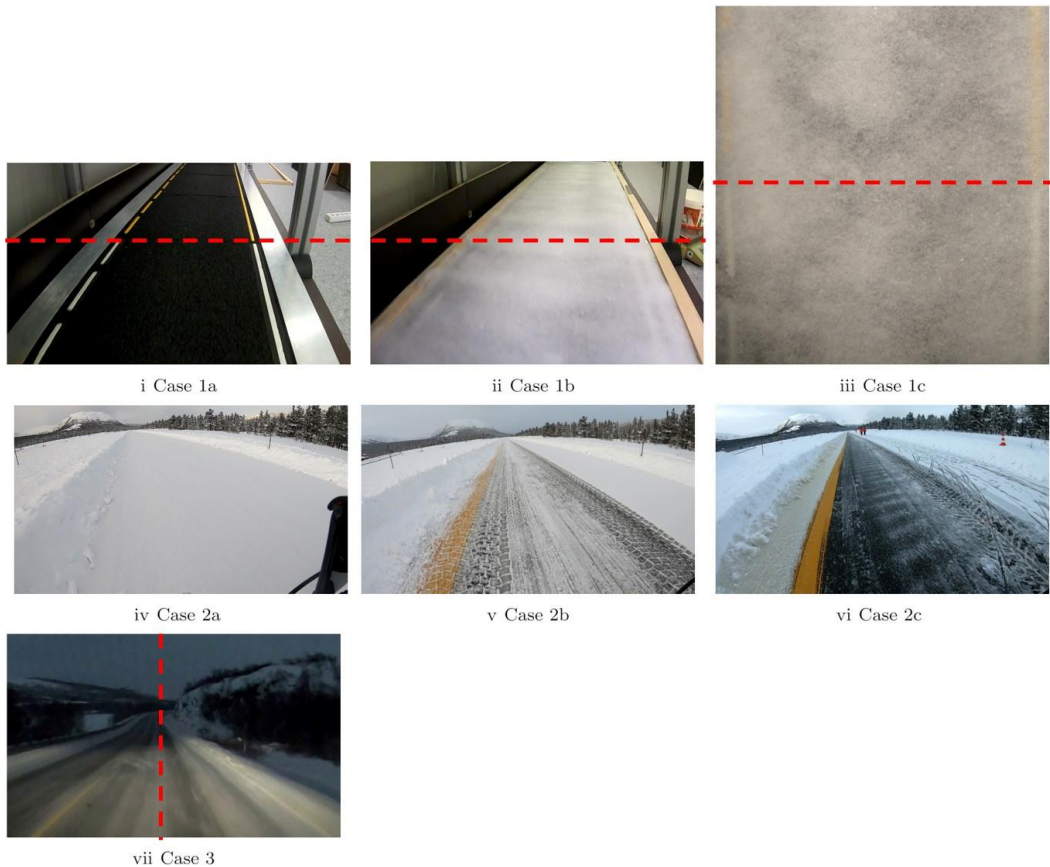


Figure 3 The images used from each of the seven cases.

For the different cases, video was captured using a GoPro Hero 7 camera. In addition, a Canon EOS 5D camera was used for taking birds-eye view images for Case 1c. The GoPro Hero 7 captured video at a resolution of 3840x2160 at 60 frames per second (GoPro, 2020). The Canon EOS 5D was equipped with 50 mm lens and images were shot in RAW format at 6720 x 4480 resolution.

The first scenario was a laboratory setting where a scaled-down road model with both yellow and white road markings was used, and artificially created snow could be produced and applied on site at a given depth. The GoPro and Canon cameras were used to provide different view

perspectives of the test setup. The second scenario was a closed airfield with a wide yellow centerline covered in snow. The airfield strip was filmed using a GoPro attached to a bicycle. Filming occurred at a snow depth of 2.5 cm, and then again after two different snow removal procedures had been performed. Lastly, field footage from a public road with white and yellow road markings was collected via a GoPro attached to the windshield providing an example of snowy and low ambient light conditions.

Table 1 Description of the seven cases of video and image capture

Case	Description	Markings		Camera
		White	Yellow	
1a	Laboratory, 1:10 road model, bare road	Yes	Yes	GoPro Hero7
1b	Laboratory, 1:10 road model, 0.5 cm snow, rear-view mirror perspective	Yes	Yes	GoPro Hero7
1c	Laboratory, 1:10 road model, 0.5 cm snow, birds-eye perspective	Yes	Yes	Canon EOS 5D
2a	Airfield strip, 2.5 cm snow	No	Yes	GoPro Hero7
2b	Airfield strip, plowed	No	Yes	GoPro Hero7
2c	Airfield strip, brushed	No	Yes	GoPro Hero7
3	Low light conditions on public road	Yes	Yes	GoPro Hero7

3.1 LABORATORY IMAGE CAPTURE (CASES 1A, 1B AND 1C)

The experiment was performed in a snow laboratory which consists of a narrow lane (50 cm x 2 m) with a moving equipment rig that can move back and forth above it. In the lane, a miniature road was constructed consisting of six consecutive tiles of asphalt, approximately 30 x 30 cm in size. Cameras were passed over the scaled down road under two different road conditions: bare road and 0.5 cm of snow.

The road was made by scaling down the asphalt and road markings to make the geometry consistent with a real-world road. The miniature road geometry was made based on the template in **Figure 4** (Statens vegvesen, 2019). The design standard in **Figure 4** corresponds to the minimum requirements when upgrading an existing road in Norway (values given in meters). The miniature road model was made for one lane (right-hand side), with a dashed center line and a continuous edge/fog line. The geometry of the road markings was given by the Norwegian standard for road marking, N302 (Statens Vegvesen, 2015). Roads with speed limits at or below 60 km/h and total width below 7.5 meters should use a width of 0.1 m for both center line and edge/fog line. Given the available space in the track of the snow lab, this allowed for the creation of a 1:10 model of the road.

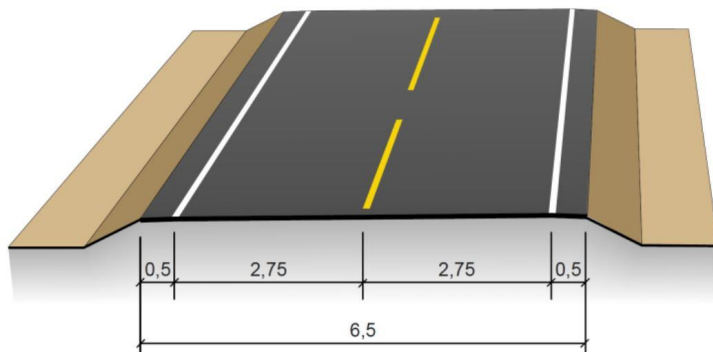


Figure 4 Minimum requirements for upgrading existing roads (values in meters) (Statens vegvesen, 2019)

On the first three tiles white thermoplastic road marking was used, followed by three tiles where yellow thermoplastic road marking was applied. The road marking pattern consisted of nine meter long dashes with three meter long spacing (**Figure 5**), this is in accordance with the standard for a 60 km/h road in the condition where the sight distance is too short for safe overtaking (Statens Vegvesen, 2015). The thermoplastic marking was applied to the road with the use of a heat gun following the same procedures as used by road crews. The finished result is shown in **Figure 5**. The thermoplastic marking product used was white and yellow ViaTherm 31H 25.

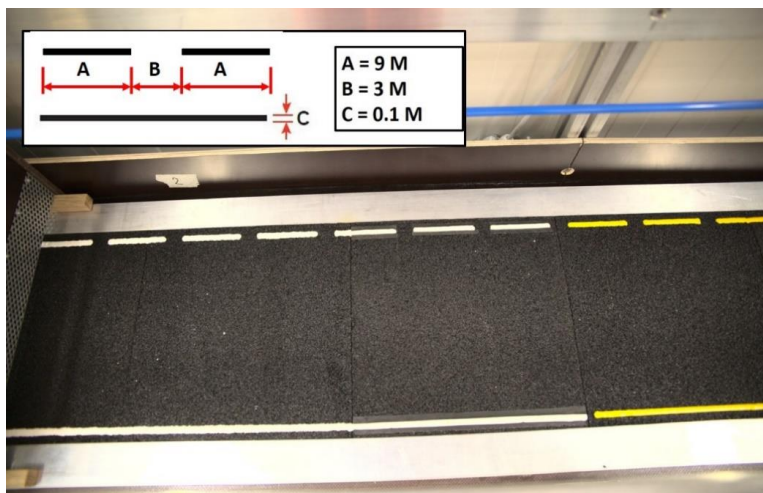


Figure 5 Applied thermoplastic road marking to 1:10 scale.

The GoPro was mounted in the rig above the scaled-down road. The height was chosen to be 11 cm above the road which is 1/10 the eye height definition used in road design in the U.S. (AASHTO, 2011) and similar to the height of a rear-view mirror where the camera for a lane

detection system generally is mounted. The cameras were positioned to have the road model in view and focus.

3.1.1 Snow production and application

Snow was produced in the lab using a snow machine (Giudici et al., 2017). The snow produced was a loose dendritic snow with a density of 302 kgm^{-3} . This density is found in settled snow (Armstrong and Paterson, 1982). In the snowy condition, the road was covered in a 0.5 cm layer of snow. To apply the layer of snow, a sifter was crafted for the experiment to try to achieve an even layer of snow that fit with custom wooden frames of 0.5 cm height **Figure 6**.



Figure 6 Sifting tool (left) and the applied 0.5 cm snow layer with the wooden frame (right)

3.1.2 Similitude

Similitude is a term used to describe the similarity between a model and the original. Generally, the scale effects for a phenomenon increase with the scale factor given by **Equation 1**, where L_P is a length in the real world application and L_M the corresponding length in the downscaled model (Heller, 2011). The inverse of the **Equation 1** gives the scale $1:\lambda$.

$$l = \frac{L_P}{L_M} = 10 \quad \text{Equation 1}$$

Geometric similarity requires that all lengths and dimensions be scaled down according to λ . For the road model described this will hold true for the lane width and markings, as well as the camera height. The height of the markings will not be to scale and, therefore, the volume of marking will also be larger than the scale factor would suggest. The heating of the thermoplastic removes any hard edges as in real-life road application. Lastly, the particle size and height of the snow is not scaled down as this was not achievable in the lab.

The material used for the road model is an asphaltconcrete type with stones up to 2 mm in size (Ab2), especially manufactured for lab use. Asphaltconcrete is commonly used in the top layer of the road construction for average annual daily traffic volumes between 3000 and 15 000. The stone sizes used in asphaltconcrete are 4, 8, 11, 16 and 22 mm (Statens vegvesen, 2005). The 2

mm stone size used at 1:10 scale is therefore within the range of stone sizes found in real life asphaltconcrete application, i.e. between 0.4 and 2.2 mm.

The set-up of the camera rig provides a model geometry similar to a car with a camera in the rear-view mirror sensor cluster. The cameras passed over the scaled road at speeds of 1/10 of 30 km/h. There was no interaction between the cameras and the snow or road and therefore no forces to scale down. The cameras detect light particles that are scattered from the road surface, road marking, snow, and surroundings. In addition to the moving GoPro camera, a Canon EOS 5D camera was used to take still photos in a birds-eye view.

If scaled up, the snow depth used would correspond to a real-life depth of 5 cm. However, the greater depth of snow, the more visible light is reflected from the snow itself (Perovich, 2007). More light reflected from the snow means less light hitting the road model. This causes overall brighter images with low chances of seeing the underlying road and markings. The physical interaction of light, snow and road marking is the same for the road model as for a full-scale road and using 0.5 cm deep snow was therefore assumed to produce a situation closest to a real-world road with a 0.5 cm depth of snow.

According to McEvoy and Castañer (2003) the amount of light reflected from new snow is between 80 and 90 percent of the incident light, although depth is not specified for these values. Furthermore, how much light is reflected from the snow and road model to the camera is dependent on several factors including the angle of incident light, the angle of the viewer, and the properties of the snow (age, density, particle size) (O'Neill and Gray, 1972; Perovich, 2007). In outside conditions both the zenith angle, i.e. how high the sun is in the sky, and the azimuth angle, i.e. the sun's position relative to the north, will affect the reflection of light from a snow surface, known as the albedo. In the lab setting, the artificial light is mounted in the roof making the zenith angle and the amount of ambient light constants. The two viewing angles represented by the moving GoPro camera and the Canon camera taking stills, will experience different amounts of reflected light from the snow and road model. The greater viewing zenith angle for the GoPro camera, θ_{v1} , theoretically suggests a lower reflection of light than for the smaller viewing angle for the Canon camera, θ_{v2} , (Kokhanovsky et al., 2005) as shown in **Figure 7**.

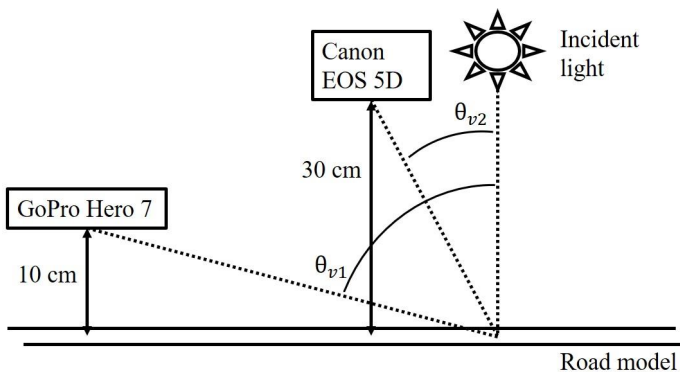


Figure 7 Zenith viewing angles for GoPro and EOS cameras

3.2 AIRFIELD TEST TRACK IMAGE CAPTURE (CASES 2A, 2B AND 2C)

An airfield with a wide yellow center line was the second scenario for image capture. The videos were captured using a bicycle with the camera mounted on the bar as shown in **Figure 8**.

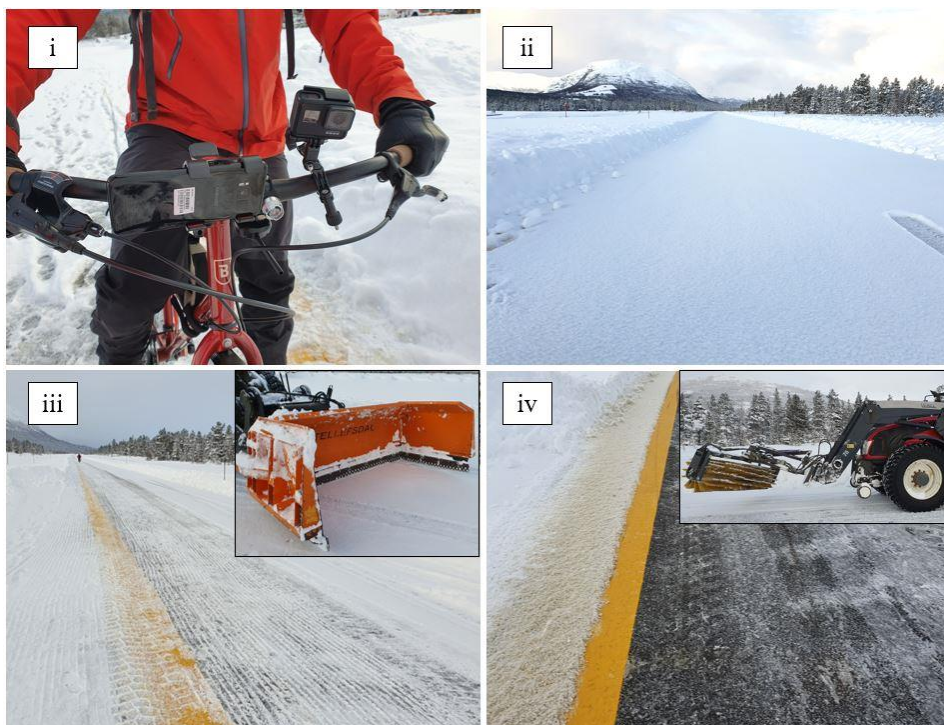


Figure 8 i) Video capture set-up for airfield scenario, ii) 2.5 cm snow coverage on test track, iii) Test track after snow removal by ribbed plow and iv) Test track after snow removal by brush

The camera height was 1 meter above the ground. Videos were recorded under three different conditions. The first was a 2.5 cm coverage of natural snow (**Figure 8ii**). The second video was taken after a ribbed plow with rib height of 2 cm had been applied to the test track (**Figure 8iii**). Finally, the third video was shot after the same part of the test track had been brushed (**Figure 8iv**). The yellow road marking was 43.5 cm wide of type ViaTherm 31H 25. The snow had a temperature of -2.5 degrees Celsius and the air temperature was -5.5 degrees Celsius. The snow had a density of 99.7 kgm^{-3} typical for damp new snow. For the first snow removal procedure, the ribbed plow left 2cm ribs of snow, however the wheels of the tractor subsequently passed over the road marking and adjacent road surface creating a varying snow coverage from 0 to 2 cm (**Figure 8iii**). After the second snow removal procedure, the brushing process, the road marking appeared to be close to bare while the adjacent road surface had small amounts of snow with the asphalt clearly seen underneath (**Figure 8iv**).

3.3 PUBLIC ROAD IMAGE CAPTURE (CASE 3)

Videos were also captured from public road driving. In this case, the GoPro camera was mounted on the inside of the front wind shield slightly to the left of the rear-view mirror. The video was recorded on European route 6 (latitude 9.366) at 15:30 on December 2nd, 2019. This represents a challenging scenario with low ambient light due to the sun being low in the horizon and the weather overcast, as well as a snow coverage of between 0 and 2 cm of snow and snow drift. The road marking on this road was the same type of thermoplastic material (Viatherm 31H 25) as in the other cases, with a yellow dashed centerline and white solid edge line. The air temperature was -5.2°C and road surface temperature -7.3°C .

3.4 LANE DETECTION PROCEDURE

From the videos captured in each of the cases, every 10th frame was extracted to create images for comparing color spaces. One frame was selected manually for each case and converted to different color spaces using OpenCV, Matplotlib and Python. The images were imported as RGB images using the Matplotlib function *imread* and subsequently converted to other color spaces using the functions *cv2.COLOR_RGB2GRAY*, *cv2.COLOR_RGB2HLS*, *cv2.COLOR_RGB2HSV* and *cv2.COLOR_RGB2YUV*. Note that the OpenCV function uses HLS as the color space most often referred to as HSL. The images from the different color spaces were then split into their separate color channels for comparison. The images were assessed by visual inspection. In addition, histograms of the different cases and color spaces were created to assess the change in pixel intensity between the road marking and the surroundings. In the histograms distinct peaks or troughs corresponding to the white or yellow marking, signify lane markings that are detectable by thresholding or by identifying gradients of pixel values.

4 RESULTS

The seven images, one for each of the cases (**Figure 3**) were imported as RGB and converted to grayscale, HSL, HSV and YUV color spaces. Grayscale images have 1 channel while the color spaces consist of three channels. This gives 17 different representations of each image, one for the grayscale image and four for each color space (the three separate channels plus all channels combined). To assess how the color representation affects the visibility of the white and yellow markings, respectively, the images will be analyzed visually and then using histograms for each of the color channels.

4.1 GRAYSCALE REPRESENTATION

Converting images to grayscale representation is a common way of turning a 3-channel image into a single channel image. In **Figure 9**, the images representing each case are shown in grayscale representation.

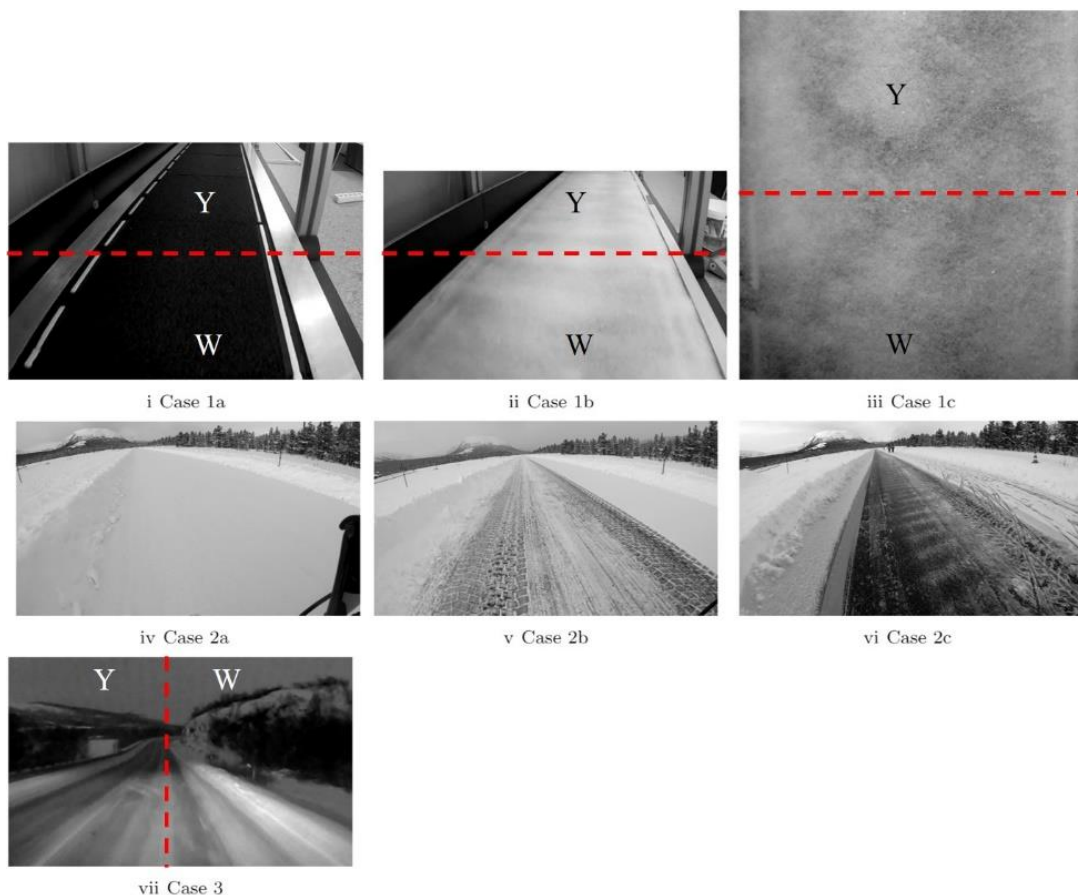


Figure 9 Grayscale representation of cases

Case 1a (**Figure 9i**), the bare road model, represents an ideal situation for lane detection: new road marking, new asphalt, and good lighting. The markings are clearly visible in grayscale as they were in the RGB version of the image, with the yellow markings appearing slightly grayer in the grayscale image, as expected. In cases 1b (**Figure 9ii**) and 1c (**Figure 9iii**), the road model is covered in 0.5 cm of snow. The road markings hard to visually detect in case 1b where the camera was placed at an angle representative to that of a camera in vicinity of the rear-view mirror. When the image is taken directly overhead, case 1c, the white lane lines are visible in the lower part of the image. In the upper half, the yellow markings again appear grayer than the white markings making them road marking hard to see.

In case 2a (**Figure 9iv**) the field test with 2.5 cm snow, the road marking is not visible. In 2b (**Figure 9v**) and 2c (**Figure 9vi**) different snow removal procedures have been performed. In the RGB images (**Figure 3**) the yellow markings were clearly visible, but more difficult to see in the grayscale images.

Case 3 (**Figure 9vii**) shows a snowy public road in low ambient light. Both the yellow lane marking on the left side and the white road marking on the right side are visible in the grayscale representation, as they were in RGB color space. However, the markings and snow are of similar intensity in the images, which might make the edge between road surface and road marking challenging to identify.

In summary, the road markings appear distinct and much lighter in color than the adjacent asphalt when the road is bare but a visual inspection of the images indicates that lane detection may be more problematic under snow cover for the conventionally used RGB and grayscale images. Both white and yellow road markings will, in grayscale images, have pixel intensities similar to parts of the snow coverage. This is especially evident in Case 2b (**Figure 9v**).

In the following section, the images are assessed in the color spaces RGB, HSL, HSV and YUV by visual inspection and using histograms. Based on the visual inspection of the cases in RGB and grayscale presentations, cases 1b and 2a will be omitted. In the first instance, case 1c will make for a better comparison between the white and yellow markings as these appear at the same distance and in equal quantities in the image. For case 2a, the road marking is not visible and will therefore not provide additional information in other color spaces or corresponding histograms.

4.2 COLOR SPACE REPRESENTATION

The images analyzed are cases 1c, 2b, 2c and 3. The images are shown in the four color spaces RGB, HSL, HSV and YUV and in their respective channels.

Case 1a (**Figure 10**) shows an ideal situation for lane detection. In the upper part of the images there is yellow markings and in the lower part white markings with the transition between the marking colors indicated by the red dashed line. **Figure 10** shows the four color representations: RGB, HSL, HSV and YUV in the top row, and the three separate channels they are made up of in the color spaces respective columns. A mask has been added manually to focus on the road and lane marking rather than the adjacent metal edges in the lab setting. For RGB, the white marking is visible in all channels, while the yellow seems most prominent in the R channel, slightly less so in the G and not very prominent in the B channel. For the HSV color space, neither white or yellow marking is visible in the H-channel, the yellow marking is clear while the white marking is more muted in the S- channel, while the white marking is most prominent in the V-channel. For the HSL representation, the H- and S- channels show similar result to the HSV color space. The HSV-V channel on the other hand, shows the yellow marking more clearly than the HSL-S channel. In the rightmost column, the YUV representation of the image, the Y-channel shows both markings clearly, while the U- and V- channels highlight the yellow marking. The difference between the YUV-U and YUV-V channels being that the former represents the yellow marking as the darkest part of the image, while the latter conversely represents it as the lightest part of the image. This difference will make the YUV-U histogram form a trough representing the marking while the YUV-V channel will show the road marking as a peak.

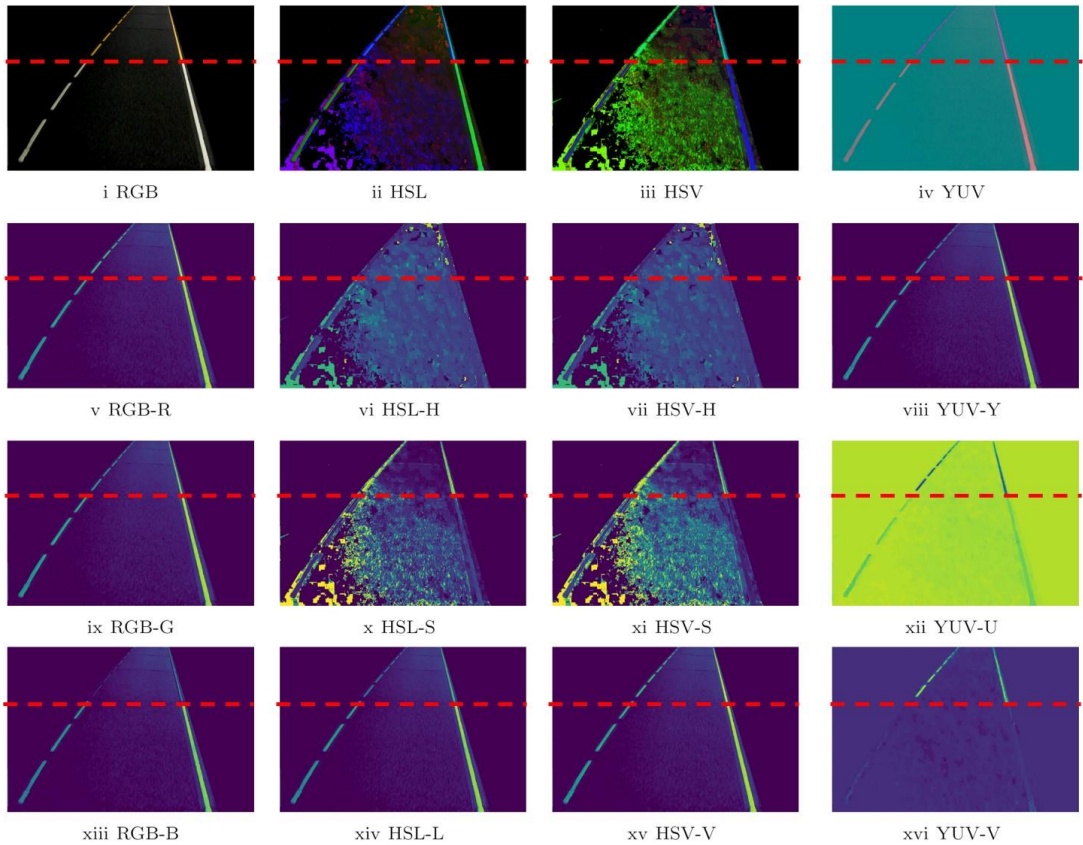


Figure 10 Case 1a in RGB, HSL, HSV and YUV color spaces and corresponding channels

Next, the images featuring different snow coverages will be presented in the respective color spaces. First, case 1c, the road model with 0.5 cm snow coverage in birds-eye view (**Figure 11**). There is white marking in the lower end of the image and yellow marking above the red dashed line. The effect of the different color space representation is the same for case 1c as it was for the previous case, 1a. However, the snow cover makes the markings that appeared clearly in Case 1a challenging to see in Case 1c. In the bare road case (1a) four channels enhanced only the yellow marking: HSL-S, HSV-S, YUV-U and YUV-V. Interestingly, these channels seem to work even better for the 0.5 cm snow coverage but only for the yellow marking. The white elements, represented by the white road marking and the snow, are no longer clearly visible.

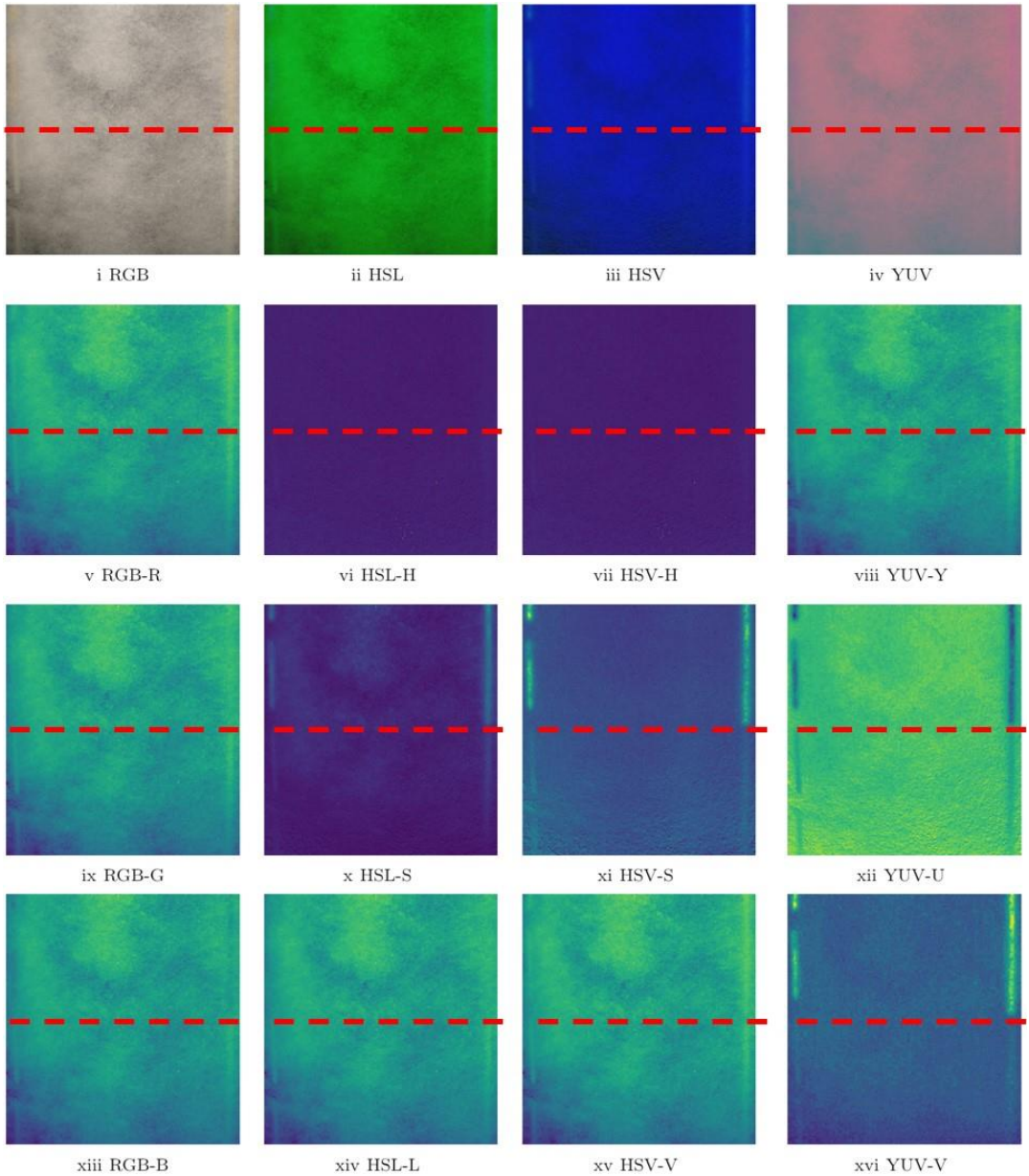


Figure 11 Case 1c in RGB, HSL, HSV and YUV color spaces and corresponding color channels

The next 2 figures show the airfield images in different color spaces. Case 2b, the image after snow plowing (**Figure 12**) is therefore presented, followed by case 2c, the image after brushing (**Figure 13**). In these two cases, there is only yellow marking.

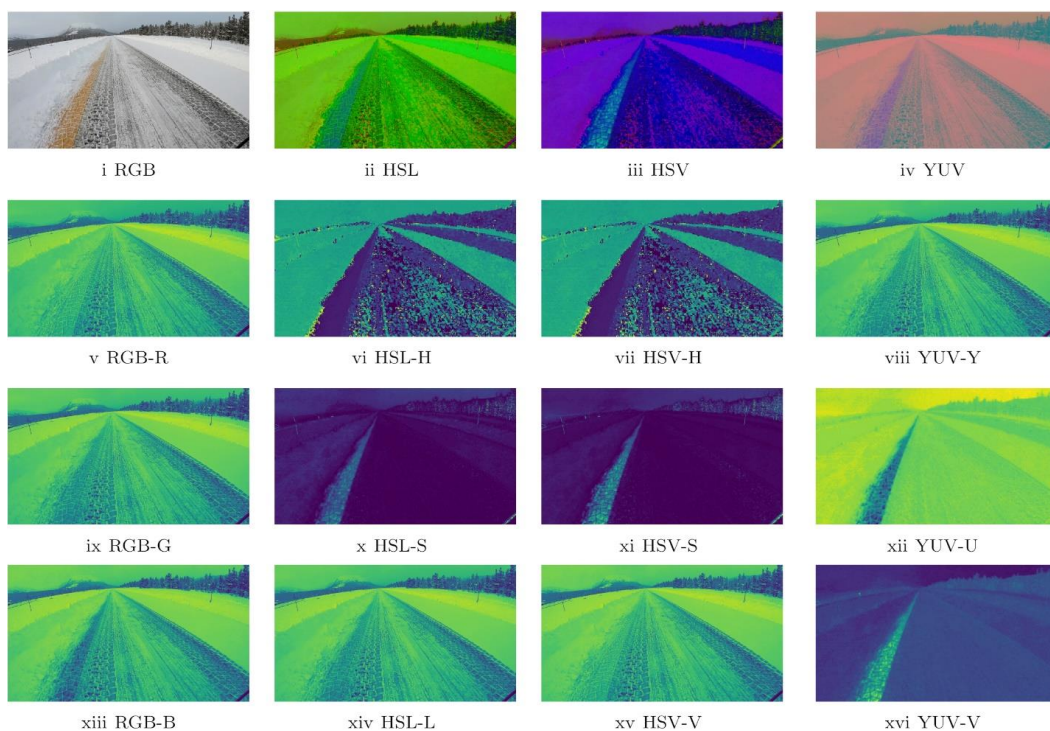


Figure 12 Case 2b in RGB, HSL, HSV and YUV color spaces and corresponding color channels

For case 2b, the yellow road marking is clearly visible to the human eye in the RGB image. However, when considering the separate channels of the image, the marking is harder to detect. In the RGB-R channel the tire track from the tractor is clearer than the road marking. In the RGB-G channel it is hard to distinguish the road marking, tire track and other elements of snow. In the RGB-B channel the marking is visible and similar in pixel value to the right edge of the snow removal area. The channels that look most promising in terms of visibility and contrast of the yellow marking are HSL/HSV-S, YUV-U and YUV-V, as in the two previous cases. HSL-L and HSV-V channels are not suited to enhance the road marking, while the HSL/HSV-S channel in this case shows the markings but with low contrast to the road surface on the right hand side.

The airfield strip after snow has been removed by brush, case 2c, is shown in **Figure 13**.

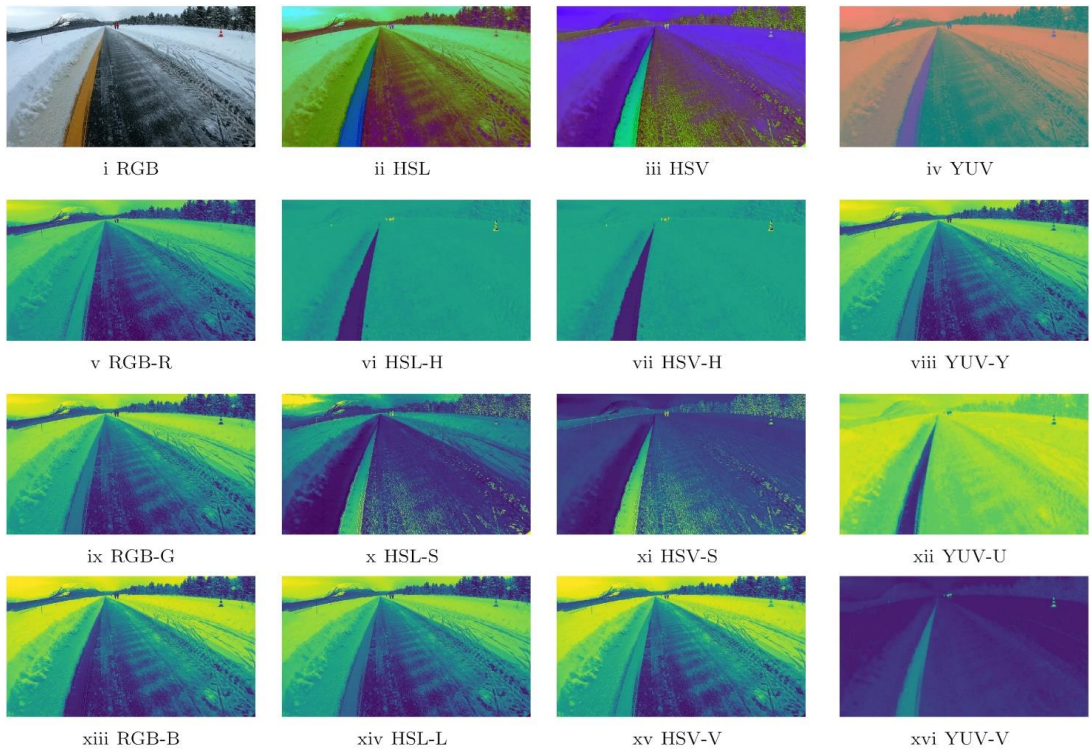


Figure 13 Case 2c in RGB, HSL, HSV and YUV color spaces and corresponding color channels

In case 2c, the brushing of the snow coverage has removed most of the snow on the right hand side of the yellow road marking, while the snow coverage on the left hand side of the marking remains mostly intact. Having snow on one side of the yellow marking and dark road surface on the other creates an interesting situation in terms establishing contrast between the road and road marking in images. In the RGB image, the yellow color is clearly seen, but when considering the separate channels usually used in analyses, the contrast is low between the snow and the marking in the RGB-R channel, and conversely, between the marking and the road surface in the RGB-B channel. In the RGB-G channel the road marking does provide a contrast to the snow and road surface, but the pixel values are also similar to the snow which would make it challenging to separate the marking from longitudinal snow elements. In the HSL image, the marking is hard to separate from the snow, however the HSL-H and HSL-S channels highlight the yellow marking in light versus dark pixel representation. The same channels in the HSV image, HSV-H and HSV-S show similar results, while the HSV image provides a better separation of road marking to snow and road surface than the HSL image. The HSV-V channel and HSL-L channel are not optimal to enhance the yellow marking, as in case 1c and 2b. The YUV image representation provides an identifiable color for the yellow marking, like the RGB and the HSV images. Considering the separate channels, the YUV-Y channel is poorly suited to detect lane markings, while the YUV-U and YUV-V channels separate the yellow marking from both the snow and the dark road surface in opposite ways.

The final scenario, case 3, considers an image taken in the afternoon (15:30) driving on a public road (**Figure 14**). There is a yellow road marking on the left-hand side and white road marking on the right-hand side. In **Figure 14** the white road marking is visible in all the RGB channels, but the contrast to the snow next to it is not high. The H-channels from the HSL and HSV representations are inapt to show the lane markings. In the S-channels for these two color spaces, the yellow marking is visible, but not the white. The HSL-L and HSV-V channels provide similar results as the RGB channels, where the lines are visible, but have low contrast to other elements of the scene. The YUV and YUV-Y representations of the image are not favorable in locating the lane markings, while the YUV-U and YUV-V channels provide what seems like the highest contrast between the yellow road marking and the snow and road surface.

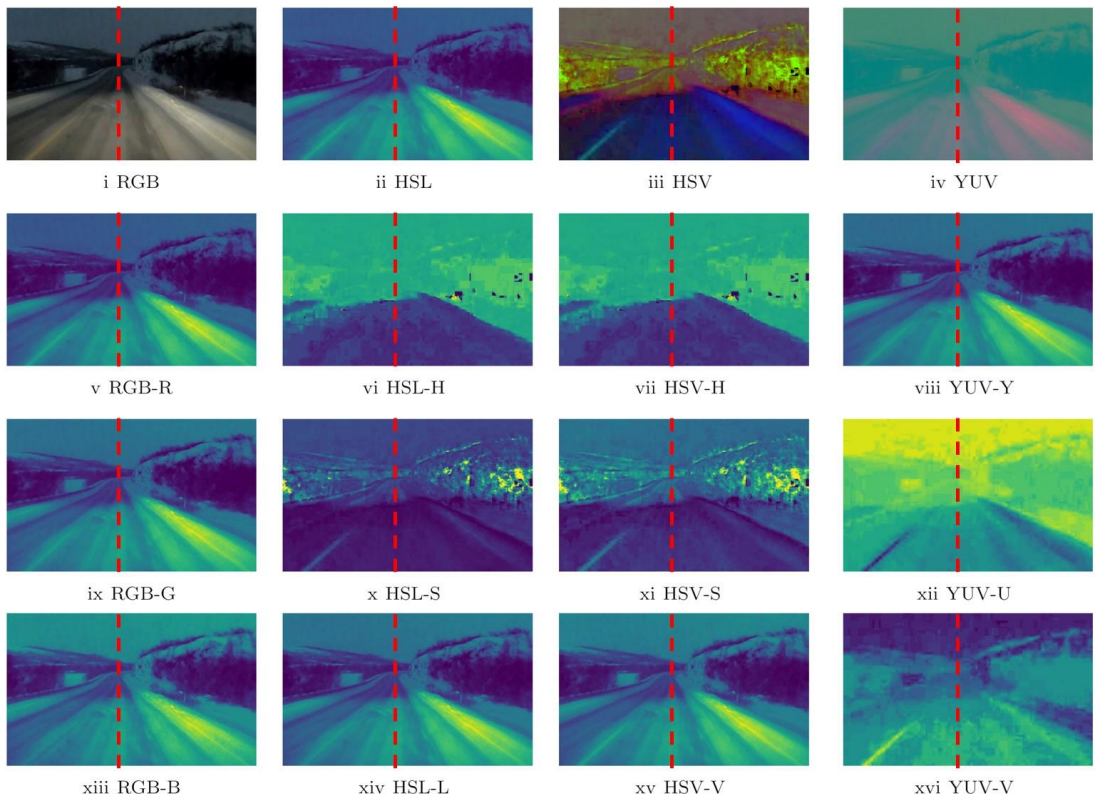


Figure 14 Case 3 in RGB, HSL, HSV and YUV color spaces with corresponding color channel

In summary, a consistent set of color channels: HSL-S, HSV-S, YUV-U and YUV-V, seem to amplify the visibility of the yellow marking in the four images of snow conditions (cases 1c, 2b, 2c and 3). In case 1c, the airfield strip with snow on the left hand side and almost bare road on the right hand side, the color spaces HSL/HSV-H also set the road marking apart from the rest of the image. For the white markings (case 1c and 3), the highest visibility was in the three RGB-channels, YUV-Y, HSV-L and HSV-V.

The visual analyses of the visibility of white and yellow road markings in snowy conditions are summarized in **Table 2**. Case 1a has been grayed out as this image does not have snow in it and serves as a reference for the bare road situation.

Table 2 Visual assessment of visibility of white and yellow markings in different color channels where ‘+’ means the marking is somewhat visible and ‘++’ that the marking is clearly visible.

Image Case	Gray	RGB-R	RGB-G	RGB-B	HSL-H	HSL-S	HSL-L	HSV-H	HSV-S	HSV-V	YUV-Y	YUV-U	YUV-V
1a W	++	++	++	++			++			++	++	+	
1a Y	++	++	++	+		++	+		++	++	++	++	++
1c W		+	+	+			+			+		++	
1c Y	+	+				+			++	+	+	+	++
2b				+	+	++		+	++			++	++
2c	+	+	+	+	++	++		++	++	+	+	++	++
3 W	+	+	+	+			+			+	+		
3 Y	+	+	+			+			+	+	+	++	++

From **Table 2** the color channels that provide the highest visibility overall are HSL-S, HSV-S, YUV-U and YUV-V. The visibility in snowy conditions is higher for yellow markings than for white markings in these instances. **Table 2** summarizes a subjective way of visually analyzing images. The following section will therefore establish an objective assessment of the visibility of the road markings using histogram plots.

4.3 HISTOGRAMS OF PIXEL VALUES

Whether lane markings are detected by thresholding or by using gradients, lane detection algorithms generally rely on distinct changes in pixel values to establish edges. The four images of snowy conditions (Cases 1c, 2b, 2c and 3) are therefore assessed with regard to changes in pixel values through sets of histogram plots. The plot is produced by adding the individual pixel intensities for each column of pixels for a given color channel. The pixel column is on the x-axis and the summed pixel values on the y-axis. The aim is to achieve a clear indication of where the road marking is in the image given by a distinct rise or fall in the sum of pixel values. When the pixels representing the road markings are light in color they will have high intensity values creating high sums and, thus, peaks in the plot. In instances where the road marking appears as the darkest part of the image, the road marking pixels have a low sum and should create a visible trough in the plot. The more distinct the peak or trough is in the plot, the more ideal the image is for lane detection will be. Plots with no clear peaks or troughs mean that the road marking is challenging to identify in the image. The next sections will first present the traditional representations, RGB and grayscale, and then the alternative representations, HSL, HSV and YUV for the selected cases with snow and visible markings: Case 1c, 2b, 2c, and 3.

4.3.1 Case 1c

For Case 1c, the top half of the image has yellow markings, and the bottom image has white markings. To compare the white and yellow markings, two histogram plots are made: one for the lower half (white markings) and one for the upper half (yellow markings). In **Figure 15**, the RGB-channels and the grayscale representation are shown. In these histograms, there is a peak on the right side of the image where the continuous lane marking is, for both white and yellow

marking. The dashed line does not produce a peak higher than those of the road surface. The peak is most distinct in RGB-R for both colors, while RGB-G and -B also provide peaks that for white markings. The RGB-B channel has a trough for the yellow continuous marking which would be hard to discern from the rest of the minima in the plot. The grayscale histograms show peaks for both white and yellow markings, however, the white marking peak is significantly more prominent than the yellow marking peak. Again, only the continuous lines are detected in the histogram plots.

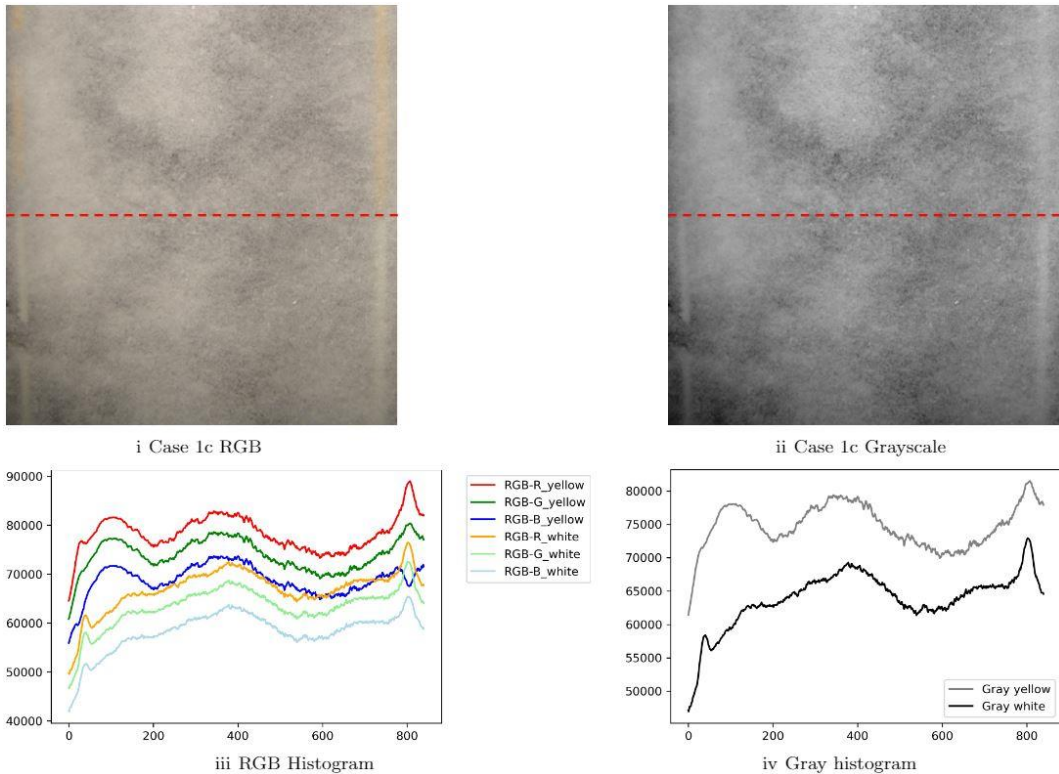


Figure 15 Case 1c RGB and Grayscale histograms

Figure 16 shows the histograms for the channels of the HSL, HSV and YUV color spaces. The histograms on the left-hand side show all channels and the histograms on the right-hand side show the channels that appear to be most suited to detect the lane markings in terms of changes in pixel value. In the HSL and HSV plots, the HSL-S channel has been highlighted as it shows distinct peaks for both the dashed and the continuous line. The HSL-L channel has a peak for the continuous white line only. In the top right-hand side plot the difference between the visibility of the yellow markings is evident with the yellow markings providing clear peaks for both dashed and continuous lines.

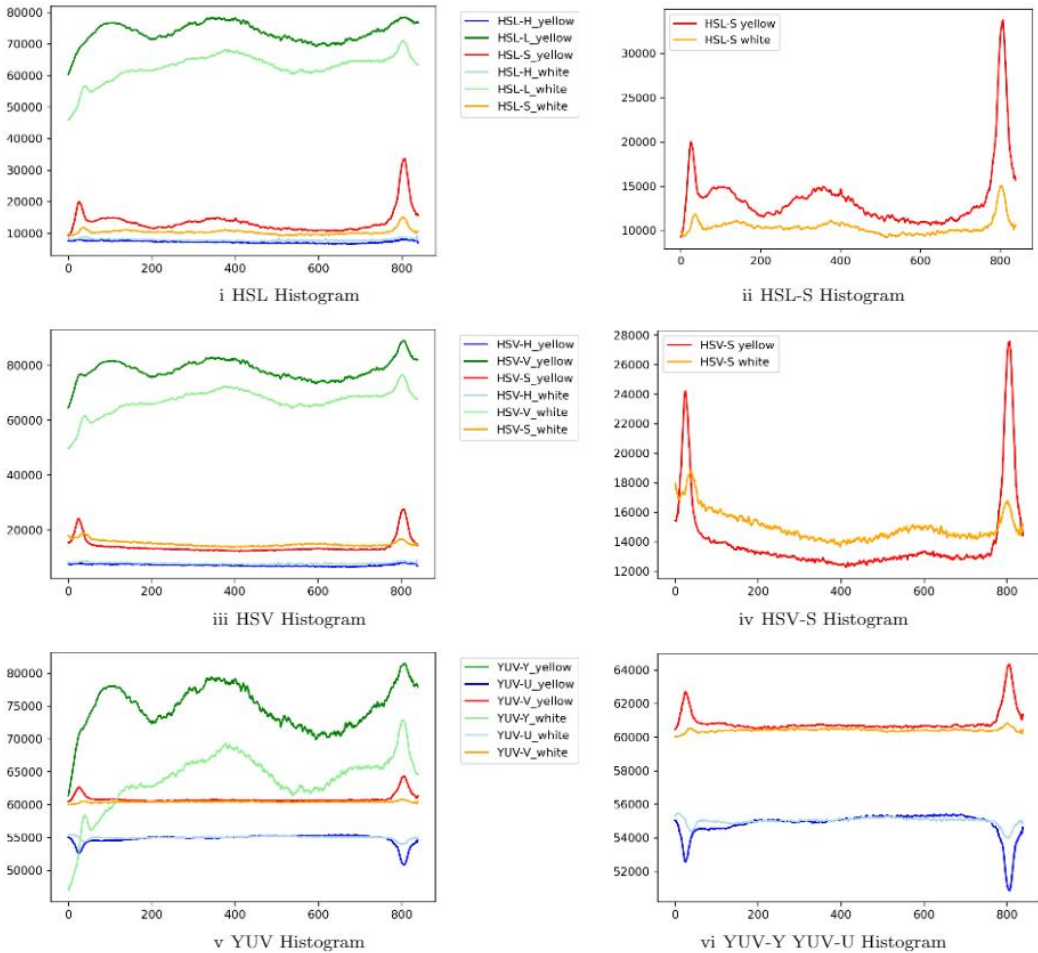


Figure 16 Case 1c HSL, HSV and YUV histograms

The same effect is seen in the HSV plots, where the HSV-S plots have very distinct peaks for the road marking and low sums for the columns representing the rest of the image. For the YUV representations, the V- and U-channels show the most distinct peaks, where the road markings have significantly higher values than the surrounding surfaces. In these channels, both the dashed line (left) and the continuous line (right) can be detected in contrast to the RGB and grayscale histograms which only detected the continuous lines. The YUV-U channel shows the road markings appear as troughs but in this case, as opposed to the RGB-B plot, the troughs would be identifiable as local/global minima. The histogram plots are consistent with the findings in the previous section (**Table 2**), where the HSL/HSV-S and YUV-U/V channels provided the highest visibility of the yellow marking in snowy conditions.

4.3.2 Case 2b

In Cases 2b and 2c, there is only a continuous yellow marking. The histograms are created based on the lower half of the images, focusing on the area of the image with the lane marking. **Figure 17** shows the histograms for Case 2b as represented by RGB and grayscale images. In Case 2b it is not possible to separate a threshold or peak that represents the road marking from the surroundings in either the RGB or grayscale histogram plots.

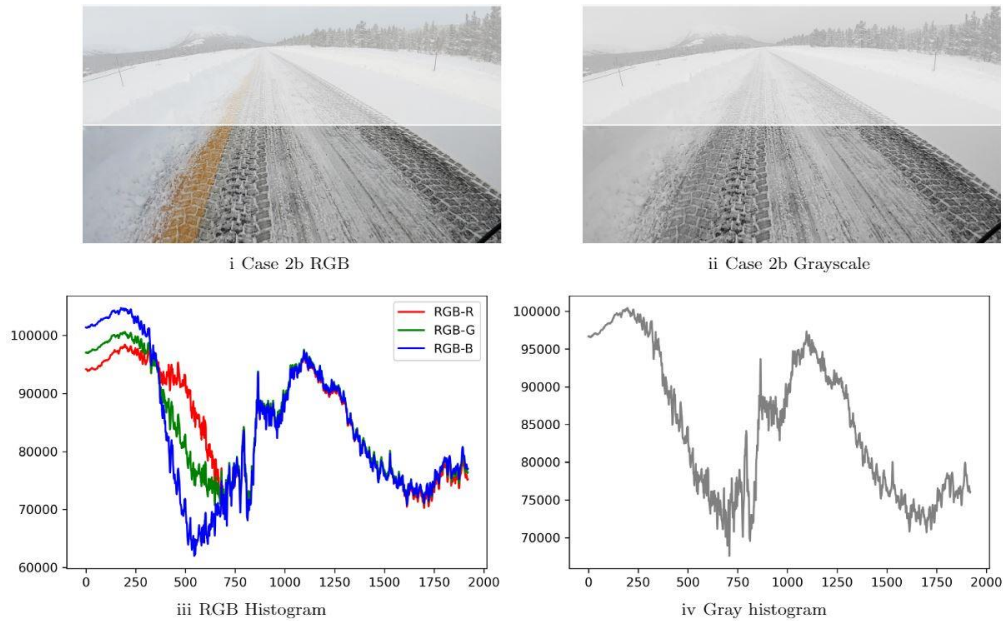


Figure 17 Case 2b RGB and grayscale histograms

In **Figure 18**, the histograms for the HSL, HSV and YUV representation of the Case 2b image are shown. On the left-hand side the three channels of the color spaces are plotted, while the right-hand side highlights the channels that provide the best detection of lane markings. In the HSL representation, the S-channel provides the most prominent peak. This is also true for the HSV histogram. In Case 2b, the YUV-U and YUV-V channels also produce a distinct trough and peak respectively, this is consistent with the findings in the visual inspection.

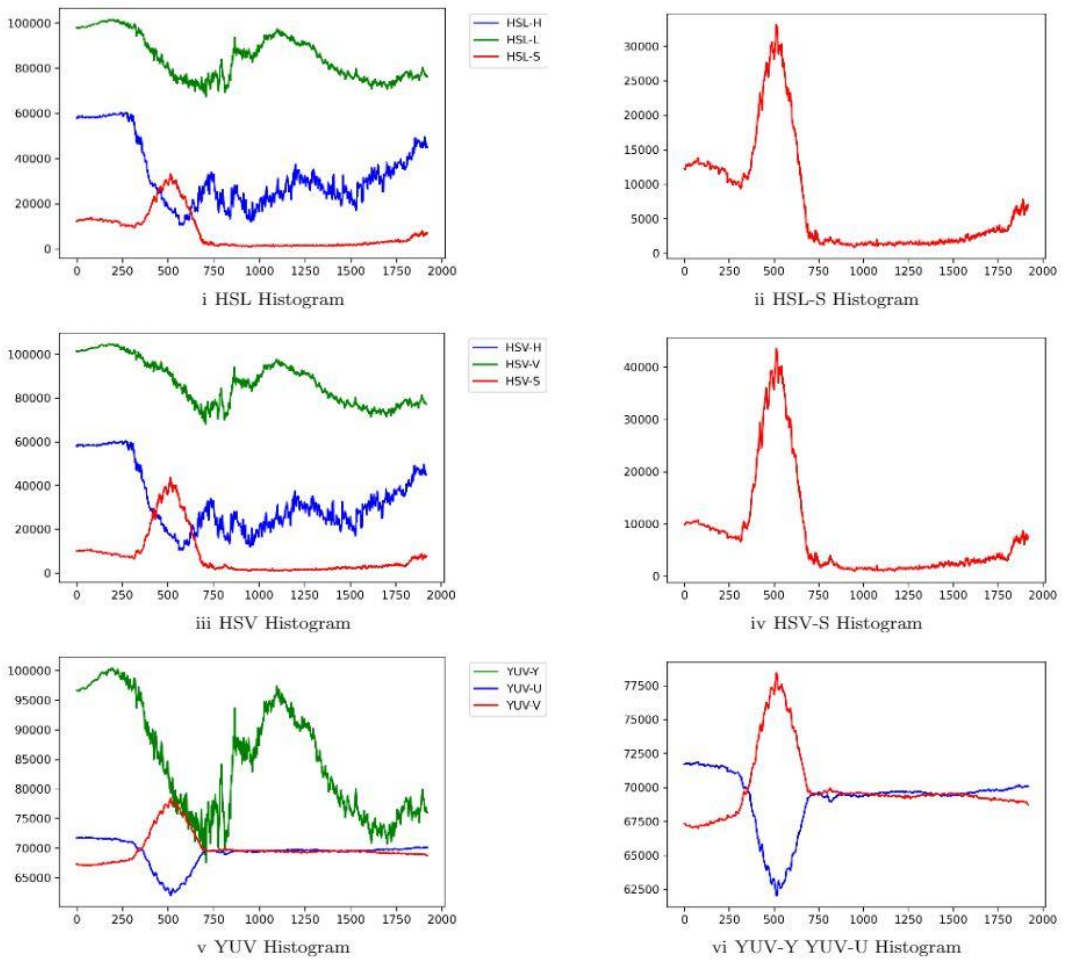


Figure 18 Case 2b HSV HSL and YUV histograms

4.3.3 Case 2c

The RGB and grayscale histograms for Case 2c are shown in **Figure 19**. As in the previous case, 2b, these representations are not well suited to detect the single continuous yellow road marking.

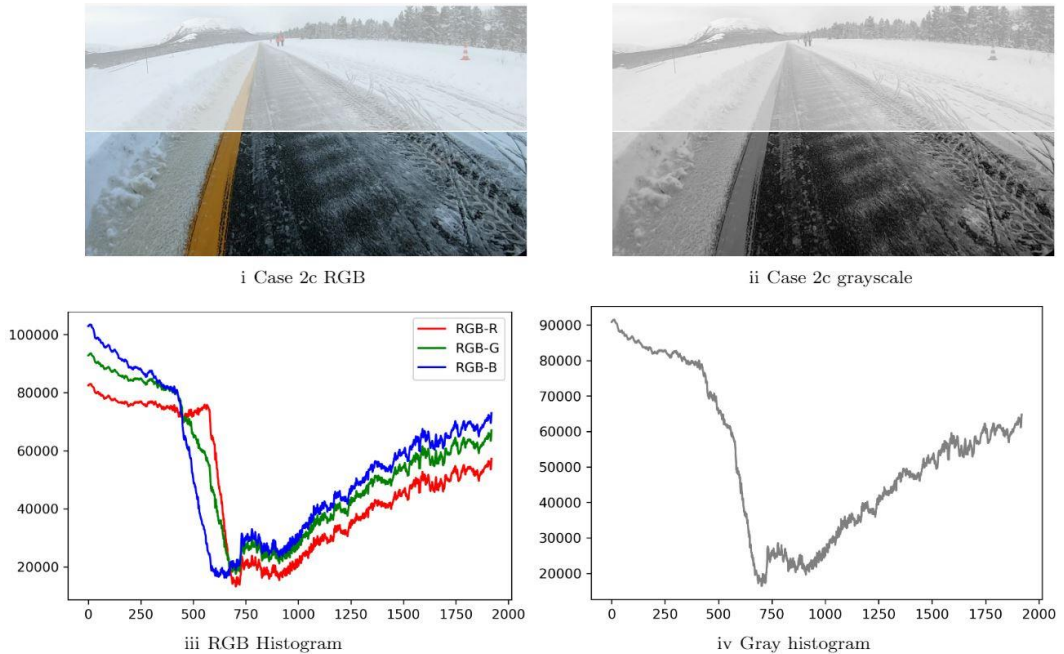


Figure 19 Case 2c RGB and grayscale histograms

In the HSL, HSV and YUV representation in **Figure 20**, the H- and S- channels of the HSL and HSV color spaces, as well as the U- and V- channels of the YUV representations, all show identifiable peaks for the yellow road marking. For the HSL and HSV color spaces, the H-channel is particularly successful at isolating the road marking as the only peak in contrast to both the snow and almost bare road. When the road marking pixels form the clear local or global maxima the image representation is well suited for lane detection as there are no peaks that can be misidentified as road markings. This echoes the result seen in the summary of the visual inspection in **Table 2**.

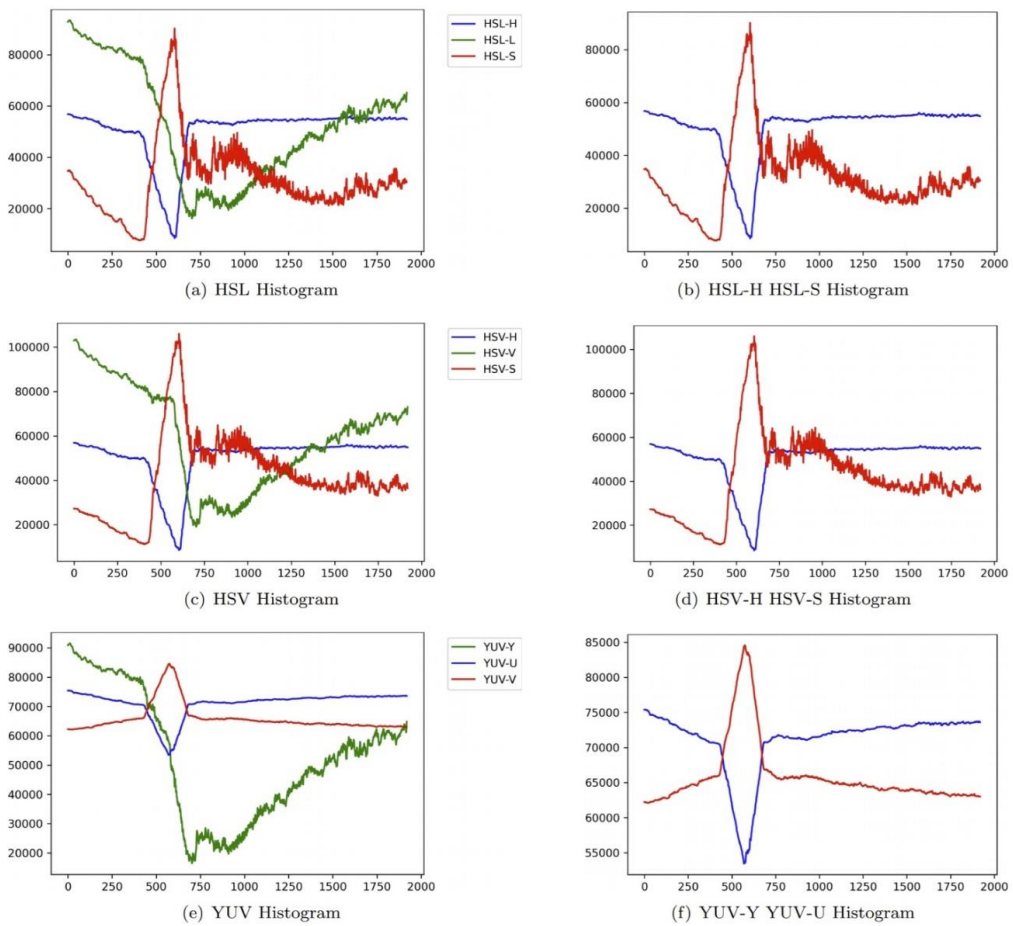


Figure 20 Case 2c HSL HSV and YUV histograms

4.3.4 Case 3

Case 3 has a yellow dashed line on the left-hand side and a white continuous line on the right-hand side of the image. In this case, the part of the image used in creating the histograms is the very lower end of the image as indicated below the white line in **Figure 21**. This section of the image provides a continuous section of both yellow and white marking. The RGB and grayscale histograms are also shown in **Figure 21**. The histograms for these conventionally used image representations are not suited to identify either the white or the yellow marking.

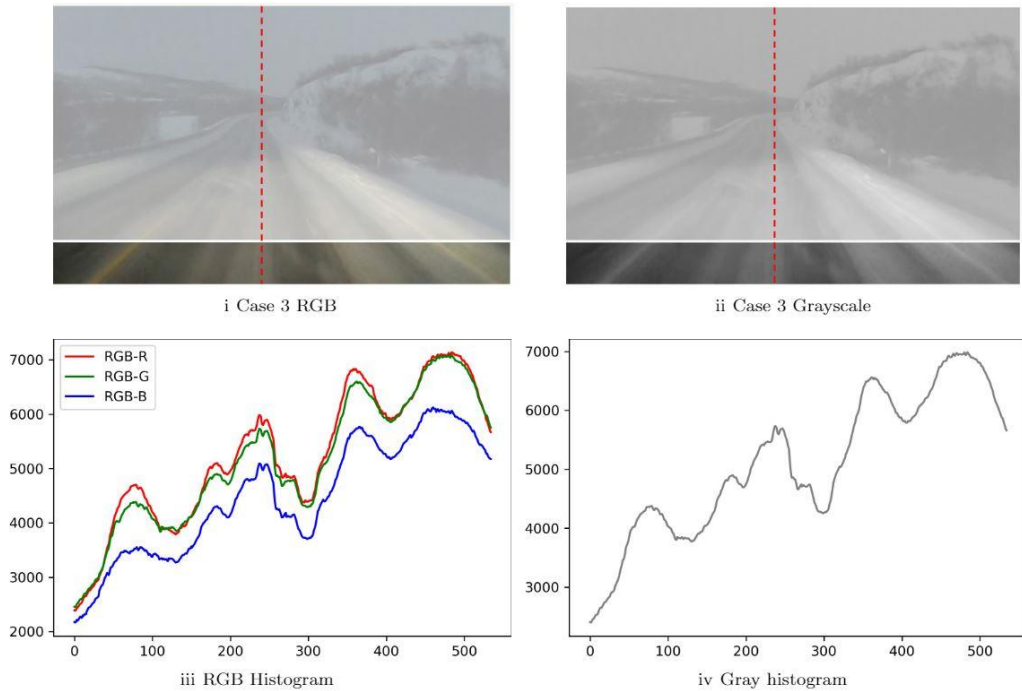


Figure 21 Case 3 RGB and grayscale histograms

The HSL, HSV and YUV histograms for Case 3 are shown in **Figure 22**. In this case, the only channels that provide visible peaks are the HSL-H and HSV-H channels. A peak large enough to separate it from the rest of the plot is seen on the left-hand side, i.e. stemming from the yellow road marking, while the white road marking's pixel values are not distinguishable from the surrounding environment. In Case 3, the YUV channels are not able to pick out any road marking.

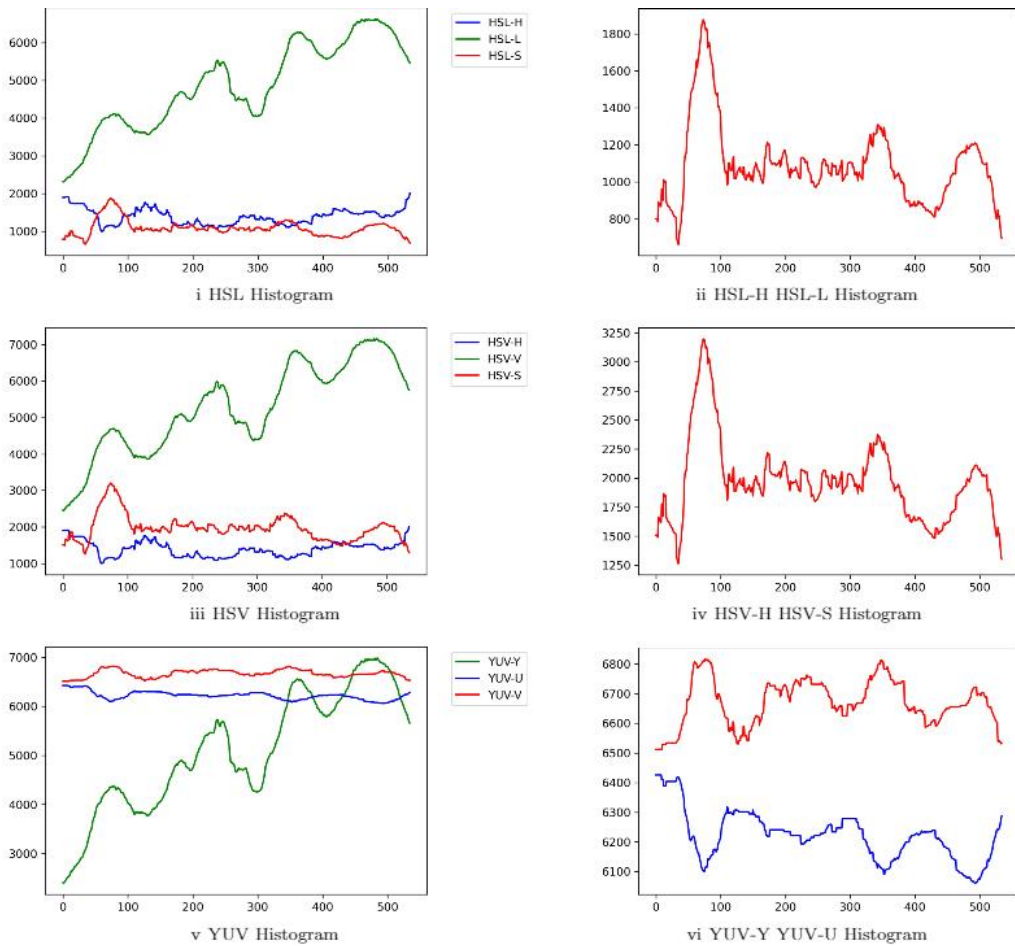


Figure 22 Case 3 HSL HSV and YUV histograms

The visibility of the white and yellow road markings based on the histogram analyses have been summarized in **Table 3**.

Table 3 Summary of visibility of road markings based on histogram plots where ‘+’ means the marking is somewhat visible and ‘++’ that the marking is clearly visible.

Image Case	Gray	RGB-R	RGB-G	RGB-B	HSL-H	HSL-S	HSL-L	HSV-H	HSV-S	HSV-V	YUV-Y	YUV-U	YUV-V
1c W	+	+	+	+		+	+		+	+	+	+	+
1c Y		+				++			++	+	+	++	++
2b						++			++			++	++
2c					++	++		++	++			++	++
3 W													
3 Y						++			++				

The results from the analyses of the histogram plots is in line with the findings for the visual inspection (**Table 2**). In both cases the color channels HSL-S, HSV-S, YUV-U and YUV-V perform the best in identifying lane markings in snowy conditions. However, in Case 3 the YUV-U and V channels do not provide identifiable peaks for the white or yellow markings.

5 DISCUSSION

The aim of the paper was to determine whether yellow road marking could be beneficial for automated lane detection in snowy conditions. From the seven initial cases (one image depicting a bare road and six images depicting snowy roads) five images were chosen as most appropriate for analyzes by visual inspection and four images by using histogram plots.

The visual analyses were performed for the five cases 1a, 1c, 2b, 2c and 3, followed by histogram plots of the intensity values of the pixels in the different color channels for the four cases with snowy conditions: Cases 1c, 2b, 2c and 3. The histogram plots provided an objective and machine friendly interpretation of the visibility of the lane markings. The results of these analyses were summarized in **Table 2** and **Table 3**, and when compared yield similar results. The most common image representations, RGB and grayscale, work well for lane detection on bare roads (Case 1a). However, for snowy conditions, Case 1c was the only case where the lane marking was visible in RGB and grayscale histogram plots and then only for the white continuous line (**Table 3**). HSV-S and HSL-S channels provide high visibility in all four cases. Of these two, the HSV-S provides the most distinct peaks for the lane marking and lowest pixel value for the surroundings. In Case 2c, the H-channels of the HSV and HSL color spaces highlight the yellow marking well, however this is not the true for the other cases. The U- and V-channels of the YUV image representation are successful in identifying the lane marking in the three conditions with good ambient light, Cases 1c, 2b and 2c. In Case 3, the yellow marking appear to be visible to the human eye in the U- and V-channels (**Figure 14**), but the histogram representation (**Figure 22**) show that there is no identifiable peak for machine vision. The low light conditions, video capture at about 80 km/h, snow and snowdrift provide low contrast between lane marking and road surface. Case 3 represents driving at around rush hour (15:30) on a European route, i.e. a road of high standard, in Norway. It is thus a realistic case for winter driving and makes the fact that the HSV-S channel has a clear peak for the yellow marking even more promising.

Two cases with both white and yellow road marking were analyzed, Cases 1c (birds-eye view of 0.5 cm snow in lab) and 3 (public road with low ambient light). The results show that the white marking is hard to detect in all color spaces, supporting the theory presented that white marking is hard to distinguish from the snow. As the snow and white road marking have similar pixel values in the various color spaces, this suggests that for snowy conditions yellow marking can provide higher visibility of lane markings for camera-based lane detection applications.

Regarding snow depth, the image analysis shows that a relatively uniform coverage of 0.5 cm is problematic for a GoPro Hero 7 camera recording at an angle comparable to a camera in the rear-view mirror instrument cluster of vehicles. The same snow depth is less problematic photographed in birds-eye view and with the Canon EOS 5D. The difference in visibility of the

road marking from the GoPro at eye height to the Canon EOS 5D taking images from a birds-eye view could be related to the fact that the latter camera produced higher quality images, that the GoPro was moving, as well as the angle of the camera. The GoPro position in both the lab and airfield images is close to the eye height of a human driver as well as the height of many sensor clusters used for ADAS applications. A higher position of the camera and a smaller zenith angle might be beneficial for lane detection by camera in snow.

In the airfield test track, the first image was from a snow depth of 2.5 cm at which lane detection is not possible with the given equipment. Performing snow removal by using a ribbed plow with a rib height of about 2 cm was sufficient to make the road marking possible to detect. The color of the lane marking is clearly visible in the HSL-H, HSV-H, YUV-U and YUV-V channels after plowing with the ribbed plow, and it would be interesting to investigate whether the pattern left by the combination of plow and plow tires have a negative effect on establishing lines for lane keeping. Considering other methods of winter maintenance, the effect of salting of the road would also be worth investigating in terms of how it affects the visibility of lane markings.

6 CONCLUSION

This paper has investigated how the visibility of white and yellow road markings in snowy conditions is affected by different color space representations using three different scenarios: a laboratory model, a closed airfield, and public roads. The aim of the study was to determine whether yellow road markings could be beneficial for camera-based lane detection in snow. Images were analyzed by visual inspection and using histogram plots of the pixel intensities. Visually, RGB color channels and grayscale images provided poor visibility of road markings in snowy conditions. Among the HSL, HSV and YUV color spaces and their respective channels, the HSL-S, HSV-S, YUV-U and YUV-V channels provided the clearest depictions of the lane markings. The yellow markings had consistently better visibility than the white markings. The histogram plots gave similar results, with the HSL/HSV-S and YUV-U/V channels providing the most distinct peaks indicating a higher likelihood of automated identification and positioning of lane markings in the images. The HSV-S channel provided highest visibility overall. Again, the yellow road marking produced the clearest peaks indicating that yellow road markings are beneficial for automated driving in snow.

The results suggest that snow depths of 0.5 cm can cause problems for camera-based lane detection when there is a relatively uniform snow coverage. Snow removal procedures that leave parts of the road marking exposed were shown to be effective in making road marking visible in color images but also leave patterns that could be confusing for edge detection. Where markings were partially covered by snow after snow removal procedures the grayscale images were not able to detect lanes. Further investigation into snow removal procedures for camera-based lane detection is recommended to establish what snow depth cause lane keeping systems to struggle.

This research suggests that yellow road markings are beneficial for automated lane detection based on cameras. More research on the visibility of yellow versus white road markings for both human and automated drivers is encouraged especially considering the trend towards removing yellow road markings in the Nordic countries.

Further investigations could include:

- A more comprehensive investigation of the effect of snow depth on camera-based lane detection.
- The effectiveness of different winter maintenance approaches, including the effect of salting on the visibility of road markings in snowy conditions
- The effect of different camera characteristics and the position of the camera on the accuracy of automated lane detection
- How different types of road markings, e.g. color and thickness, affect camera-based lane detection.
- How different types of road surfaces, e.g. color and texture, affects camera-based lane detection

Road markings are a universally used means of leading and regulating traffic. Adapting infrastructure design and maintenance to support automated driving features relies on both the strategies of road authorities and the hardware and software solutions developed by the vehicle industry. Cooperation between these agents will be beneficial in implementing safe and efficient automated driving features.

REFERENCES

- Acharjya, P.P., Das, R., Ghoshal, D., 2012. Study and Comparison of Different Edge Detectors for Image Segmentation. *Glob. J. Comput. Sci. Technol. Graph. Vis.* 12, 29–32.
- Aldibaja, M., Sukanuma, N., Yoneda, K., 2017. Improving localization accuracy for autonomous driving in snow-rain environments. *SII 2016 - 2016 IEEE/SICE Int. Symp. Syst. Integr.* 212–217. <https://doi.org/10.1109/SII.2016.7844000>
- Aly, M., 2008. Real time detection of lane markers in urban streets, in: *IEEE Intelligent Vehicles Symposium, Proceedings*. Eindhoven, Netherlands, pp. 7–12. <https://doi.org/10.1109/IVS.2008.4621152>
- American Association of State Highway and Transportation Officials, 2011. *A Policy on Geometric Design of Highways and Streets*, 6th ed. American Association of State Highway and Transportation Officials, Washington DC, USA.
- Anisetti, M., 2009. Fast and Robust Face Detection, in: Jeong, J., Damiani, E. (Eds.), *Multimedia Techniques for Device and Ambient Intelligence*. Springer-Verlag US, New York, USA. https://doi.org/10.1007/978-0-387-88777-7_3
- Armstrong, R.L., Paterson, W.S.B., 1982. The Physics of Glaciers. *Arct. Alp. Res.* 14, 176. <https://doi.org/10.2307/1551118>
- Bar Hillel, A., Lerner, R., Levi, D., Raz, G., 2014. Recent progress in road and lane detection: A survey. *Mach. Vis. Appl.* 25, 727–745. <https://doi.org/10.1007/s00138-011-0404-2>
- Blake, D.M., Wilson, T.M., Gomez, C., 2016. Road marking coverage by volcanic ash: an experimental approach. *Environ. Earth Sci.* 75. <https://doi.org/10.1007/s12665-016-6154-8>
- Carlson, P.J., Park, E.S., Andersen, C.K., 2009. Benefits of pavement markings: A renewed perspective based on recent and ongoing research. *Transp. Res. Rec.* 2017, 59–69. <https://doi.org/10.3141/2107-06>
- Chen, C., Seff, A., Kornhauser, A., Xiao, J., 2015. DeepDriving: Learning Affordance for Direct Perception in Autonomous Driving, 2015 IEEE International Conference on Computer Vision (ICCV). Santiago. [https://doi.org/10.1016/S1573-4285\(07\)00003-8](https://doi.org/10.1016/S1573-4285(07)00003-8)
- Chetan, N.B., Gong, J., Zhou, H., Bi, D., Lan, J., Qie, L., 2020. An Overview of Recent Progress of Lane Detection for Autonomous Driving, in: *Proceedings - 2019 6th International Conference on Dependable Systems and Their Applications, DSA 2019*. IEEE, Harbin, China, pp. 341–346. <https://doi.org/10.1109/DSA.2019.00052>
- European Union Road Federation, 2012. *Marking the way towards a safer future an ERF Position PaPer on how road Markings can Make our road safer*. Brussels, Belgium.
- Finnish Transport and Communications Agency, 2020. *New road markings and traffic signs [WWW Document]*. Road Traffic Act 2020. URL <https://www.traficom.fi/en/transport/road/new-road-markings-and-traffic-signs> (accessed 11.2.20).
- Giudici, H., Dahl Fenre, M., Klein-Paste, A., Rekilä, K.-P., 2017. A technical description of

- LARS and Lumi: Two apparatus for studying tire-pavement interactions. *Routes/Roads Mag.* 49–54.
- Gruyer, D., Magnier, V., Hamdi, K., Claussmann, L., Orfila, O., Rakotonirainy, A., 2017. Perception, information processing and modeling: Critical stages for autonomous driving applications. *Annu. Rev. Control* 44, 323–341. <https://doi.org/10.1016/j.arcontrol.2017.09.012>
- Heller, V., 2011. Scale effects in physical hydraulic engineering models. *J. Hydraul. Res.* 49, 293–306. <https://doi.org/10.1080/00221686.2011.578914>
- Hernández, D.C., Kurnianggoro, L., Filonenko, A., Jo, K.H., 2016. Real-time lane region detection using a combination of geometrical and image features. *Sensors (Switzerland)* 16. <https://doi.org/10.3390/s16111935>
- Huang, A.S., Moore, D., Antone, M., Olson, E., Teller, S., 2009. Finding multiple lanes in urban road networks with vision and lidar. *Auton. Robots* 26, 103–122. <https://doi.org/10.1007/s10514-009-9113-3>
- Kaur, J., Agrawal, S., Vig, R., 2012. A Comparative Analysis of Thresholding and Edge Detection Segmentation Techniques. *Int. J. Comput. Appl.* 39, 29–34. <https://doi.org/10.5120/4898-7432>
- Kokhanovsky, A.A., Aoki, T., Hachikubo, A., Hori, M., Zege, E.P., 2005. Reflective properties of natural snow: Approximate asymptotic theory versus in situ measurements. *IEEE Trans. Geosci. Remote Sens.* 43, 1529–1535. <https://doi.org/10.1109/TGRS.2005.848414>
- Kusano, K.D., Gabler, H.C., 2015. Comparison of Expected Crash and Injury Reduction from Production Forward Collision and Lane Departure Warning Systems. *Traffic Inj. Prev.* 16, 109–114. <https://doi.org/10.1080/15389588.2015.1063619>
- Lee, C., Moon, J.H., 2018. Robust lane detection and tracking for real-time applications. *IEEE Trans. Intell. Transp. Syst.* 19, 4043–4048. <https://doi.org/10.1109/TITS.2018.2791572>
- Li, L., Luo, W., Wang, K.C.P., 2018. Lane marking detection and reconstruction with line-scan imaging data. *Sensors (Switzerland)* 18, 1–23. <https://doi.org/10.3390/s18051635>
- Lin, Q., Youngjoon, H., Hahn, H., 2010. Real-time lane detection based on extended edge-linking algorithm, in: 2nd International Conference on Computer Research and Development, ICCRD 2010. IEEE, Kuala Lumpur, Malaysia, pp. 725–730. <https://doi.org/10.1109/ICCRD.2010.166>
- Lundkvist, S.-O., Fors, C., 2010. Lane Departure Warning System – LDW Samband mellan LDW:s och vägmarkeringars funktion VTI notat 15-2010. Linköping, Sweden.
- Markvart, T., Castañer, L., 2003. Practical Handbook of Photovoltaics: Fundamentals and Applications, Practical Handbook of Photovoltaics: Fundamentals and Applications. Elsevier Ltd, Oxford, UK. <https://doi.org/10.1016/B978-1-85617-390-2.X5000-4>
- Narote, S.P., Bhujbal, P.N., Narote, A.S., Dhane, D.M., 2018. A review of recent advances in lane detection and departure warning system. *Pattern Recognit.* 73, 216–234. <https://doi.org/10.1016/j.patcog.2017.08.014>

- Nitsche, P., Mocanu, I., Reinthaler, M., 2014. Requirements on tomorrow's road infrastructure for highly automated driving, in: 2014 International Conference on Connected Vehicles and Expo, ICCVE 2014 - Proceedings. IEEE, Shenzhen, China, pp. 939–940. <https://doi.org/10.1109/ICCV.2014.7297694>
- O'Neill, A.D.J., Gray, D., 1972. Solar radiation penetration through snow. Proc. UNESCO-WMO-IAHS Symp. Role Snow Ice Hydrol. Vol. 1 1, 229–249.
- Perovich, D.K., 2007. Light reflection and transmission by a temperate snow cover. *J. Glaciol.* 53, 201–210. <https://doi.org/10.3189/172756507782202919>
- Pike, A., Carlson, P., Barrette, T., 2018. Evaluation of the Effects of Pavement Marking Width on Detectability By Machine Vision : 4-Inch vs 6-Inch Markings. Virginia, USA.
- Pike, A.M., Bommanayakanahalli, B., 2018. Development of a Pavement Marking Life Cycle Cost Tool. *Transp. Res. Rec.* 2672, 148–157. <https://doi.org/10.1177/0361198118758012>
- Podpora, M., Korbaś, G.P., Kawala-Janik, A., 2014. YUV vs RGB—Choosing a Color Space for Human-Machine Interaction. *Position Pap. 2014 Fed. Conf. Comput. Sci. Inf. Syst.* 3, 29–34. <https://doi.org/10.15439/2014f206>
- Razmi Rad, S., Farah, H., Taale, H., van Arem, B., Hoogendoorn, S.P., 2020. Design and operation of dedicated lanes for connected and automated vehicles on motorways: A conceptual framework and research agenda. *Transp. Res. Part C Emerg. Technol.* 117, 102664. <https://doi.org/10.1016/j.trc.2020.102664>
- Rezwaniul Haque, M., Milon Islam, M., Saeed Alam, K., Iqbal, H., 2019. A Computer Vision based Lane Detection Approach. *Int. J. Image, Graph. Signal Process.* 11, 27–34. <https://doi.org/10.5815/ijigsp.2019.03.04>
- Samuel, M., Mohamad, M., Saad, S.M., Hussein, M., 2018. Development of Edge-Based Lane Detection Algorithm using Image Processing. *JOIV Int. J. Informatics Vis.* 2, 19. <https://doi.org/10.30630/joiv.2.1.101>
- Schnell, T., Zwahlen, H.T., 2000. Computer-Based Modeling to Determine the Visibility and Minimum Retroreflectivity of Pavement Markings. *Transp. Res. Rec.* 1708.
- Shladover, S.E., 2018. Connected and automated vehicle systems: Introduction and overview. *J. Intell. Transp. Syst. Technol. Planning, Oper.* 22, 190–200. <https://doi.org/10.1080/15472450.2017.1336053>
- Statens vegvesen, 2019. Håndbok N100 - Veg- og gateutforming. Vegdirektoratet, Oslo, Norway.
- Statens vegvesen, 2005. Asfalt 2005-materialer og utførelse Håndbok 246. Vegdirektoratet, Trondheim, Norway.
- Statens Vegvesen, 2015. Vegoppmerking Tekniske bestemmelser og retningslinjer for anvendelse of utforming. Statens vegvesen, Oslo, Norway.
- Sternlund, S., 2017. The safety potential of lane departure warning systems—A descriptive real-world study of fatal lane departure passenger car crashes in Sweden. *Traffic Inj. Prev.* 18,

S18–S23. <https://doi.org/10.1080/15389588.2017.1313413>

- Stevic, S., Dragojevic, M., Kronic, M., Cetic, N., 2020. Vision-Based Extrapolation of Road Lane Lines in Controlled Conditions, in: 2020 Zooming Innovation in Consumer Technologies Conference (ZINC). Novi Sad, Serbia, pp. 174–177. <https://doi.org/10.1109/zinc50678.2020.9161779>
- Storsæter, A.D., Pitera, K., McCormack, E.D., n.d. The Automated Driver as a New Road User. *Transp. Rev.* <https://doi.org/10.1080/01441647.2020.1861124>
- U.S. Department of Transportation, 2009. Manual on uniform traffic control devices for streets and highways. Washington DC, USA.
- Vadeby, A., Kjellman, E., Fors, C., Lundkvist, S.-O., Berne Nielsen, V., Cato Johansen, T., Nilsson, C., 2018. ROMA state assessment of road markings in Denmark, Norway and Sweden - Results from 2017.
- Wang, X., Hänsch, R., Ma, L., Hellwich, O., 2014. Comparison of different color spaces for image segmentation using graph-cut. *VISAPP 2014 - Proc. 9th Int. Conf. Comput. Vis. Theory Appl.* 1, 301–308. <https://doi.org/10.5220/0004681603010308>
- Xing, Y., Lv, C., Chen, L., Wang, Huaji, Wang, Hong, Cao, D., Velenis, E., Wang, F.Y., 2018. Advances in Vision-Based Lane Detection: Algorithms, Integration, Assessment, and Perspectives on ACP-Based Parallel Vision. *IEEE/CAA J. Autom. Sin.* 5, 645–661. <https://doi.org/10.1109/JAS.2018.7511063>
- Xuan, H., Liu, H., Yuan, J., Li, Q., 2017. Robust Lane-Mark Extraction for Autonomous Driving under Complex Real Conditions. *IEEE Access* 6, 5749–5765. <https://doi.org/10.1109/ACCESS.2017.2731804>
- Yi, S.C., Chen, Y.C., Chang, C.H., 2015. A lane detection approach based on intelligent vision. *Comput. Electr. Eng.* 42, 23–29. <https://doi.org/10.1016/j.compeleceng.2015.01.002>
- Yinka, A.O., Ngwira, S.M., Tranos, Z., Sengar, P.S., 2014. Performance of drivable path detection system of autonomous robots in rain and snow scenario, in: 2014 International Conference on Signal Processing and Integrated Networks, SPIN 2014. IEEE, Dehli, India, pp. 679–684. <https://doi.org/10.1109/spin.2014.6777041>
- Zhang, L., Yin, Z., Zhao, K., Tian, H., 2020. Lane detection in dense fog using a polarimetric dehazing method. *Appl. Opt.* 59, 5702. <https://doi.org/10.1364/ao.391840>

Appendix E

Code for Data Analyses in Paper III

LISTING E.1: Example of code used to create data input for logistic binary regression analyses.

```
# This is code used to create data sets analysed in publications
# by Ane Dalsnes Storsøter. The code shows examples of merging
# vehicle data with different sample rates, continuous and
# discrete, and the creation of data sets used to perform
# binary logistic regressions to correlate data from a lane
# departure warning (LDW) system and a mobile
# retroreflectometer.

import pandas as pd
import numpy as np
#from datetime import datetime
import datetime as dt
#import traces
import matplotlib.pyplot as plt
from mpl_toolkits.mplot3d import Axes3D
import seaborn as sns
import sklearn as sk
import pandas as pd
import xticks
GPSdata= pd.read_csv(r"VehicleData.txt",usecols=[n,n+1,n+2],
                    low_memory=False,names=['T','Longitude','Latitude'])
DiscreteLane= pd.read_csv(r"VehicleData.txt",usecols=[x,x+1],
                          low_memory=False,names=['T2','LaneDetn'])
VehicleSpeed= pd.read_csv(r"VehicleData.txt",usecols=[y,y+1],
                           low_memory=False,names=['T3','VehSpeed'])
AmbLight= pd.read_csv(r"VehicleData.txt",usecols=[z,z+1],
                      low_memory=False,names=['TAmb','AmbLight'])
GPSdata = GPSdata.dropna(how='all')
DiscreteLane = DiscreteLane.dropna(how='all')
VehicleSpeed = VehicleSpeed.dropna(how='all')
AmbLight = AmbLight.dropna(how='all')

#Set date to today's date but leave time stamp:
dateUsed = '2019-08-30_21:30:44'
dateCorr = '2019-08-30_21:28:00'

# Lane detection is the sampling rate to match due to its
```

```

# categorical nature. Resampling lane detection will create
# falsely continuous values. Therefore, we want to downsample
# vehicle speed and average the values, upsample lat and long
# with interpolation, and upsample retromesurements with
# interpolation.

#Converting time to datetime
VehicleSpeed.index = pd.to_datetime(VehicleSpeed['T3'],
                                     unit='s',origin=pd.Timestamp(dateUsed))
GPSdata.index = pd.to_datetime(GPSdata['T'], unit='s',
                               origin=pd.Timestamp(dateUsed))
DiscreteLane.index = pd.to_datetime(DiscreteLane['T2'],
                                     unit='s', origin=pd.Timestamp(dateUsed))
AmbLight.index = pd.to_datetime(AmbLight['TAmb'], unit='s',
                                 origin=pd.Timestamp(dateUsed))

#Clean up columns.
GPSdata['Time'] = GPSdata['T']
VehicleSpeed['Time'] = VehicleSpeed['T3']
del GPSdata['T']
del VehicleSpeed['T3']

#Merging GPS and Vehicle speed with interpolation.
GPSVehSpeed = pd.merge_ordered(GPSdata, VehicleSpeed,
                              left_on='T', right_on='T3', how='outer',
                              fill_method='ffill')
GPSVehSpeed.head(15)

#Clean up columns.
DiscreteLane['Time'] = DiscreteLane['T2']
del DiscreteLane['T2']

# Making index datetime format.
GPSVehSpeed.index = pd.to_datetime(GPSVehSpeed['Time_y'],
                                   unit='s', origin=pd.Timestamp(dateUsed))

#Clean up columns.
GPSVehSpeed['Time'] = GPSVehSpeed['Time_y']
del GPSVehSpeed['Time_y']

# Merge gps data, vehicle speed and discrete lane data
# with interpolation.
GPSSpeedLane = pd.merge_ordered(GPSVehSpeed,
                               DiscreteLane, left_on='Time', right_on='Time',
                               how='outer', fill_method='ffill')

#Clean up columns.

AmbLight['Time'] = AmbLight['TAmb']
del AmbLight['TAmb']

# Merge gps, speed, lane det with ambient light.
GPSSpeedLaneAmb = pd.merge_ordered(GPSSpeedLane, AmbLight,
                                   left_on='Time', right_on='Time',
                                   how='outer', fill_method='ffill')
GPSSpeedLaneAmb.head(15)

```

```

#Plot for sanity check:
GPSSpeedLaneAmb.plot(x='Time', y= 'AmbLight')

#Done merging vehicle data at different sample rates,
# now to add laser data (retroreflectometer).
# Reading files:
df = pd.read_csv(r"LaserDataPart1.csv",sep=';',skiprows=n,
                usecols = ['Time', 'Latitude','Longitude',
                            'Valid_Scans_Left','Retro_Left_Average',
                            'Retro_Left_Contrast','Odometer','Vehicle_Speed'])
df2 = pd.read_csv(r"LaserDataPart2.csv",sep=';',skiprows=n,
                 usecols =['Time', 'Latitude','Longitude',
                            'Valid_Scans_Left','Retro_Left_Average',
                            'Retro_Left_Contrast','Odometer','Vehicle_Speed'])

# Making sure vehicle speed is in the same units for
# vehicle and retroreflectometer:
df['Vehicle_Speed']=0.277777778*df['Vehicle_Speed']
df2['Vehicle_Speed']=0.277777778*df2['Vehicle_Speed']

# Concatenate data sets to get the data set that matches
# the vehicle data in time:
frames = [df, df2]
laserFullBothWays = pd.concat(frames,ignore_index=True)

# Changing time columns to datetime format for both
# vehicle and retroreflectometer data:
laserFullBothWays['TimePlot'] = \
    pd.to_datetime(laserFullBothWays['Time'])
GPSSpeedLaneAmb['TimeMerge'] = \
    pd.to_datetime(GPSSpeedLaneAmb['Time'], unit='s',
                  origin=pd.Timestamp(dateCorr))

# Sanity check:
laserFullBothWays.dtypes

GPSSpeedLaneAmb.dtypes

# Merge Vehicle data with retroreflectometer data:
VehicleLaser = pd.merge_ordered(GPSSpeedLaneAmb,
                                laserFullBothWays,left_on='TimeMerge',
                                right_on='TimePlot',fill_method='ffill',
                                how='outer')
VehicleLaser.head(5)

# Plotting to check that data is overlapping and correct:
ax3 = VehicleLaser.plot(x='Time_y', y='VehSpeed',
                       linewidth=3.3)
ax4 = VehicleLaser.plot(x='Time_y', y='Vehicle_Speed',
                       color='g', ax=ax3)

print(ax3 == ax4)

# Position data (lat,lon) is not always accurate.
# Performing additional sanity check that the merge is
# correct by correlation vehicle speed measure in

```

```

# vehicle and by retroreflectometer:
VehicleLaser['VehSpeed'].max()
VehicleLaser[['VehSpeed']].idxmax()
print(VehicleLaser[VehicleLaser.VehSpeed ==
                VehicleLaser.VehSpeed.max()])
print(VehicleLaser[VehicleLaser['Vehicle_Speed'] ==
                VehicleLaser['Vehicle_Speed'].max()])
VehicleLaser.shape

# Creating sections of data needed for analyses:
VehicleLaserFormer = VehicleLaser[286940:1200000]
VehicleLaserLatter = VehicleLaser[1200001:2787897]

# Plots to check:
ax321 = VehicleLaserFormer.plot(x='Time_y', y='VehSpeed',
                               linewidth=3.3)
ax432 = VehicleLaserFormer.plot(x='Time_y', y='Vehicle_Speed',
                               color='g', ax=ax321)
print(ax321 == ax432)

# More plots to check:
ax33 = VehicleLaserLatter.plot(x='Time_y', y='VehSpeed',
                               linewidth=3.3)
ax44 = VehicleLaserLatter.plot(x='Time_y', y='Vehicle_Speed',
                               color='g',
                               ax=ax33)
print(ax33 == ax44)

# Even more plots to check:
ax01 = VehicleLaserFormer.plot(x='Time_y', y='Latitude_x',
                               linewidth=3.3)
ax02 = VehicleLaserFormer.plot(x='Time_y', y='Latitude_y',
                               color='r', ax=ax01)
ax01.set_ylim(59.3,60)
print(ax01 == ax02)

# Some more plots:
ax011 = VehicleLaserFormer.plot(x='Time_y', y='Longitude_x',
                                linewidth=4)
ax022 = VehicleLaserFormer.plot(x='Time_y', y='Longitude_y',
                                color='r', ax=ax011)
ax011.set_ylim(10.6,11)
print(ax011 == ax022)

# Some plots:
ax1 = VehicleLaserLatter.plot(x='Time_y', y='Latitude_x',
                              linewidth=3.3)
ax2 = VehicleLaserLatter.plot(x='Time_y', y='Latitude_y',
                              color='g', ax=ax1)
ax1.set_ylim(59.3,60)
print(ax1 == ax2)

# Plots:
ax11 = VehicleLaserLatter.plot(x='Time_y', y='Longitude_x',
                               linewidth=3.3)
ax22 = VehicleLaserLatter.plot(x='Time_y', y='Longitude_y',
                               color='g', ax=ax11)

```

```
ax11.set_ylim(10.6,11)
print(ax11 == ax22)

# Look at discrete lane detection in a histogram:
VehicleLaserLatter.hist(column='LaneDetn')

# Change discrete values to binary values:
laneBinary = []
for value in VehicleLaserLatter["LaneDetn"]:
    if value == 0:
        laneBinary.append("0")
    elif value == 1:
        laneBinary.append("0")
    elif value == 2:
        laneBinary.append("1")
    elif value == 3:
        laneBinary.append("1")
    else:
        laneBinary.append("0")

VehicleLaserLatter["laneBinary"] = laneBinary
VehicleLaserLatter["laneBinary"] = \
    VehicleLaserLatter["laneBinary"].astype(int)

#New plot of LaneDet values to validate conversion to
# binary set.
VehicleLaserLatter.hist(column='laneBinary')

# Change discrete values to binary values:
laneBinary2 = []
for value in VehicleLaserFormer["LaneDetn"]:
    if value == 0:
        laneBinary2.append("0")
    elif value == 1:
        laneBinary2.append("0")
    elif value == 2:
        laneBinary2.append("1")
    elif value == 3:
        laneBinary2.append("1")
    else:
        laneBinary2.append("0")

VehicleLaserFormer["laneBinary"] = laneBinary2
VehicleLaserFormer["laneBinary"] = \
    VehicleLaserFormer["laneBinary"].astype(int)

#New plot of LaneDet values to validate conversion to
# binary set.
VehicleLaserFormer.hist(column='laneBinary')

# Plot:
ax17 = VehicleLaserFormer.plot(x='Time_y', y='Latitude_x',
                               linewidth=3.3)
ax27 = VehicleLaserFormer.plot(x='Time_y', y='Latitude_y',
                               color='g', ax=ax17)
print(ax17 == ax27)
```

```
# Create files for statistical analyses:  
# County road night:  
VehicleLaserLatter.to_csv(r'CountyRoadNight.csv')  
# Freeway night:  
VehicleLaserFormer.to_csv(r'FreewayNight.csv')
```


Appendix F

Code for Image Analyses in Paper IV

LISTING F.1: Example of code used for converting images to different color spaces and creating corresponding histograms.

```
#!/usr/bin/env python
# coding: utf-8

# In[1]:

# This is an example of code used to produce different color
# space representations and histograms for the paper
# "Camera-Based Lane Detection - Can Yellow Road Marking
# Facilitate Automated Driving in Snow?" Authors: Ane Dalsnes
# Storsæter, Kelly Pitera and Edward McCormack,
# submitted to the Journal of Field Robotics in December 2020.
# The aim of the paper was to investigate if yellow road
# marking could be beneficial for camera-based lane detection.
# Code by Ane Dalsnes Storsæter.

# Import libraries
import matplotlib.pyplot as plt
import matplotlib.image as mpimg
import numpy as np
import cv2
import math

# In[2]:

# Setting title to make it easier to find and sort the images
# that are produced. Change this title when changing images or
# if you don't want to overwrite previously produced images and
# plots.
title= "Case_1a_test_"

# Reading image from local folder, replace with own location.
img = mpimg.imread('testImages/1a_croppedROI.jpg')

# Addressing the three color channels to be used to show and
```

```
# plot the respective color channels.
R = img[:, :, 0]
G = img[:, :, 1]
B = img[:, :, 2]

# Finding the shape of the image, used to do simple slicing.
h, w, c = img.shape
print('width:␣␣', w)
print('height:␣', h)
print('channel:', c)

# Removing axis on image, showing image and saving image.
# Set the save location to a folder that exists and update
# the savefig-location.
plt.axis('off')
plt.imshow(img)
plt.savefig('C:/Cases/'+title+'RGB'+'.jpg', dpi=300,
           bbox_inches='tight', pad_inches=0)

# In[3]:

# For Case 1a, the image is not sliced in half, instead
# the pixel row to separate white from yellow markings is
# set manually. Creating upper half of image
# (yellow marking).
sub_image = img[0:430,:]

# Showing upper part of image
plt.axis('off')
plt.imshow(sub_image)

# In[4]:

# The lower part of the image is also manually set in
# this case.
sub_image2 = img[500:1344,:]

# Showing lower part of image (white marking)
plt.axis('off')
plt.imshow(sub_image2)

# In[5]:

# In Case 1a the upper and lower part of the image have
# different color marking. As the difference between
# these two markings, in terms of visibility in color
# spaces and histograms, is the aim of the paper the
# upper and lower parts of the image are plotted separately
# to look at differences.

# Histograms are found by using the np.sum function and
```

```

# plotted for upper (yellow) and lower (white) parts of
# the image for the three different color spaces of the RGB
# color space.

Rlow = np.sum(R[500:1344,:],axis=0)
Rhigh = np.sum(R[0:430,:],axis=0)
Glow = np.sum(G[500:1344,:],axis=0)
Ghigh = np.sum(G[0:430,:],axis=0)
Blow = np.sum(B[500:1344,:],axis=0)
Bhigh = np.sum(B[0:430,:],axis=0)
plt.plot(Rhigh, color = 'red', label = 'RGB-R_yellow')
plt.plot(Ghigh, color = 'green', label = 'RGB-G_yellow')
plt.plot(Bhigh, color = 'blue', label = 'RGB-B_yellow')
plt.plot(Rlow, color = 'orange', label = 'RGB-R_white')
plt.plot(Glow, color = 'lightgreen', label = 'RGB-G_white')
plt.plot(Blow, color = 'lightblue', label = 'RGB-B_white')

plt.legend(bbox_to_anchor=(1.05, 1), loc='upper_left')
plt.savefig('C:/Cases/'+ title+'RGBhisthighlow'+'.jpg',
            dpi=300, bbox_inches='tight', pad_inches=0)

# In[6]:

# Plotting only the upper part of the image,
# i.e. yellow marking.

plt.plot(Rhigh, color = 'red', label = 'RGB-R_yellow')
plt.plot(Ghigh, color = 'green', label = 'RGB-G_yellow')
plt.plot(Bhigh, color = 'blue', label = 'RGB-B_yellow')

plt.legend(bbox_to_anchor=(1.05, 1), loc='upper_left')
plt.savefig('C:/Cases/'+ title+'RGBhisthigh'+'.jpg',
            dpi=300, bbox_inches='tight', pad_inches=0)

# In[7]:

# Plotting only the lower part of the image,
# i.e. white marking.

plt.plot(Rlow, color = 'red', label = 'RGB-R')
plt.plot(Glow, color = 'green', label = 'RGB-G')
plt.plot(Blow, color = 'blue', label = 'RGB-B')
plt.legend(bbox_to_anchor=(1.05, 1), loc='upper_left')
plt.savefig('C:/Cases/'+ title+'RGBhistlow'+'.jpg',
            dpi=300, bbox_inches='tight', pad_inches=0)

# In[8]:

# Highlighting the channels that give the most
# distinct peaks at the position of the road markings.

```

```

plt.plot(Rhigh, color = 'red', label = 'RGB-R␣yellow')
plt.plot(Ghigh, color = 'green', label = 'RGB-G␣yellow')
plt.plot(Bhigh, color = 'blue', label = 'RGB-B␣yellow')
plt.plot(Rlow, color = 'orange', label = 'RGB-R␣white')
plt.plot(Glow, color = 'green', label = 'RGB-G')
plt.plot(Blow, color = 'blue', label = 'RGB-B')
plt.legend(bbox_to_anchor=(1.05, 1), loc='upper left')
plt.legend()
plt.savefig('C:/Cases/'+title+'Rhist_highlow'+'.jpg',
            dpi=300, bbox_inches='tight', pad_inches=0)

# In[9]:

plt.plot(Rhigh, color = 'red', label = 'RGB-R yellow')
plt.plot(Ghigh, color = 'green', label = 'RGB-G␣yellow')
plt.plot(Bhigh, color = 'blue', label = 'RGB-B␣yellow')
plt.plot(Rlow, color = 'orange', label = 'RGB-R white')
plt.plot(Glow, color = 'lightgreen', label = 'RGB-G␣white')
plt.plot(Blow, color = 'blue', label = 'RGB-B')
plt.legend(bbox_to_anchor=(1.05, 1), loc='upper left')
plt.legend()
plt.savefig('C:/Cases/'+title+'Ghist_highlow'+'.jpg',
            dpi=300, bbox_inches='tight', pad_inches=0)

# In[10]:

plt.plot(Rhigh, color = 'red', label = 'RGB-R yellow')
plt.plot(Ghigh, color = 'green', label = 'RGB-G␣yellow')
plt.plot(Bhigh, color = 'blue', label = 'RGB-B␣yellow')
plt.plot(Rlow, color = 'orange', label = 'RGB-R white')
plt.plot(Glow, color = 'green', label = 'RGB-G')
plt.plot(Blow, color = 'lightblue', label = 'RGB-B␣white')
plt.legend(bbox_to_anchor=(1.05, 1), loc='upper left')
plt.legend()
plt.savefig('C:/Cases/'+title+'Bhist_highlow'+'.jpg',
            dpi=300, bbox_inches='tight', pad_inches=0)

# In[11]:

# Converting the RGB image to grayscale
gray = cv2.cvtColor(img, cv2.COLOR_RGB2GRAY)

# Showing image and saving image
plt.axis('off')
plt.imshow(gray, cmap='gray')
print(gray.shape)
plt.savefig('testImages/gray.jpg')
plt.savefig('C:/Cases/'+title+'gray'+'.jpg', dpi=300,
            bbox_inches='tight', pad_inches=0)

```

```

# In[12]:

# Making histogram plots for the upper and lower part of
# the image for the grayscale representation
histogramgraylow = np.sum(gray[0:430,:],axis=0)
histogramgrayhigh = np.sum(gray[500:1344,:],axis=0)
plt.plot(histogramgraylow, color = 'gray',
         label = 'Gray□white')
plt.plot(histogramgrayhigh, color = 'black',
         label = 'Gray□yellow')

plt.legend()
plt.savefig('C:/LD/Cases/'+title+'grayhist_highlow'+'.jpg',
          dpi=300, bbox_inches='tight', pad_inches=0)

# In[13]:

# Converting the RGB image to HSL color space, OpenCV
# uses the order HLS.
hls = cv2.cvtColor(img, cv2.COLOR_RGB2HLS)

# Naming the three color channels of the HLS
# representation.
H = hls[:, :, 0]
L = hls[:, :, 1]
S = hls[:, :, 2]

# Finding the shape of the image
he, wi, ch = hls.shape
print('width:□□', wi)
print('height:□', he)
print('channel:', ch)

# Showing and saving the HLS representation
plt.imshow(hls)
plt.axis('off')
plt.savefig('C:/Cases/'+title+'HLS'+'.jpg', dpi=300,
          bbox_inches='tight', pad_inches=0)

# In[14]:

# Separating the upper and lower part of the image to
# produce histogram plots for the lower and upper part
# of the image.

Hlow = np.sum(H[500:1344,:],axis=0)
Hhigh = np.sum(H[0:430,:],axis=0)
Llow = np.sum(L[500:1344,:],axis=0)
Lhigh = np.sum(L[0:430,:],axis=0)
Slow = np.sum(S[500:1344,:],axis=0)
Shigh = np.sum(S[0:430,:],axis=0)

```

```

# Plotting the histograms for the lower part of the
# image (white)
plt.plot(Hlow, color = 'blue', label = 'HSL-H')
plt.plot(Llow, color = 'green', label = 'HSL-L')
plt.plot(Slow, color = 'red', label = 'HSL-S')
plt.legend()
plt.legend(bbox_to_anchor=(1.05, 1), loc='upper_left')
plt.savefig('C:/Cases/'+title+'HLShistlow'+'.jpg',
            dpi=300, bbox_inches='tight', pad_inches=0)

# In[15]:

# Plotting the histograms for the L-channel from the
# HSL image, comparing the white marking
# (lower part of image) to the yellow marking
# (upper part of image).

plt.plot(Llow, color = 'lightgreen',
         label = 'HSL-L_white')
plt.plot(Lhigh, color = 'green',
         label = 'HSL-L_yellow')

plt.legend()
plt.savefig('C:/Cases/'+title+'HSL-Lhist_highlow'+'.jpg',
            dpi=300, bbox_inches='tight', pad_inches=0)

# In[16]:

# Plotting the histograms for the H-channel from the
# HSL image, comparing the white marking
# (lower part of image) to the yellow marking
# (upper part of image).

plt.plot(Hlow, color = 'lightblue', label = 'HSL-H_white')
plt.plot(Hhigh, color = 'blue', label = 'HSL-H_yellow')

plt.legend()
plt.savefig('C:/Cases/'+title+'HSL-H_histhighlow'+'.jpg',
            dpi=300, bbox_inches='tight', pad_inches=0)

# In[17]:

# Plotting the histograms for the S-channel from the
# HSL image, comparing the white marking
# (lower part of image) to the yellow marking
# (upper part of image).

plt.plot(Slow, color = 'orange', label = 'HSL-S_white')
plt.plot(Shigh, color = 'red', label = 'HSL-S_yellow')

plt.legend()

```

```

plt.savefig('C:/Cases/'+title+'HSL-Shistlow'+'.jpg',
            dpi=300, bbox_inches='tight', pad_inches=0)

# In[18]:

# Converting the RGB image to HSV color space and naming
# the three color channels

hsv = cv2.cvtColor(img, cv2.COLOR_RGB2HSV)
H2 = hsv[:, :, 0]
S2 = hsv[:, :, 1]
V = hsv[:, :, 2]

# Showing and saving the HLS representation
plt.imshow(hsv)
plt.axis('off')
plt.savefig('C:/Cases/'+title+'HSV'+'.jpg', dpi=300,
            bbox_inches='tight', pad_inches=0)

# In[19]:

# Separating the white (low) from the yellow (high) in
# the histogram plots

H2low = np.sum(H2[500:1344, :], axis=0)
H2high = np.sum(H2[0:430, :], axis=0)
Vlow = np.sum(V[500:1344, :], axis=0)
Vhigh = np.sum(V[0:430, :], axis=0)
S2low = np.sum(S2[500:1344, :], axis=0)
S2high = np.sum(S2[0:430, :], axis=0)

plt.plot(H2low, color = 'blue', label = 'HSV-H')
plt.plot(Vlow, color = 'green', label = 'HSV-V')
plt.plot(S2low, color = 'red', label = 'HSV-S')

plt.legend(bbox_to_anchor=(1.05, 1), loc='upper_left')
plt.savefig('C:/Cases/'+title+'HSVhistlow'+'.jpg',
            dpi=300, bbox_inches='tight', pad_inches=0)

# In[20]:

# Plotting the histograms for the H-channel from the
# HSV image, comparing the white marking
# (lower part of image) to the yellow marking
# (upper part of image).

plt.plot(H2low, color = 'lightblue', label = 'HSV-H_lowwhite')
plt.plot(H2high, color='blue', label = 'HSV-H_lowyellow')

plt.legend()
plt.savefig('C:/Cases/'+title+'HSV-Hhist_highlow'+'.jpg',

```

```
        dpi=300, bbox_inches='tight', pad_inches=0)

# In[21]:

# Plotting the histograms for the S-channel from the
# HSV image, comparing the white marking
# (lower part of image) to the yellow marking
# (upper part of image).

plt.plot(S2low, color = 'orange', label = 'HSV-S□white')
plt.plot(S2high, color='red', label = 'HSV-S□yellow')

plt.legend()
plt.savefig('C:/Cases/'+title+'HSV-Shist_highlow'+'.jpg',
           dpi=300, bbox_inches='tight', pad_inches=0)

# In[22]:

# Plotting the histograms for the V-channel from the
# HSV image, comparing the white marking
# (lower part of image) to the yellow marking
# (upper part of image).

plt.plot(Vlow, color = 'lightgreen',
         label = 'HSV-V□white')
plt.plot(Vhigh, color='green', label = 'HSV-V□yellow')

plt.legend()
plt.savefig('C:/Cases/'+title+'HSV-Vhist_highlow'+'.jpg',
           dpi=300, bbox_inches='tight', pad_inches=0)

# In[23]:

# Converting the RGB image to YUV color space and naming
# the three color channels

yuv = cv2.cvtColor(img, cv2.COLOR_RGB2YUV)

Y = yuv[:, :, 0]
U = yuv[:, :, 1]
V2 = yuv[:, :, 2]

# Showing and saving the image
plt.axis('off')
plt.imshow(yuv)
plt.savefig('C:/Cases/'+title+'YUV'+'.jpg', dpi=300,
           bbox_inches='tight', pad_inches=0)

# In[24]:
```



```

# Separating the white (low) from the yellow (high) in
# the histogram plots

Ylow = np.sum(Y[500:1344,:],axis=0)
Yhigh = np.sum(Y[0:430,:],axis=0)
V2low = np.sum(V2[500:1344,:],axis=0)
V2high = np.sum(V2[0:430,:],axis=0)
Ulow = np.sum(U[500:1344,:],axis=0)
Uhigh = np.sum(U[0:430,:],axis=0)

plt.plot(Ylow, color = 'green', label = 'YUV-Y')
plt.plot(Ulow, color = 'blue', label = 'YUV-U')
plt.plot(V2low, color = 'red', label = 'YUV-V')
plt.legend(bbox_to_anchor=(1.05, 1), loc='upper_left')
plt.savefig('C:/Cases/'+title+'YUV_hist'+'.jpg',
            dpi=300, bbox_inches='tight', pad_inches=0)

# In[25]:

# Plotting the histograms for the Y-channel from the
# YUV image, comparing the white marking
# (lower part of image) to the yellow marking
# (upper part of image).

plt.plot(Ylow, color = 'lightgreen', label = 'YUV-Y_white')
plt.plot(Yhigh, color = 'green', label = 'YUV-Y_yellow')

plt.legend()
plt.savefig('C:/Cases/'+title+'YUV-Yhist_highlow'+'.jpg',
            dpi=300, bbox_inches='tight', pad_inches=0)

# In[26]:

# Plotting the histograms for the U-channel from the
# YUV image, comparing the white marking
# (lower part of image) to the yellow marking
# (upper part of image).

plt.plot(V2low, color = 'orange', label = 'YUV-V_white')
plt.plot(V2high, color = 'red', label = 'YUV-V_yellow')

plt.legend()
plt.savefig('C:/Cases/'+title+'YUV-Vhist_highlow'+'.jpg',
            dpi=300, bbox_inches='tight', pad_inches=0)

# In[27]:

# Plotting the histograms for the V-channel from the
# YUV image, comparing the white marking
# (lower part of image) to the yellow marking

```

```
# (upper part of image).

plt.plot(Ulow, color = 'lightblue', label = 'YUV-Uwhite')
plt.plot(Uhigh, color = 'blue', label = 'YUV-Uyellow')

plt.legend()
plt.savefig('C:/Cases/'+title+'YUV-Uhist_highlow'+'.jpg',
            dpi=300, bbox_inches='tight', pad_inches=0)

# In[28]:

# Plotting the histograms for the U- and V- channels
# from the YUV image, only for the yellow marking.

plt.plot(Uhigh, color = 'blue', label = 'YUV-Uyellow')
plt.plot(V2high, color = 'red', label = 'YUV-Vyellow')

plt.legend()
plt.savefig('C:/Cases/'+title+'YUV-UVhist_highlow'+'.jpg',
            dpi=300, bbox_inches='tight', pad_inches=0)
```

ISBN 978-82-326-6579-2 (printed ver.)
ISBN 978-82-326-5241-9 (electronic ver.)
ISSN 1503-8181 (printed ver.)
ISSN 2703-8084 (online ver.)